DTU Library

3D printing of bio-based concrete composites for construction

Christ, Julian

Publication date:
2023

Document Version
Publisher's PDF, also known as Version of record

[Link back to DTU Orbit](#)

Citation (APA):
Christ, J. (2023). *3D printing of bio-based concrete composites for construction*. Technical University of Denmark.

3D printing of bio-based concrete composites for construction

Julian Christ

PhD Thesis

3D printing of bio-based concrete composites for construction

Julian Christ

PhD thesis

DTU

Technical University of Denmark

Lyngby, Denmark

February 2023

3D printing of bio-based concrete composites for construction

Julian Christ

PhD thesis, February 2023

Supervisors

Principal Supervisor:
Associate Professor Holger Koss, Technical University of Denmark, DTU Construct - Department of Civil and Mechanical Engineering, Denmark

Co-supervisor:
Professor Lisbeth M. Ottosen, Technical University of Denmark, DTU Sustain – Department of Environmental and Resource Engineering, Denmark

Assessment Committee

Chairperson:
Senior Researcher Ana Teresa Macas Lima, Technical University of Denmark, DTU Sustain - Department of Environmental and Resource Engineering, Denmark

Examiner 1:
Associate Professor Roberto Naboni, University of Southern Denmark, Department of Civil and Architectural Engineering, Denmark

Examiner 2:
Senior Researcher Maris Sinka, Riga Technical University, Department of Civil Engineering, Latvia

IV

Preface

This thesis was submitted to fulfill the requirements of a PhD degree. The project was carried out at the Technical University of Denmark (DTU) at the Department of Civil and Mechanical Engineering (DTU Construct) and the Department of Environmental and Resource Engineering (DTU Sustain), previously called the Department of Civil Engineering (DTU Byg). The research was carried out as a collaborative project between the Section for Materials and Durability and the Section for Structures and Safety. The project was supervised by Associate Professor Holger Koss (DTU Construct) and co-supervised by Professor Lisbeth M. Ottosen (DTU Sustain).

Local experimental facilities of the Department of Civil Engineering (DTU Byg), Department of Civil and Mechanical Engineering (DTU Construct), Department of Mechanical Engineering (DTU Mek) and the National Food Institute (DTU Food) were used. In addition, experimental work was carried out at the University of South Brittany (UBS), France, and at the Department of Geosciences and Natural Resource Management at the University of Copenhagen (KU).

This PhD project was the first funded project at DTU Civil Engineering that researched experimentally 3D concrete printing and connected biologically based binders in concrete composites. Due to the novel character of the project, it was part of the PhD to 1.) accumulate knowledge in the interdisciplinary fields of organic chemistry/biochemistry, robotics, rheology, processing engineering, and 3D printing; 2.) purchase and build-up research infrastructure like large-scale 3D printing facilities and lab equipment for biologically based materials; and 3.) establish national and international networks for knowledge exchange and use of research equipment.

During the project, a protection of intellectual property through a patent application was pursued. The technology of using a biologically based concrete composite for 3D printing, as presented in this thesis, was deemed novel by the supervisors, the DTU patenting office (DTU Tech transfer) and the PhD student itself by literature- and patent-based novelty search. The patent process has been ongoing since 2019. Therefore, the dissemination of the here presented journal publications was postponed to the end of the PhD study. The here presented content is not in conflict with any current patenting process.

Additional work, such as communication activities, supervision of Master thesis projects and special course projects, attending courses on all University levels, and teaching activities were done during the course of this PhD study. A list of these can be found in Appendix 0.I, 0.II, 0.III, and 0.IV.

The content of the document reflects the major findings of a three-year research project. All documentation and recognition of other's work was done to the best of the PhD student's knowledge and belief.

Lyngby, February 2023

Acknowledgements

I would like to thank my supervisors Holger Koss and Lisbeth M. Ottosen without whom I would have not been able to conduct and finish my PhD project. Their support and discussions were central to the success of this research, including defining the research idea and supporting me in receiving the necessary funding. In addition, I would like to thank Jessica Fernandoy-Bak for introducing me to the academic world.

Without the trust and financial support from VILLUM FONDEN and DTU, I would not be able to present this work. I am very thankful for the opportunity that was given to me. Being able to spend time on education and research is one of the sweetest fruits of prosperity that our society has earned. I am grateful that DTU and VILLUM FONDEN contribute to this ambitiously.

I furthermore owe my gratitude to all the collaborators from other scientific fields, which I have found along the way. The input of many different disciplines in this interdisciplinary project has widened my horizon and exceeded the portfolio of DTU. Here, I would like to thank especially Thor Engelsen, Emil Engelund Thybring and Arnaud Perrot without naming the many more that did contribute.

It was an honor for me to meet so many talented young engineers in teaching and supervision activities. Especially through the supervision of seven student projects, I have learned a lot and their results contributed largely to what I know today.

Finally, I would like to thank my family and friends: my companion Marte Teksum Haugland and our daughter Sigrid Christ-Teksum, who are the foundation and motivation for what I do, my parents Ute Künzel-Christ and Markus Christ with partners for their love and support, my brother Manuel Christ with family, as well as the rest of my family in Germany and Norway.

Abstract

This thesis presents a proof-of-concept study on using biopolymer binders as cement replacement in 3D printing mortars to enable advanced flow properties and therefore, paving the way for the realization of highly optimized structures for minimum material consumption.

The construction sector is one of biggest polluters and emitters of CO_2 worldwide. Therefore, recent research focuses on minimization of waste and emissions, and reducing, reusing and recycling. 3D printing of concrete shows the potential of increasing the productivity of the sector and, at the same time; enhancing its environmental performance by enabling the realization of optimized structures with a minimum of material use. In addition, no formwork is required for building, which significantly decreases the amount of waste for concrete structures.

Since the printing of concrete materials requires advanced rheological properties that let the material stiffen rapidly after extrusion, the printing of cementitious materials is usually connected with the use of a high share of Portland cement, presenting a drawback in its environmental performance. Its slow setting characteristics limit the placing of material to a, broadly seen, vertical build up. This restrains the possibilities of minimizing material use by realization of optimized structures.

This research project therefore investigates the potential of replacing the cementitious binders with biologically-based materials. The research focuses on natural polymers, which usually use low extraction temperatures. Some of the natural polymers showed thermoreversible properties, both in pure form, as well as in a concrete composite with mineral aggregates. This allowed for the use within a temperature-controlled print-head and rapid stiffening after extrusion.

14 natural polymers are evaluated for the use as binder in printing concrete. Both polysaccharides and proteins prove elevated potential for the application. The materials are assessed for their mechanical strength, and rheological- and printing properties.

Within a composite of biopolymer and mineral aggregates, gelatin showed the highest mean compression strength (37MPa and 59.5MPa, respectively for mammal and cold water fish gelatin), as well as the largest yield strength development in the fresh state under cooling from 50-20°C (0.1kPa-106kPa).

The research proves that a concrete composite from biopolymers and mineral aggregates can be used as structural material and as filament in a temperature-controlled extrusion process. Its mechanical strength could be measured in the same order of magnitude as for cementitious printing materials. Its temperature controlled rheological stiffening as fresh material made it possible to print advanced free-form constructions up to an unsupported inclination of 80°. This enables the construction of freely shaped geometries and highly optimized structures without the use of CO_2 intensive Portland cement.

Table of Contents

1.   Introduction

Photo: media_k (Mikal Schlosser) taken as requested by Julian Christ, biologically-based concrete composite.

In the last decades, the quality of life has increased significantly in many parts of the world: prosperity, quality and variety of food, hygiene and medical care have increased and improved. Consequently, the global average life expectancy rose from 46 years in 1950 to 71 years in 2015 (Roser et al., 2019). Even if the total birth rate declined during this time period (The World Bank, 2019), the older reached ages caused a tripling in global human population from 2.5 billion in 1950 to 7.8 billion in 2020 (Roser et al., 2020). Because human population and consumption of goods increases, increasing amounts of energy, mostly from fossil fuels (Ritchie et al., 2020) are being consumed and large amounts of waste are being produced, causing an environmental and climatic crisis. Especially the amount of anthropogenic greenhouse gas emissions like CO_2 has increased drastically since the industrialization, causing a warming of our climate (IPCC, 2022). To sustain prosperity by limiting climate change, the Paris Agreement (United Nations, 2015), signed by 193 states, was prepared by the United Nations, setting ambitious goals to reduce greenhouse gas emissions. Both the energy supply and manufacturing industry must be modernized to emitting less. Radically new ideas and implementations are therefore necessary to replace current technologies.

The building construction and operations industry is one of the industries that is in change. It is the most emitting industry with 39% of global CO_2 emissions (Global Alliance for Buildings and Construction et al., 2019) and largest contributor to solid waste generation. The production of cement alone is responsible for over 8% of global CO_2 emissions (Monteiro et al., 2017). This is due to the energy intensive production that is burning raw materials at over 1450°C. To fuel the process, non-renewable energy sources are often used. The chemical process of burning limestone, releases additional CO_2. The large cement consumption of 4.4 billion metric tons (Garside, 2022), adds to the emissions being three times higher than the ones associated with aviation (Teter et al.,

2020). Even a complete transition to renewable energy in the production process, would not remove the CO_2 emissions caused by the sector, because the chemical process of burning the raw materials would still release significant amounts of green-house gasses. It is therefore deemed necessary to lower the consumption by replacing the cement with alternative materials or reducing the used amount per built volume. A rethinking of construction technology as we know it today is necessary with disruptive, more environmentally competitive technologies as an outcome.

In addition to the environmental and climatic concerns of the construction sector, its productivity stagnated or even declined over the last 40 years (Castagnino et al., 2016). While other sectors automated and digitized many processes, the construction industry is traditionally rather slow in adapting to technological changes (Castagnino et al., 2016) and still depends largely on the availability of manual labor. To satisfy the demand for housing and infrastructure connected to demographic changes like urbanization and increase in population, the sector is forced to boost its technological capabilities with digital tools, modular construction and automation through robotics and 3D printing technologies (Whittington, 2021). These allow for more environmentally friendly handling of building materials by more effectively placing material with computer numerical controlled systems, and by adopting new materials and technologies that would need large amounts of manual labor when manufactured analogously.

1.1. Rethinking building and construction materials

In recent years, more environmentally compatible material technologies have been applied and researched, bringing a general shift from the use of ubiquitously processed virgin materials to less energy intensive-, locally sourced-, biologically based- and recycled materials.

One group of materials gaining popularity are bio-based materials such as wood, wood composites or fibrous materials, such as hay. The general principle of capturing atmospheric CO_2 in biologically based materials through the plants' photosynthesis processes and storing it in building materials adds positively to its overall environmental impact.

Also earth-based materials have regained popularity in western countries. Known and used for centuries (Pacheco-Torgal and Jalali, 2012), the materials present hydrophilic properties, fire resistance and large thermal mass. This makes them attractive as building materials. By using little to no added binding material, the bulk is mainly held together by the binding properties of clay. The material is either being processed by compacting through ramming or by stacking of uncompacted wet soil (Hamard et al., 2016).

However, concrete remains having beneficial properties, especially in terms of its workability and durability: it can be casted into almost any shape, pumped in a liquid state and becomes stone after hardening. The mineral aggregates used for the materials are non-renewable, but are abundantly available. The major concerns in terms of our climate remains with the binder production. Alternative binders are searched for but Portland cement remains the most used.

There are several strategies for reducing the climatic impact of concrete without altering the currently applied building processes. One of those is adding various supplementary cementitious materials, like fly ash (Paris et al., 2016), calcined clay (Cao et al., 2021), geopolymers (Singh et al., 2015) or silica fume that can replace some of the Portland cement binder (Lothenbach et al., 2011). These supplementary cementitious materials are often resourced from industrial waste products and reduce therefore the overall greenhouse gas emissions and environmental impact of the applied concrete.

A second strategy for making concrete 'greener' is to change the energy source used in concrete production. Around 50% of the concrete's CO_2 emissions origin from the energy use from burning raw materials (Surahyo, 2019), others from the chemical process. The required energy production is often based on carbon intensive fossil fuels. The combustion chambers of the concrete plants can also burn alternative secondary materials like waste tires, -wood or -plastics that would add positively to the overall sustainability (Surahyo, 2019).

Another way to make concrete structures more sustainable is using less: building components from concrete can be recycled and reused, mechanical properties can be improved so that a smaller cross-section is sufficient to withstand the building's loading conditions and the durability of materials can be increased to make buildings last a longer period of time (Surahyo, 2019).

Current research suggests that binder for concrete can be also produced through bio-mineralization by microbiological systems or enzymes (Jain et al., 2021). These use the CO_2 from the air as substance to precipitate calcite and such bind the aggregates in concrete.

Both replacing some of the Portland cement binders and reducing the used amount of concrete are identified as methods for reducing the overall climatic and environmental impact of concrete. Efforts are being made through optimization of current building techniques or through the application of digital processes like 3D printing.

1.2.   3D printing of concrete

Especially within the last 5-10 years, additive manufacturing methods for concrete structures are being developed, making the use of formwork redundant (Paul et al., 2018)(Schutter et al., 2018)(Perrot, 2019) and enabling the realization of structures with higher complexity than possible to build with conventional casting methods.

For 3D printing of constructions, many materials such as concrete, plastics (Teizer et al., 2016), earth (Kontovourkis and Tryfonos, 2020)(Perrot et al., 2018a), steel (Buchanan and Gardner, 2019) or bio-based fibrous composites (Sinka et al., 2020) have been investigated. The most widespread one is concrete, due to its known suitable properties for construction purposes such as fire resistance, workability, strength and robustness. Several additive manufacturing methods for concrete were developed, such as mesh-mold manufacturing (Hack and Lauer, 2014), or shotcrete printing (Dressler et al., 2020). However, particle-bed 3D printing and especially extrusion-based 3D printing remain the most researched and used for constructions. In all processes, material is placed with a computer numerical controlled system. Therefore, higher levels of accuracies and a reduced amount of manual labor can be achieved during the building phase, compared to analogue building processes.

Particle-bed printing (see Figure 1-1)(Lowke et al., 2018) operates in a way that the aggregates of the concrete composite are being stacked, layer-by-layer with the help of a roller. The printing area is therefore empty at first and contains lose aggregate particles after the application of the first layer. These particles are then being selectively bound with a computer numerically controlled extrusion system (see example in Figure 1-1). The extruded volume can be cementitious, or water, if the actual binder is already mixed within the applied particles (Lowke et al., 2018). When the intended areas of the current particle layers are bound, the next layer of particles is applied. After the whole object is built in this way and the cementitious material is cured, the unbound particles are removed and the object is done. A large benefit of this process is that the unbound particles are still supporting the unhardened material matrix. The binder then has time to cure without the need for extensive early-age yield strength. Therefore, a large degree of geometrical freedom and detail can be reached with this process (see Figure 1-1). Still, for the construction of larger structures,

extrusion based 3D printing systems are usually used since they are not limited by the size of the printing bed, and no excess material must be removed after printing.

Figure 1-1 (Left) An example object produced by particle-bed printing. A large degree of detail and geometrical freedom is seen, as well as the limited building volume. This picture was taken at the ETH Zurich and shows work of Benjamin Dillenburger's team. See more at (Dillenburger and Hansmeyer, 2016), Picture: Julian Christ at a visit at the ETH Zurich within the DigitalConcrete Conference. **(Right)** Selectively bound particles from the D-shape 3D printer. Picture from: (Lowke et al., 2018)

In extrusion-based 3D concrete printing (Paul et al., 2018)(Schutter et al., 2018)(Perrot, 2019), the fresh concrete material is pre-mixed and is used within a specific open time. While the unused material is stored in a vessel, the currently printed mortar is brought to a nozzle by either a hopper or a pump. The material flows through an auger to control extrusion and is deposited through a nozzle onto the print bed or preceeded layers (see Figure 1-2). Compared to particle-bed processes, sufficient support is necessary to any time to keep the freshly extruded layers in place. Less geometrical freedom than particle processes are reachable with his method. The extrusion system is usually traversed by either a robot arm (e.g. in (XTree, 2023)) or a gantry printer (e.g. in (COBOD, 2023). Robot arms can work with a high level of accuracy and deposit material outside its actual dimensions, i.e., structures larger than the printer can be realized. Gantry printers, on the

other hand, show an easy setup, which is why they are mostly used for on-site printing. A picture of such a process and an example print from the Danish company COBOD (COBOD, 2023) can be seen in Figure 1-2. A gantry printer has been used in this print.

Figure 1-2 (Left) Example of extrusion based 3D printing at COBOD (see more at (COBOD, 2023)). Clearly visible is the extrusion of the wet material and deposition on the preceeded layers. (Right) extrusion-based 3D printed house from COBOD at Copenhagen – Nordhavn, Denmark. Pictures: Julian Christ at COBOD within a visit of the Danish Society for Structural Science and Engineering.

The process of extrusion-based 3D printing is mostly known for its smaller scale polymer prints that use thermoplastic filaments. This material is heated within the print head and sets right after extrusion through cooling. This principle is not possible for cementitious materials, which are through their rather slow setting behavior less well suited for 3D printing processes. To create constructions without the use of formwork in extrusion based 3D concrete printing, the material needs to show special rheological properties. Firstly, the material needs to be flowable to be pumpable and extrudable, i.e. the material needs to be deformable enough to force it through a nozzle (see Figure 1-2). Right after extrusion, the material needs to build up sufficient strength to support itself and keep the material in place (Roussel, 2018). This happens through the thickening properties of fresh cementitious concretes at rest, i.e. thixotropy. This strength, however, is much

weaker than the strength that can be developed during the setting of the cement and the strength that can be produced by small-scale polymer extrusions through the principle of thermoplasticity. Enhancing these early-age yield strengths and rheological behavior of the fresh concrete, is the key for advancing extrusion-based 3D concrete printing.

Improving the material's rheological properties enables better solidification right after extrusion either through optimizing the bespoken thixotropic behavior and structural build-up of the material (Le et al., 2012)(Panda et al., 2018)(Roussel, 2018)(Mechtcherine et al., 2020) or an additional two-component system that injects accelerators into the nozzle of the extruder (Wangler et al., 2022)(Gosselin et al., 2016). However, for advanced printing properties, higher shares of cement or admixtures are usually used than for conventional concrete composites (Kaszyńska et al., 2020). This is done to support the stiffening of the materials, presenting a drawback on environmental performance of the method.

Still, extrusion-based 3D printing of concrete can remove the need for formwork and can place material, computer numerical controlled, in a three dimensional space. This can be utilized for the realization of structurally optimized buildings, which reduces the amount of material needed to support the structure.

1.3. 3D printing of optimized constructions

To reduce the amount of material used per built-volume and to increase productivity and sustainability, structural design can be optimized significantly by using algorithms to reduce structural materials to a minimum amount. This can, e.g., be done by structural optimization through topology optimization algorithms (Bendsøe and Sigmund, 2003). Topology optimization algorithms take a specific set of loading conditions that the building is exposed to during its

lifetime and optimize the design performance of structural parts through an iterative process. Through advancing processing power of computers and algorithms, this has increased in popularity in civil engineering, especially for large-scale building designs to save significant amounts of material (Zegard et al., 2020)(Tsavdaridis et al., 2018). A drawback for the realization of the designs is the usually connected complexity of the shape that is connected with high consumption of formwork materials and costs during the construction phase. 3D printing can deliver an alleviation of these formwork dependencies and ease the realization of these structurally complex parts.

Several studies have been conducted to minimize the material use through topology optimization and realizing the results by 3D printing technologies, e.g. (Meibodi et al., 2017)(Vantyghem et al., 2020a)(Martens et al., 2017) (see also Figure 1-3). The computer algorithms are not the limiting factor for the maximum degree of optimization, it is the process and material constrains that decide for the degree of material minimization. Specific designing programs that fit the material and process constrains were therefore developed (Martens et al., 2017).

Figure 1-3 (Top) post tensioned and topology optimized concrete beam produced with extrusion based 3D printing (Vantyghem et al., 2020a). Picture from: (Vantyghem et al., 2020b) (Bottom) Optimize building slab, produced with help of 3D printing. The picture was taken at the ETH Zurich and reflects the work of the BLOCK research group (see more at: (Block Research Group, 2023)) Picture: Julian Christ at a visit at the ETH Zurich within the DigitalConcrete conference. Both building components use significantly less material than a conventionally manufactured building component.

Figure 1-3 shows two optimized designs, realized by 3D printing. In the top figure, an extrusion-based method is utilized and in the bottom, a particle bed printing method was used. The higher degree of detail that can be reached in particle-bed printing is clearly visible. This can minimizes the material need.

The constrains for extrusion based printing do not only lay in the level of detail but also in the degree of freely placing material, e.g. with overhangs. Figure 1-4 shows a topology optimized design without printing constrains. To realize these kind of structures with extrusion-based 3D

printing, a large degree of overhangs is necessary to construct without the use of support through

formwork. The general setting behavior of cementitious printing mortar for extrusion-based 3D

printing is rather slow and difficult to control. Largely seen, merely vertical build-up is used, not

allowing for highly optimized, organically shaped constructions as presented in Figure 1-4.

Overhangs in extrusion-based 3D concrete printing are strongly limited and less explored (Brun et

al., 2020)(Vantyghem et al., 2020a)(Gosselin et al., 2016). Still, extrusion-based methods are the

preferred when 3D printing buildings due to its larger print volume and easy applicability to on-

site production.

Figure 1-4 Example of a result of a topology optimization algorithm. The result shows an optimized structural design of an arctic shelter with wind loading, for further information see (Christ et al., 2019a)(Christ, 2016). The detailed character of the structure and the overhangs are difficult to realize without the use of formwork.

Advanced material properties are being searched for to enable the construction of architecturally

advanced buildings and optimized structures. (Vantyghem et al., 2020a) and (Schutter et al., 2018)

identified the rheological properties in 3D concrete printing and the thereby defined the lack of

overhang geometries as the limiting factor for constructing highly structurally optimized building

components. With more advanced material properties, less material is needed. However, the need

for more suitable material properties in 3D printing concretes is usually also connected with an

increased use of Portland cement. Finding alternative materials that have advanced rheological properties with a better environmental performance can be a solution.

1.4. 3D printing in construction with bio-based materials

To increase the environmental performance of the process and reduce cement or aggregate consumption, or to improve the building material's hygrothermal or mechanical properties, bio-based materials are being used to 3D printed constructions.

Research shows that bio-based fibers in 3D printing mortar reduces shrinkage cracking, increases ductile behavior, and improves mechanical properties by keeping its workability for the printing process (Luhar et al., 2020). The fibers are used for reinforcing cementitious, earth based (Ferretti et al., 2022) or other materials as either an addition to normal aggregates (Luhar et al., 2020) or as primary aggregates (Sinka et al., 2020) (see Figure 1-5 right).

Natural fibers and wood based products are also used as aggregates for polymer bound composite in 3D printing for constructions (Bove and Uricek, 2022)(Kromoser et al., 2022). In this case, the material is extruded with a temperature-controlled print-head, using a wood based composite with a thermoplastic polymer matrix or starch.

Researchers have explored natural polymers as reinforcing additives to be used in a printing process for earth-based structures (Perrot et al., 2018a). Natural polymers have also been used as filament for printed architectural sculptures (Soldevila et al., 2014). All natural polymers used in these research's were polysaccharides, which can be extracted from seaweed or crustaceans. A rather recent research shows that bovine protein extracted from blood can be used to print natural polymer bound soil. This research was intended for space exploration (Biggerstaff et al., 2021; Rosa et al., 2020).

Figure 1-5 3D printing of biologically based materials. Examples of (left) water-based hydrogel printing at the Massachusetts Institute of Technology (Soldevila et al., 2014), picture from (DesignNews, 2014) and (right) natural fibers with a fast setting binder at Riga Technical University, picture from (Sinka et al., 2020).

A rethinking of material takes place in the 3D printing construction sector, to find more sustainable alternatives to conventional concrete composites. This study aims on finding a biological material that not only allows for a reduction or a replacement of cementitious materials, but also to discover materials with flow- and mechanical properties specifically suited for 3D printing in construction.

1.5.   Research objective

On the background of a changing climate and a decrease or stagnation of the productivity of the construction sector, this PhD project aims on contributing to a sustainable change through material innovation. 3D concrete printing can support the digitalization of processes in construction that lead to material savings and simultaneously increases productivity through automation. This can decrease the global housing shortage.

In the field of 3D printing of concrete, increased activity can currently be observed, especially in extrusion-based processes that aim at the construction of full-scale buildings on-site. These

processes can place material with a computer numerical controlled system freely in a three dimensional space and can therefore place material where it is needed in a structural component, i.e. material can be saved. Since the process can work without formwork, additional material consumption can be avoided. The specific rheological requirements for the material, usually imply large consumption of CO_2-intensive binders like Portland cement. The setting characteristics of these binders are difficult to control and have limitations in their geometrical freedom.

This project's aim is to build onto the recent developments in 3D concrete printing, but wants to replace the CO_2–intensively produced binder Portland cement by more sustainable alternatives that can support the fast setting behavior of 3D printing filaments. A structural building material is therefore presented and investigated for the specific application in 3D concrete printing.

Instead of cementitious binders, the intention is to use natural polymers that are abundant and easily accessible in nature. These can be workable in conjunction with water and increase their strength under drying. By applying these materials as binders in concrete, they could alleviate the climate and environmental impact of 3D printed concrete because the extraction methods normally require temperatures of less than 100°C, instead of the high temperature requirements of ~1450°C for Portland cement. In addition, the chemical process that emits large amounts of CO_2 during burning of the raw materials for Portland cement production could be circumvented.

In addition to their strength increase under drying, natural polymers show setting characteristics, such as thermoplasticity and thermosetting, which cannot be found in cementitious materials. This could be beneficial for the printing properties of the material, enabling high degrees of geometrical freedom and thus a higher degree of structural optimization of building components. Since water is used to make the material workable, the intended natural polymer composites would undergo an extensive drying process during curing. This drying process is eased by constructing without

formwork and by realizing thin-walled and slender geometries that have a high surface area. Such structures can easily be built with extrusion-based 3D printing.

This research presents a fundamental rethinking of building and construction as we know it. The delivered material innovation levers on novel and digitalized building technologies and aims on paving the way to construction of optimized building components with a minimal material consumption. The researched material is potentially a more sustainable alternative to the cementitious concrete composites that are used today. **This work presents a proof-of-concept study for building structural building components with this material.** *The project vision is further elaborated in Appendix 1.I.*

In the earliest studies of this research project (see Appendix 1.II), it was shown that an example composite from sand and the natural polymer mammal gelatin (bone glue) – heated, cast, cooled and dried – shows comparable mechanical properties to a cementitious concrete. The composite was evaluated for a potential use in a 3D printing application. It was deemed that the workable and mechanical properties are suitable for further investigation of the research's objective. It could prove the research potential.

1.6. Order of this thesis

The study tests several kinds of natural polymers as binder in a concrete composite on its mechanical properties to prove their potential as load carrying material. Furthermore, the composite's flow properties are characterized in the material's fresh state to test the applicability to 3D printing processes. It was later chosen to continue the study with thermoplastic natural polymers. A temperature controlled printing process was therefore developed and the possibilities of creating free form and optimized structures were tested. As Figure 1-6 shows, the order of this

thesis was designed accordingly: After introducing the overall topic, the major three objectives 'Mechanical properties', 'Rheological properties' and 'Printing process' were managed as chapters.

This thesis is written as a publication based work. I.e., the thesis is a compilation of publications that were prepared during the course of this PhD study. The major three journal publications are embedded as chapters in the main body of this thesis. The underlying publication strategy was developed with the intention to form this cohesive thesis. The journal papers are introduced and discussed prior to the inclusion of the paper and in an overall discussion section. Other conference publications and posters are appended and referred to throughout the text. The structure of this thesis and connected publications are elaborated in the following numbered list, corresponding to the chapter numbers of this thesis, and summarized in Figure 1-6. An overview of the publications is presented in Table 1-1.
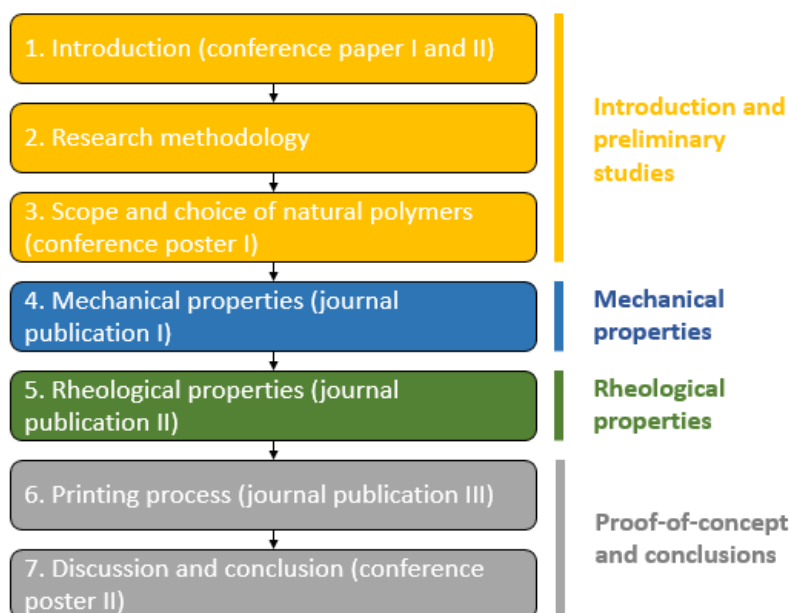
Figure 1-6 Structure of this thesis: The left shows the thesis' chapters and connected publications, while the right clusters the chapters into a superstructure. Color scheme is related elaborated overall research methodology in Figure 2-1.

1. **Introduction and preliminary studies** (marked yellow in Figure 1-6):

   The research idea and preliminary studies, as well as placement in the State-of-the-Art can be read in the introductory chapter of this thesis, and in the associated conference papers, included in Appendix 1.I and Appendix 1.II.

2. **Research methodologies** (marked yellow in Figure 1-6) are explained in the second chapter of this thesis

3. **Scope and choice of natural polymers** (marked yellow in Figure 1-6): The scope of this thesis is defined in this chapter (Chapter 3) and a choice of 14 natural polymers as subjects is presented. Furthermore, a preliminary assessment limited this selection of the 14 natural polymers down to six. These six natural polymers showed elevated potential for the use as binder in a composite for 3D printed constructions. The associated conference poster publication is included in Appendix 3.I.

4. **Mechanical properties** (marked blue in Figure 1-6): The six natural polymers with elevated potential from Chapter 3 were assessed on their suitability as load carrying material by testing the mechanical properties of a composite from sand and the respective natural polymers. It was found that two of the six natural polymer composites are especially suitable as load carrying material. This is presented within the journal publication I, i.e. Chapter 4.

5. **Rheological properties** (marked green in Figure 1-6): In this chapter, two natural polymers from Chapter 4 showed thermoplastic behavior are

assessed in printability studies and rheometer experiments. This is presented within the journal publication II, i.e. Chapter 5.

6. **Printing process** (marked grey in Figure 1-6): In this chapter, a printing setup working with a temperature controlled print-head to extrude mammal gelatin composite materials is presented. Gelatin was chosen because it was found to be the most suitable in terms of its rheological properties in Chapter 5, as well as its mechanical properties, shown in Chapter 4. This is presented within the journal publication III, i.e. Chapter 6.

7. **Discussion and conclusion** (marked grey in Figure 1-6): In this chapter, the main findings of this research are discussed and compiled. The proof-of-concept is presented in this chapter and a concluding remark is given. The connected conference poster publication can be seen in Appendix 7.I.

Table 1-1: Titles of publications

Publication	Title
Conference paper I	On the Ecology of Climate & Structures
Conference paper II	A concrete composite from biologically based binders and mineral aggregates for constructional 3D-printing
Conference poster I	Potential of natural polymers as alternative binder for 3D printing concretes
Conference poster II	Gelatin as biologically-based binder in temperature-sensitive printing mortar for advanced free form constructions
Journal paper I	Screening of natural polymers as binder in concrete composites
Journal paper II	Rheological characterization of temperature-sensitive biopolymer-bound 3D printing concrete
Journal paper III	Multi-axial 3D printing of biopolymer-based concrete composites in construction

1.7.   Terminology in this thesis

1.7.1. Concrete/mortar

In construction, concretes and mortars are colloquially defined as a composite material from cementitious binders and mineral aggregates. Concrete uses aggregates with maximum diameters of more than 2mm. Similar materials with less than 2mm of maximum diameter are defined as mortar. This wording intends the conventional utilization of concrete as primary structural material and mortar as interlayer for brick constructions.

With the advent of extrusion based 3D concrete printing, these definitions are softened, meaning that the description of mortar and concrete are not necessarily longer connected to the maximum grain size. Usually, extrusion based processes do not allow for larger diameters than 2mm but the materials, which would conventionally be defined as mortar, are still intended for a concrete application, i.e. to build primary structural building components. The term concrete, as well as mortar is used in this field. A clash of definitions can be identified between application and aggregate size. This is also identifiable in research publications that aim on testing the strength of 3D printed concrete/mortar. Both, standardization for mortar/cement testing and the standardization for concrete testing are used (e.g. in (Wolfs et al., 2019) and (Inozemtcev et al., 2018)). The standardization for concrete testing is usually scaled down to 3D printed sample sizes.

Not only are the aggregate sizes in the term concrete not strictly defined, also the types of materials themselves are not strictly limited to cement and mineral aggregates: E.g. the term 'Holzbeton', or wood concrete, describes a concrete that has merely wood (non-mineral) as an aggregate and was widely used in houses in the German Democratic Republic (Wagner, 2017). Another example is polymer concrete (Ohama, 2008), which is e.g. used for constructing swimming pools or structures that are exposed to toxic or corrosives matter. This type of concrete does not use cementitious

binders but uses either thermoplastic or thermosetting polymers in conjunction with mineral aggregates.

The author of this thesis acknowledges the softened definition and discussions around the term 'concrete' and 'mortar'. The author defines the investigated technology, the composite material of biopolymers and smaller mineral aggregates, as a mortar for primary structural applications and uses therefore the words concrete and mortar as synonyms. Analogously to polymer concrete, the proposed material also uses a natural polymer as binder matrix and can therefore be defined as a biopolymer concrete/mortar.

1.7.2. Hydrogel, biopolymer and natural polymer

The choice of natural polymers as primary subject in this thesis is further elaborated in Chapter 3. The word biomaterial defines a broad variety of materials that are either originating from nature or are used for medical or biologically related applications and is not clearly defined - similar to the word biopolymer. Biopolymers can either be defined as polymers occurring in nature, or as polymers synthetically produced from natural sources. Natural polymers are one group that are naturally occurring biopolymers. Most of the chosen and explained natural polymers in this thesis are also hydrogels, i.e., water based gels. Therefore, the words biopolymer, natural polymer and hydrogel are used as synonyms.

1.7.3. Mammal gelatin / bone glue

As further introduced in Chapter 3, bone glue is one of the oldest known glues to human kind. The glue consists of gelatin that is made from mammals. The words bone glue and mammal gelatin are both used in this thesis.

1.8.   **Novelty of this work**

3D printing of polymers has its origin in the 1980s. The method of building sliced objects with polymers is almost half a century old. Concrete extrusion techniques for 3D printing first started to accelerate in the 2010s. Still, it has become a widely acknowledged field with many research and development branches, first houses were built with the technology and various processes and materials were proposed. This thesis aims on advancing this field to incorporate natural polymers based concrete composites and connected printing processes. In the following, selected work prior to this study is presented.

1.8.1. 3D printing of concrete and for construction

3D printing for construction purposes is in existing literature mainly reflected within extrusion-based 3D printing of concrete. The technology is often presented as a construction revolution because building processes can be automated on-site and the use of formwork becomes redundant.

Table 1-2 Selected material that reflects the current state in 3D concrete printing and general 3D printing in construction

Reference	Title	Summary or findings
(Bos et al., 2016)	Additive manufacturing of concrete in construction: potentials and challenges of 3D concrete printing	Reviewed in 2016 some of the first applications and developments of 3D concrete printing
(Buswell et al., 2018)	3D printing using concrete extrusion: A roadmap for research	Identified a rapidly increasing trend for construction applications of additive manufacturing (with concrete). Additionally, methods and materials for printing and testing are reviewed.
(Mechtcherine et al., 2020)	Extrusion-based additive manufacturing with cement-based materials – Production steps, processes, and their underlying physics: A review	Mechtcherine et al. review the underlying physics and failure modes in extrusion-based 3D printing of cementitious materials. Common failure modes are material failure or loss of stability.

(Lyu et al., 2021)	Overview of the Development of 3D-Printing Concrete: A Review	Lyu et al. reviews printing materials like geopolymers, Portland cement, geopolymers as well as connected admixtures and fiber reinforcements. Connected print head designs for extrusion-based 3D printing are presented and reviewed.
(Ali et al., 2022)	A critical review of 3D printing and digital manufacturing in construction engineering	Ali et al. Review currently used materials such as concrete, plastics and metals for the 3D printing in construction. Connected concrete printing processes like particle bed printing and extrusion-based processes are presented.

Table 1-2 shows five review papers, which are published between 2016-2022. Mainly focusing on concrete, the studies show that cementitious 3D concrete printing is an established field of research. Other materials are also present in 3D printed construction applications; such as metals, polymers or geopolymers.

1.8.2. 3D printing with natural polymers in small scales

Small-scale desktop printers are mainly used for prototyping applications. Conventionally used materials are acrylonitrile butadiene styrene (ABS), Nylon or the biopolymer polylactic acid. Also other applications onto biomedicine and food are thought of where, inter alia, natural polymers are used.

Table 1-3 Selected material which shows that natural polymers are used for 3D printing of smaller scale objects

Reference	Title	Summary or findings
(Godoi et al., 2016)	3D printing technologies applied for food design: Status and prospects	The paper reviews 3D printing applications in the food sector and presents applied materials like chocolate, meat, dough and natural polymers like xanthan gum or gelatin. Connected extrusion based or melt extrusion based 3D printing techniques are presented.
(Ngo et al., 2018)	Additive manufacturing (3D printing): A review of materials, methods, applications and challenges	A general review of 3D printing is given, also the application of hydrogels onto biomedical 3D printing is elaborated.

	3D bio-printing technology for body tissues and organ regeneration	For medical applications, neural tissues, cartilage, skin and bone can be 3D printed. Biopolymers are used.
(Biazar et al., 2018)		

Table 1-3 shows that natural polymers like gelatin and xanthan gum are applied on 3D printing for food applications (Godoi et al., 2016). Hydrogels made from natural polymers are applied to 3D printing of medical components like skin and bone tissue (Biazar et al., 2018)(Ngo et al., 2018).

1.8.3. Natural polymers in construction materials

Natural polymers are a large group of polymers that is usually easily retrievable from nature. E.g. wood and hay contain several kinds of natural polymers and are conventionally used in construction. As presented in Table 1-4, also other uses of these polymers for construction purposes also exist. For this thesis, especially applications as binder or stabilizer were of interest.

Table 1-4 Selected material that shows the application of natural polymers on construction materials.

Reference	Title	Summary or findings
(Donayre et al., 2018)	Eco-friendly Improvement of Water Erosion Resistance of unstable Soils with Biodegradable Polymers	The natural polymers chitosan and carrageenan are used to increase the water resistance of soils.
(Guihéneuf et al., 2020)	Effect of bio-stabilizers on capillary absorption and water vapor transfer into raw earth	The biopolymers linseed oil, xanthan gum, casein and tannins are tested as stabilizers for earth based construction materials.
(Khatami and O'Kelly, 2013)	Improving Mechanical Properties of Sand Using Biopolymers	Agar and starch are used to increase the cohesion of mechanically weak soil.
(Rosa et al., 2020)	On designing biopolymer bound soil composites (BSC) for peak compression strength	Bovine blood protein is proposed as a binder for soil to form a construction material.
(Rizvi et al., 2019)	Fuel Resistance Asphalt Binder: Mixing Procedure and Fuel Damage Resistance	Uses mammal gelatin as additive in asphalt to increase the resistance against fuel damage.
(Perrot et al., 2018b)	Strategies for optimizing the mechanical strengths of raw earth-based mortars	In this study, alginate is used as a biopolymer reinforcement for earth-based materials.

(Menasria et al., 2017)	Using Alginate Biopolymer To Enhance the Mechanical Properties of Earth-Based Materials	Alginate is used as a reinforcement for earth-based construction materials
(Nakamatsu et al., 2017)	Eco-friendly modification of earthen construction with carrageenan: Water durability and mechanical assessment	Carrageenan is used as stabilizer in earth-based construction materials
(Seok, 2005)	Manufacturing method for building panel of yellow earth	A manufacturing method for a panel of yellow earth that includes seaweed extracts, pine needles and starch.
(Aday et al., 2017)	Carrageenan-based superabsorbent biopolymers mitigate autogenous shrinkage in ordinary Portland cement	A carrageenan based additive is presented for Portland cement that reduces shrinkage cracking.
(Lv et al., 2013)	Structure and characterization of sulfated chitosan superplasticizer	A chitosan based superplasticizer is presented for cement paste and concrete materials.
(Mignon et al., 2016)	Use of methacrylated alginate for self-healing concrete	The natural polymer alginate is presented as additive for self-healing cementitious concrete. During the occurrence of cracks, these polymers swell and close these openings.

Table 1-4 shows that natural polymers are used in construction. Their application in composite materials for the built environment is versatile. Natural polymers are used as cementitious concrete additives (Mignon et al., 2016), (Lv et al., 2013), (Aday et al., 2017) for rheology or shrinkage cracking control. Natural polymers are also applied in pavement composite materials (Rizvi et al., 2019). They can also be used as a stabilizer for earthen construction by increasing the water resistance or the mechanical strength (Seok, 2005), (Nakamatsu et al., 2017), (Menasria et al., 2017), (Perrot et al., 2018b), (Rosa et al., 2020), (Khatami and O'Kelly, 2013), (Guihéneuf et al., 2020), (Donayre et al., 2018). Most of these researches primarily utilize the cohesive properties of the contained clay in soil. However, some also use non-cohesive soils like sand and stabilize the particles with natural polymers, e.g. (Rosa et al., 2020). The production method is usually compaction.

1.8.4. 3D printing in construction with natural polymer-(composites)

3D printing in construction is by now an established field within civil engineering. The use of composites and other extrudable materials are applied to 3D printers to construct buildings. Simultaneously, natural polymers are researched as additives for cementitious concretes and as stabilizers within earthen constructions. Therefore, some existing research incorporates natural polymers within 3D printing of buildings.

Table 1-5 Selected papers that show the application of natural polymer composites in 3D printing in construction

Reference	Title	Summary or findings
(Yuelin, 2018)	Preparation method of 3D printing mortar with high thermal insulation performance	A specific formulation and method of a thermal insulating cementitious composite for 3D printing is presented. The formulation includes the natural polymer cellulose.
(Muhammad et al., 2020)	Cement-based direct ink for 3D printing of complex architected structures	Uses a cementitious material formulation for 3D printing that includes cellulose.
(Biggerstaff et al., 2021)	Determining the yield stress of a biopolymer-bound soil composite for extrusion-based 3D printing applications	Tests the rheological behavior of a bovine blood protein with lunar regolith for the application on construction scale 3D concrete printing
(Perrot et al., 2018a)	3D printing of earth-based materials: Processing aspects	3D printing of earth based construction materials with the addition of alginate.
(Soldevila et al., 2014)	Water-based robotic fabrication: Large-scale additive manufacturing of functionally graded hydrogel composites via multi-chamber extrusion	3D printing of architectural structures with a combination of the natural polymers chitosan, sodium alginate and organic aggregates.
(Luhar et al., 2020)	Sustainable and renewable bio-based natural fibers and its application for 3d printed concrete: A review	Presents a review and outlook on the applications of bio-based fibers as reinforcement in 3D printed concrete structures.

Table 1-5 shows that natural polymers have been applied in the field of 3D printing for construction purposes. As additives in cement-based printing concretes, natural polymers function as rheology modifying agents or as reinforcement. (Perrot et al., 2018a) uses the natural polymer as additive

to print earth based materials. Also some isolated studies can be found (Biggerstaff et al., 2021) where a blood protein is used to test a composite with lunar soil regolith as 3D printing mortar for space exploration applications. Architectural structures could be printed with natural polymers and organic aggregates (Soldevila et al., 2014).

1.8.5. *3D printing in construction with temperature controlled extruder for polymers or polymeric concretes*

Small polymer printers for prototyping applications that extrude thermoplastic materials are widely used. The realization of larger objects is possible by scaling up this principle. The printers can then also be applied for construction purposes.

Table 1-6 Selected papers that show the application of thermoplastic extruders on 3D printing of constructions.

Reference	Title	Summary or findings
(Bove and Uricek, 2022)	WOHN - Homes as a Service	This company uses large-scale temperature controlled extruders to build houses from polypropylene and fibrous fillers.
(Burgos, 2023)	First 100% bio-based 3D printed home unveiled at the University of Maine	A house was printed with a temperature controlled extruder using fibrous fillers and polylactic acid.
(Krcma et al., 2021)	Use of polymer concrete for large-scale 3D printing	Presents a polymer concrete from glass sand and polypropelene that is intended as 3D printing filament for construction applications.
(DUS, 2023)	DUS - 3D print Canal house	Ongoing project of constructing a house from thermoplastic polymers with large-scale, temperature controlled printers.

Table 1-6 shows some examples of previous research on constructing with thermoplastic materials. The presented studies use either polypropylene or polylactic acid as a thermoplastic polymer. (Krcma et al., 2021) uses a combination of polypropylene and glass sand as polymeric concrete composite.

1.8.6. Novelty

As Sections 1.8.1-1.8.5 show, 3D printing for construction has been widely explored. Construction projects are being pursued with material mixtures that can be computer numerically controlled extruded. Especially wide application and research activity finds extrusion-based 3D printing of cementitious concretes (see Section 1.8.1).

Simultaneously, natural polymers are explored in composites for construction materials. The use in earthen materials can increase their water resistance and mechanical strength for geotechnical applications or earthen constructions. For earthen constructions, the binding properties of clay are usually being increased by the addition of natural polymers. Some studies also use local sand for these applications which is then stabilized or bound with natural polymers (see Section 1.8.3). The usual construction method is by ramming or compacting. Some studies also show the application on 3D printing of clay-based or cementitious composites (see Section 1.8.4). Natural polymers are also applied on various other 3D printing disciplines like additive manufacturing for medical application or food (see Section 1.8.2).

Generally, the application of purely natural polymer and sand based building materials has not been explored widely. In addition, the novelty of this thesis lays on the intention to develop a concrete composite with a, for the application, designed grain size distribution. This mineral's aggregates shall be bound with natural polymers exclusively, which are expected to act as a binding matrix, similar to cementitious binders. To be able to apply this composite to extrusion-based 3D printing, the composite needs to be workable and can therefore not be produced by ramming or compaction. Therefore, a quite large water content is necessary. The water content needs to be reduced by drying after construction. It is generally more difficult to cast or to produce bulky parts of materials that require drying. Large ratios of surface-area to volume are beneficial. The novelty

of the material innovation levers therefore on the 3D printing application where slender constructions can be realized and allow for a fast drying processes.

Further, there is novelty in the exploration of the fast thermoplastic setting behavior of the natural polymer-based concrete. This study applies the fresh biopolymer concrete mix within a heated extruder to a large-scale 3D printing process. Even if temperature controlled printing processes exist (see Section 1.8.5), its connection to a workable natural polymer-based concrete composite, prior to this study, is not known to the author.

2.   Research methodology
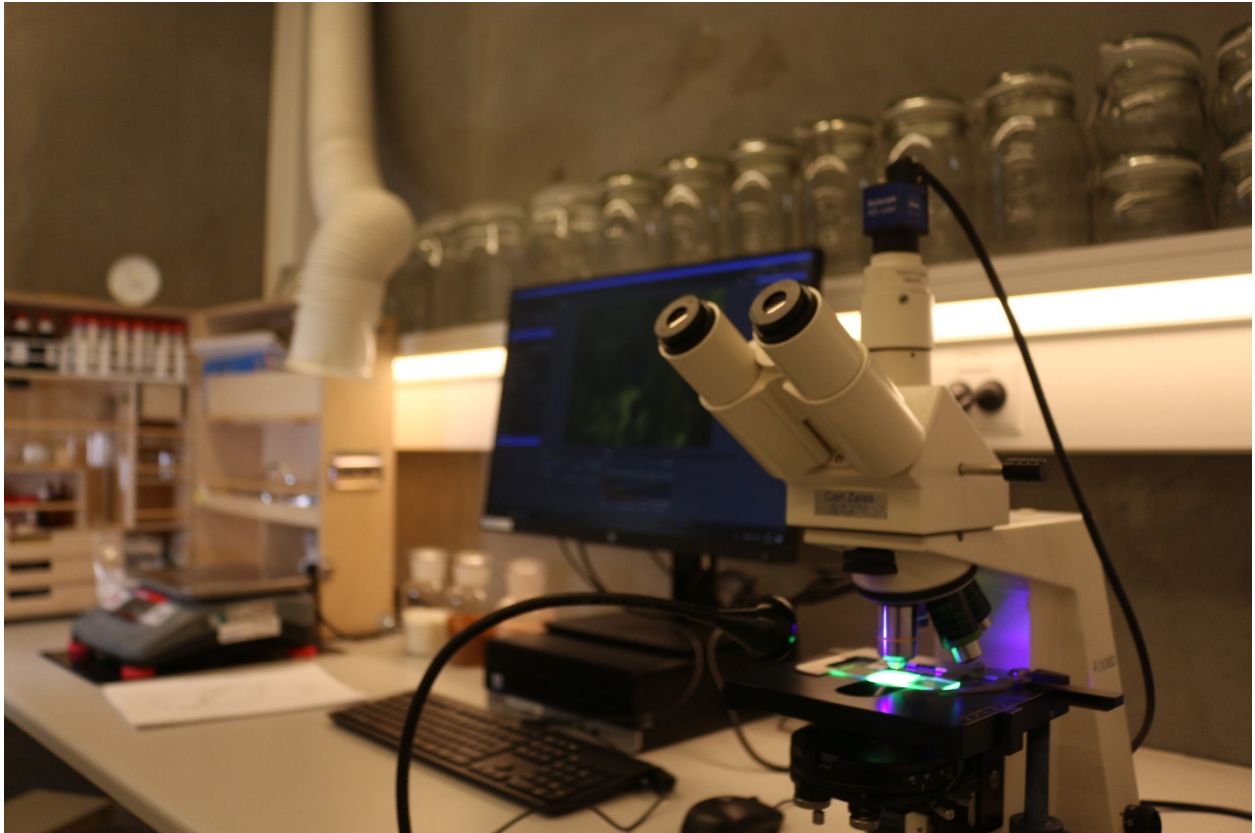
Photo: Julian Christ. The project laboratory.

This chapter provides an overview of the underlying research methodologies and discussions of this PhD project. In the following, the thesis' fundamental research questions are presented and elaborated. These were designed to address the problem statements introduced in Chapter 1. To address these research questions, experimental methodologies were carefully chosen to ensure the reliability of the collected data. The chosen and discarded experimental methods are presented and the choices are justified. Furthermore, this chapter will provide a comprehensive description of the overall sequence of the conducted research.

2.1.   Research questions

The underlying research questions of this project are designed to prove the concept of building 3D printed, load-carrying structures with biologically-based concrete composites. Furthermore, advantageous setting properties of these materials should be tested for the material's suitability to 3D print free-formed structures and therefore pave the way for the application of high degrees of structural optimization and material minimization. The main points of interest are the material load carrying capabilities (mechanical strength), the material setting properties during extrusion (rheological properties) and finally, the behavior of the material when applied in a tailored printing process. The research questions were designed accordingly:

The first research question aims on demonstrating the structural strength of the proposed material and determining the most appropriate natural polymer binders for the application:

1. *Is it possible to build something from a concrete composite from natural polymers and mineral aggregates?*

When working with the first research question, the later needed process parameters were not defined , so non-thermoplastic materials were also tested at this stage. It was deemed possible that

the thermosetting characteristics of some of the natural polymers presented in Chapter 3 could be beneficial for a printing process. The further direction of this thesis research was determined on the basis of the mechanical tests presented in Chapter 4. The thermoplastic materials were chosen for further investigation. This was due to the testing of the thermoplastic hydrogel gelatin resulting in especially good mechanical properties.

The second research question focuses on these thermoplastic hydrogels and aims on elaborating their 3D printing capabilities as a binder in a concrete composite:

2. ***Is it possible to use these composites to 3D print structures?***

The thermoplastic hydrogels were expected to show good setting characteristics for 3D printing of concrete. These rheological properties are intended to realize free-form constructions and to pave the way for building highly optimized structures. The third research question aims on proving the concept of applying the natural polymer based concrete composites to a printing process and showing its ability to enable freely shaped constructions. The research question can be formulated as:

3. ***Do the advanced setting characteristics enable the realization of freely formed constructions?***

These three research questions were to some extent addressed simultaneously throughout the three year long process of this study. However, in this thesis, these questions are answered in chronological order to guide the reader. A publication strategy allocating these research questions to three main journal publications was developed. These are presented here in this PhD thesis as Chapter 4-6. An overview of the connection between publications and research questions is shown in Figure 2-1.

Research methodology
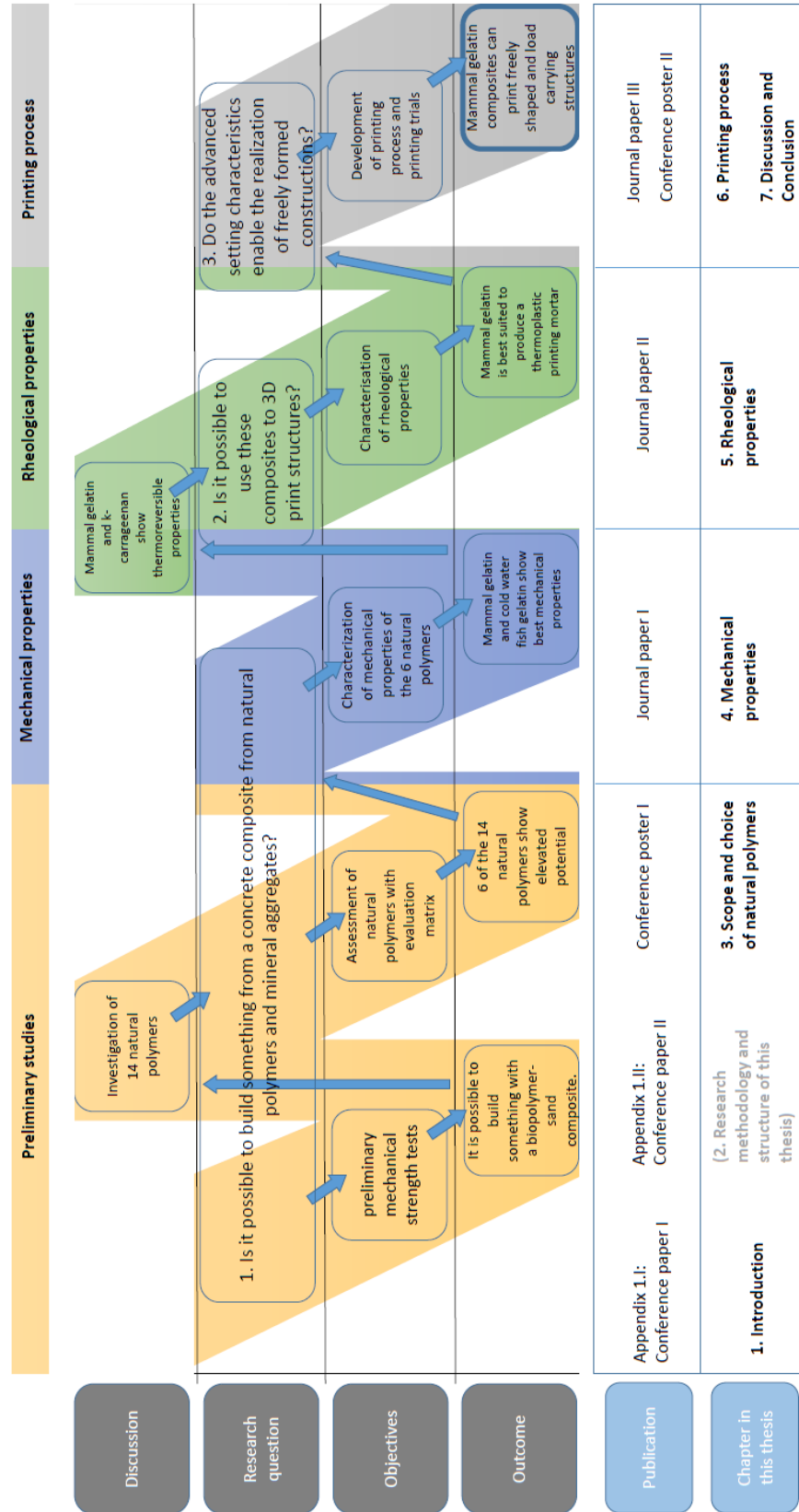
Figure 2-1 Research methodology, publication strategy and structure of this thesis. On the horizontal axis, the publication strategy and connected structure of this publication-based PhD dissertation are shown. In the vertical dimension, the content and discussions of the respective research stages are shown.

As shown in Figure 2-1 the first research question is addressed within Chapter 1 to Chapter 4. First, a preliminary study investigating the research potential of the material combination of natural polymers and mineral aggregates was conducted. Then, the research was broadened to investigate 14 different polymers. The 14 natural polymers were then narrowed down to 6 within a preliminary assessment by excluding 8 that showed low potential for the application as binder in a construction material. The remaining 6 were assessed on their mechanical properties. As a result, a reflected overview over whether or not it is possible to build with natural polymers is given, addressing the first research question.

Furthermore, Figure 2-1 shows that the second research question is addressed by characterizing the rheological properties of the material. Whether or not a material is 3D printable, depends on the flow properties. These were investigated, especially aiming on describing the rheological change during extrusion. Printing trials were conducted. By answering the first research question, especially the thermoplastic binders showed good potential. Rheological tests are purely focused on the thermoplastic binders, as these showed most potential when addressing the first research question.

As shown in Figure 2-1, the third research question is addressed by designing a printing process with a robotic arm which can traverse a print head. Since the most promising materials evaluated by answering the first two research questions were thermoplastic, the printing head was designed so that it could extrude heated material. Printing trials were conducted to visualize the materials rheological properties and the potential of the innovation. Special focus was laid on overhang structures, since these require high setting control. This is elaborated in Chapter 6.

The final proof-of-concept is shown and discussed in Chapter 7.

2.2.   Order of the conducted research work

This chapter will present the order of the conducted research. It will give insights on how the work was organized to address the research questions identified in the previous section. Since this thesis' structure, presented in Figure 2-1 deviates slightly from the order of the conducted research, the latter is elaborated here:

1. At the beginning of this study, preliminary experiments were conducted to answer the first research question. The potential for use in construction of the proposed materials was evaluated. Digital manufacturing was already envisaged but at this point not further specified. As Figure 2-1 shows, these studies were recorded within 'Conference Paper II', which can be seen in Appendix 1.II. These preliminary studies were conducted with one, freely chosen natural polymer, i.e., mammal gelatin or bone glue. Compression strengths in the order of magnitude of construction materials were observed. Additionally, fast stiffening with temperature change was noticed during the production of the samples.

2. The preliminary experiments, presented in Appendix 1.II, showed that one natural polymer had suitable binding properties within a concrete composite for the application on load carrying structures. Fast solidification characteristics were also observed. A vision of 3D printing highly optimized structures with a print-head specifically designed for utilizing the material's fast setting properties was developed. This vision can be read in Appendix 1.I, i.e., in 'Conference Publication 1' (see Figure 2-1).

3. It was expected that mammal gelatin was not the only binding natural polymer. The study was therefore expanded with 13 other natural polymers that were found in literature. This is further elaborated within Chapter 3 of this thesis and in 'Conference Poster I' (see Appendix 3.I).

4. This project was the first of its kind in experimental 3D concrete printing and biologically based composites at the Department of Civil Engineering at DTU. Research infrastructure and a scientific network needed to be built. The PhD student procured and setup a large robotic arm, designed a print head and arranged a laboratory for both printing and biologically based composites. Simultaneously, knowledge about 3D printing of concrete, biological materials, rheology of composites, robotics and organic chemistry was obtained through literature studies, attending University courses (see Appendix 0.II) and conferences. The student established scientific collaboration, for the use of research infrastructure and exchange of knowledge. A network was built to other departments at DTU (DTU Food, DTU Mechanical Engineering, DTU Biotechnology, DTU Ballerup), as well as other Universities, such as the University of Copenhagen and the University of Southern Brittany. At this stage, studies on the topics of 'Mechanical strength', 'Rheological properties' and 'Printing process' (see Figure 2-1) were prepared simultaneously, as networking, accumulation of knowledge and especially the buildup of research infrastructure, e.g. the robotic arm described in point 4 was time intensive.

5. Development of methodologies for testing mechanical strength and rheological properties, as well as print head design and mixing methodologies of the material in a reproducible fashion proved to be challenging. This was especially due to the large water content and the associated shrinkage and fast drying behavior of the binders. Also, the thermal history of the natural polymers, the non-homogeneity of the dried composite samples and the high variability in concentrations (see Chapter 4 for further explanations) needed to be addressed. In addition, the fresh materials were prone to drying and slippage in rheometer experiments, especially under changing temperature conditions. Heated large-scale

extruders for fresh biologically based concrete did not exist prior to this work. Current models could not be adapted because the developed material dried in the conventionally applied open hoppers. Generally, a significant amount of methodology development was done to eliminate errors and ease the reproducibility of the study. Other studied methodologies aimed on broadening this research with durability studies, the development of larger print heads and mechanical testing of printed samples (see Chapter 2.3). These, could however not be developed to satisfy high scientific quality within the time scope of the study and were therefore left for future work. These methodologies and the time intensive establishment of research infrastructure and collaborations were taking place simultaneously. The finally applied methods are presented in Chapter 2.3.

6. The 14 natural polymers were pre-evaluated as binder in a composite for extrusion with a caulking gun. It was shown that all natural polymers are somewhat printable and highly dependent on the potential printing process used (e.g. two component system, temperature controlled, etc.). As not all of these processes could be developed and tested within the period of this study, an evaluation based on the mechanical properties of the binders was performed.

7. Simultaneously to the activities presented in point 6, the 14 natural polymers were reduced to a number of 6 natural polymers by a preliminary assessment which is presented in Chapter 3. This was done to limit the number of experimental investigations.

8. The mechanical and binding properties of the binders and composites were then evaluated. It was found that gelatin is the most promising binder (see Chapter 4). The setting mechanisms of gelatin were evaluated as thermoplastic.

9. A temperature-controlled print head which can extrude temperature sensitive concrete composites was developed (see Chapter 5 and Chapter 6).

10. Temperature-controlled rheological- and printing methodologies were defined and the suitability of temperature-sensitive composites in a 3D printing process evaluated. Since another binder, carrageenan showed especially rapid stiffening under temperature change, this binder was included in the further analysis.

11. A printing methodology was designed for both binders mentioned in point 8 and 10, already before the rheological experiments were completed. This was done to prove the benefits of their fast setting characteristics. Therefore, the printing of freely formed overhang structures was the objective.

12. To optimize the material processing and printing methodologies, a large number of preliminary printing trials ere conducted (see the final method description in Chapter 6).

13. The final proof-of-concept was done by evaluating the gelatin-based composite, as it was the most promising in terms of rheological and mechanical properties. A large printed overhang structure and a printed topology optimized structure showed that the concept of building robotically with a bio-based concrete composite in a free-form fashion could be proven.

14. Scientific literature and patents were reviewed continuously throughout the duration of the research.

2.3. Applied, adapted and alternative methodologies

As mentioned in Section 2.2, extensive methodology testing, adaptation and development was done to create results with high scientific quality and reproducibility. In the following, the applied methodologies, as well as the adapted and alternative methodologies are elaborated.

2.3.1. *Applied methodologies*

Table 2-1 shows an overview over the applied experimental methodologies in this thesis. Please

find the corresponding descriptions and justifications in the respective appendices and chapters

(compare to Figure 1-6 and Table 1-1).

Table 2-1 List of experimental methodologies for the respective publications (see respective Chapters and publications in Figure

1-6 and Table 1-1 for further explanations)

Publication	Title	Aim	Methods
Conference paper I	On the Ecology of Climate & Structures	This paper aims on outlining the intentions behind the development of 3D printed biologically based structures and sets it in perspective with the research group's work.	- review of literature - review of research group's topics
Conference paper II	A concrete composite from biologically based binders and mineral aggregates for constructional 3D-printing	This paper evaluates, based on a preliminary study, whether the composition of biopolymers and sand has potential for the application as 3D printed building material.	-casting of compression prisms and cylinders after EN196-1 and demolding for drying '-shrinkage testing with two separate length-of-prism-measurements - density measurement through weight and volume - testing of connected drying period by weighing
Conference poster I	Potential of natural polymers as alternative binder for 3D printing concretes	This work aims on finding the most promising biopolymer binders from 14 natural polymers on the basis of a preliminary study.	- observation of mixing solutions with respective bio-based binders - assessment of additional information
Journal paper I	Screening of natural polymers as binder in concrete composites	Aims on evaluating the potential of six natural polymers for the use as binder in concrete composites on the basis of mechanical properties and polymer-structure-property relations	- tensile bones mechanical testing of biopolymer films cut with laser cutter - sieving analysis after EN 933 - solubility measurements - adhesion testing of biopolymer films with roughened silica glass surfaces and tensile testing - composite compression tests with concentration sweep and extruded samples - density measurements with volume and weight measurements - shrinkage measurements with composite's sample dimensions under drying - scanning electron microscopy (SEM) to image the failure surface

			- Fourier Transform Infrared Spectroscopy (FT-IR) to identify molecular principles -light microscopy to investigate fraction of hydrogel film samples
Journal paper II	Rheological characterization of temperature-sensitive biopolymer-bound 3D printing concrete	Aims on evaluating the potential of two biopolymer composites as filament in a temperature controlled 3D printing process. Temperature dependent rheological properties are evaluated.	- printability assessment with self-built moving traverse and self-built extruder - yield shear strength test with rheometer, cup and shear vane setup, covered with polymer foil - oscillatory rheometer plate-on-plate tests of both pure gel and composite with cover hood and bentonite to prevent drying of the sample, with varying plate sizes.
Journal paper III	Multi-axial 3D printing of biologically-based concrete composites in construction	Aims on demonstrating the free form possibilities with the biologically based concrete composite and temperature controlled printing.	-robotic arm traversing mechanism -self-built ram extruder and printing process with material placed in tube bags to prevent drying - multi-axial slicing methodologies to enlarge the free-form possibilities of the material and process
Conference poster II	Gelatin as biologically-based binder in temperature-sensitive printing mortar for advanced free form constructions	Sums up the major findings of this PhD study.	-rheological test of yield strength development - compression tests of casted cubes - interface adhesion of printed sample -printing of topology optimized sample

2.3.2. Adapted or alternative methodologies

An extensive number of methodologies were tested, discarded or adapted. The most relevant of those are presented in this chapter, and justifications are given on why they were not further applied.

Alternative methodologies to the ones used in Chapter 4 (journal paper I):

I)   *Casted bone samples, following the standard for plastics after ASTM D638* (ASTM International, 2014) were produced for testing the pure tensile strength of the natural

polymers and evaluating the cohesive strength. Molds, as seen in Figure 2-2, were produced with computer-numerical-controlled milling machines.

The sample production method was adapted further due to large shrinkage of the material. Trials for reducing the shrinkage of the casted samples were conducted. This proved not feasible. Figure 2-2 shows the largest possible reduction in shrinkage. As an alternative, films were produced and cut after drying.

Figure 2-2 Molded tensile bone samples preparation inspired by ASTM D638 (ASTM International, 2014). The large amount of shrinkage during drying making it impossible to test these samples. Pictures: Julian Christ

II)   *Production of composite compression test samples with the same binder concentration* was attempted to reach a 'fair' comparison between the tested natural polymers. This was only possible by ignoring the solubility limit of the binders (see further discussions in Chapter 4). Some of the binders could not reach high levels of solution concentrations and therefore, only a few binders could be placed in the composite samples, while other binders could reach higher concentrations. The binders with higher concentrations were then scaled down to fit the concentrations of the binders with low solubility limits. The compression strengths were then compared.

This methodology was used in journal paper I, but extended with further concentration sweeps. It was found that the solubility limit is one of most important factors for producing a high density and -strength composite (see Chapter 4). This factor could therefore not be excluded in a valid comparison of binders.

An additional issue was identified for testing low binder concentrations. Low binder concentrations lead to inhomogeneous distribution of binder in the dried composites due to osmotic pressure differences during the drying process. Figure 2-3, shows a vacuum epoxy impregnated sample where the uneven binder distribution is visible. More binder can be found close to the drying surface, while the inner areas of the cross-section show lower binder contents. This is not an issue for higher concentrations. The issue was eliminated by scaling down sample sizes and by testing concentration sweeps instead of samples with the same binder concentrations.
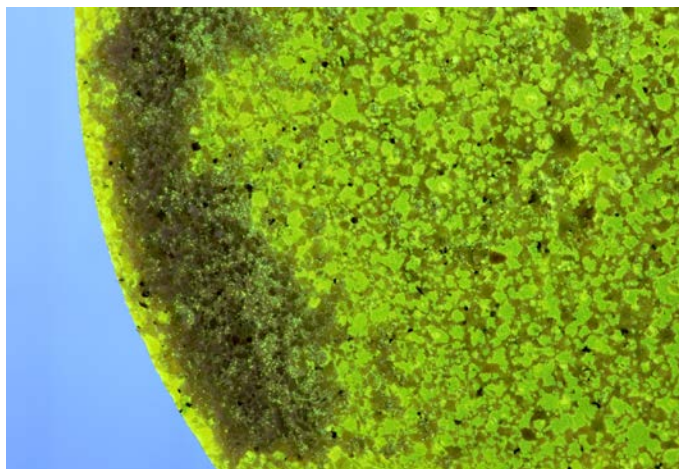
Figure 2-3 Vacuum impregnated sample with fluorescence epoxy resin. The pore space of the material is shown in green color. It is visible that more of the biopolymer binder is found close to the drying surface. Picture: Julian Christ

III)   *Food testing standards were evaluated for testing the mechanical strengths of binders.* Food testing standards like the Bloom strength test (Bloom, 1925) were evaluated to compare the natural binders on their cohesive and adhesive strengths.

These standards were discarded because close to all food standards test the gels in a non-dried state. Concentration sweeps (see Figure 2-4) with subsequent extrapolating of the concentration values to dry state were attempted. This, however lead to a low quality of the results.
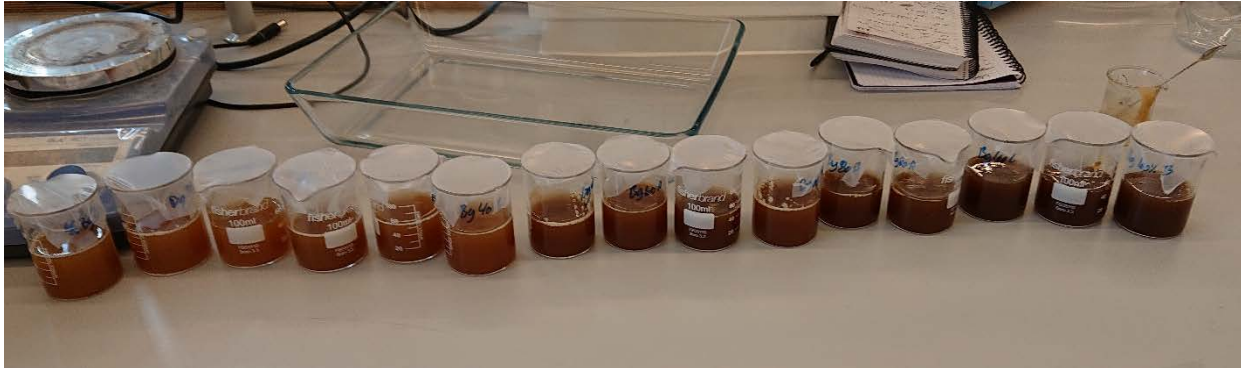
Figure 2-4 Concentration sweep of gelatin for Blooms test. The aim was to extrapolate the results to receive the compression strength of the dry gel. Picture: Thor Engelsen

IV)   *Testing of natural polymer composite after cement and mortar standards* (Dansk Standard, 2016). These standards were utilized in the preliminary study, which is included in Appendix 1.II.

Adaptation for further studies: Some of the casted concentrations, especially those with high water contents led to extensive molding. Concentration sweeps were therefore not possible with these bulky samples. In addition, uneven drying behavior as shown in point II) (Figure 2-3) was identified for especially the large sample sizes, and was avoided by using smaller sample sizes.

V)   *Thermogravimetric analysis (TGA)* was tested for receiving information about the chemical composition of the materials (see Figure 2-5).

Infra-red spectrometer data was preferred because this also shows the interactions between polymers and mineral aggregates (see Chapter 4).
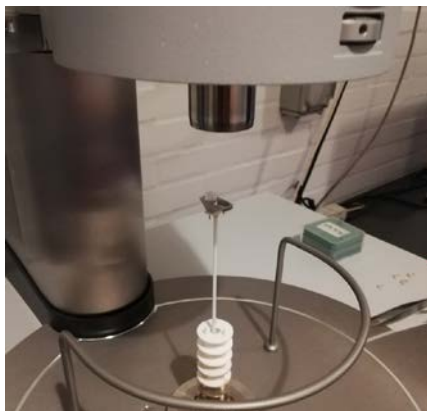
Figure 2-5 TGA Sample holder with biopolymer sample. Picture: Julian Christ

VI)   *Durability studies (mold growth, heat- and water exposure tests)* were conducted to

investigate the durability of the material (see Figure 2-6). The intention was to

measure mechanical strength during heat exposure, water soaking and mold growth in

humid environments.

This work was excluded from this thesis since the sample preparation proved to be

challenging for these tests, similar to the quantification and comparison of mold

growth. Further methodology development would be required. These durability

studies were evaluated to be non-essential to answer the presented research questions

from Section 2.1 and were left for future studies.
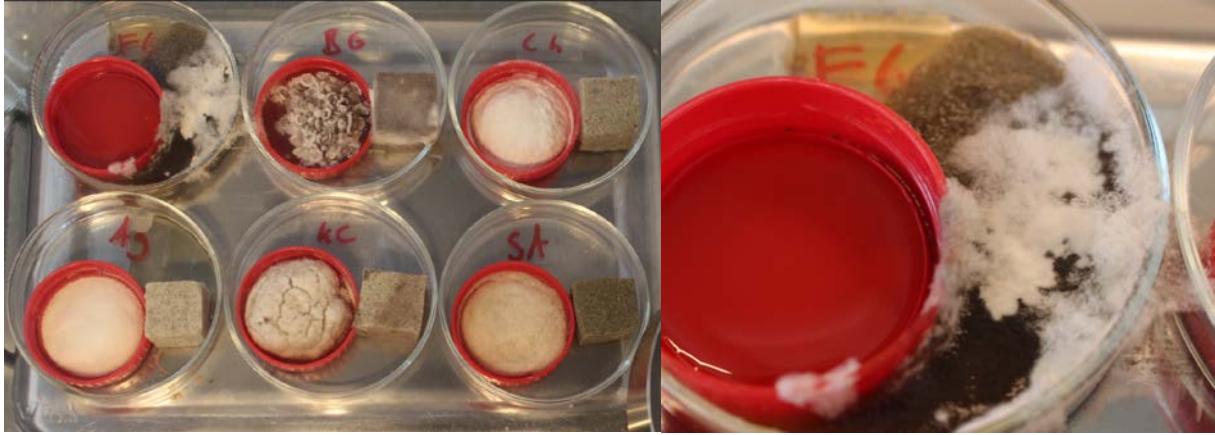
Figure 2-6 Mold growth tests. Some of the natural polymers and respective composites were exposed to a humid environment to reach a comparison on which materials show the highest mold resistance. Pictures: Julian Christ

VII) *Thin sections of composite samples, vacuum impregnated with epoxy resins for light microscopy* were produced to investigate interface properties between binders and sand (see Figure 2-3).

This method was discarded because the Scanning Electron Microscopy images (SEM) (see Chapter 4) allowed for better conclusions.

VIII) Additives like glycerol, glutaraldehyde and cellulose were investigated for improving the mechanical strength of the binders.

This was discarded and not further pursued because the screened concentrations resulted in decreased cohesive strengths and because the addition of additives to the binders was deemed non-essential for answering the research questions presented in Section 2.1. The evaluation of additives for improvement of mechanical strength, durability or rheological studies is left for further work.

Alternative methodologies, investigated for Chapter 5 (journal paper II):

I) *Vicat apparatus tests according to (DS-EN-196-3, 2016)* were adapted to reach a quick screening method for comparison of the binders within a workable composite,

without extensive Rheometer testing as presented in Chapter 5. The Vicat needle
diameter was changed and the thickness of the vessel was adapted to a printing layer
thickness, allowing for recording of the setting characteristics during cooling of one
of the natural polymer composites.

This method was discarded because the adapted needle width only worked for testing
the setting characteristics of one of the composites. Composites with the remaining
binders reached very varying setting properties. The adapted Vicat setup did therefore
not enable testing of all the composite's setting characteristics and comparison was
not possible. Rheometer testing was therefore preferred.

II)   *Rheometer testing* was tried in alternative setups than the ones used in Chapter 5.
Standard plate-on-plate, bob-in-cup, and vane-in-cup testing geometries were
attempted. For cup geometries, the particle sizes and high viscosity were usually the
cause of errors. For plate-on-plate geometries, extensive drying of the sample,
especially for elevated temperatures, caused large errors in the results. Cover fluids
(see Figure 2-7) were applied to the exposed sample surfaces. Varying types of oil or
grease were tested but discarded because they either drained away from the sample
during testing and hence did not prevent drying, or altered the tested properties due to
their own flow characteristics. These tests were further developed to the
methodologies used in Chapter 5.

Figure 2-7: Grease (black) was applied to the rheometer testing of the natural polymer composite with a plate-on-plate testing geometry to prevent drying of the sample. Unfortunately, the grease influenced the results and the methodologies were adapted further. Pictures: Julian Christ

Alternative methodologies, investigated for Chapter 6 (journal paper III):

I)   *Off-the-shelf print head setups* were evaluated for their suitability for extruding the proposed composite. Both polymer extruders and concrete extruders were evaluated. These setups were discarded because concrete printing heads are not equipped with a heating system for controlling and elevating the temperature. Hoppers for concrete extruders are usually open, which does not allow for avoidance of drying, especially when the prepared mixture needs to be kept at a set temperature (see Chapter 5 and 6). Large-scale extruders for thermoplastics are usually made for granulates and homogeneous thermoplastics without 'larger' aggregates. Therefore, it was decided to develop a suitable extruder from scratch.

II)   *Larger extruder, as the presented in Chapter 6:* A larger extruder for realizing larger structures was designed. In principle, the designed larger extruder works like the extruder presented in Chapters 5 and 6, but hosts a larger material volume of around 20 liters. See a sketch of the extruder in Figure 2-8. The material is kept warm within

a vessel and a piston feeds the material to the nozzle. The extrusion is controlled by an auger. An additional stepper motor was intended to control the direction of the nozzle to allow for a variety of nozzle shapes.

The building and testing of the extruder is left for further work because it could not be realized within the time frame of this thesis. Furthermore, building a larger extruder was deemed non-essential to answering the central research questions. The smaller extruder used in the study proved to be sufficient.
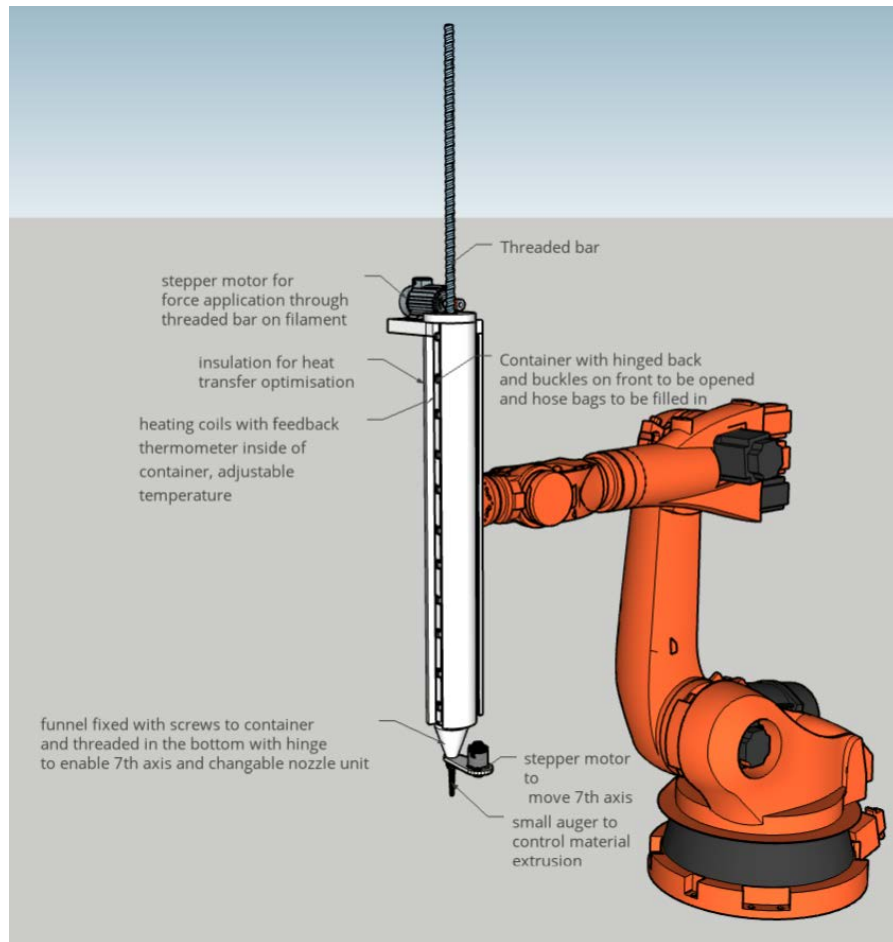
Figure 2-8 Extruder development for robotic arm and heated thermoplastic natural polymer and mineral aggregate composites. Picture: Julian Christ

3.   Scope and choice of natural polymers

Photo: Julian Christ. Mammal gelatin, as purchased in granular form.

As introduced, the aim of this PhD-study is to deliver a proof-of-concept for the application of biologically based polymers as binder in a concrete composite for 3D concrete printing. A focus on natural polymers is given. This chapter aims on justifying this chosen scope, i.e. the choice of natural polymers as primary objective and gives a preliminary evaluation of the investigated specific natural polymers.

3.1. Natural polymers

The field of polymer chemistry consists of a large number of varying types of polymers. Even though inorganic polymers exist (e.g. geopolymers), the largest variety of polymers can be classified as organic compounds (Vollmert, 1973). These organic polymers can be sub-divided into synthetic, semi-synthetic and natural polymers (see Figure 3-1).
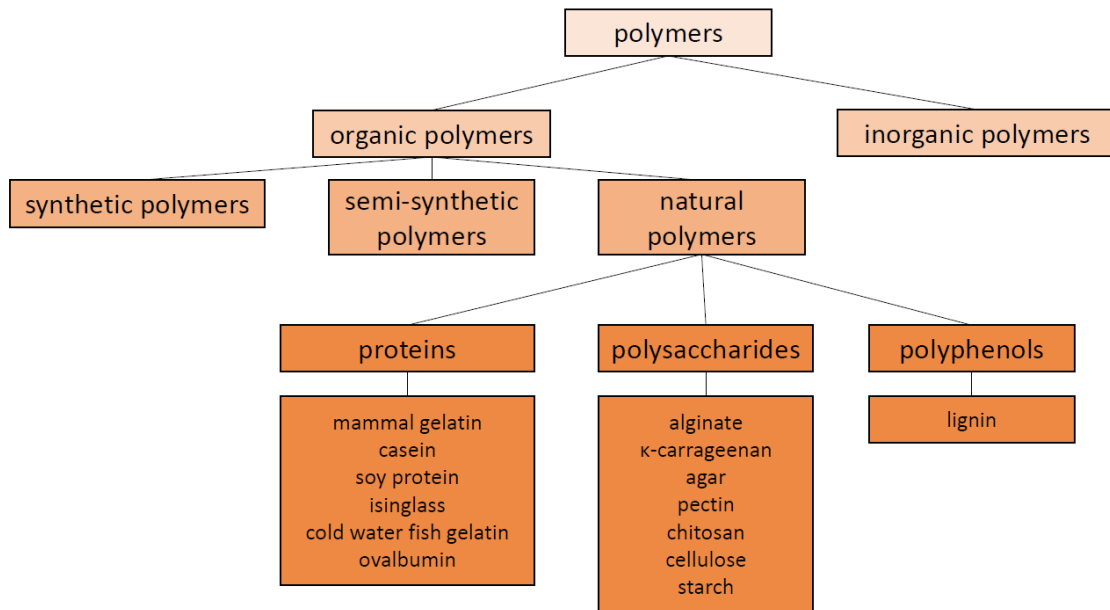
Figure 3-1 Overview of polymer classification and list of investigated natural polymers in this thesis

Synthetic polymers are a well known type of polymer. Engineered and altered to specific applications, they commonly use petroleum as a resource. The known beneficial properties of fast rheological change with temperature in form of a thermoplastic make them moldable and extrudable for many applications. They can be defined as one of the most important anthropogenic materials of current time. The durability of these materials do not only add to its usability: The lack of recyclability of synthetic plastics also confronts humanity with major waste management issues. Many of the polymers are threatening ecosystems and ending up in human food chains. These synthetic polymers are widely applied in 3D printing of various scales. Due to the potential environmental threat after its lifetime, as well as the non-renewable character of the petroleum-based raw materials, these polymers were not chosen as objective in this thesis.

Natural polymers (see Figure 3-1), on the other hand, are widely available in biomass and are the basis of every life. These polymers are used in nature for example for structural purposes (e.g. cellulose, chitin, and protein), energy storage (proteins and fatty acids), binders (e.g. lignin) or information storage (e.g. DNA). Natural polymers can be easy accessible and abundant. Some of the most abundant natural polymers are cellulose, chitin and lignin. While most cellulose and lignin are found in dry land plants, chitin is a structural polymer found in exoskeletons of crustaceans and in fungi. A large variety of properties can be derived from these types of biopolymers.

The term biopolymer can define natural polymers. However, the term can also include semi-synthetic polymers like e.g. biologically-based Polyethylene Terephthalate (PET). These materials are synthesized from ethanol, produced from biomass instead of petroleum. This material presents similar threats to the environment as synthetic polymers, once produced.

The PhD study aims on utilizing the known benefits in rheological properties of polymers to enhance 3D printed concrete. A thermosetting or thermoreversible behavior of the binders should ease the 3D printing of the concrete composite. Since the aimed application to structural building components require large amounts of material, easy accessibility and abundance of the polymers was important, as well as a renewable resourcing. The focus was therefore laid on natural polymers.

3.2.   Choice of investigated natural polymers

Fourteen natural polymers were chosen for consideration as binder in the 3D printed concrete composite to reach a broad overview and comparison. A list of the chosen polymers can be seen in Figure 3-1: six proteins, seven polysaccharide and one polyphenol were selected. These were identified by a literature search within the following references that are a collection of wood adhesives, biopolymers and applications of bio-based building materials (Frihart and Lorenz, 2018)(Thomas et al., 2013)(Sonebi et al., 2019). The selected natural polymers are elaborated in the following.

3.2.1. Proteins
Mammal gelatin, isinglass, cold water fish gelatin is produced from the structural protein collagen, the most important and abundant protein in mammals (Thomas et al., 2013). The gel is made by decocting connective tissue, bones, and hide to denature the collagen and form, by partial hydrolysis, gelatin. Mammal gelatin is also known as bone glue and is one of the world's oldest known adhesives. It is originally used for carpentry, cabinet- and instrument making, and restoration. Some research efforts partially applied gelatin to replace asphalt in pavement (Rizvi et al., 2019). Other researchers applied mammal proteins from blood to bind soil (Rosa et al., 2020). Cold water fish gelatin and mammal gelatin show similar properties. Gelation takes place

by swelling in water. A thermoreversibility can be denoted for all three gelatins. However, a significantly lower gelling point can be observed for cold water fish gelatin than for mammal gelatin (Nitsuwat et al., 2021). Similar to cold-water fish gelatin is Isinglass, but swim bladders are utilized instead of other parts of the fish.

Casein is the main protein in milk. The protein is mostly applied for food purposes, but also the application as adhesive is known. The protein forms a weak curd with water under elevated temperature, or is acid induced. (Frihart and Lorenz, 2018)

Soy protein can be isolated from the soy plant. It is commonly applied in food, cosmetics and adhesives for wooden boards (Frihart and Lorenz, 2018)(Thomas et al., 2013). The globular proteins can be dissolved in water and denatured under heating to form a polymer network. This thermosetting principle under elevated temperature forms a weak curd that can then be dried. When cooling, the gel stiffens. The protein is extracted as a side product of the soy oil production.

Ovalbumin is the protein in egg white. It denatures under the addition of heat and sets. The protein is easy accessible within the egg and its application as a wood adhesive is known (Frihart and Lorenz, 2018). Mostly, the protein is used as food or for medical applications.

3.2.2. Polysaccharides

Sodium alginate is extracted from brown seaweed and is a sodium derivative of Alginate (Thomas et al., 2013). Sodium Alginate is extracted by acid and ethanol treatment of seaweed (Saji et al., 2022). For its gelation, it does not need heat (Thomas et al., 2013) but gels under the influence of calcium ions and acids. The biopolymer is primarily applied as a thickener in food, biomedical and environmental applications (Guo et al., 2020). In construction, the hydrogel can function as an accelerator (Engbert et al., 2020) and superabsorbent polymer (Mignon et al., 2016) in concrete. Also, the application in stabilized earth is researched (Galán-Marín et al.,

2010)(Guihéneuf et al., 2020)(Menasria et al., 2017).

κ-Carrageenan is a polysaccharide extracted with alkaline treatment from red seaweeds (Thomas et al., 2013)(Y. Liu et al., 2022) under a temperature of around 100°C. The carrageenan is known for its gelling, thickening, and stabilizing properties for biochemical and food applications (Błaszak et al., 2018)(Mokhtari et al., 2021). The gelling appears under the influence of heat at around 55℃ or with the addition of a catalyst. It has previously been attempted in construction to use carrageenan as a superabsorbent polymer (Aday et al., 2017) or to modify earthen construction (Nakamatsu et al., 2017).

Agar is, just like sodium alginate and κ-carrageenan derived from seaweed (Thomas et al., 2013). Its structure is similar to κ-carrageenan and it melts and gels at elevated temperatures as a solution with water. Decocting red algae extracts the agar. Besides food, medical and cosmetic (Thomas et al., 2013) applications, the material is found to stabilize sandy earth (Khatami and O'Kelly, 2013). The gelling occurs under heat and a gelling temperature of 30-40℃ (Thomas et al., 2013). The gel has thermoreversible properties.

Pectin is a polysaccharide that is present in almost all terrestrial plants, but mostly in fruits and vegetables. Pectin is present in their cell walls where it acts as a binder. Pectin is commonly used to make jams (Thomas et al., 2013). Pectin-gels are acid induced with addition of sugar, or with an ion solution. Most commonly, pectin is extracted from fruits, e.g. lemon fruit or apples, where they are most abundant.

Chitosan is a natural polymer made by deacetylation of chitin, the second most abundant polysaccharide on earth. Chitosan can be extracted from the exoskeletons of shellfish like crab or shrimp (Thomas et al., 2013). Gelling occurs in slightly acidic solutions and without heat. The gel

is used in cosmetics, biomedical and food applications (Rinaudo, 2006). In construction, the gel was applied for architectural sculptures (Soldevila et al., 2014), for improvement of earth erosion properties (Donayre et al., 2018), and as additive for concrete (Lv et al., 2013).

Cellulose is a high molecular weight structural polymer that is abundant in plants. It can be pulped with either chemical or mechanical pulping from wood. Cellulose itself does not have gelling properties with water and does not dissolve (Thomas et al., 2013).

Starch is found in close to all plants. It has thermoplastic/thermosetting properties in water. Once heated, the starch structure denatures and sets to a gel. The new polymer network thickens when cooled down. Starch is usually applied as thickener for foods, but is also applied to make adhesives or films (Thomas et al., 2013).

3.2.3. Polyphenol

Sodium/Calcium lignosulfonate: Lignin is an abundant organic polymer that is a side product of the paper making industry. Lignin changes the permeability of cell walls in plants and acts as a binder for cellulose fibers. It can be pulped mechanically or chemically. Lignosulfonate is water soluble and conventionally extracted from wood. (Haghdan et al., 2016)

3.3. Preliminary evaluation of the 14 natural polymers

In the scope of this study, it was not possible to evaluate all 14 natural polymers on their mechanical strength, rheological properties and the printing application. The 14 presented natural polymers (see Figure 3-1) were therefore evaluated on a preliminary basis. Based on their aimed application, the natural polymer binders should present good binding properties, fast setting for good printability, an abundance for the use as construction material, easy accessibility of the

material and should ideally not be used as food. These evaluation criteria were evaluated qualitatively on known characteristics of the binder and experimental studies.

3.3.1. Preliminary evaluation criteria

To evaluate the binders, five main evaluation criteria were identified: Binding properties, setting characteristics, abundance, extraction of material and ethical concerns. These were justified in the following and are summed up in Table 3-1.

Binding properties: For the natural polymer to be utilizable as a binder in a composite with mineral aggregates, strong cohesion and adhesion were beneficial. Within this category, the binders were evaluated qualitative on their expected ability to bind aggregates in a fresh state.

Setting characteristics: A general setting behavior is necessary for the use as binder in a workable composite. Both, thermosetting properties, like a setting with the addition of acid or ionic solutions, as well as viscosity change or solidification with temperature change were evaluated as positive. Fast setting, or drastic and rapid change in viscosity were additionally evaluated as positive.

Abundance: The utilization of the natural polymers as binder in construction materials requires a certain abundance in order to satisfy the large volumes needed for construction purposes. High abundance of the raw materials is wanted to increase the potential for application.

Extraction of material: The natural polymers are not always occurring in its pure form. The material needs to be extracted - the more elaborate the process, the higher the final costs. The natural polymer binder should therefore be easy accessible.

Ethical concerns: Almost all 14 presented polymers can be used as food for human consumption or feed for animals. A direct competition with the human food chain can therefore

be identified. The competition eases when the material is present as a secondary resource, i.e. waste material. Ideally, the natural polymer is present as an unused secondary resource that can be utilized for other applications, as the proposed in this thesis.

Table 3-1 shows a connected rating system for the introduced categories. The performance of the 14 natural polymers on these requirements were evaluated on experimental basis and on the basis of the information and references given in Section 3.2. The categories 'binding properties' and 'setting characteristics' were evaluated on the basis of experimental studies. All other categories were assessed qualitatively on the basis of Section 3.2.

Table 3-1 Rating system for performance indicators of natural polymers. The rating reaches from '++' (very good) to '- -' (very bad). The connected categories are elaborated in Section 3.3.1.

Category	++	+	o	-	--
Binding properties	forms hydrogel with strong adhesive and/or cohesive properties	forms hydrogel with adhesive or cohesive properties	forms hydrogel without cohesive or adhesive strength	forms a thick suspension but does not gel	Suspension with low viscosity
Setting characteristics	sudden thermoset or sudden thermoplastic viscosity change	thermoplastic / thermoreversible or thermoset	does not show sudden viscosity change but high viscosity	low viscosity change of suspension by temperature change	No viscosity change
Abundancy	very high abundancy	high abundancy	mediocre abundancy	relatively rare	rare
Extraction	natural polymer is present in its pure form in nature	easy accessibility by e.g. decocting of raw material	extraction by addition of simple additives (eg. acids)	complex extraction method	complex, energy intensive industrial process necessary for extraction

	no ethical concerns - secondary material that is currently not reused	low ethical concerns - primary material, no food application	secondary material, reusable as food for human consumption or feed	primary material, usable for food or feed	use of large quantities of life stock
Ethical concerns					

3.3.2. Experimental studies

To evaluate the setting and binding properties of the respective natural polymers, the polymers were prepared as a solution with varying solvents and the temperature was elevated or a second component was added to evoke their potential setting characteristics. The used materials, the preparation methods, as well as the respective observations are documented in Table 3-2.

Table 3-2 Observations on binding properties and setting characteristics of the respective natural polymers. The table shows the material specification, preparation method and the connected observations.

Natural polymer	Product and provider	Preparation method	Observation on setting and binding characteristics
Mammal gelatin	'Bone glue granulate' from Dictum, #450145	Solution in water, elevated in temperature	forms thermoreversible gel as solution in water with cohesive and adhesive properties
Casein	'Bio casein protein - Neutral' from AlpenPower	(i) solution in water and elevated in temperature, (ii) solution with acid	weak thermoset induced by elevated temperature and/or acid
Soy protein	'Soy protein - 100% isolate' from Greenfood	solution in water, elevated temperature	weak thermoset induced by elevated temperature, low adhesive properties as gel.
Isinglass	'Isinglass glue granulate' from Dictum, #450142	Solution in water, elevated in temperature	forms thermoreversible gel as solution in water with cohesive and adhesive properties
Cold water fish gelatin	'Gelatin from cold water fish skin' from Sigma-Aldrich, #G7765-1L	Solution in water, elevated in temperature	forms thermoreversible gel as solution in water with cohesive and adhesive properties

Ovalbumin	'Eiklar Pulver' from Hoosier Hill Farm	Solution in water, elevated in temperature	thermosets with elevated temperature as solution in water, has cohesive strength
Alginate	'Sodium Alginate' from Sigma-Aldrich, #W201502	(i) solution in water, (ii) solution in water with the addition of Ca^{++} ion-solution	no effect of elevated temperature; forms thick gel as solution in water; sudden setting when Ca^{++} ion-solution is added. Has cohesive gel strength, weak adhesive properties.
κ-carrageenan	'κ-carrageenan - sulfated plant polysaccharide' from Sigma-Aldrich, #22048-100G-F	solution in water, elevated in temperature,	forms thermoreversible gel as solution in water, can also gel in conjunction with K+ ion-solution. Strong cohesive properties, weak adhesion.
Agar	'Agar - extra pure' from Merck KGaA - Emprove Essential, #1.01615.1000	Solution in water, elevated in temperature	Thermoreversible hydrogel in water. Cohesive strength, low adhesion.
Pectin	'Pectin from citrus peel' P9135 from Sigma Life Science	solution in weak acid with addition of sucrose; elevated temperature	Forms thermoreversible gel with sucrose and acid.
Chitosan	'Chitosan from shrimp shells' from SIGMA, #50494-100G-F	solution in weak acid, to increase solubility, temperature was elevated	acid induced gelation; elevated temperature did not have an influence on the gel's viscosity
Cellulose	'Pure Microcrystalline Cellulose' from eBay, #201373404104	solution in water, elevated temperature	no setting or binding properties; elevated temperature had no effect
Starch	'Maizena - corn starch' from Unilever Food Solutions	solution in water, elevated temperature	forms thermoreversible gel as solution in water, thermosets at elevated temperature
Lignin	'Sodium/Calcium lignosulfonate' from alibaba.com	solution in water, elevated temperature	no setting or binding properties; elevated temperature has no effect

3.3.3. Assessment on the basis of additional information

Based on the information given in Section 3.2, the natural polymers were evaluated on their abundance, complexity of extraction, and ethical concerns. These findings are shown in Table 3-3.

Table 3-3 Preliminary assessment on the basis of additional information. The criteria abundance, material extraction and ethical concerns were assessed qualitatively based on the information and references given in Section 3.2.

Natural polymer	Abundance	Material extraction	Ethical concerns
Mammal gelatin	is a type of gelatin made from mammal collagen. Collagen is the most abundant protein in mammals.	can be extracted by soaking and decocting animal tissue in water.	gelatin can be used as food. However, butchery waste such as hide and bone are often used as fodder. Large amounts are available.
Casein	occurs in high concentration in mammalian milk.	can be extracted by pH adjustment, fermentation, heat treatment.	Milk and the protein casein are a food source. The milk from which casein can be extracted is a primary food that needs live stock to be produced.
Soy protein	soy is a farming product that is produced in large quantities.	the protein is extracted by extrusion as a side product of the soy oil production.	The secondary product is mostly utilized in fodder or foods.
Isinglass	is a type of gelatin made from the fish sturgeon. The protein is obtained from the fish's swim bladder. No large amounts are available of this bladder.	can be extracted by soaking and decocting the animal tissue in water.	large amounts of fish would be necessary to be produce the significant quantities needed for the use in construction.
Cold water fish gelatin	is a type of Gelatin made from fish protein. The protein is obtained from the fish's skin and is available in larger amounts as fishery waste.	can be extracted by soaking and decocting animal tissue in water.	Fish skin is a secondary resource form the fishing industry. Some fisheries reuse the waste for animal fodder; others do not process the waste any further.
Ovalbumin	occurs as egg protein from poultry.	available in the egg in high concentration, easy to purify.	needs live stock to be produced and is a primary product for foods.

Alginate	occurs in brown algae that is an abundant form of seaweed.	extraction by acid and ethanol treatment, chemically simple extractions.	Brown algae can be used as food. Sodium alginate can be used as a food additive. Only small amounts of algae are being utilized as food.
κ-carrageenan	occurs in red algae that is an abundant form of seaweed.	Can be produced by alkaline treatment and decocting/rapid cooling of red algae.	Red algae can be used as food. κ-carrageenan can be used as a food additive (thickener). Only small amounts of algae are being utilized as food.
Agar	occurs in red algae that is an abundant form of seaweed.	Can be produced by decocting of red algae.	Red algae can be used as food. Agar can be used as a food additive. Only small amounts of algae are being utilized as food.
Pectin	produced from citrus peels or apples. Both are farmed products and side products of juice production. Pectin is available in low concentrations from these wastes.	can be extracted with hot acidic solutions.	secondary resource of juice production.
Chitosan	Is made from Chitin. Chitin is one of the most abundant polysaccharides and occurs in exoskeletons of crustaceans and in mushrooms.	Produced by deacetylation of Chitin. Deacetylation can be done by treatment with alkaline solution.	Chitin is a secondary resource from the fishing industry. Chitin has limited value for food application.
Cellulose	is abundant in almost all plants.	does occur in high concentrations in plants and can be pulped chemically or mechanically as e.g. done for the paper industry.	low value as food or fodder.
Starch	is found in almost all plants and is used for energy storage.	can be purified by washing and grinding.	is one of the most used carbohydrates in food.
Lignin	one of the most abundant natural polymers. Is a side product of the paper industry.	can be pulped by varying extraction methods - chemically, mechanically.	Low value as food or fodder.

3.3.4. Overall preliminary assessment

The overall preliminary assessment of the 14 presented natural polymers on the basis of the five evaluation criteria can be seen in Table 3-4. The information, summarized in Section 3.3.2 and Section 3.3.3 was used for the rating. The rating system presented in Table 3-1 was applied.

Table 3-4 Overall preliminary assessment of 14 natural polymers for the use as binder in 3D printed construction material. The assessment was based on the five categories of binding properties, setting characteristics, abundance, raw material extraction and ethical concerns

	Natural polymer	Category A: Binding properties	Category B: Setting characteristics	Category C: Abundance	Category D: Raw material extraction	Category E: Ethical concerns	Overall Rating
Protein	Mammal gelatin	++	+	+	+	o	5
	Casein	o	++	o	o	-	1
	Soy protein	o	++	o	+	-	2
	Isinglass	++	+	--	+	--	0
	Cold water fish gelatin	++	+	o	+	o	4
	Ovalbumin	+	++	o	++	--	3
Polysaccharides and others	Alginate	+	++	+	-	+	4
	κ-carrageenan	+	++	+	+	+	6
	Agar	+	+	o	+	+	4
	Pectin	+	+	-	o	o	1
	Chitosan	+	+	+	o	+	4
	Cellulose	--	-	+	-	+	-2
	Starch	+	+	+	+	-	3
	Lignin	--	--	+	-	+	-3

The categories 'binding properties' and 'setting characteristics' were evaluated on the basis of the experimental observations, shown in Table 3-2. It can be seen that especially the gelatin based binders present a high rating in terms of their binding properties (rated with '++'). The gelatins form both, a strong adhesion and cohesion in the fresh state. Other materials, such as carrageenan or agar form a good cohesion but develop no tack, i.e. adhesion. Cellulose and the presented lignin

do not show any tack or cohesive properties once prepared after the method presented in Table 2-1. These were therefore negatively rated. Sudden setting characteristics could be observed e.g. for carrageenan with temperature change or for alginate with the addition of an ion solution and were therefore evaluated as positive. Cellulose and lignin did not present any setting in a solution with water and were therefore evaluated as negative.

The criteria 'abundance', 'raw materials' and 'ethical concerns' were assessed on the basis of the given information in Table 3-3. The abundance for isinglass e.g. was evaluated as negative since a specific part (swim bladder) of a specific fish is used. Ovalbumin was evaluated positively in terms of its material extraction since the material occurs in a very pure form. Ethical concerns are present especially for virgin materials that can be used for food or that use large amounts of life stock to be produced. Ovalbumin or isinglass were identified as such. Materials that were evaluated as positive are e.g. lignin, cellulose or alginate. These have no or just limited food applications or are a side product of other industries.

Within this preliminary assessment, the score was calculated by, e.g., identifying a positive rating of '+' as +1 and a double negative rating '- -' as -2. The overall score for each natural polymer was calculated as the sum of all categories. This score can be seen in Table 3-4. The evaluation of a negative overall score was graded as 'red' and a low potential for further investigation could be derived. This was the case for lignin and cellulose. The overall score of 0 to 3 was graded as 'yellow' and connected to a medium potential for further investigation. Six natural polymers showed an elevated potential for further investigation. These scored higher or equal to 4 and are mammal gelatin, cold water fish gelatin, alginate, carrageenan, agar, and chitosan.

This preliminary assessment of the 14 natural polymers allowed to focus the study on the six natural polymers. The choice reflects the knowledge gained from the experimental studies and the

information presented in this chapter. Other combinations of the materials or chemical alteration through other incorporated components might be possible and change this evaluation. These, however were not further pursued and were evaluated as out of scope for this study.

The content of this chapter was published in form of a conference poster (see Appendix 3.I).

.

4.   Mechanical properties

Photo: Julian Christ. A composite from sand and a natural polymer. Sample for testing of the mechanical strength.

A key parameter for the application of materials for construction purposes are the mechanical properties. Whether or not a material has load bearing abilities is decisive for this application. The presented composite of natural polymers and sand was therefore tested on its mechanical strength to answer research question 1, presented in Section 2.1. It was intended to test and compare the identified six natural polymers from Chapter 3 on their applicability as a binder in a concrete composite. These six natural polymers were: κ-carrageenan, sodium alginate, agar, chitosan, mammal- and cold-water fish gelatin.

As primarily decisive for structural applications, the compression strength and connected working principles of the composite were in focus and assessed in this chapter. The aim was to identify the best working natural polymer binder for load carrying applications and to investigate chemical structure-property relations for the binder's adhesion and cohesion strengths. Concentration sweeps were conducted to find the maximum compression strength for each natural polymer composite, which were then compared. Some of the natural polymers showed good cohesive and/or adhesive binding properties in the fresh state (see Chapter 3). These properties were further investigated and quantified in the dry state as they are highly relevant for the mechanical strength development. Furthermore, general chemical properties of the natural polymers that are responsible for their binding characteristics were identified to allow conclusions on why the identified natural polymers do or do not bind mineral aggregates.

This chapter is presented in form of a journal paper. This publication can be referenced as:

J. Christ, T. K. Engelsen, E. Thybring, L. Ottosen and H. Koss. 'Screening of natural polymers as binder in concrete composites'. *Submitted to*: Construction and Building Material, 2023, manuscript reference no.: CONBUILDMAT-D-23-02616.

Screening of natural polymers as binder in concrete composites

Julian Christ[a],*, Thor Engelsen[a], Emil Engelund Thybring[b], Lisbeth M. Ottosen[a], Holger Koss[a]

[a]*Technical University of Denmark, Brovej 118, 2800 Lyngby, Denmark*

[b]*University of Copenhagen, Department of Geosciences and Natural Resource Management, Rolighedsvej 23, 1958 Frederiksberg C, Denmark*

Abstract

Six natural polymers were tested as binders in a novel concrete composite for construction. Cubic composite samples were made from the different binders and sand, and the compression strengths were evaluated. Concentration sweeps found the highest strength for each natural polymer composite. The polymer's mechanical performance was then compared with its cohesive and adhesive strength and discussed based on their molecular properties. The adhesion was found to be essential to the composite's compression strength. Gelatin and chitosan showed good adhesive properties. Gelatin presented the highest mean compression strength (59.6MPa) at a concentration of 30g binder per 100g sand. The lowest mean compression strength was found for κ-carrageenan with 1.6MPa. Gelatin-based composites were found to be most suitable for structural purposes due to their mechanical performance.

Keywords: thermoplastic resin, mechanical properties, strength, mechanical testing

4.1.　　　Introduction

The construction industry is one of the biggest CO2 emitters worldwide. Cement production alone causes over 8% of global CO2 emissions under production (Monteiro et al., 2017). Research and development are conducted, focusing on replacing cement and concrete with more sustainable building materials. Environmentally compatible alternatives are biologically-based materials like wood or hay that store atmospheric CO2. Also, mineral cement replacements for concrete that use waste- or less energy-intensive materials like fly ash (Paris et al., 2016), calcined clay (Cao et al., 2021), or geopolymers (Singh et al., 2015) are explored as potential alternatives. Earth-based materials (Laborel-Préneron et al., 2016) that use local resources and the binding properties of unfired clay to form structural elements have also gained increased interest. These earth-based materials usually use smaller amounts of cement as stabilizers (Walker and Stace, 1997)(Sri Bhanupratap Rathod and Venkatarama Reddy, 2021) for increased durability and strength. In recent years, biologically-based stabilizers have been added to soil-based materials for this purpose (Muguda et al., 2020)(Guihéneuf et al., 2020). Raw earth materials, from pure clay to sand-clay composites (Wang et al., 2022), are explored, locally sourced, and unrefined. Two of the most common bio-stabilizers for earth constructions are sodium alginate (Perrot et al., 2018b) and xanthan gum (Muguda et al., 2021). Since the materials can be locally sourced, these composites have also gained interest for space exploration (Rosa et al., 2020)– in any case, they are using locally resourced aggregate and clay materials.

Simultaneously with this development, automation processes, like extrusion-based 3D printing (Buswell et al., 2018), are being developed to increase the construction sector's productivity and decrease the amount of material through optimal placement (Schutter et al., 2018). The advent of 3D printing in construction has led to the development of novel material mixtures that include

Portland cement concrete, polymers, and earth-based materials. Recently, also natural polymer-based materials have found their application for 3D printing in construction (Soldevila et al., 2014)(Biggerstaff et al., 2021)(Menasria et al., 2017). The material is used as a pure natural polymer or as a binder in a composite with earthen materials and sand. Printed objects generally have a thin-walled design, which eases drying processes and makes it possible to use a high share of water in water-dissolved binding materials, such as natural polymers. For a composite to be 3D printable, the material must be workable and present a yield strength (Roussel, 2018) to hold its shape under gravitational loading at its early age. Some natural polymers have unique rheological properties in the wet stage, such as shear thinning or thermoplasticity. These properties are beneficial for 3D printing (Christ et al., 2023).

This paper investigates concrete composites from mineral aggregates and natural polymers for future use in extrusion-based 3D concrete printing (3DCP). The material will not use clay-based binders as seen previously in (Menasria et al., 2017) but instead produce a binder matrix with only natural polymer materials. The focus is on its mechanical performance but is also connected to the manufacturing and testing of boundary conditions that are essential for 3DCP, like workability and yield strength in the early stage. Six natural polymers shown in a preliminary study have elevated potential to be used as a binding material in composites for construction purposes (Christ et al., 2020). This paper investigates these six natural polymers: κ-carrageenan, sodium alginate, agar, chitosan, mammal gelatin, and cold-water fish gelatin. The first four are polysaccharides, while the other two are proteins. The mechanical strength of varying composite concentrations, densities, and shrinkage values are tested, and the structure-property relations are discussed.

4.1.1. Polysaccharides

a) *κ-carrageenan* is a polysaccharide extracted with alkaline treatment from red seaweeds (Thomas et al., 2013)(Y. Liu et al., 2022) under a temperature of around 100°C. Its chemical structure can be seen in Figure 4-1a). The carrageenan is known for its gelling, thickening, and stabilizing properties for biochemical and food applications (Błaszak et al., 2018)(Mokhtari et al., 2021). The gelling appears in an aqueous solution under the influence of heat at around 55°C. Previous attempts were made using carrageenan as a superabsorbent polymer for concrete structures (Aday et al., 2017) and modifying earthen construction (Nakamatsu et al., 2017).
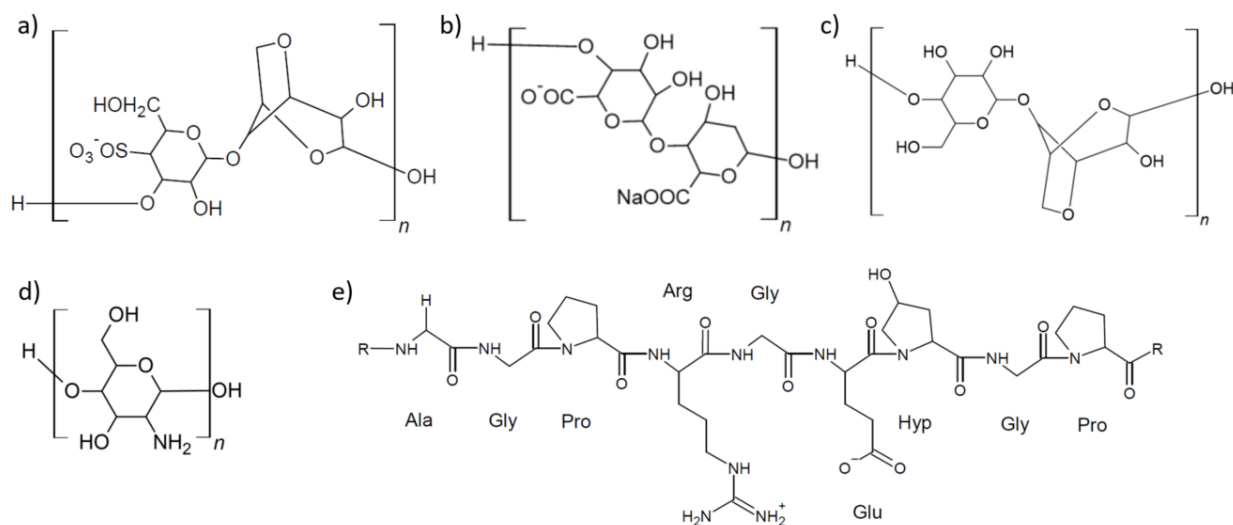
Figure 4-1 Chemical structure of a) κ-carrageenan, adapted from (Thành et al., 2002); b) sodium alginate, edited from (Homayouni et al., 2007); c) agar, edited from (Minghou et al., 1988); d) chitosan, edited from (Baxter et al., 1992); e) gelatin, edited from (Deshmukh et al., 2017).

b) *Sodium alginate* is extracted from brown seaweed and is a sodium derivative of alginate (Thomas et al., 2013). Sodium alginate is extracted by acid and ethanol treatment of seaweed (Saji et al., 2022). The chemical structure is seen in Figure 4-1b). For its gelation, it does not need additional heat (Thomas et al., 2013) but gels under the influence of calcium ions and acids at room temperature. The biopolymer is primarily used as a

thickener in food, biomedical and environmental applications (Guo et al., 2020). In construction, the hydrogel can function as an accelerator (Engbert et al., 2020) and superabsorbent polymer (Mignon et al., 2016) for cementitious binding. Also, the application stabilized-earth was researched (Galán-Marín et al., 2010)(Guihéneuf et al., 2020)(Menasria et al., 2017).

c) *Agar* is like sodium alginate and κ-carrageenan derived from seaweed (Thomas et al., 2013). Its structure is similar to κ-carrageenan (see Figure 4-1c)), and it melts and gels at elevated temperatures as a solution with water. Decocting red algae extracts the agar. Besides food, medical and cosmetic applications (Thomas et al., 2013), the material is found to stabilize sandy earth (Khatami and O'Kelly, 2013). The gelling occurs at a temperature of 30-40ºC (Thomas et al., 2013). The gel has thermoreversible properties.

d) *Chitosan* is a natural polymer made by the deacetylation of chitin, the second most abundant polysaccharide on earth. Chitosan can be extracted from the exoskeletons of shellfish like crabs or shrimp (Thomas et al., 2013). Its molecular structure can be seen in Figure 4-1d). Gelling occurs in slightly acidic solutions and without heat. The gel is used in cosmetics, biomedical and food applications (Rinaudo, 2006). In construction, the gel was used for architectural sculptures (Soldevila et al., 2014), for improvement of earth properties, i.e., preventing or delaying erosion (Donayre et al., 2018), and as an additive for concrete (Lv et al., 2013).

4.1.2. Proteins

e) *Mammal- and cold-water fish gelatins* are produced from the structural protein collagen, the most abundant protein in mammals. The gel is made by decocting connective tissue, bones, and hide to denaturalize the collagen and form, by partial hydrolysis, gelatin. This

gelatin is also known as bone glue and is one of the world's oldest known adhesives. It is used for carpentry, cabinet- and instrument making, and restoration. Some research efforts partially used gelatin to replace asphalt in pavement (Rizvi et al., 2019). Other researchers used mammal proteins from blood to bind soil (Rosa et al., 2020). The molecular structure of the gelatin protein can be seen in Figure 4-1e). Cold-water fish gelatin and mammal gelatin show similar structures and properties. Gelation takes place by swelling in water. A thermoreversibility can be denoted for both gelatins. However, a significantly lower gelling point can be observed for cold-water fish gelatin than for mammal gelatin (Nitsuwat et al., 2021).

4.2.   Materials and Methods

4.2.1. Aggregates

Sea sand from the Great Belt region in Denmark was used at a size of 0-2mm. Due to the cubic specimen size of 20mm for the compression tests (see Section 4.2.11), the maximum grain size was reduced to 1mm by sieving to ensure homogeneous mechanical properties. The grading curve of the sieved sand corresponds to EN 933 (Dansk Standard, 2013) and is shown in Figure 4-2. The sand offers a grading of 0-1mm and has its largest mass in the sizes of 0.25-1mm. A fine particle content (below 0.063mm) of 0.4%-wt. and a moisture content of 0.06%-wt. was observed.
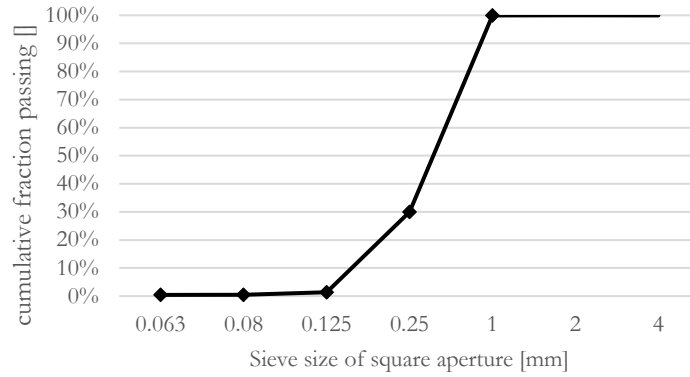
Figure 4-2 Grading curve of sand from the Big Belt region in Denmark, sieved to a maximum grain size of 1mm. Grain size distribution was recorded after EN 933 (Dansk Standard, 2013).

As shown in the bright field microscope images in Figure 4-3, the sand grains are of sub-rounded shape. The mineralogical composition was identified with an X-ray diffractometer as SiO_2 and $CaCO_3$. A minor $CaCO_3$ amount of 2.1%-wt. was measured in a Scheibler apparatus as CO_2 release analysis under the presence of acid.
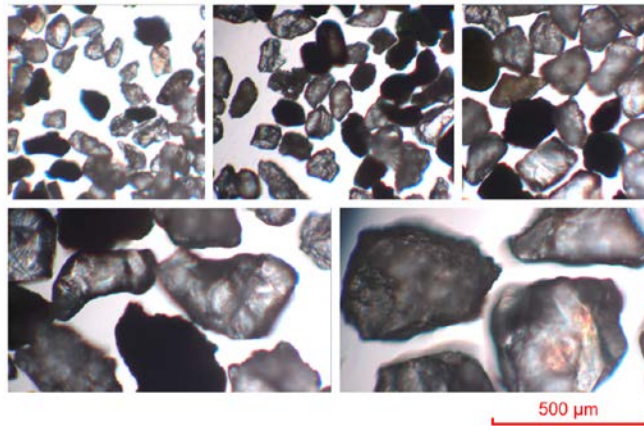
Figure 4-3 Brightfield microscope images from sieving analysis with 10x objective, showing retained grains on sieves of the following sizes (from top left to bottom right): Pan, 0.063mm, 0.08mm, 0.125mm, 0.250mm. The scale bar applies to all images.

4.2.2. κ-carrageenan

κ-carrageenan in powder form was purchased from Sigma-Aldrich (product number 22048). The binder was prepared by soaking the powder in water with various concentrations, as described in Section 4.3. The solution was heated in an oven and an adjusted temperature of 120°C until melting

and gelling occurred. During heating, the gel was placed in a non-ventilated container to prevent drying and hence a change of concentration. To identify the chemical composition of the material and ease reproducibility of this study, a Fourier-transform infrared (FT-IR) spectrum of the raw material with the most significant peaks identified can be seen in Appendix 4.I. See also Section 4.2.15.

4.2.3. Sodium alginate
Sodium alginate in powder form was purchased from Sigma-Aldrich (product number W201502). At room temperature, the gel was prepared by soaking the material in water under occasional stirring with concentrations, as shown in the following sections. An FT-IR-spectrum of the used material with the most significant peaks can be seen in Appendix 4.I.

4.2.4. Agar
Agar was purchased in powder form from Sigma-Aldrich (product number 1.01615.1000). Like κ-carrageenan, the gel was prepared by soaking the powder in water at room temperature and subsequently heating it to 120°C in an electric oven until the solid content of the solution was dissolved. During the heating phase, the gel was placed in a non-ventilated container to prevent drying and hence a change of concentration. The material was mixed with the concentrations as specified in the following sections. An FT-IR-spectrum of the used material with the most significant peaks can be seen in Appendix 4.I.

4.2.5. Chitosan
Chitosan from shrimp shells was purchased in powder form from Sigma Aldrich with product number 50494. The gel was produced by soaking the powder in a 2%w/v acetic acid solution at room temperature for 24h, after which it was fully dissolved. To remove air entrainments, the solution was heated to approximately 80°C. The material was mixed at concentrations as specified in the following sections. An FT-IR-spectrum of the used material with the most significant peaks can be seen in Appendix 4.I.

4.2.6. Mammal gelatin

Mammal gelatin was purchased in granular form from DICTUM (DICTUM, 2019) with the product number 450141. The material was prepared by soaking the material for one h in water at room temperature. The last solid content was removed by heating the solution to 60°C with a magnet-stirring heating plate. The material was mixed at the concentrations as specified in the following sections. An FT-IR-spectrum of the used material with the most significant peaks can be seen in Appendix 4.I.

4.2.7. Cold-water fish gelatin

Gelatin from cold-water fish skin was purchased in granular form from Sigma-Aldrich with the product number G7041. The gelatin was prepared by soaking it in water at room temperature and dissolving it under a slightly elevated temperature with a magnet-stirring heating plate until homogeneity could be assumed. The material was mixed with the concentrations, as specified in the following sections. An FT-IR-spectrum of the used material with the most significant peaks can be seen in Appendix 4.I.

4.2.8. Solubility limit

The used hydrogel binders exhibit natural solubility limits, i.e., the amount of raw granulate or powder that can be dissolved in water or acetic acid. The limit was tested by gradually increasing the amount of solute in the respective solvent, possibly heating it to a workable temperature (depending on the hydrogel type - see Section 4.2.2-4.2.7). The highest concentration mixable by keeping its workability, was defined as the solubility limit shown in Figure 4-4.

	κ-Carrageenan	Sodium Alginate	Agar	Chitosan	Mammal Gelatin	Cold Water Fish Gelatin
□ max %	8%	15%	6%	8%	150%	200%
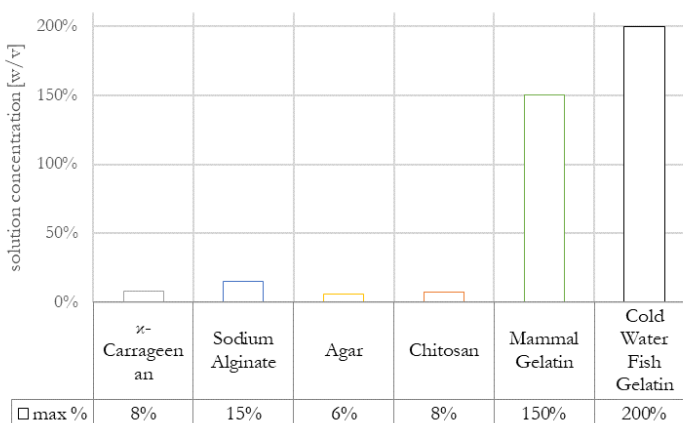
Figure 4-4 Solubility limits of hydrogels without losing its workability – concentrations are given in [%-w/v]

4.2.9. Tensile strength of the dried binder films

The cohesive strengths of the dried binder, as used in the final composite, is a key parameter.

However, since the hydrogels exhibited a high shrinkage during drying, the mechanical strength

of the binders could not be tested with shape-casted samples. Instead, films were produced by

drying with the undried hydrogel solution concentrations of 5% (k-carrageenan), 2.5% (sodium

alginate), 4% (agar), 5% (chitosan), 5% (mammal gelatin), and 5%-w/v (cold-water fish gelatin).

Other hydrogel concentrations were tried but discarded due to the formation of cracks and strong

warping under drying. The hydrogel solution concentration before drying was expected not to

influence the final mechanical strength of the dried films significantly since the dried concentration

would be the same.

The hydrogels were prepared as described in Section 4.2.2-4.2.7 and filled into large Petri dishes

to a filling height of around 1cm. To prevent strong adhesion, the Petri dishes were nano-coated

with a glass spray from the company NASIOL. The dishes were kept under room temperature of

23°C and air humidity of 40-50% in a well-ventilated environment with a steady airflow. Due to

the varying concentrations, the time for drying varied. A fully conditioned sample could be

assumed when the thickness of the film was constant over time. Due to the thinness of the produced

films of around 0.1mm, a fast adaptation to the surrounding moisture conditions was assumed.

The films were cut into bone-shaped samples with a laser cutter to prevent unintended breakage

through blade cutting. The cut dimensions specified in Figure 4-5 were inspired by ASTM D638

– 14 but broadened to reach better robustness for handling the samples.
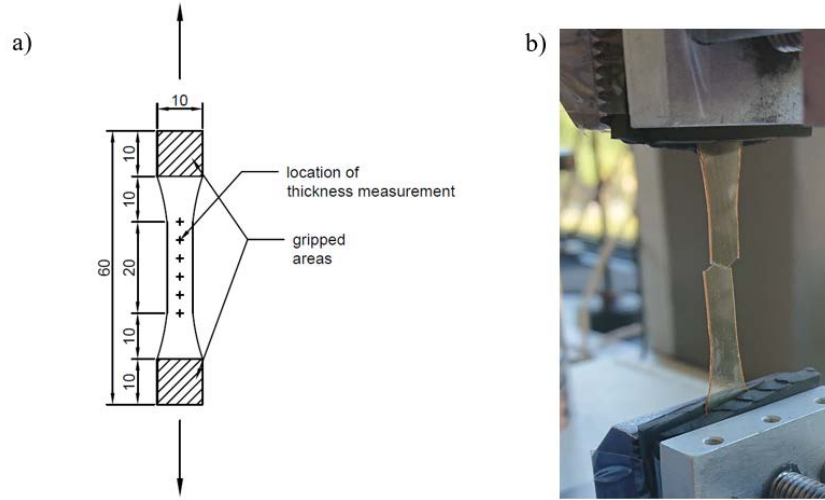
Figure 4-5 The dimensions of tensile samples from the film. The shape was inspired by ASTM D638 – 14. a) working principle
and dimensions in [mm]. b) a photo of the actual test.

To determine the cross-section of the sample's failure area and to compute the maximum stress

after testing, the thickness of the samples was measured at six locations, as shown in Figure 4-5,

with the gravitational dial gauge 'S_Dial nano' from SYLVAC.

The tensile tests were conducted with a TA.XT.plus Texture Analyser and a 300N load cell.

Testing was conducted in deflection-controlled made with a rate of 2mm/s. The samples were held

at the locations specified in Figure 4-5 with aluminum grippers coated with a 1mm thick rubber to

prevent sliding.

The tensile strength at breaking was calculated with the following:

$$f_{T,u}(MPa) = \frac{F_{max}\ (N)}{w_{failure}(mm) \cdot t_{failure}(mm)} \qquad (4.1)$$

here F_{max} is the maximum force measured, $w_{failure}$ the width at the failure position and $t_{failure}$

the thickness at the failure position, possibly interpolated between two of the five measured values. Samples were excluded when the failure occurred at the grippers. A minimum of 13 valid samples for each hydrogel was used for the presented results.

4.2.10. Adhesion tests

The adhesion capability of the binding materials to the sand grains was determined. Therefore, a silica glass plate was roughened with an eccentric grinder with sanding paper of the roughness 80. After that, the glass with a thickness of 3mm was cut into 20mm squared pieces and connected with epoxy resin to a substrate material from stone, as illustrated in Figure 4-6.
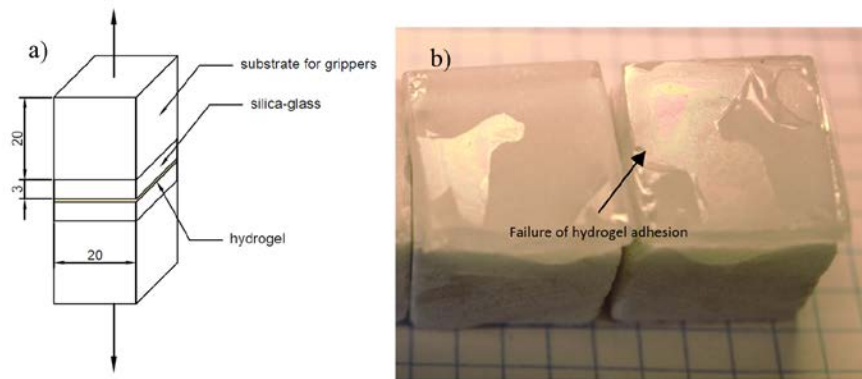
Figure 4-6 The adhesion tensile tests – a) dimensions and working principle [mm], b) failed adhesion sample with visible hydrogel interface.

The hydrogels were prepared with a concentration of 5%-w/v, as described in Sections 4.2.2-4.2.7. The binder was used to adhere to two of the roughened glass surfaces. The samples were left for drying for 96 hours under the same conditions as the tensile samples in Section 4.2.9.

After drying, the adhesive tensile properties between the binder and the glass surface were measured analog to Section 4.2.9. The maximum stress was calculated with the recorded maximum force at breakage and the adhesion surface area.

Two failure modes could be expected, i.e., the binder's cohesion and adhesion failure. Therefore, it was controlled by light microscopy that the failure occurred between silica glass and binder, representing the intended adhesion failure.

4.2.11. Compression tests of composite

Composite cubes were tested in compression. The shapes were inspired by the cubed samples of EN196 (Dansk Standard, 2016), the norm for cementitious mortar testing. Smaller dimensions of the cubes were chosen to compensate for the long drying time of the material and the intended slender constructions made from 3D printing. A homogenous mechanical behavior of the composite is reached by defining the side length as at least 3.5 times greater than the largest grain size dimension as described in EN 12390 (Dansk Standard, 2013). A length of 20mm was chosen. In earlier trials it was observed that hydrogels can migrate to exposed surfaces while drying and, thus, alter the material's homogeneity. Smaller sample sizes were also chosen to limit the migration distances, adding to the uniformity of the sample.

For all samples, the dry mass of the binder to the mass of sand was noted as composite concentration, and the solution concentration of the binder in water specifies the material's wet state.

Compression cubes were prepared in 2 batches: Batch #1 used a small concentration of 0.73g dried binder to 100g sand and solution concentrations of 2% (κ-carrageenan), 4% (sodium alginate), 2% (agar), 3.75% (chitosan), 4% (mammal gelatin) and 5%-w/v (cold-water fish gelatin). Batch #2 tested a variety of composite concentrations, which are described in Section 4.3.

For batch #2, the solubility limit solution concentrations from Figure 4-4 were chosen for mixing. The hydrogels were prepared as described in Sections 4.2.2-4.2.7. The hydrogels were then blended with a spatula for 2-3 min into the sand until homogeneity was achieved. The material was cast into a squared pipe mold with the inner dimensions of 20x20x20mm, opened at the top and bottom. After cooling, the material could be removed from the form with a stamp and left for hardening under ambient conditions, as described in Section 4.2.9. For this methodology, the material needed to exhibit sufficient yield strength to keep its shape after demolding in the fresh

state and good workability to be moldable. Concentrations with greater water content, as in Sections 4.3.4 and 4.3.5, could not be mixed since the material could not sustain its shape after demolding. This goes in line with the intended 3DCP application

The drying time of the binders varied immensely due to the varying concentrations and binders. With a fine-scale (Sartorius M-power), the decrease in weight was recorded every 24 hours. The samples were conditioned when the weight did not decrease for three successive days. The drying duration was between 7 and 19 days, depending on the concentration and binder. To avoid inhomogeneous drying, the cubes were turned 180º every two days.

Due to the largely varying strengths and compression forces necessary to fracture the samples, the TA.XT.plus Texture Analyser with a 300N load cell was used as a basis for all tests. Would the maximum compression force exceed 300N, an Instron actuator with a 10kN load cell was used to record the maximum compressive force. A deflection-controlled test was performed with a speed of 2mm/s. For almost all samples, a clear maximum could be identified. For some of the samples, an elastomer-like behavior was observed. For these cases, the compressive strength was determined by the yielding point of the composite.

4.2.12. Density
In the dried state, the density of the composite materials was determined by the weight of the samples, measured with the fine-scale Sartorius M-power, divided by the volume of the cubes. The volume was calculated from the specimen's averaged dimensions, measured with a digital caliper.

4.2.13. Shrinkage
Shrinkage was measured by comparing the final side length of the compression samples described in Sections 4.3.4 and 4.3.5 in the dried state with the original dimensions after demolding in the wet state. The length was measured with an electronic caliper.

4.2.14. SEM
Scanning electron microscopy pictures (SEM) were recorded with 250x magnification, 15kV, and

100Pa pressure. The long exposure of the samples to the electron beam before recording images was avoided since it would illuminate the binders by electrostatic charging. The fracture surface of composite samples with the optimum concentration for mechanical strength, as described in Section 4.3.6, were investigated after compression failure to conclude on the failure mechanisms of binder and aggregate.

4.2.15. FT-IR

A PIKE Technologies GladiATR testing setup was used on a Nicolet 6700 FT-IR Fourier-Transform Infrared Spectrometer (FT-IR) to identify the properties of molecular structures. The spectral range between 400-4000cm-1 of the hydrogel batches was recorded in four different states: 1) Raw, dried granular or powder from suppliers; 2) Films prepared analogously to Section 4.2.9, 3) wet binder hydrogels prepared as in Section 4.2.2-4.2.7 with the solubility limit concentrations of Section 4.2.8, that are being dried during the testing on the FT-IR apparatus, and 4) composites, that were dried during testing.

The recorded spectrum allows to conclude on the molecular structure and composition of the sample. The spectral fingerprint of the investigated materials shall help in understanding the chemical composition of the raw binder materials and their response to the drying process as hydrogels in the fresh composite material. The preparation and application of the samples done in the following steps:

1) granular material was ground to powder. All powders were applied onto the measurement crystal and pressed firmly to its surface by the instrument fixation pin (Figure 4-7 a).

2) For the films, a small plate was used to secure contact of the films with the measurement surface and full light beam reflection (Figure 4-7 b).

3) and 4) The wet material was applied directly onto the measurement surface covering the whole crystal. A ventilated plastic hood was placed over the sample to circulate dry air to accelerate the

drying process (Figure 4-7 c).
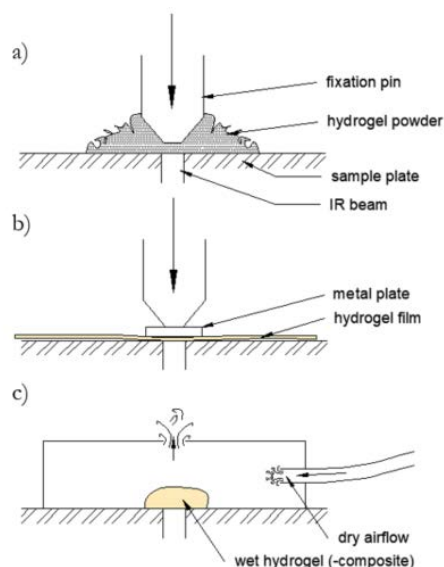
Figure 4-7 The FT-IR testing of a) powder, b) film, and c) drying gel samples.

Background tests were performed and subtracted from the measured spectrum for all samplings. For 1)-2), three tests were recorded for each type of material. For drying tests as in 3)-4), samplings were repeated every 5 min to record a concentration drift caused by reducing free water. After the changes seemed to stagnate, the tests were stopped.

4.3.   Results and discussion

4.3.1. Cohesive tensile strength

The cohesive tensile strengths of the hydrogel film samples are shown in Figure 4-8. The tensile strength of all samples was between ~50-160 MPa. The polysaccharides, presented as the first four values starting from the left, show the highest cohesive strengths with mean values in the range of 80.8MPa-142.9MPa. The protein binders of mammal gelatin and cold-water fish gelatin are presented as the last two values in Figure 4-8. Their mean tensile strengths were lower than all polysaccharide films, with 57.7MPa-71.2MPa. All samples of films showed a brittle and sudden failure. One representative failure location for each hydrogel can be seen in Figure 4-9. All

biopolymer films refer in the order of magnitude to the strengths of other biopolymer-based films

used for packaging (Rhim and Ng, 2007) or medical applications (Khunawattanakul et al., 2010).
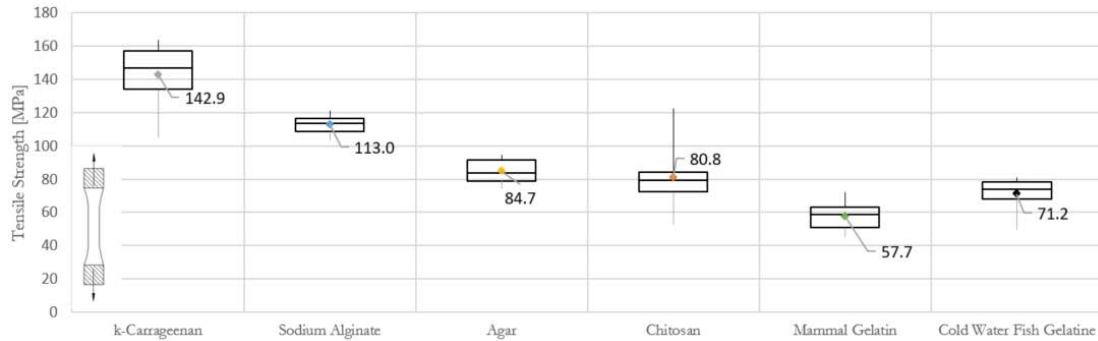
Figure 4-8 Cohesive ultimate tensile strength of dried hydrogel films. The box charts show the median, upper and lower quartile

and maximum and minimum measured values. The dot marker with number identifies the mean. n≥13
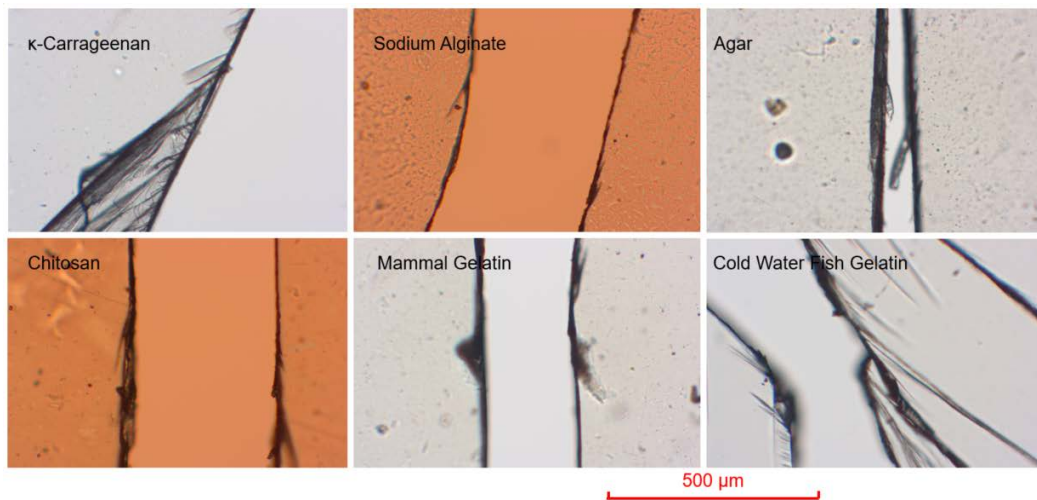
Figure 4-9 The breakage of tensile samples according to results presented in Figure 4-8. All films measured show a brittle failure.

4.3.2. Adhesive tensile strength

The adhesion strength of the dried hydrogels to silica glass can be seen in Figure 4-10. All values

are located between 0-1.5MPa. The polysaccharide-hydrogels were generally weaker (0.063MPa-

0.61MPa) than the protein-based binders (0.731MPa-1.022MPa). κ-carrageen had the lowest

adhesion strength measured, followed by agar. Chitosan had the strongest adhesion of the

polysaccharides (0.61MPa). Cold-water fish gelatin showed the highest value of the protein

binders with 1.02 MPa. Mammal gelatin was the weakest protein binder, performing better than

the polysaccharide binders.

The interfacial strength between silica-glass and the dried hydrogel can be considered significantly lower than the cohesive tensile strength recorded and shown in Figure 4-8. The measured cohesive strength was at least 33 times larger than the adhesive strength. The relative tendencies between the hydrogel adhesion strengths in Figure 4-10 were opposite to the cohesion strengths in Figure 4-8, i.e., a strong cohesion was connected with a lower adhesion strength and the opposite.
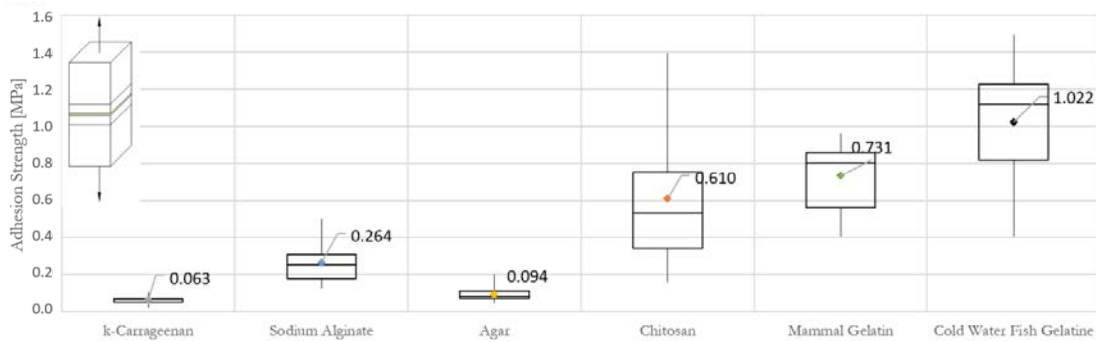
Figure 4-10 The adhesive ultimate tensile strength on roughened silica glass. The box charts show the median, upper and lower quartile and maximum and minimum measurements. The dot marker with number identifies the mean. n≥7

4.3.3. Composite compression strength with an equal composite concentration

Figure 4-11 shows the compressive strength of composites with a low but equal dried composite concentration of 0.73g/100g sand. Chitosan reached the largest mean compression strength of 3.01MPa. Within the polysaccharide binders, similar tendencies as for the adhesive tensile strength in Figure 4-10 were observed. Sodium alginate presents the second-largest strength, κ-carrageenan, and agar has a weak strength.
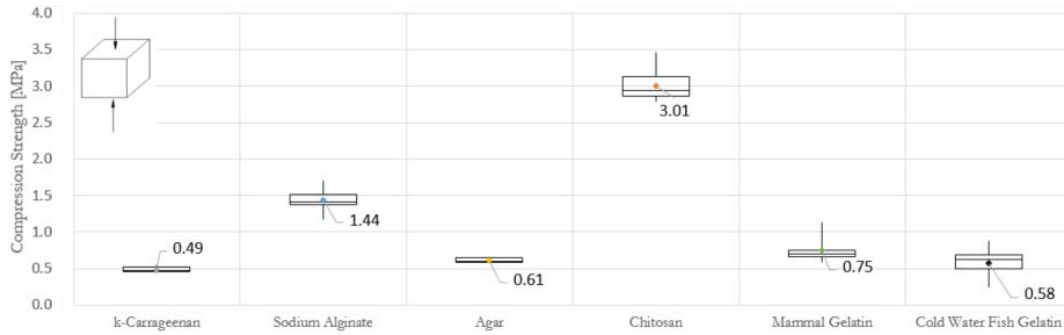
Figure 4-11 The composite compression tests – low, equal composite concentration of 0.73g/100gsand. The box charts show the median, upper and lower quartile and maximum and minimum measurements. The dot marker with number identifies the mean. n=10

In this composite with low composite concentration, the binder is not acting as a matrix since the dried binder content is significantly lower than the amount of sand. The binder is expected to hold the sand grains in place, adhering to the contact surfaces between the sand grains. Since the cohesion of the material is significantly larger than the adhesive strength, the interface is expected to fracture first. Therefore, the composite strengths in Figure 4-11 follows the adhesion strength of the polysaccharides displayed in Figure 4-10.

The protein binders, however, do not follow this trend. Mammal and cold-water fish gelatin composites showed a heterogenization under drying for this low concentration. During testing and failure, it could be observed that the binder concentration was higher at the surfaces of the cubes compared to locations in the center of the cubes. Chitosan is the most effective binder for small concentrations.

4.3.4. *Polysaccharide bound composite compression strength – concentration sweep*

In Figure 4-12, the composite compression strength of the polysaccharide binders is shown in dependency on its dried binder content. The tendencies between the hydrogel types are the same as presented for the composites with equal and low binder content in Figure 4-11 and the adhesive strength in Figure 4-10. Chitosan had the highest compression strength, sodium alginate second, and agar and κ-carrageenan had the lowest strength. Two scenarios can be identified for the composite's maximum strength distribution: 1) chitosan has a peak value at the concentration of 2g dried binder content per 100g sand. 2) sodium alginate, κ-carrageenan, and agar show an increasing strength for an increasing binder content. The maximum measured concentrations of Figure 4-12 were also the sampling limit due to the material's low yield strength in the early age state. Higher concentrations could not hold their shape after demolding and were therefore excluded. The composites without sufficient yield strength do not qualify for the intended use in a 3D printing process.
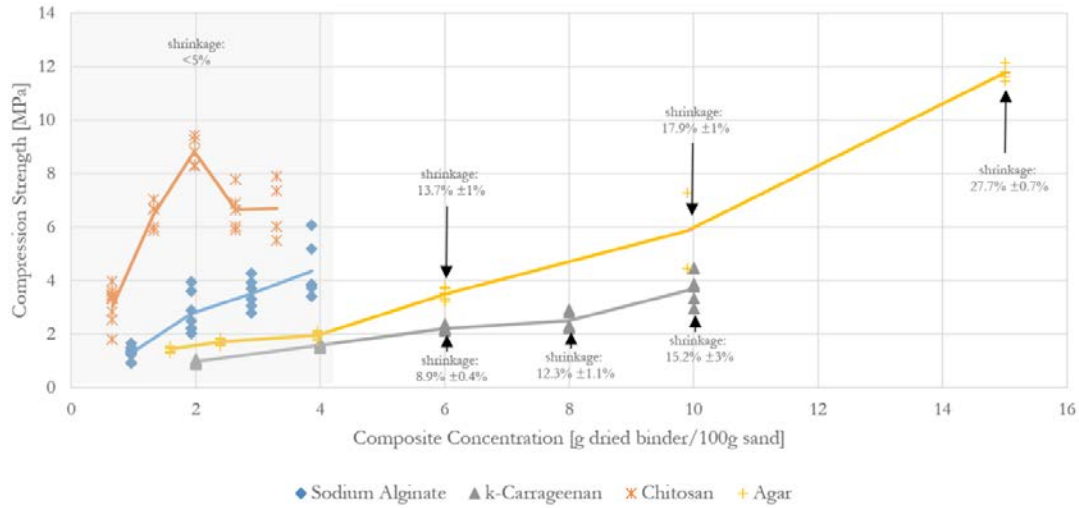
Figure 4-12 The composite compression tests concentration sweep – polysaccharide composites
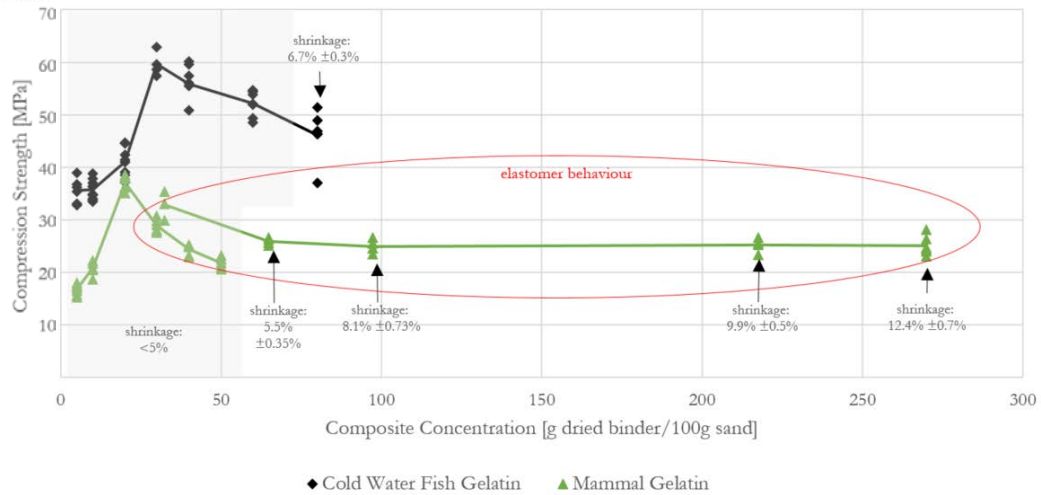
Figure 4-13 The composite compression tests concentration sweep – protein binders

Shrinkage of the respective concentrations was measured and can be seen in Figure 4-12. A more than 5% shrinkage was considered unsuitable for the composite's construction application. The optimum strength without exceeding the 5% shrinkage limitation of sodium alginate, κ-carrageenan, and agar can be reached at around 4g dried binder content per 100g sand (composite concentration). The highest mean compression strength of κ-carrageenan, sodium alginate, agar, and chitosan can be identified with 1.58MPa, 4.35MPa, 1.96MPa, and 8.81MPa, respectively, for the tested concentrations and limited by shrinkage of 5% (see Figure 4-14).

In comparison, (Nakamatsu et al., 2017) reports a compression strength of 4MPa for an earth-based composite stabilized with a 2% w/v k-carrageenan solution. (Galán-Marín et al., 2010) presents a 3.77MPa maximum compression strength of 19.75%wt sodium alginate stabilized earth material. (Menasria et al., 2017) shows a maximum of 7MPa for kaolin clay with 5%wt sodium alginate. All references use clay-based soils. Compared to the here-tested bound sand composite, the values of the clay-based composite seem to be similar or higher. This is expected due to the binding properties of the clay materials. Generally, the compression strengths of earth and sand-based composites seem to be in the same order of magnitude. (Khatami and O'Kelly, 2013) presents stabilized sand with 4%wt agar for geotechnical applications. Compression strength of 490kPa was reported and hence lower than the here tested. Contrary to this study, (Khatami and O'Kelly, 2013) use a different sample preparation methodology, allowing the biopolymer solution to penetrate through the already-shaped sand sample.

4.3.5. *Protein-bound composite compression strength – concentration sweep*

The strength of varying concentrations of the protein binders mammal gelatin and cold-water fish gelatin is shown in Figure 4-13. The cold-water fish gelatin shows for all concentrations higher values than the mammal gelatin. Both offer a maximum peak below 50g dried binder concentration per 100g sand. The maximum peak of mammal gelatin is at 30g dried binder/100g sand concentration with a mean compression strength of 37.8MPa. The maximum peak of cold-water fish gelatin was measured at a slightly higher concentration of 40g dried binder/100g sand with a mean compression strength of 59.61MPa. Generally, a brittle failure mode could be observed for the lower concentrations. For the higher concentrations of mammal gelatin, a plateau was identified at around 26MPa. These compression tests showed an elastomer-like behavior.

A critical shrinkage value of 5% for both binders is reached around 50g/100g composite concentration. The critical value is larger for the cold-water fish gelatin than for the mammal

gelatin.

(Rosa et al., 2020) presents a study with similar objectives to this study. (Rosa et al., 2020) uses the blood protein bovine serum albumin to bind sand. The maximum compression strength in (Rosa et al., 2020) was 22.7MPa at a 16% binder/sand ratio, thus lower than the here-tested proteins. Since the testing speed and sample sizes differed from this study, it cannot be concluded which of the proteins is better suited as a binder for sand.

4.3.6. *Maximum compression strength of composites*

The protein-bound composites could be documented with a higher compression strength and dried binder concentration than the polysaccharide-bound composites. When collecting the compression strengths at optimum binder concentration with consideration of the 5% shrinking limit, the maximum compression strengths in Figure 4-14 could be identified. When comparing the graph with the adhesive strengths of Figure 4-10, the tendencies seem to be similar: cold-water fish gelatin, mammal gelatin, and chitosan showed the highest strength, while agar and κ-carrageenan reached the lowest strength. Since the cohesive strength was significantly larger than the adhesive strength, the adhesive strength is considered to be critical for the composite's failure behavior.

		κ-Carrageenan	Sodium Alginate	Agar	Chitosan	Mammal Gelatin	Cold Water Fish Gelatin
■	max strength [MPa]	1.58	4.35	1.96	8.81	37.08	59.61
□	concentration [g dried binder/100g sand]	4	3.7	3	2	20	30
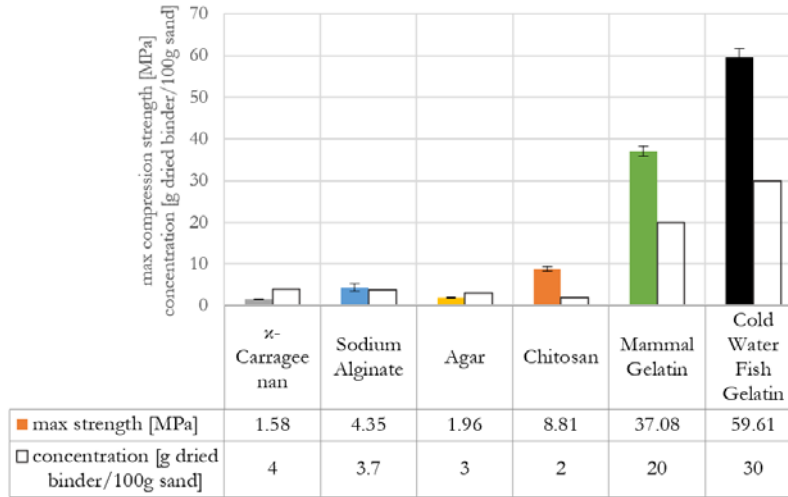
Figure 4-14 The maximum compression strength in dependency on its respective composite concentration. These results were extracted from Figure 4-12 and Figure 4-13.

Figure 4-15 shows the SEM images of a fractured surface after a compression strength test of the optimum concentrations (see Figure 4-14). The interface properties are well visible. Figure 4-15 shows, from left to right, increasing adhesion properties and the highest possible concentration for the proteins. In Figure 4-15a), d) (agar and κ-carrageenan), the weakest adhesion can be identified. The grains barely have contact with the aggregates. On the contrary, Figure 4-15c),f) (mammal- and cold-water fish gelatin) show good adhesion and a high concentration of dried binder. The grains are held in place after the compression failure.
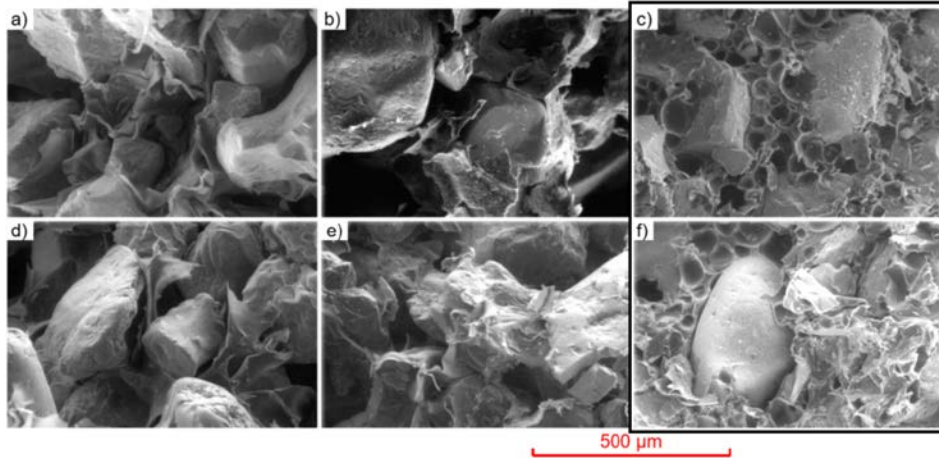
Figure 4-15 The SEM image of compression failure surface of highest strength composite concentration as in Figure 4-14: a) agar, b) sodium alginate, c) mammal gelatin, d) k-carrageenan, e) chitosan f) cold-water fish gelatin. Protein binders in a black frame.

Figure 4-15 also shows the difference in binder solution concentration. As shown in Figure 4-4, the protein binders could be mixed with a significantly higher concentration than the polysaccharide binders maintaining their workability. During drying, the evaporating water causes the formation of pores in the composite. Therefore, the least binding effect can be seen in Figure 4-15a-b) and d-e) for the binders with high initial water content. The polysaccharide binders connect the sand grains rather than represent a binder matrix. A matrix can be identified for the protein binders in Figure 4-15c) and f). The large initial concentration of the binder solution leaves less water in the fresh composite. The binder volume decreases with the amount of evaporated water, and more material remains from the protein binders than from the polysaccharides. This relation could also be identified in Figure 4-16 by plotting the initial water content of the composites with the highest compression strength over their respective density. It can be seen that the density increases with decreasing initial water content, i.e., a decrease in pore space. The initial water content is also correlated to the strength of the composite: The larger the initial water content, the lower the strength.
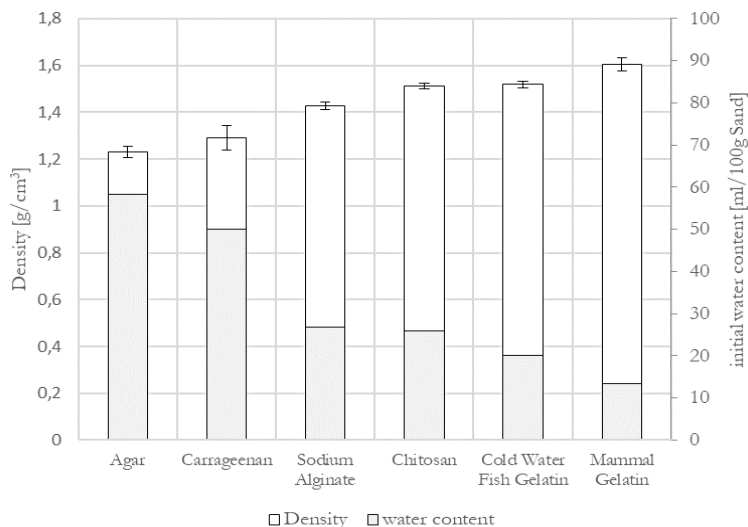
Figure 4-16 The density and initial water content of composite cubes with optimum binder content (see Figure 4-14). The error bars show the standard deviation. Both bars have their origin in zero. n=4

4.3.7. FT-IR and structure-property relations

The FT-IR spectra of the six different hydrogels can be seen in Appendix 4.I. The spectra were recorded and juxtaposed in powder form and processed dried film as described in Section 4.2.15. Before and after processing, chitosan, mammal gelatin, and cold-water fish gelatin do not change their FT-IR spectra significantly (compare Appendix 4.I), indicating that the processing of the granulate did not denature its original molecular form. The gel preparation could be reversed by drying. K-carrageenan, agar, and sodium alginate seem to change their properties in terms of thickening significantly when being heated or dissolved in water. A change can also be observed in the IR spectrum between raw powder form and processed film (see Appendix 4.I). Peak changes between wavenumbers 1250cm-1-1750cm-1 could be observed.

The interface properties between the silica sand grains and the hydrogels were expectedly dependent on the electrostatic interactions. The silicate surfaces of the aggregate are usually negatively charged in aqueous solutions (Behrens and Grier, 2001). The adhesion was therefore expected to be dependent on polar or charged molecular groups of the polymer, such as the partly

protonated amine groups of chitosan in acidic solutions.

Sodium alginate and κ-carrageenan have a negative charge (see Figure 4-1). This is expected to justify their lack of adhesion to the silicate materials. On the contrary, the protein binders of mammal gelatin and cold-water fish gelatin have a large variety of differently charged amino acids (see Figure 4-1), giving them a good chance for adhesion.

Chitosan shows, in addition to its hydroxyl groups, an amino group. Hydroxyl groups are present in all presented polymers and do not seem to justify good adhesion. In acidic solutions, the amino groups are partly protonated and, therefore positively charged (Samimi Gharaie et al., 2018)(Donayre et al., 2018), which is expected to be the reason for the strong adhesion of the hydrogel. (Yong et al., 2022) and (Mokhtar et al., 2018) both reported an FT-IR spectrum shift in chitosan caused by electrostatic interactions between the amino group of the chitosan and an oxygen atom of another molecule. A connected amide band II shift can also be seen in the FT-IR spectrum in Appendix 4.II. As seen in Figure 4-17, this can also be observed for this chitosan composite. Figure 4-17 refers to Appendix 4.II, where IR spectra were recorded under drying for pure gel and composite. Figure 4-17a) shows the amide band II peak for these two scenarios. It can be seen that the two scenarios develop with varying tendencies under drying. An electrostatic interaction between the amino group and the silica grains is expected.
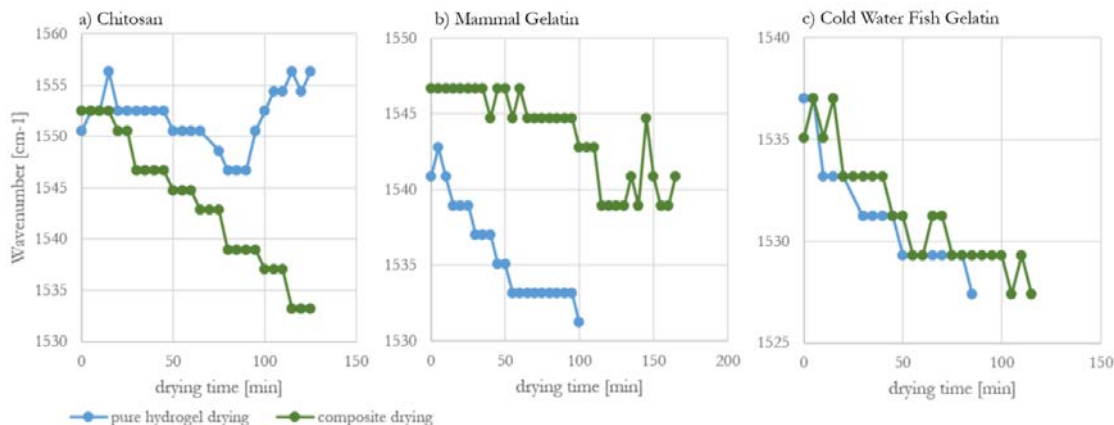
Figure 4-17 The FT-IR recordings of amide band II shift during drying for a) chitosan, b) mammal gelatin, and c) cold-water fish gelatin. Respectively recorded under drying of the pure hydrogel (blue) and composite under drying, i.e., a hydrogel with sand (green). The plotted peak can be identified in the FT-IR spectrum in Appendix 4.II.

Since mammal- and cold-water fish gelatin have also (charged) amino groups (see Figure 4-1), an electrostatic interaction was also expected in this case. Figure 4-17b) and c) show the amide II bands for mammal gelatin and cold-water fish gelatin. Mammal gelatin shows varying amide II band sweeps under drying for the pure and composite states. No altering shift could be observed for cold-water fish gelatin. Shifts in the amide II band are observed for pure hydrogel and composite. Due to the large variety of sequences and amino acids, a more complex interaction between sand grain and biopolymer is expected for gelatins, and no general interactions can be stated.

The polysaccharides κ-carrageenan, agar, do not show a significant shift in their peaks, as seen in Appendix 4.II. Sodium alginate shows minor shifts compared to composite and pure hydrogel, which could be due to the intermolecular interactions of the sodium ion Na+. However, this could not be verified.

In summary, the biopolymers with mostly uncharged hydroxyl- or negatively charged groups do not show good adhesion (κ-carrageenan, agar, sodium alginate). The molecules with various side groups (cold-water fish gelatin, mammal gelatin) and positively charged amino side groups

(chitosan, cold-water fish gelatin and mammal gelatin) seem to work well in adhesion. They can contribute to forming a strong composite with silica sand.

4.4.   Conclusion

The six natural polymers κ-carrageenan, sodium alginate, agar, chitosan, mammal gelatin, and cold-water fish gelatin were tested for their suitability as binding material in a structural biologically based concrete composite with sand. As a boundary, the materials should show both good workability and yield strength in the fresh state to sustain their shape under gravitational loading and to be moldable. All the natural polymers could make a composite material with sand that could withstand compression forces to a certain extent. The proteins functioned the best to bind sand.

It was shown that all natural polymers in a dried state proved strong cohesion properties. The polysaccharides (κ-carrageenan, sodium alginate, agar, and chitosan) absorb more water per unit mass than the proteins. Therefore, denser materials could be reached with the protein binders mammal gelatin and cold-water fish gelatin. The weakest adhesion to silicate materials was found for κ-carrageenan and agar. The strongest adhesion was found for protein binders due to their complex and varying amino acid structure. Also, chitosan adhered well and showed the strongest adhesion of the polysaccharides binders. Generally, the adhesion strength was found to be significantly lower than the cohesion strength, presenting an early failing interface in the composite. The adhesion strength of the biopolymers correlates, therefore, to its composite strength. Of the polysaccharides, chitosan was found to form the strongest composites, with a composite concentration of 2g dried binder/100g sand. It reaches the highest compression strength with the least amount of binding material. The protein binders proved to form the strongest composite of all natural polymers tested at a concentration of 20-30g dried binder/100g sand.

Chitosan, mammal gelatin, and cold-water fish gelatin adhere well to the silicate aggregates and form strong composites. The cold-water fish gelatin can be dissolved in the highest concentration and forms, the strongest composite with a strength of around 60MPa.

The compression strength of natural polymer-bound sand composites; especially gelatin-bound sand composites can present mechanical strengths in the same order of magnitude as cementitious concrete composites and is, therefore, applicable to constructions.

Acknowledgments

5. Rheological properties

Photo: media_k (Mikal Schlosser) taken as requested by Julian Christ, printing of biologically-based concrete composite.

In Chapter 4, all six natural polymer composites with the varying binders of κ-carrageenan, sodium alginate, agar, chitosan, mammal gelatin, cold water fish gelatin, presented some mechanical strength and could therefore be identified as load carrying material. However, the mechanical strengths of the composites varied largely. The gelatin-based composites were identified as the most suitable for load bearing applications, while the polysaccharide composites showed weaker strengths.

For the application on a 3D printing process, the natural polymers are expected to show fast setting rheological properties after extrusion. The presented six natural polymers can create a change in rheological properties differently, either by a thermosetting process or a thermoplastic principle (see also Chapter 3).

The further investigated natural polymers, the intended utilization principle (thermosetting or thermoplastic) and the connected printing process was decided, based on the investigated mechanical properties in Chapter 4. Since gelatin showed the best mechanical properties, the connected thermoplastic principle of the material was utilized.

Both gelatins, cold water fish gelatin and mammal gelatin, show this thermoplastic setting principle. However, cold water fish gelatin was observed to have a significantly lower gelling point than mammal gelatin. The gelling point of cold water fish gelatin is below normal ambient temperature, which could lead to issues with an intended printing process that relies on temperature change and cooling in ambient conditions. Mammal gelatin, in the contrary, showed a solidified state under normal ambient conditions. Its composite was therefore chosen as the primary material for further investigation.

Chitosan and sodium alginate did not show any setting with temperature change (see also Chapter 3) and were therefore excluded from further studies. κ-carrageenan however, could show a very sudden and strong thermoreversibility with temperature change. This was elaborated as interesting for a temperature controlled printing process and therefore included in further investigations.

In the following, the temperature dependent rheological properties of a mammal gelatin and κ-carrageenan based composite are investigated and compared. The understanding of the flow characteristics aimed on designing the printing parameters, i.e. printing temperature and process constrains.

The content of this chapter is presented in form of a journal publication. The reference information can is:

J. Christ, A. Perrot, L.M. Ottosen, H. Koss. 'Rheological characterization of temperature-sensitive biopolymer-bound 3D printing concrete'. *Submitted and currently under review in*: Building and Construction Materials, 2023, manuscript reference no.: CONBUILDMAT-D-23-01335.

Rheological characterization of temperature-sensitive biopolymer-bound 3D printing concrete

Julian Christ[a],*, Arnaud Perrot[b], Lisbeth M. Ottosen[a], Holger Koss[a]

[a]Department of Civil Engineering, Technical University of Denmark, Brovej 118, 2800 Lyngby, Denmark

[b]Univ. Bretagne Sud, UMR CNRS 6027, F-56100 Lorient, France

Abstract

3D concrete printing materials with advanced rheological properties are being developed to realize more structurally optimized and sustainable structures. However, traditional mixtures use large shares of cementitious materials presenting reduced sustainability. In this paper, thermo-reversible mammal gelatin and κ-carrageenan are explored as alternative binders for temperature-controlled concrete printing. Rheological properties were found suitable at solution concentrations of 80-120%-w/v mammal gelatin in a 40%-w/w biopolymer-aggregate composite and 3%-w/v κ-carrageenan in a 50%-w/w composite at temperatures of, respectively, 50°C and 65°C. The corresponding yield stress increase from 0.1-107kPa under cooling to 20°C demonstrated good buildability.

Keywords: gelatin, κ-carrageenan, 3D printing, concrete, biopolymer, yield stress, modulus of elasticity, printability

5.1. Introduction

3D concrete printing (3DCP) shows the potential to drastically reduce environmental impact and increase the economic efficiency of the construction sector (Paul et al., 2018)(Schutter et al., 2018)(Perrot, 2019). The process lowers geometrical constraints by making formwork redundant (Y. Liu et al., 2022) and placing material freely in a three-dimensional space. Sophisticated optimization algorithms can design building components with optimum material usage, which 3DCP can then realize. The degree of geometrical complexity that can be built with 3DCP is the limiting optimization factor which defines its environmental performance (Schutter et al., 2018). Therefore, the urge to reach higher degrees of freedom can be identified (Vantyghem et al., 2020a)(Gosselin et al., 2016). Broadly seen, 3DCP is limited to a vertical build-up since the setting characteristics of cementitious composites are relatively slow and difficult to control, limiting, in theory, possible high degrees of optimization. Conventionally, the process either relies on (1.) the thixotropic behavior and structural build-up of the material (Le et al., 2012)(Panda et al., 2018)(Roussel, 2018)(Mechtcherine et al., 2020) or (2.) an additional two-component system that injects accelerators into the nozzle of the extruder (Wangler et al., 2022)(Gosselin et al., 2016). Since aggregate size is limited by the scale of the printer's nozzle, both processes require higher cement content than conventional concrete composites (Kaszyńska et al., 2020), presenting a drawback on environmental performance even if the use of structural optimization can save material.

Other printing materials like geopolymers (Panda et al., 2018)(Lim et al., 2018), clay and earth-based materials (Kontovourkis and Tryfonos, 2020)(Perrot et al., 2018a), polymers (Teizer et al., 2016) and bio-composites (Sinka et al., 2020) are being explored for use in 3D printing for construction to improve the environmental compatibility. Also, concrete composites that replace

the cementitious content with natural polymer hydrogels show potential for building applications (Christ et al., 2019b)(Rosa et al., 2020). Some of these hydrogels have temperature-sensitive properties, i.e., thermo-reversibility, which can ease the setting control of the material during the print via an increase of the temperature during the pumping and extrusion steps.

This research investigated the printability and connected rheological properties of biopolymer-concrete-composites made from the hydrogels mammal gelatin (MG) or κ-carrageenan (kC) and mineral aggregates. It identifies the potential benefits compared to cementitious printing materials.

Hydrogel-bound composites can obtain compression strengths in the order of magnitude as conventional concretes (Christ et al., 2019b). Resourced from butchery waste (Gomez-Guillen et al., 2011) and seaweed (Thomas et al., 2013), the production of hydrogel binders is potentially more environmentally friendly through lower production temperatures of around 100°C (Gomez-Guillen et al., 2011)(Refilda et al., 2009), compared to cement (~1450°C).

Similar composites for 3D printing in constructions were investigated by (Biggerstaff et al., 2021)(Soldevila et al., 2014). However, the use of kC and MG in a heated extruder for construction applications is still unexplored.

Besides these construction applications, the hydrogel binders MG and kC are known as thickeners in food (Nhari et al., 2012)(Błaszak et al., 2018) and the biomedical industry (Foox and Zilberman, 2015)(Mokhtari et al., 2021). Another application is in the field of 3D printing of human organs and food (Biazar et al., 2018)(Godoi et al., 2016).

This research presents a printability assessment of hydrogel-based concrete with different binder concentrations, binder-to-sand ratios, and printing temperatures. Concretes with printable properties were evaluated and related to rheological properties such as complex modulus, loss

factor, and yield stress under varying temperatures and shearing strains in oscillatory and rotational rheometry.

5.2. Materials

5.2.1. Aggregates

A silica sand with a maximum grain size of 250µm was used for all experiments. As conventionally chosen for extrusion-based printing processes (Buswell et al., 2018), small grain sizes were selected to enable a smooth print process. Additionally, the exclusion of larger particles ensures homogenous behavior in rheometer tests with a plate-on-plate setup without excessive gap size (>8 times the maximum grain size) (Ranjbar et al., 2021). The grading curve was performed using EN 933 (Dansk Standard, 2012) and is shown in Figure 5-1. The sand shows its greatest mass within the grain sizes of 90-250µm. A low fine particle content (below 0.063mm) of 0.78%-wt. and a moisture content of 0.03%-wt. were recorded.
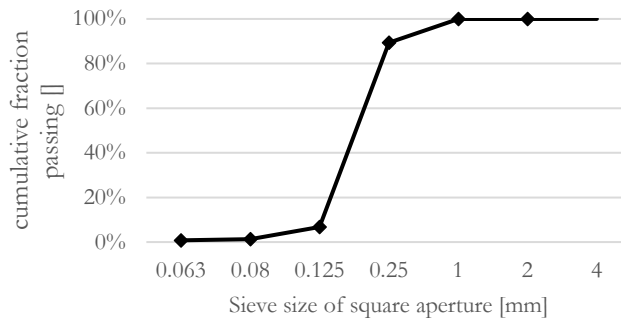
Figure 5-1 Grading curve of used silica sand specified with 0.09mm-0.25mm, quantified after EN 933 (Dansk Standard, 2012)

The light microscopy pictures in Figure 5-2 present sand grains with sub-rounded to sub-angular geometrical properties. The mineralogical composition was identified with an X-ray diffractometer as merely consisting of SiO_2.
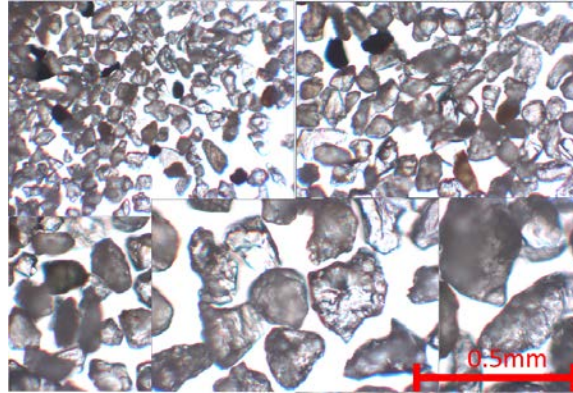
Figure 5-2 Light microscope recordings from sieving analysis of used sand with 10x objective, showing retained grains on sieves (from top left to bottom right): Pan, 0.063mm, 0.08mm, 0.125mm, 0.250mm.

5.2.2. *Hydrogel-binder*

This study investigated two hydrogel binders, one protein binder and one polysaccharide binder. The protein binder is MG, and the polysaccharide binder is a κ-type carrageenan. Both binders are hydrogels chosen due to their thermoplastic phase change character (Campo et al., 2009)(Aykin-Dinçer et al., 2017). MG was purchased as granular material through the tool manufacturer DICTUM (DICTUM, 2019) (Art. Nr.: 450141). kC was used in powder form and obtained from Sigma-Aldrich (Mat. Nr.: 22048-100G-F).

Generally, both binding materials were prepared as hydrogels by mixing with water and heating the solution over the material's specific gel point. To produce a concrete composite material, heated sand is added to the binder. Under mixing, a homogenous composite material can be made that solidifies when cooled. The maximum strength of the hydrogel-bound composite materials is reached by fully or partially removing the water through drying or conditioning. Previously, mean compression strengths of over 20MPa could be recorded for MG composite (Christ et al., 2019b) samples conditioned to average environmental moisture and temperature states in Denmark.

5.2.2.1.Mammal gelatin

MG is a biopolymer produced by partial hydrolysis of collagen through decocting, alkaline or acidic treatments of animal skin, connective tissue, or bones (Nhari et al., 2012). The extracted biopolymer is a protein made of long-chained polymer strands of various amino acids. An amino acid analysis could show that the used MG is primarily made up of the amino acids Glycine (32.6 mol-%), Proline (12.23 mol-%), and Alanine (11.2 mol-%). The gelatin consists of randomly placed polymer coils when heated as a solution. Under cooling, these random coils partially regain the collagen structure, an approximately 300nm long triple-helix structure that is cross-linked through hydrogen bonds. Relevant for the formation of these, for the gelation responsible helix structures, are primarily Proline and Hydroxyproline (Schrieber and Gareis, 2007). The content of these amino acids could be identified in the used MG as 12.34 mol-% and 9.26 mol-%, respectively.

Gelatin is a thermo-reversible material, i.e., heating and cooling cycles can be repeated and lead to similar phase change characters with gelling points around 15-30°C (Matsunaga and Shibayama, 2007). However, an irreversible denaturalization process of the gelatin polymer network occurs when heated to temperatures that approach boiling temperature or above (Tice and Moore, 1952).

5.2.2.2. κ-carrageenan

kC is a hydrogel that is extracted from red seaweeds (Rhodophyceae) (Błaszak et al., 2018) with alkaline treatment (NaOH or Ca(OH)2) under a temperature of ~100°C (Y. Liu et al., 2022). The polymer consists of repeating D-galactose and 3,6-anhydrogalactose units. The definition κ-kappa originates thereby from the number and placement of ester-sulfate groups. Correspondingly, the types ι iota and λ lambda also exist but exhibit different solubility and temperature-dependent

properties (Błaszak et al., 2018). Like the MG gelling behavior, the kC hydrogel undergoes a coil to helix transition by cooling, i.e. gelling. However, its gelling temperature is around 55°C (Laureano-López et al., 2022) and thereby significantly higher than MG. The helix arrangement is evoked by the κ-unit residue (Piculell, 2020).

5.3. Methods

Three performance criteria were used to assess the materials' rheological properties suitable for application on 3D concrete printing: 1. Evaluation of printability by extruding four layers of material through a modified caulking gun to assess buildability and extrudability as key parameters of printability, 2. Oscillatory rheometry with a plate-on-plate geometry to assess rigidity under the influence of varying temperature and shear strain, and 3. destructive rotational rheometry with shear-vane in cup geometry to measure yield stress development over temperature and time.

In (1.), several concentrations were evaluated as printable. With minor adjustments, these printable compositions were then tested in (2.) and (3.): To be able to draw more detailed conclusions, it was intended to keep most of the parameters identical for (2.), even though they did not show optimal results in (1.). For (3.), merely the highest printable concentration was tested.

For all testing protocols, especially for high temperature testing, drying was identified as the most significant challenge since the rheology is significantly affected. It was avoided by keeping the vapor pressure at an equilibrium state by adding moisture and water around the sample, increasing the relative humidity of the samples' surroundings, and shielding the samples from non-saturated air. The methodologies presented are the result of trials without any measures that could prevent drying, with different oils and greases as cover fluids for rheometer testing and continuous addition

of moisture without any coverage. These measurements were discarded and improved. The presented methodologies showed the least significant errors.

5.3.1. *Printability assessment*

5.3.1.1.*Extrusion system*
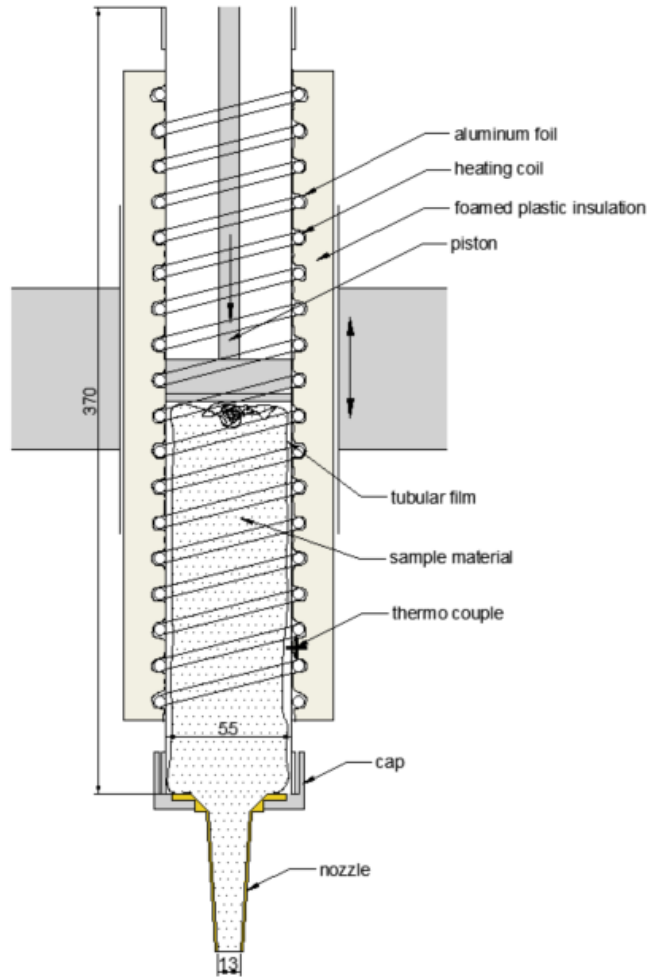
Figure 5-3 The heated ram extruder system, which was mounted on a movable- sled. Tubular films were used to store and refill material. Dimensions are given in [mm]

Similar to (Soltan and Li, 2018) and (Shakor et al., 2019), a caulking gun was used in the printability assessment. An automatic caulking gun DEWALT DCE581E with a 600ml capacity was utilized as an extruder basis. The caulking gun is an off-shelf ram extrusion system that can

apply pressure (1.05 MPa according to the user manual) on its 5.5 cm diameter piston (DeWALT, 2018) (see Figure 5-3).

The cartridge that held the hydrogel concrete was made from aluminum and had a length of 37cm. The speed of the piston was kept constant for all tests at 40mm/min, accepting minor variations due to changing resistance under progressing extrusion state. A relation between applied force and total friction, dependent on filling state of the cartridge, could be identified in (Perrot et al., 2014). The caulk gun was connected to a cylindrical nozzle with an inner diameter of 13mm.

The caulk gun was adapted and equipped with adjustable heating: Around the aluminum tube, a heating coil was applied and insulated with foam rubber. By adding a temperature switch connected with a thermocouple mounted between the foam rubber and the aluminum, the temperature outside the cartridge but inside the insulating layer could be controlled. A drawing of the heated extruder system can be seen in Figure 5-3. Since aluminum has a high thermal conductivity, an insignificant temperature difference between the outside and inside of the cartridge was assumed. Thus, the adjusted value on the temperature switch presented the temperature conditions on the inside of the cartridge.

5.3.1.2. Moving traverse

The extruder was mounted on a traversing sled to obtain a linear print and constant layer height (see Figure 5-4), restraining all movements except the traversing direction. The sled rolled along two rails with a total length of ~2m and a distance of 40cm. The extruder head was mounted vertically in the center of the sled, still allowing for vertical adjustment of printing height. The layer height was kept constant at 10mm. After a printed layer, the caulking gun was adjusted manually to the next layer height.
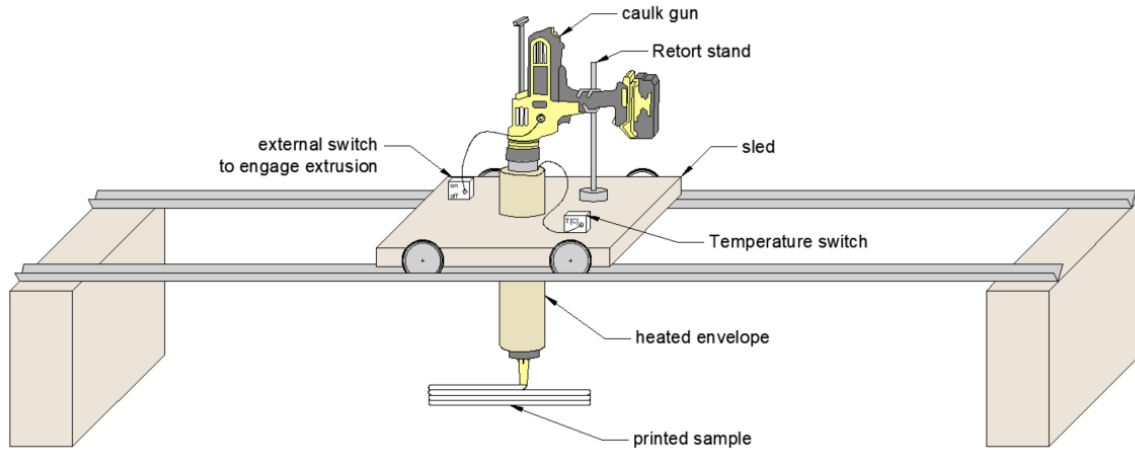
Figure 5-4 Moving travers with extrusion system, mount, temperature switch and four layers of extruded sample.

5.3.1.3.Material preparation

Both hydrogels investigated show phase change properties and are sensitive to temperature (Campo et al., 2009)(Aykin-Dinçer et al., 2017). The same accounted for the fresh composites investigated. Due to a possible dependency of temperature on handling history, a strict protocol was followed for the tests, keeping shearing and temperature history similar:

1) Soaking of MG {kC} in water, 2) Heating of solution in an oven at 70°C {90°C} (1h), 3) addition of preheated sand at 70°C {90°C}, 4) mixing with a spatula under heating from a heating plate for 3 min, where after homogeneity was assumed.

Subsequently, all material mixtures were filled into tubular films, made from 50μm {100μm} thick low-density polyethylene with a width of 80mm (see Figure 5-3) to avoid drying. The volume of each sample was 200-300ml. The material tubes were stored for a short time under cooled conditions until used in the printability assessment.

5.3.1.4.Mixtures

The material's rheological properties vary with temperature, binder to sand ratio, and the binder solution concentration. Therefore, an experimental matrix was designed to indicate the influence

of all three parameters mentioned. The corresponding nomenclature was defined by MGxxByy (xx%-MG-granulate-wt./H2O-vol.) (yy% MGgelxx-wt./sand-wt.).

MG: The concentration of MG150 presents one of the largest mixable concentrations without loss of workability. The solution concentrations investigated were 60%, 80%, 100%, 120%, 150%-w/v of MG. The binder to sand ratios were chosen with 0.3, 0.35, 0.4, 0.45, and 0.5, and temperatures of 30°C, 35°C, 40°C, 50°C, and 70°C.

kC: Similarly, the kC compositions of 2%, 3%, 4%-w/v were selected with the corresponding binder to sand ratios by weight of 0.4, 0.5, and 0.6 with the printing temperatures of 45°C, 65°C, and 85°C.

5.3.1.5. Experimental procedure

The cooled tubular films were heated in an electric oven to the specific testing temperatures specified in Section 5.3.1.4. The extruder was heated to the same temperature. After one hour of heating, the tubular film bag was placed inside the extruder and cut open closest to the nozzle. After the nozzle was put back on, and the extruder was set in the moving traverse, the setup was ready for the experiment.

The nozzle extruded the material with a maximum velocity of 10mm/s during the tests. Depending on the material consistency and the resistance to the piston, the extrusion rate varied slightly. Hence, the printing speed was accordingly adjusted to avoid tearing of the material. The print speed was 5-10mm/s. The layer height and the nozzle's distance to the preceding layer were kept constant at 10mm. The produced samples had a length of 15cm. After each layer, the extruder was stopped to keep a layer time of 90s. If the material did not show sufficient yield strength to stay

inside the cartridge, the material flow was stopped during the waiting period by clogging the nozzle.

Given that the material could not pass the nozzle under pressure, the material was defined as not extrudable. If it could be extruded, but the four layers (each 10mm height) were deviating more than 5mm in total (total height <35mm), the material was defined as not buildable.

5.3.2. Rheological characterization

The rheological characterization of 3D printing composites requires the determination of mainly three parameters: the apparent elastic modulus to prevent buckling (Wolfs et al., 2018), the yield stress to prevent the structure from collapsing at the basis (Perrot et al., 2016) and the description of the viscosity for pumping and extrusion (Mechtcherine et al., 2020)(Roussel, 2018)(Ranjbar et al., 2021). To ensure the stability of the printed shape, the initial elastic modulus of printable cementitious materials ranges between 10 to 100 kPa and the initial yield stress between few hundreds Pa to a couple of kPa. This roots in the requirement for great rigidity and static yield stress after extrusion to enable the buildability of the material and a liquid state material during extrusion to avoid segregation and clogging. The complex modulus G^*, loss factor $\tan(\delta)$, and yield stress τc have been measured and computed for the rheological tests. Since the materials have both solid and liquid-like behaviors for most tests under temperature change, the complex modulus in conjunction with its loss factor was used to describe and quantify the visco-elastic behavior.

The yield stress build-up and consistency change were expected to be mainly due to the temperature change and the connected polymer folding to helix-like structures (Rhein-Knudsen et al., 2015). Additionally, the thixotropic build-up due to particle flocculation can contribute to the yield stress development over time. The rheological tests aimed to mimic the shearing and temperature process of the actual printing procedure: 1. Initial state – Heated material in extruder

cartridge at printing temperature, 2. Extrusion – Shearing of material, 3. Deposition – material at rest and initial cooling, 4. Temperature set - Cooling of material to ambient temperature. The influence of aggregate particles in the hydrogel composite was studied and compared with the rheological properties of the raw binding material. All tests were made in at least triplicates.

5.3.2.1.Testing setup

Oscillatory tests: All rheological tests were performed with an Anton Paar MCR 702 Rheometer. A plate-on-plate testing geometry was used with diameters of 25mm (PP25) and 50mm (PP50), respectively, for the composite materials and the pure hydrogels. The larger plate geometry was chosen to decrease the torque error measured under low friction for the pure binders. A heated lower plate was used for temperature control of the sample. With a gap size of 1mm for pure hydrogels and 2.5mm for suspensions, the temperature gradient inside the sample was assumed to be negligible.

Like (Ranjbar et al., 2021), the gap size was more than eight times the maximum grain size to ensure a homogeneous behavior. To prevent drying, a hood from foamed plastic was made with an inner diameter of 9cm and an outer diameter of 13cm, covering the sample space. As shown in Figure 5-5, the inner surfaces were covered with a bentonite-water mixture with sufficient yield stress to stay at the inner surfaces of the foamed plastic, to keep the testing environment moisturized. The bentonite was mixed with a water-to-bentonite ratio of 2.35. Additionally, the foamed chamber was moisturized throughout all tests with sprayed water through the recess on the foamed hood's top.
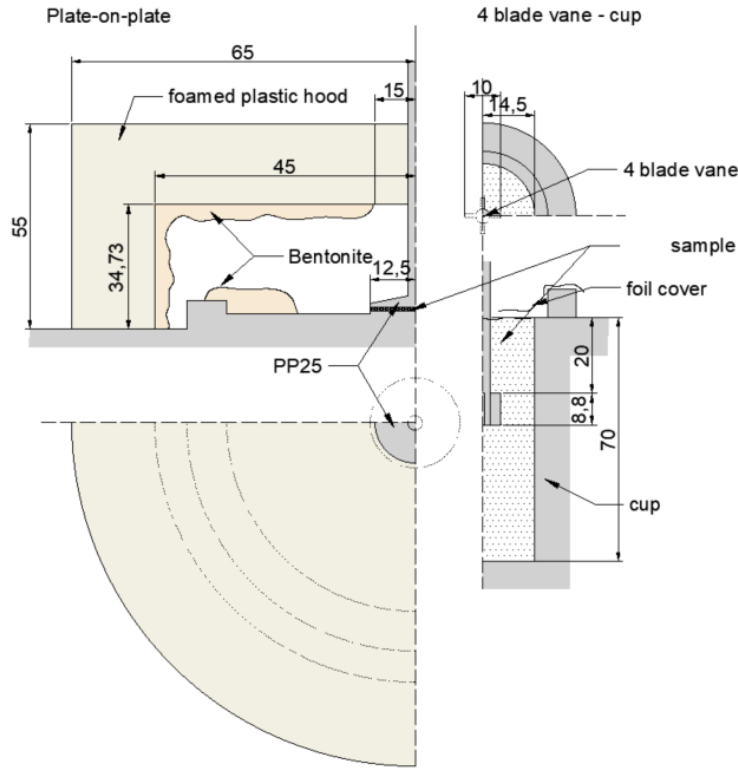
Figure 5-5 Setup to measure rheological parameters by oscillatory shear rheometry (left) through a plate-on-plate setup and determination of yield strength (right) in rotational fashion with four blade vane-cup setup. Both samples were protected against drying. Dimensions are given in [mm].

Rotational destructive testing of yield stress: The same Anton Paar MCR 702 Rheometer was used for rotational tests. Similar to (Ma et al., 2018), a four-blade vane–cup setup was chosen, as presented in Figure 5-5. The material was placed to a height of 70mm in the cup with a diameter of 29mm. The 4-blade vane probe with a height of 8.8mm and a diameter of 10mm was then approx. 2 cm fully submerged into the sample. The exposed sample surface was moisturized by water spray and covered by a thin plastic film. The film was not to any time in direct contact with the torque-inducing parts of the rheometer.

5.3.2.2.Data analysis

Oscillatory tests: G* denotes both the modulus of elasticity of viscoelastic (VE) fluids and VE solids and can be defined as the vector sum of the real component, or storage modulus G' and the imaginary component, or loss modulus G'':

$$G^* = G' + iG'' \tag{5.1}$$

The tangent of the phase angle δ in

$$G^* = |G^*| \cos(\delta) + i|G^*|\sin(\delta) \tag{5.2}$$

can be identified as the loss factor $tan(\delta)$, denoting the relative magnitude between G' and G''. Being that G' describes the properties of a viscoelastic solid and G'' describes a VE fluid, $tan(\delta) > 1$ is defining a fluid. In contrast, $tan(\delta) < 1$ represents a VE solid.

The gel point TG is defined as the temperature for this physical state transition.

I.e.:

$$T_G = T(tan\delta = 1) \tag{5.3}$$

Yield stress: The yield stress is the maximum shear stress applied on a sample at yielding failure with T as the maximum torque at this point. A cylindrical shearing surface was assumed with the dimensions of the 4-blade vane (see Figure 5-5) geometry of D=10mm (R=5mm) and H=8.8mm. The corresponding yield stress τ_c could be calculated by:

$$\tau_c = \frac{T}{2\pi R^2(H + \frac{2R}{3})} \tag{5.4}$$

5.3.2.3.Mixtures and preparation of samples
In the printability assessment described in Section 5.3.1., the concentrations of MG60B35, MG80B40, MG100B40, MG120B40, MG150B45, kC03B50 and kC04B50 were evaluated as well printable (see Section 5.4.1).These printable compositions were further investigated with minor adjustments: To draw more detailed conclusions, all parameters were kept constant but the solution concentration. The compositions of MG60-150B40 and kC03-04B50 were selected to be measured within rheometer tests at the corresponding printing temperatures of 50°C (MG), 65°C (kC03), and 85°C (kC04). In similar fashion, the pure binder compositions of MG60-150 and kC03-04 were investigated.

Yield stress measurements were merely conducted using the highest concentration of kC04B50 and MG150B40.

Like Section 5.3.1.3, the materials were prepared by 1. Soaking, 2. Heating and mixing, 3. addition of heated sand. To prevent the mixtures from drying and repeated heating and cooling cycles, the batches were split into several samples of ~10ml and filled into Ziplock bags. The bags were stored in cooled conditions until testing. The application procedure for MG {kC} is as follows:

1) A Ziplock bag with the material was emerged in 70°C {95°C} water for 30s {180s}, 2) The PP25 or PP50 probe is lowered 90s {240s} past the start of heating. 3) The excess material is removed to reach material application states as shown in Figure 5-5. 4) The sample space is moisturized with water spray (plates and bentonite in the hood). 5) Hood is closed. 6) The test is started 210s {360s} past the start of heating.

5.3.2.4.The testing protocol for amplitude strain sweep of hydrogel solution
An oscillatory amplitude strain sweep of the binder solutions was conducted by recording 30 data points with a maximum recording time of 90s each. The strain sweep was done logarithmic,

starting from 0.0005% and reaching 100%. After the material application, the instrument was defined with a resting time of 2 min. The tests were conducted at the respective testing and printing temperatures of 50°C (MG60-MG150), 65°C (kC03), and 85°C (kC04). A generally low frequency of 3Hz was chosen. A large diameter PP50 setup was used to increase the measurements' torque and reduce errors. A gap size of 1mm was defined.

5.3.2.5.The testing protocol for the temperature sweep of binder solution
An oscillatory temperature sweep was conducted by recording 46 data points with a recording length of 15s each. The temperature was varied with a magnitude of 2.5°C/min during the recording. This gradient was chosen by approximating a constant cooling rate for a printed layer. Because the cooling rate varies significantly for different locations in a printed sample for different printing temperatures, a constant cooling rate enabled better comparison of the samples and allowed for better conclusions. The sample was left to rest for 2min before testing and after the application of the sample. After the temperature sweep, the data was accumulated for ten more data points to record possible time dependencies. It was tested with a frequency of 3Hz and a shear strain of 0.1%. A gap of 1mm was defined with a PP25 setup. The binders were cooled from the printing temperatures of 50°C (MG60-MG150), 65°C (kC03), and 85°C (kC04) to 20°C.

5.3.2.6.The testing protocol for the amplitude strain sweep of composite material
Like the testing protocol for the amplitude strain sweep for the pure binder solutions in Section 5.3.2.4, an amplitude strain sweep for the composite material was conducted under the same parameters. However, a PP25 setup with a gap size of 2.5mm was used instead.

5.3.2.7.The testing protocol for the structural build-up of composite material at printing temperature
The composite materials were exposed to oscillatory shear for 30 seconds with a strain amplitude of 0.5%. As can be seen in Section 5.4.2.1, this value is in the material's non-linear region, which causes a shear-thinning behavior. After, the structural build-up was measured with a strain

amplitude of 0.002%, which is in the linear elastic regime of all materials, 30 measurements were taken every 20s. A PP25 geometry was used with a gap size of 2.5mm. The materials were tested at the corresponding printing temperatures. As for other oscillatory experiments, the tests were conducted at a frequency of 3Hz.

5.3.2.8. The testing protocol for the temperature sweep of composite material
Similar to the temperature sweep of the pure binding materials in Section 5.3.2.5, the composite materials were cooled down from printing temperatures with 2.5°C/min to 20°C. Measurements were collected every 15s with a shear strain of 0.002% and 3Hz. The measurements were proceeded for 200s after reaching 20°C to record potential time-dependent effects. Like the testing procedure in Section 5.3.2.7, the materials were sheared at a strain amplitude of 0.5% before the temperature sweep to see the joint effects of thixotropic built up and temperature change. A PP25 setup was used with a gap size of 2.5mm.

5.3.2.9. Testing Protocol of composite's yield stress
The four-vane-cup setup was used to test the yield stress of the material under the temperatures of 85°C, 65°C, 45°C, 20°C and 50°C, 40°C, 30°C, 20°C, respectively for kC and MG. As in (Ma et al., 2018), a rotational test with a constant shear rate of 0.1s-1 measured the torque at failure. All samples were prepared at printing temperature, cooled down to testing temperature, and rested for 10min before testing to allow a homogeneous temperature distribution over the sample's cross-section.

5.4.   Results and Discussion

5.4.1. Printability assessment
Table 5-1 and Figure 5-6 show the results of the printability assessment.

Table 5-1 Printability assessment of MG- and kC- composites for various concentrations and temperatures. MG (kC)xx shows the dried biopolymer to water ratio (w[kg]/v[l] %). Bxx defines the wet hydrogel to sand ratio (w/w %).

	MG60					MG80					MG100					MG120					MG150				
T[°C]	30	35	40	50	70	30	35	40	50	70	30	35	40	50	70	30	35	40	50	70	30	35	40	50	70
B50	●	●	●	●	●	●	●	●	●	●	●	●	●	●	●	-	●	●	●	●	♦	-	●	●	●
B45	●	●	●	●	●	●	●	●	●	●	-	●	●	●	●	♦	●	●	●	●	♦	-	=	●	●
B40	●	●	●	●	●	=	=	=	=	=	=	=	=	=	=	♦	=	=	=	=	♦	♦	-	-	-
B35	=	=	=	=	=	-	-	-	-	-	-	-	-	-	-	♦	♦	-	-	-	♦	♦	♦	-	-
B30	♦	♦	♦	♦	♦	♦	♦	♦	-	-	♦	♦	♦	-	-	♦	♦	♦	-	-	♦	♦	♦	♦	♦

	kC02			kC03			kC04		
T[°C]	45	65	85	45	65	85	45	65	85
B40	♦	♦	♦	♦	♦	♦	♦	♦	♦
B50	♦	♦	●	♦	=	●	♦	♦	=
B60	♦	♦	♦	=	♦	♦	●	●	●

Legend:
- ● Not buildable
- = Good printability
- - printable
- ♦ Not extrudable
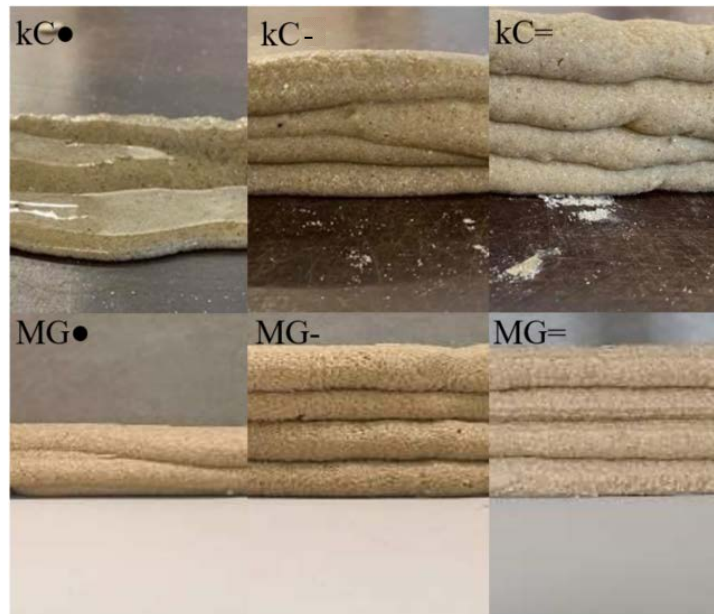
Figure 5-6 The classification of printability tests for the kC- and MG composites. The MG composites show the best printability. For legend, see Table 5-1.

Table 5-1 states the buildable, extrudable, and printable concentrations. Figure 5-6 shows respectively for kC and MG representative printing samples. Generally, the MG composites showed better printability results. MG generally exhibited no to little segregation, contrary to the low concentrations of kC. The MG also presented good robustness in the printing process, allowing

for homogeneous extrusion. A fast phase change at higher temperatures for the kC composites impeded the printing process through high sensitivity to temperature changes, causing non-homogeneous behavior during printing, clogging the nozzle.

5.4.1.1.The mammal gelatin composites

The MG composites with a binder concentration MG80-120 showed the best printability and the greatest printable concentration span (see Table 5-1). The MG150 binders tended towards high viscosity and slow extrudability, while MG60 was less buildable. A tendency towards greater buildability at lower printing temperatures and better extrudability for higher printing temperatures was observed for all specimens especially those with high binder concentrations.

5.4.1.2.kC composites

The general tendencies observed in Section 5.4.1.1 are also applicable for the kC composite materials: Higher temperatures lead to good extrudability. Low temperatures appear to have better buildability. The best printable binder concentration is kC03. A higher binder content of B50+ was needed to produce a printable material composition.

5.4.2.   The rheological characterizations of printable material

5.4.2.1.The strain amplitude sweep
The hydrogel solution

The mammal gelatin showed Newtonian behavior over the strain from 0.005-100% with VE liquid properties for all concentrations at 50°C. Figure 5-7 shows the magnitude of the complex modulus and loss factor over the hydrogel concentrations measured as the mean value over repetitions and strain. An exponential increase of the shear modulus with an increase in concentration was observed while shifting the loss factor towards solid-like material behavior. This is in consistency

with reported findings in (Wulansari et al., 1998), suggesting non-Newtonian behavior for lower concentrations.
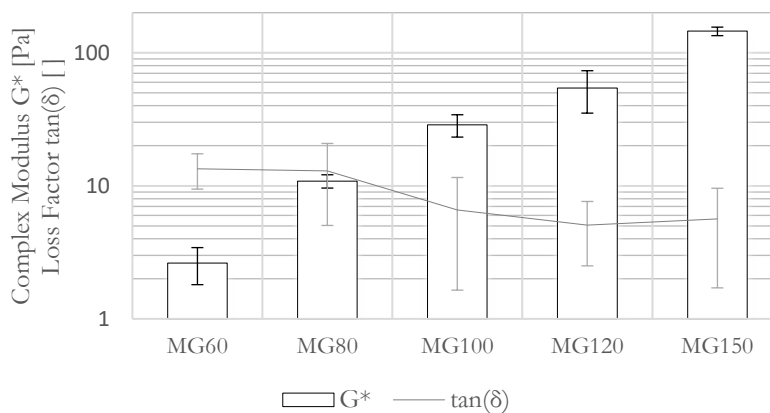
Figure 5-7 Complex modulus G* and loss factor tan(δ) of MG solution measured over increasing strain sweep (0.0005-100%) at 3Hz and 50°C. All strain sweeps showed linear behavior. Presented are mean values and standard deviations computed from at least three test repetitions and over the scope of strain.

The kC solutions at 65°C and 85°C, respectively for the concentrations of 3%-w/v and 4%-w/v, showed similar behavior for shear strains lower than 10% (see Figure 5-8). Above this threshold, shear-thinning behavior was observed.
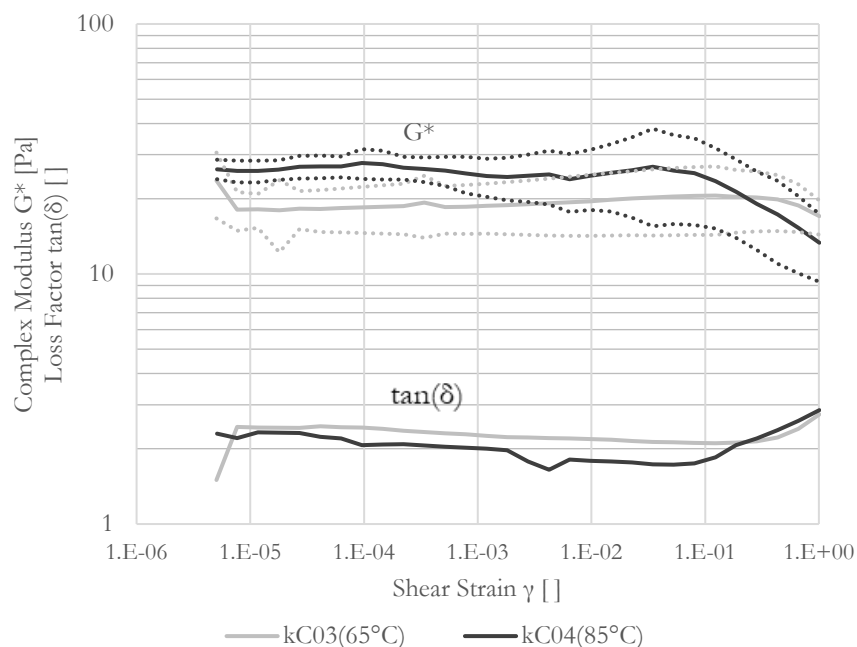
Figure 5-8 Complex modulus G* and loss factor tan(δ) of kC solution measured over increasing strain sweep (0.0005-100%) at 3Hz and 65°C, 85°C respectively for the concentrations of 3%-w/v and 4%-w/v. Standard deviation of G* shown as dashed line.

At printing temperatures, all tested hydrogels show VE liquid-like behavior. The material's complex modulus increases with increasing concentrations. Both the 3%-w/v kC concentration at 65°C and the 4%-w/v at 85°C showed a similar modulus order-of-magnitude compared to the 80-100%-w/v concentration of MG. By comparing this result with the results in Section 5.4.1., a region of G* between 10-50 Pa of the hydrogel proved to relate to good printability.

Composite

Figure 5-9 shows the results for a strain sweep of the five tested mammal gelatin composites. A non-Newtonian, shear-softening behavior was observed for large strains. A linear VE region is visible for more minor strains, proposing that, similarly to cementitious composites (De Larrard et al., 1996), a yield stress fluid can be identified. The concentration-dependent quantitative order of G* of the raw hydrogel solutions (Figure 5-7) was resembled for the high strain measurements. Low binder moduli lead to low composite moduli and high binder values to high composite values.

These tendencies cannot be observed for the settled materials at low shear. Here, the MG60B40, MG80B40 showed an increased complex modulus and, at the same time, a decrease in its loss factor, i.e., the material illustrated solid-like behavior - likely because of an elevated number of particle-particle interactions through a low viscosity solvent leading to insufficient lubrication between the particles, also justifying the printability difficulties of the MG60B40 composite material.

The results of the strain sweep of the kC composite material are shown in Figure 5-10. Despite more significant deviations, a similar behavior to the MG composites can be stated for strains below 10%, describing a linear region at low shearing and shear softening behavior for higher shear strains.
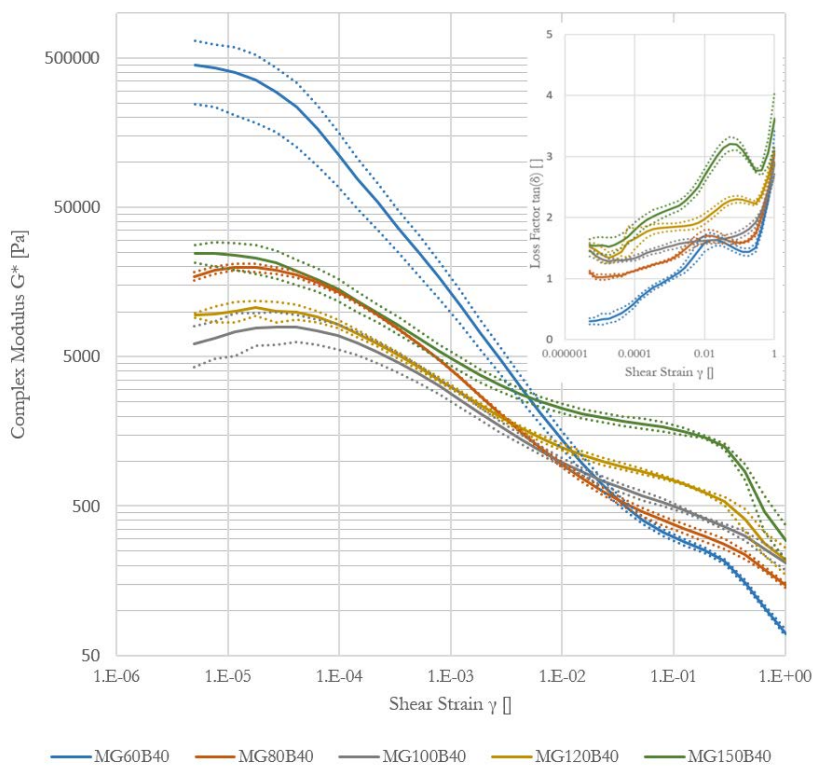
Figure 5-9 Complex modulus G* and loss factor tan(δ) of MG composite measured over increasing strain sweep (0.0005-100%) after resting the material. Recorded at 3Hz and 50°C. The standard deviations are shown as dashed lines.
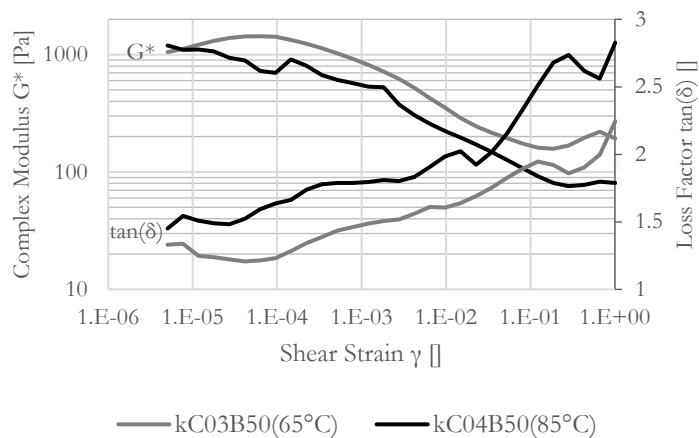
Figure 5-10 Complex modulus G* and loss factor tan(δ) of kC composite measured as increasing strain sweep (0.0005-100%) at 3Hz and at temperatures of 65°C and 85°C for the concentrations shown. The measurements are given as mean value of at least three measurements with a coefficient of variation of 13.5% and 45% respectively for tan(δ) and G*.

With its complex modulus magnitudes of ~104 Pa, the printable MG composites have significantly higher values for lower shear strains than the kC composites with ~103 Pa; leading to similar values around the order of magnitude of 10-1 kPa when sheared with a large strain. The value obtained for MG composites align with the values obtained with printable cementitious materials (Jacquet et al., 2020).

5.4.2.2. Temperature sweep
Hydrogel

Figure 5-11 shows MG's complex modulus and loss factor in time and temperature dependency. For temperatures close to 50°C, similar values were observed in Figure 5-7.
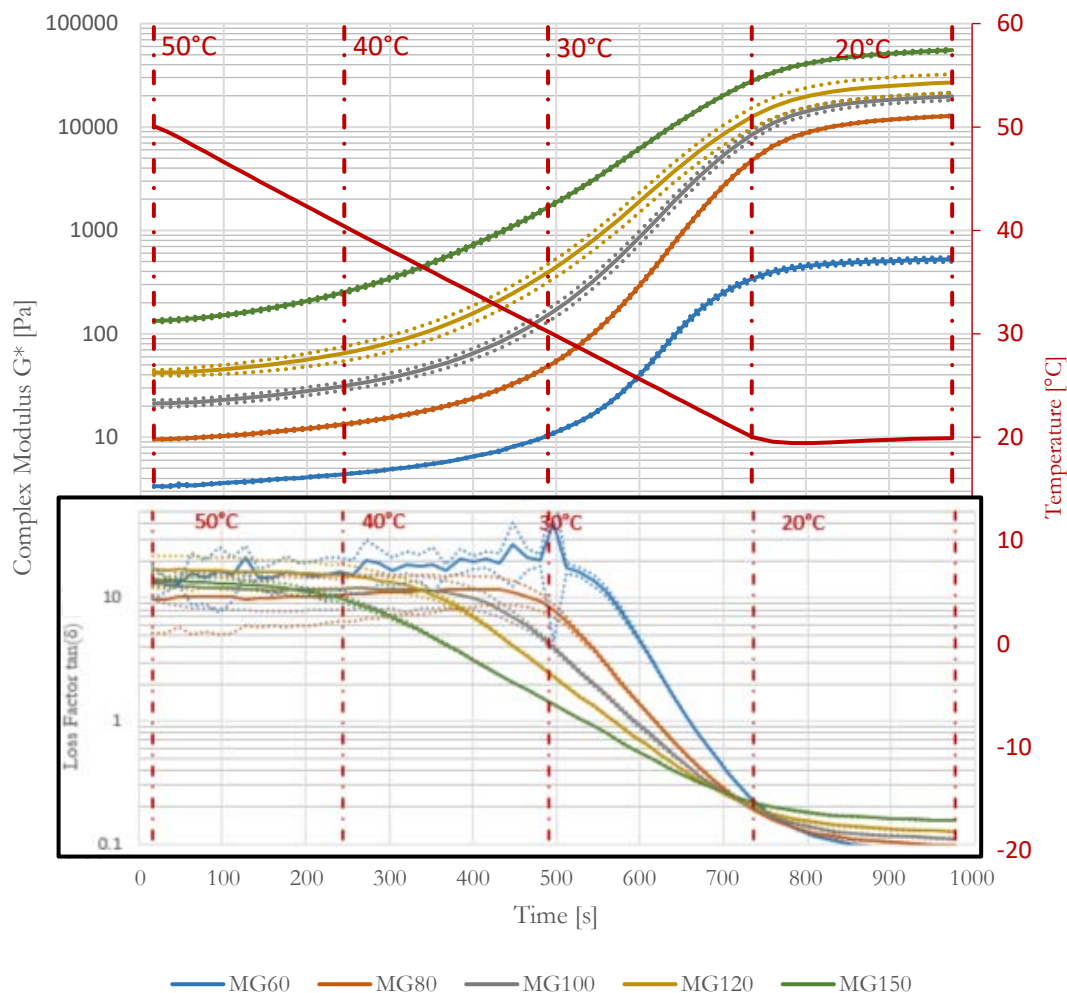
Figure 5-11 Complex modulus G* and loss factor tan(δ) of mammal gelatin measured with a constant shear strain of 0.001 and a frequency of 3Hz. The temperature profile is shown in red. Measurements are given as mean value. Standard deviations for the complex modulus are shown as dashed lines.

The general tendencies of low concentrations relating to lower modulus and the opposite remain. A general increase in G* and decrease of tan(δ) over temperature decreases could be presented. The most drastic increase in rigidity of the gels could be observed between the temperatures of 40-20°C. The exact temperature is dependent on the hydrogel's concentration: Low concentrations lead to a later (lower temperatures) drastic increase of G*. The gel transition point emphasizes this dependency as plotted in Figure 5-12. The gel point varies between 23.1°C for the lowest concentration and 28.4°C for the highest concentration.
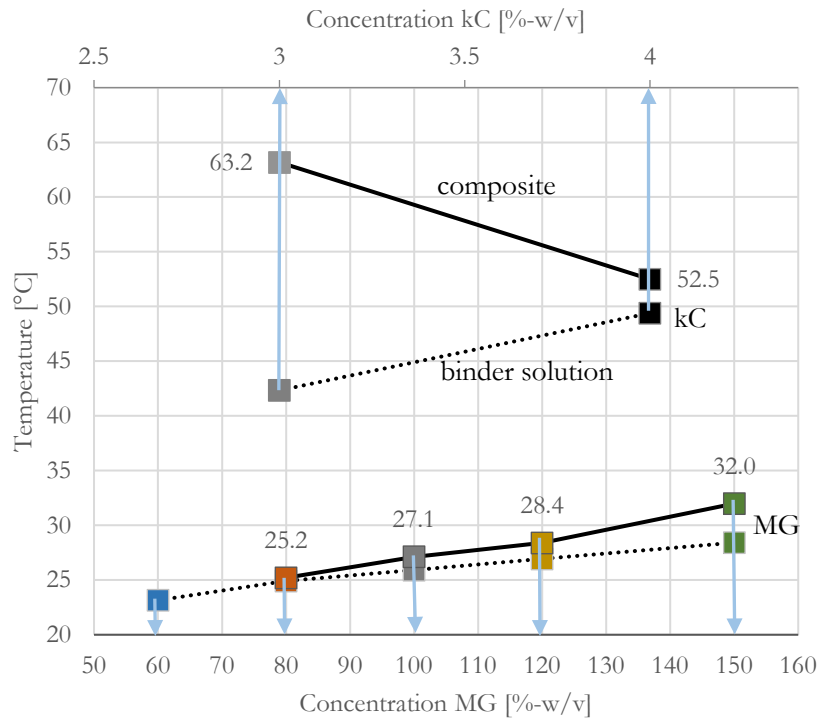
Figure 5-12 Gel-transition point of MG and kC –hydrogel and –composites. Dashed lines show hydrogels and black lines visualize the corresponding composite materials. The data describes the crossing values for tan(δ)=1 of Figure 5-11, Figure 5-13, Figure 5-14 and Figure 5-15.

From about 730s onwards, the temperature was kept constant at 20°C (compare Figure 5-11). The results suggest with a continuously increasing value of the complex modulus that the rheological behavior of the gels is not only dependent on the temperature change: A time-dependent behavior related to its temperature history could be recorded. This inertial effect decreases over time, faster for low concentration gelatins. The inertial effect could also be verified by (Guo et al., 2003), relating it with inefficient cross-linking through hydrogen bonds, with increasing effect in higher concentration gelatins.
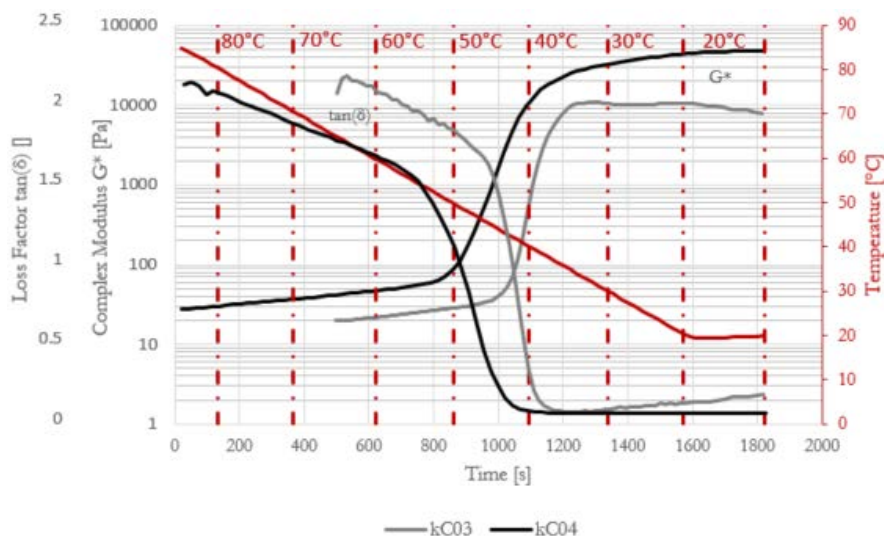
Figure 5-13 Complex modulus G* and loss factor tan(δ) of kC solution measured with a constant shear strain of 0.001 and a frequency of 3Hz. The temperature profile is shown in red. The measurements are given as mean values. Mean values for the coefficient of variation could be identified with 28% and 19%, respectively for G* and tan(δ).

The kC hydrogel exhibited a different temperature span for an increase in rigidity as shown in Figure 5-13. The most rapid rise in G* was recorded for temperatures between 35°C and 50°C. Figure 5-12 shows the significant higher gelling temperatures of 42.3°C and 49.4°C for the two concentrations. A shift towards higher modulus values with higher concentrations can be observed for the kC gel, similar to the MG. No significant time-dependent effect was observed past the termination of cooling.

Composite

A general increase of G* with a temperature decrease can be shown for the MG composite material in Figure 5-14 similar to the pure hydrogel. Adding sand to the hydrogels did not substantially alter any general temperature-dependent behavior. Similar changes in lower concentration composites were observed for the gels (Figure 5-11). The non-printable concentration MG60B40 shows the highest complex modulus at printing temperature and solid-like behavior. Again, a strong particle-particle interaction without sufficient lubrication is expected to evoke this result.

At lower temperatures, past gelling point, the rigidity of the concentrations follows expected principles from Figure 5-11, where a qualitative relation between concentration and complex modulus was observed. Likewise, the gelling point for the MG composite materials shown in Figure 5-12 follows the tendencies of the raw hydrogels. A general increase in gel point temperature can be seen, expecting that, similarly to cementitious composite materials (Carro-López et al., 2015), the mineral aggregates will absorb some of the water, decreasing the water content in the binder. Hence, altering the binder at a higher concentration.
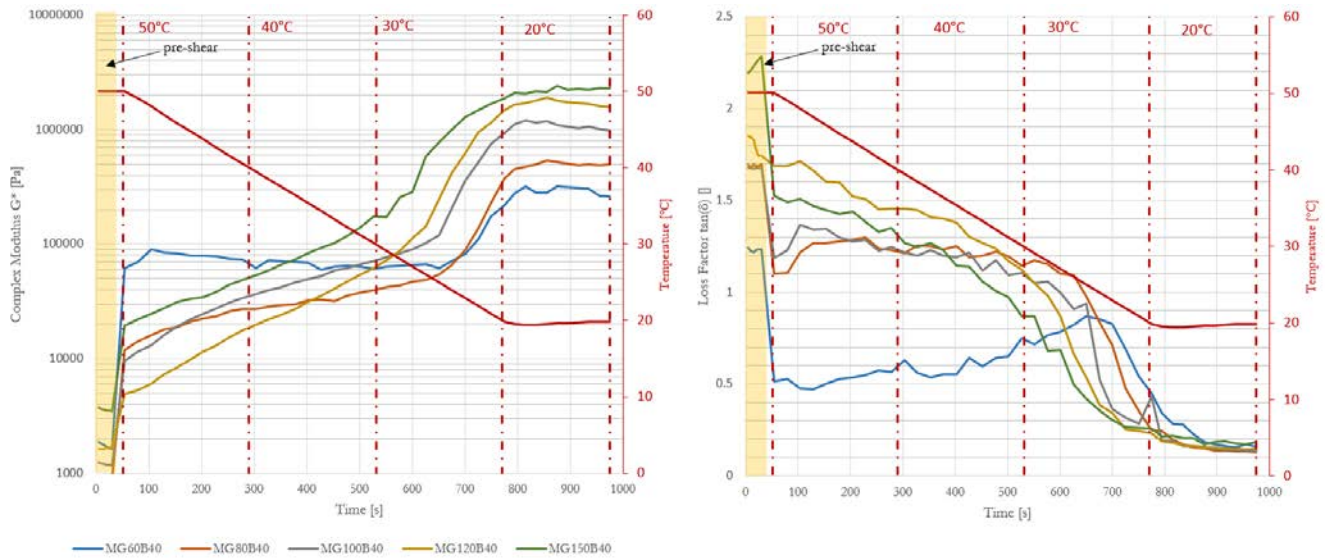
Figure 5-14 The temperature sweep of mammal gelatin composite from 50°C to 20°C. Complex modulus G* and loss factor tan(δ) measured with a constant shear strain of 0.001 and a frequency of 3Hz, pre-sheared at 50°C with a strain of 0.005. The temperature profile is shown in red. The measurements are given as mean values. Mean values for the coefficient of variation could be identified with 26% and 10%, respectively for G* and tan(δ).

Figure 5-15 shows the results of the temperature sweep of the kC composite. Like the MG60B40 concentration, a higher value of G* at printing temperature for the lower concentration of kC03B50 was observed. The elevation of the gel point (see Figure 5-12) for the concentration rises accordingly, raising it to a higher value than the kC04B50 material. Even if a high-temperature gelling point was observed for the low concentration, the corresponding complex modulus exhibits

a lower temperature for the maximum increase in rigidity. The difference in rheological change is largest for the kC04B50 concentration. Hence, it exhibits more temperature-sensitive properties.
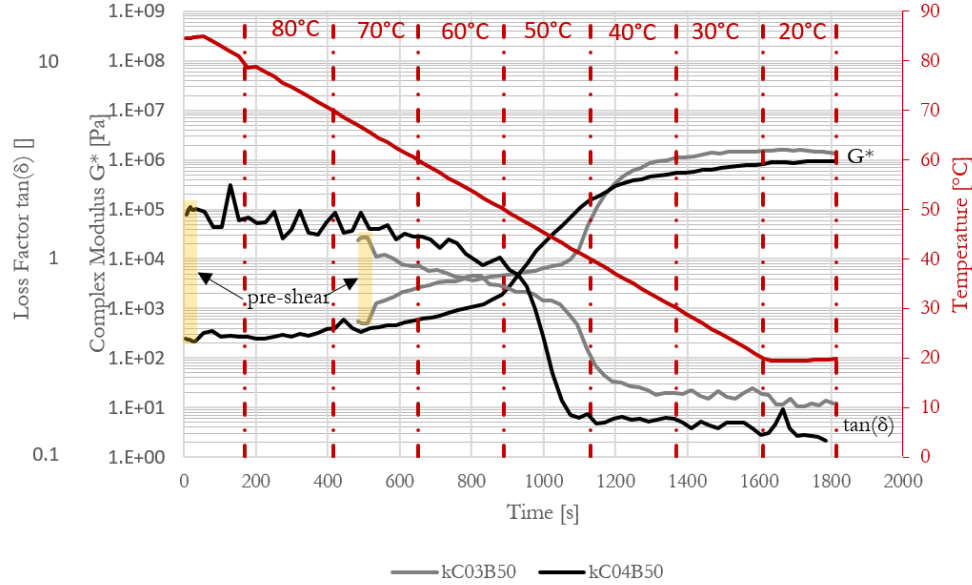
**Figure 5-15** The temperature sweep of the kC composite from 85°C and 65°C (for the concentrations shown) to 20°C. The complex modulus G* and loss factor tan(δ) measured with a constant shear strain of 0.001 and a frequency of 3Hz, pre-sheared at respective printing temperatures with a strain of 0.005. The temperature profile is shown in red. The measurements are given as mean values. Mean values for the coefficient of variation could be identified with 54% and 17%, respectively for G* and tan(δ).

Quantitatively, the MG and kC materials reach a similar complex modulus of around 1MPa when cooled, which is a high value in comparison with cement-based materials leaving a printer's nozzle. As an origin at printing temperature, the kC-composites result in lower complex modulus values than the MG-composites. Therefore, the kC differs more in its rheological behavior between printing temperature and when cooled (3-4 orders of magnitude). However, when including the shear-softening behavior of MG80B40 and MG100B40, the change in G* is like the kC-composite, but generally being one order of magnitude larger than the kC-composites. kC composites are more temperature sensitive. While MG composites exhibit both, significant shear softening behavior and temperature sensitivity.

5.4.2.3. Thixotropic build-up

The time-dependent behavior of kC and MG composites after shearing is shown in Figure 5-16. The complex modulus increases over time for all tested materials i.e., they exhibit a thixotropic behavior.
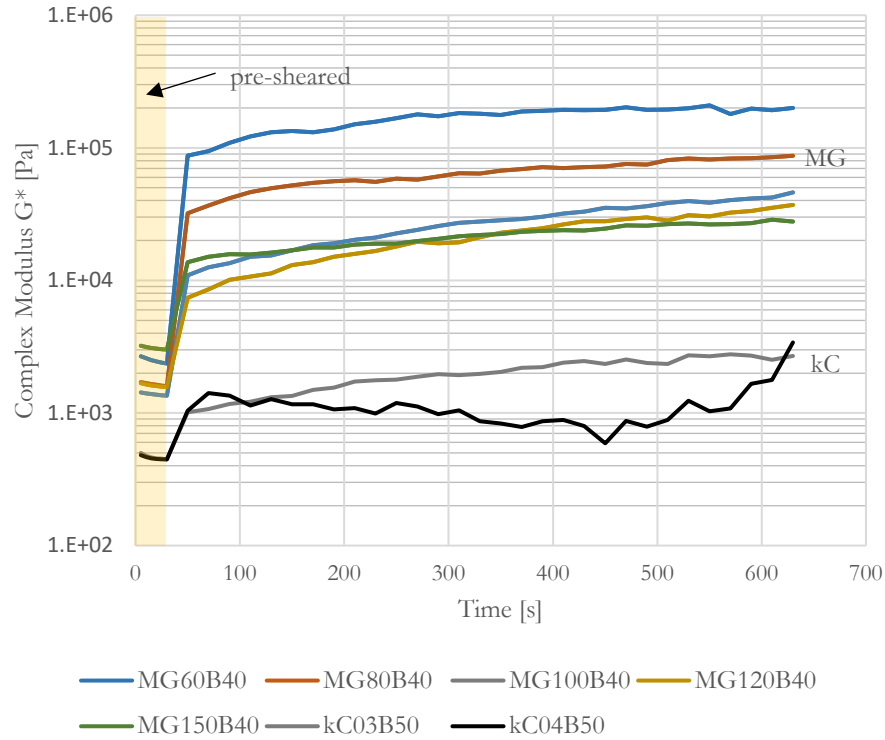
Figure 5-16 The structural build up over time for composite materials. Measured with a PP25 setup, 3Hz, strain of 0.001 and at respective printing temperatures (MG60-150B40 at 50°C, kC03B50 at 65°C and kC04B50 at 85°C). Pre-sheared with a strain of 0.005. Measurements are given as mean value. A mean coefficient of variation could be identified with 36%.

The increase of complex modulus through temperature change in Figure 5-14 and Figure 5-15 exceeded the thixotropic build-up for all concentrations. Therefore, the temperature is the most significant parameter in relation to buildability and extrudability. In future studies, the thixotropic build-up of the material can be optimized for the printing process by alternating the grain size distribution.

5.4.2.4.Yield Stress

Figure 5-17 shows the yield stress development measured over the composite's temperature. Similar to the complex modulus values in Figure 5-11, the values of the yield strength increase towards lower temperatures. MG shows the most significant yield stress increase, stretching over three orders of magnitude (0.07kPa-106kPa), while the kC composite extends over two orders of magnitude (0.05kPa-15.1kPa). Directly relating to the composite materials' gelling point in Figure 5-12, the most significant increase in yield stress is between 45-65°C (kC) and 20-40°C (MG).

It is important to note that these yield stresses for MG and kC composites align with a fast printing of cementitious materials. According to (Perrot et al., 2016), the material is theoretically able to withstand the weight of around 50cm for kC and more than 3m for MG composites which makes MG a very efficient and promising binder for 3D printing applications.
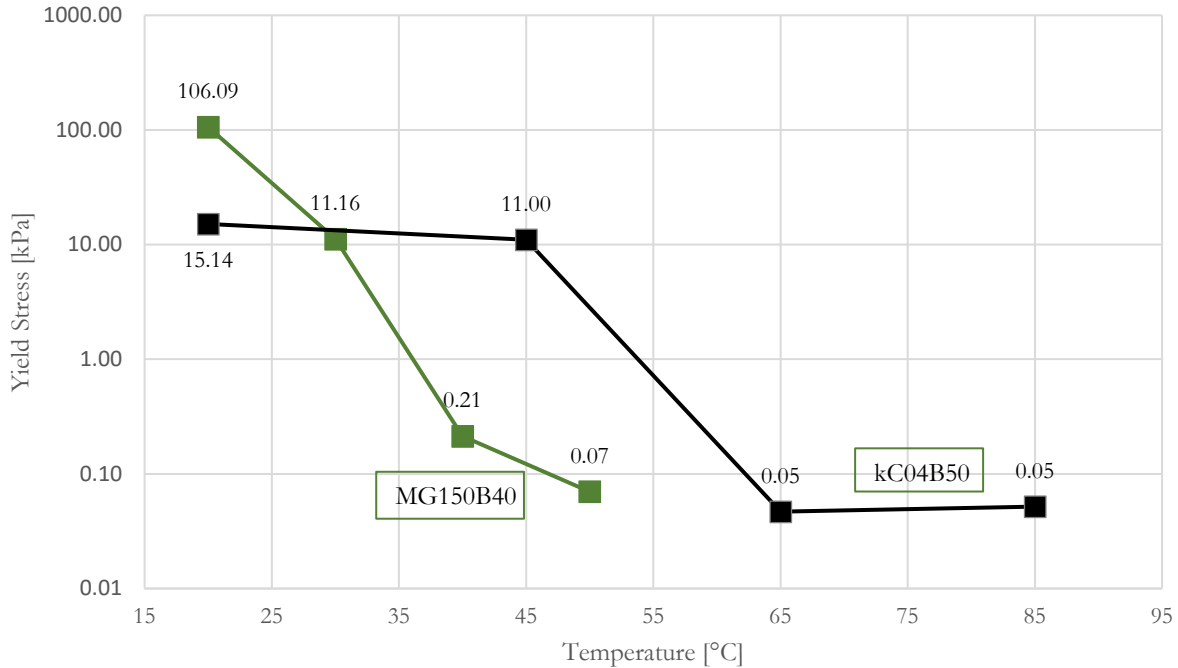
Figure 5-17 The yield stress values for MG150B40 and kC04B50 composites. A four-blade vane setup was used for the tests with a constant shear rate of 0.1s-1. The data points displayed show the maximum recorded stress at failure.

5.4.3. *Rheological properties in relation to the composite's printability*

The composites' printability originates from the rheological difference between conditions during extrusion (sheared and heated) and after extrusion (at-rest and cooled). Generally, both materials show a shear-softening behavior and thermo-reversibility, i.e., beneficial properties for their application and printability within a heated extruder.

kC composites perform best compared to MG composites in the following properties:

- *gelling point:* kC shows the highest gelling point. Exposed to environmental temperatures, the heated material cools faster. Therefore, an elevated gelling point exhibits a faster change in rheological properties after extrusion. This is beneficial for the material's buildability.

- *fast change in complex modulus:* The quickest change in complex modulus of the material (see Figure 5-15) is also elevated in temperature, which leads to a fast change in the material's rigidity. The fast rheological change is beneficial for the material's printability, but it requires a well-tuned

printing process. Especially for kC04B50, a problem with its temperature sensitivity was observed. Layer-time, extrusion- and printing speed needed to be fine-tuned to allow continuous printability. Similar problems can be described for fast-setting cementitious printing mortars (Ngo et al., 2018).

- *the lowest rigidity when heated*: kC04B50 had a significantly lower complex modulus of ~0.2kPa when heated compared to the MG composites. A good extrudability was also observed, while more force input on the extruder was needed for the MG composites.

Among the best printable **MG composites** (MG80-100B40), the beneficial properties were:

- *Gelling point:* The lower gelling point of the MG composites resulted in a lower printing temperature. This results in lower energy consumption to heat and keep the material at temperature. Contrary to the kC composites, the MG composites exhibited a robust printing process without strong dependencies on its parameters.

- *yield stress*: Both printable kC and MG composites exhibit a good buildability through its yield stress increase after cooling. However, the yield stress difference between printing- and cooled temperature is most significant for the MG composite. This could not be observed in its printability assessment, but might lead to significantly faster build rates for full-scale building components (Jayathilakage et al., 2020).

- *shear softening behavior:* The shear-softening behavior could be identified as the largest for the low concentration MG composites. Since MG60B40 did exhibit no extrudability, the shear-softening behavior of G80B40 showed the best properties of the printable composites. The thixotropic build-up after extrusion lead to good printability by not only relying on the rheological change through thermo-reversibility. This was beneficial, corresponding to the low-temperature gelling temperatures since the stiffening of the material is slower.

5.4.4. Evaluation: Best printability
The best printability was found for the MG80-120B40 composites through:

- The largest span in G* through its shear-softening/thinning behavior under extrusion with 103-102 Pa in the tested range of <100% shear strain, decreasing the materials rigidity.

- The low-temperature range for the largest increase in G* (103-106 Pa) for robustness of printing process through eased temperature control and sufficient buildability without deformation.

- The low gelling temperatures (25-28°C) for a low temperature and a low energy-consuming printing process by still allowing solidification by cooling through ambient temperatures.

- The greatest yield stress development (10-1-102kPa) for fast build rate and low plastic deformation during the process.

5.4.5. Comparison to reference printing mortars
Cementitious mortars or concretes for 3D printing conventionally rely on a purely thixotropic build-up after extrusion (Zhang et al., 2019). The shear-thinning behavior of the material enables extrudability. The related yield stress fluid properties can be described by a Herschel-Buckley or a Bingham model (De Larrard et al., 1996), presenting a linear behavior for smaller strains and a non-linear region for larger strains. As shown in (Kolawole et al., 2021), the linear-elastic region of fresh cementitious concrete composites can, with 0.4% be significantly higher as corresponding values of 0.008% for the bio-composite materials presented here. The corresponding yield stress values for the fresh state cementitious composites are significantly larger than the values of the bio-based composites at printing temperature and at rest with ~0.2-2 kPa (Yammine et al., 2008) and 0.07kPa respectively. Therefore, the shear softening and thixotropic principles are better suited

for printing processes in cementitious concrete composites. As shown in (Zou et al., 2021), the yield stress of cementitious composites at fresh state is dependent on the content of fines in the composite. Since a grain size distribution with a low fine content of 0.78%-wt. was chosen for this study, low values of the fresh properties could have been expected. The addition of fines in the here investigated bio-based materials is expected to have a similar impact on the material's yield stress and linear elastic regime. The optimization of the grain-size distribution on its printing parameters of MG composites remains to be investigated.

When cooled to ambient temperatures, the MG composite in Figure 5-17 showed a yield stress development over three orders of magnitude to 106 kPa. This being significantly larger than the yield stresses of fresh cementitious concretes of ~0.2-2 kPa (Yammine et al., 2008), a better buildability and build rate can be expected of the presented bio-composite material, possibly enabling thin-walled and higher degrees of free form in constructions. Other biopolymer bound soil composites from bovine blood proteins, tested for 3D printing, showed yield stresses in the same order of magnitude as cementitious concretes with 3-4kPa (Biggerstaff et al., 2021).

The open time of cementitious printing composites can be 30 min (Le et al., 2012) or less. This can lead to clogging and breaking of equipment connected with the printing process (Ngo et al., 2018). The presented bio-composite with thermoplastic behavior presents an open-time depending on the temperature to which it is heated or kept. If kept at printing temperature and hydrated, the open time is, in theory, infinite, disrespecting the binder's denaturing behavior.

5.5.   Conclusion

The two thermo-reversible hydrogels, mammal gelatin and κ-carrageenan, originating from mammal butchery side-products and seaweed, were investigated as binding materials in 3D

printing filaments for construction. The printing assessment within a heated extruder, cooling under ambient-temperature conditions showed that both filaments had concentration and temperature ranges for which the materials were extrudable and buildable. The tested rheological properties showed that the mammal gelatin composites exhibited the best printability. The rheological conditions between extrusion and building state exceeded the ones known for cementitious composites primarily through temperature-dependent changes. Therefore, a faster build rate and higher form stability can be expected due to quick and easy controllable yield stress development. This result could enable higher degrees of freedom in building components, leading to higher degrees of optimization and minimization of material use. As presented in this paper, the rheological properties fit this application.

6.   Printing process

Photo: media_k (Mikal Schlosser) taken as requested by Julian Christ, printing of biologically-based concrete composite with traversing mechanism and manually controlled extrusion.

In Chapter 5, the rheological principles of κ-carrageenan- and gelatin-based mortars are assessed as suitable for 3D printing processes. The thermoplastic setting of the material adds to rheological change during extrusion, compared to the thixotropic setting in cementitious mortars.

κ-carrageenan showed very sudden change in flow characteristics with temperature change. This was intended to have a positive effect on the printing process. However, the sudden rheological change was difficult to control under the simulated printing conditions. The preferred natural polymer binder for a temperature-controlled printing was therefore mammal gelatin.

The research presented in Chapter 4 and 5 showed that the mammal gelatin bound sand composites are the most suitable material for printing load carrying structures with a temperature controlled printing process, both in mechanical and rheological terms. The utilization of the thermoplastic properties for the printing process aims on increasing the freedom of printable geometry and possibly speed. The intended use of these added printing freedoms are, as introduced in Chapter 1, the realization of highly optimized structures with topology optimization. The connected need for overhang geometries and large degree of geometrical freedom in the realization process could be identified. This chapter aims on visualizing the advanced rheological properties of Chapter 5 by printing large overhang structures and thereby proving the vision, that the presented building and material concept can be applied to realize optimized structures.

A printing process with a robotic arm and a heated extruder that can keep the material at printing temperature until extrusion was designed for realizing large overhang structures. The following chapter focuses on testing the possibilities of creating these overhang constructions with the mammal gelatin based composites. Firstly, a vertical printing approach was chosen to increase continuously the overhanging degree. For this, a geometrical limit of inclination could be

identified. The study was then extended with a multi-axial printing, that could increase the overhang and layer inclination even further to show the whole capability of the printed material.

The content of this chapter is presented in form of a journal publication. The reference information can be seen below:

J. Christ, S. Leusink, H. Koss. 'Multi-axial 3D printing of biopolymer-based concrete composites in construction'. *Submitted and currently under review in*: Materials and Design, 2023, manuscript reference no.: JMADE-D-23-00609.

Multi-axial 3D printing of biopolymer-based concrete composites in construction

Julian Christ[a],*, Sander Leusink[a], Holger Koss[a]

[a] *Technical University of Denmark, Brovej 118, 2800 Lyngby, Denmark*

Abstract

This paper explores the free-form potential of 3D concrete printing with a novel concrete composite made from 80%-w/v mammal gelatin solution in water with 35%-w/w binder-aggregate. The replacement of cementitious binders in 3D printing mortar with bio-based hydrogels aims on improving sustainability and advancing the setting control through thermoplasticity. A multi-axial printing process with a KUKA robot arm and a heated ram extruder is presented. Printing trials with cylinders with 20cm diameter at varying overhangs were carried out - both with vertical- and multi-directional build direction. Through the inclination of the layers and the thermoplastic material properties, a maximum overhang of 80° could be reached. In comparison, with the same material but conventional slicing, overhangs of 40-50° could be achieved. The demonstrated freedom of shape and applicability of bio-based concrete composites could pave the way for highly optimized building components with minimum use of material, increasing the sustainability aspects of 3D concrete printing.

Keywords: biopolymer, 3D printing, concrete, gelatin, multi-axial printing

6.1.   Introduction

3D concrete printing has gained in popularity (Buswell et al., 2018)(Lyu et al., 2021) and its industrial interest is increasing (Siddika et al., 2020). The freedom to place material without the shape limitations of formwork allows the realization of architecturally advanced designs and material savings by constructing structurally optimized building components (J. Liu et al., 2022)(Tay et al., 2022)(Vantyghem et al., 2020a)(Schutter et al., 2018). Furthermore, this new technology is expected to increase the construction industry's productivity by automation of processes (WEF, 2016). The technology shows potential to lower the industry's environmental impact through material savings.

Constructing without formwork brings new challenges and sets high demands on the material's rheology. The material needs to be workable for extrusion and present high yield strengths right after deposition to support itself and further added layers under self-weight (Roussel, 2018). To enhance these properties, the current conventional material mixtures rely on a high share of cementitious material or injected accelerators to add to a fast yield strength development after extrusion (Wangler et al., 2019)(Gosselin et al., 2016). The high percentage of cementitious materials is a particular drawback on the methods environmental performance (Wangler et al., 2019). Therefore, other materials are being explored, including earth- and clay-based (Gomaa et al., 2022), polymeric- (Ali et al., 2022), geopolymer- (Panda et al., 2018)(Lim et al., 2018), or bio-based filaments (Sinka et al., 2020). In earlier studies (Christ et al., 2023), a bio-based concrete composite was explored, which was made from the hydrogel mammal gelatin and sand. It showed good printable qualities through thermoplastic phase change. Using a heated extruder, the material could increase its yield stress over three orders of magnitude (Christ et al., 2023) from extrusion to deposition, which promises good buildability. In comparison, cementitious filaments' early age

stiffening show slower and weaker early age strength development (Jayathilakage et al., 2020). Therefore, overhang geometries without the use of formwork in extrusion-based 3D concrete printing are, with some exceptions (Brun et al., 2020)(Vantyghem et al., 2020a)(Gosselin et al., 2016), little explored or strongly limited. This leaves the lack of possible overhang geometry as a limiting factor for the realization of highly structurally optimized building components (Vantyghem et al., 2020a)(Schutter et al., 2018).

For small scale extrusion-based polymer desktop printers, overhang geometries are realized by printing support structures (Ligon et al., 2017). This is, due to the large additional material use, not pursued for up-scaled concrete printing. Some advanced slicing softwares showed a multi-directional slicing approach for smaller objects and printers. This can increase the support of the printed layer by inclining the preceeded layer, making separate support structures redundant (Singh and Dutta, 2001)(Dai et al., 2018)(Wang et al., 2020). Due to the low scale, the print bed, including the object itself, can easily be tilted in this process to avoid uneven deformation. On larger scales, this is not realizable. However, with robotic fabrication, 6-axis printing can produce multi-directionally printed objects without rotation of the printing bed (Cao et al., 2022)(Dai et al., 2018). The bio-based material, presented in (Christ et al., 2023), shows the potential to exhibit the necessary shape robustness to realize multi-axial prints without bed inclination and prevent deformation due to gravitational loading.

This paper presents a method and material mixture to produce advanced free-form construction with alternative concrete composites made from gelatin and sand. A material mixture showing sufficient buildability for overhang constructions is presented. A new connected printing methodology with a heated extruder and a 6-axis KUKA robot arm that can place the thermoplastic material is introduced. Furthermore, the slicing method to create a toolpath for the KUKA robot

with a multi-directional slicing approach is presented. Finally, a comparison between vertically sliced and multi-directionally sliced objects is made to evaluate the maximum possible overhang and layer inclination for the biopolymer-based concrete. The respective failure mechanisms are being analyzed and discussed.

6.2. Materials

The bio-based concrete composite used for all samples consisted of a hydrogel binder from mammal gelatin and water mixed with sand. The mammal gelatin was purchased by the tool manufacturer DICTUM (DICTUM, 2019) (Art. Nr.: 450141) in granular form. Further specifications of the raw material can be found in (Christ et al., 2023).

Based on these results, a mixture was chosen for the tests. Earlier studies (Christ et al., 2023) showed that mixtures of 80-120%-w/v mammal gelatin solution in a 40%-w/w hydrogel-aggregate ratio present the best printable results. An 80%-w/v mammal gelatin concentration was chosen for all tests to minimize binder content. Sand with a higher fine content than in earlier studies (Christ et al., 2023) was selected to increase thixotropic effects and ease printability. The alternation of sand made it necessary to adapt the hydrogel-aggregate ratio. Through print trials and by assessing the extrudability and buildability, the hydrogel-aggregate ratio was adapted to 35%-w/w.

Sand with a specified maximum grain size of 0.18mm was used. The sand was purchased as silica sand nr.13 from Dansand A/S. A corresponding grading curve can be seen in Figure 6-1, which was experimentally determined after EN 933. The main mass of grains shows the size of 125-250μm and the mass of fine particles (<63μm) is about 5.01%-wt. The sand had a moisture content of 0.1%-wt. The light microscopy pictures in Figure 6-2 show grains with sub-rounded to sub-granular geometrical properties.
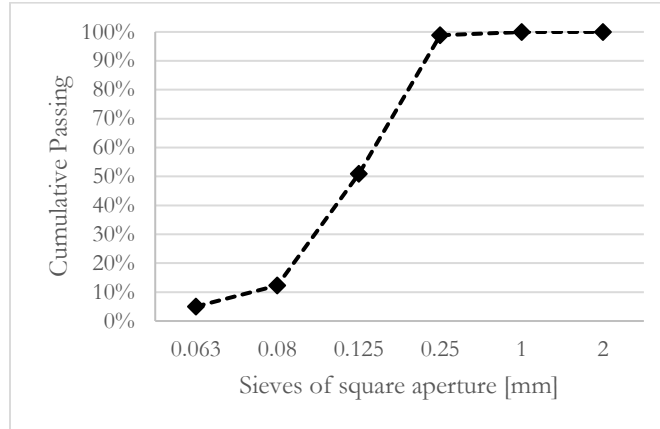
Figure 6-1 Grain size distribution of silica sand.
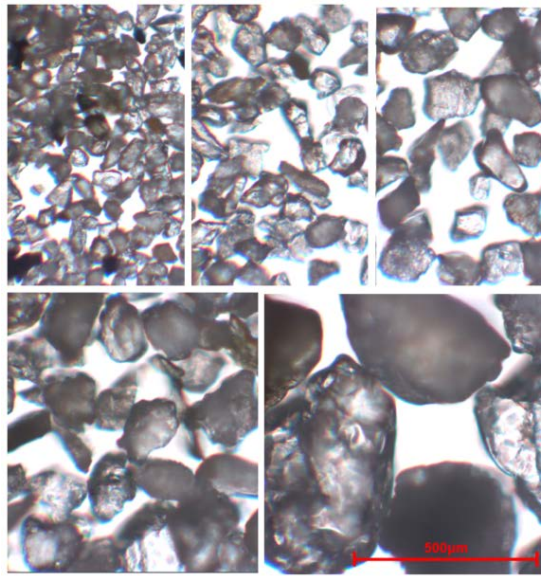
Figure 6-2 Silica sand grain geometries of varying sizes, retained in sieves: (from top left to bottom right) Pan, 0.063mm, 0.08mm, 0.125mm, 0.25mm.

6.3. Printing setup

6.3.1. Traversing mechanism

To move and control the position of the print head, a floor mounted KUKA robot KR2150 S C2 FLR ZH150/180" of type KR150, produced in 2004 with a 150kg payload was used (see Figure 6-3). The robot was controlled by a KRC2 unit that uses the KUKA robot language (KRL) for

programming.
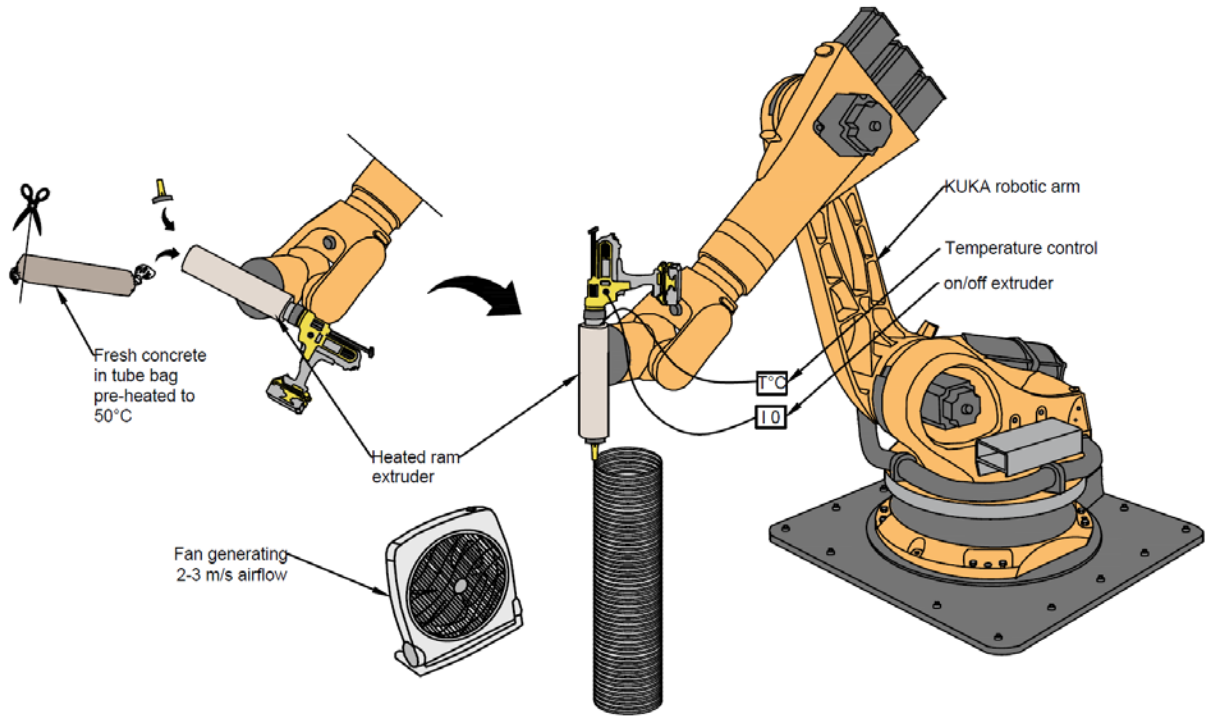
Figure 6-3 Printing setup. The tubular bag with the pre-heated material was placed in the cartridge of the ram extruder. The extruder was held and moved by a KUKA robot arm. The temperature and extrusion could be controlled by external switches. After extrusion, the material was cooled by an airflow with a speed of 2-3m/s created by a box fan.

In contrast to the three-axis gantry printers (Rahul and Santhanam, 2020)(Cao et al., 2022)(Bos et al., 2016) for concrete applications, the six axes of the robot arm allows directly for rotation around all three axes. Therefore, a tilting of the extruder for controlling the print angle is possible. Other concrete robotic printers use this additional freedom to reach difficult to access corners (XTree, 2019) or to incline the printed layer (Dressler et al., 2020)(Gosselin et al., 2016). The six-axis controllability of the robot arm is necessary to test the proposed overhang constructions with layer inclination and prove this approach as an economical off-the-shelf traversing mechanism.

6.3.2. *Extruder*

A ram extrusion system similar to (Soltan and Li, 2018) and (Shakor et al., 2019) was used. As described in (Christ et al., 2023), the ram extruder was adapted to elevate and keep the temperature of its filament. An automated caulking gun DEWALT DCE581E with a 600ml capacity was used for this purpose. According to the manufacturer, the caulking gun puts pressure of 1.05 MPa (DeWALT, 2018) on its 5.5 cm diameter piston in an aluminum cartridge of 37cm length. The standard speed of the piston is pre-defined at 40mm/min but may vary due to changes in the resistance to the extrusion process. When filled, the sum of friction on the cylinder's inner walls was higher, hence slightly slowing down the extrusion speed. The material was forced through a nozzle with a cylindrical opening of 13mm.

Figure 6-4 shows a heating coil wrapped around the extrusion cylinder with a spacing of 1.5cm and covered with an insulating foil and foamed rubber. A temperature switch was added to the heating coil and connected to a thermocouple, placed on the outside of the cartridge but underneath the insulation layer. The temperature of the aluminum cylinder could thereby be controlled and kept constant. Furthermore, an external on/off switch of the caulking gun was added to ease control. The nozzle was also insulated to prevent the material from cooling under standby time, potentially leading to clogging of the nozzle, and/or altering the extrusion's homogeneity (see Figure 6-4).
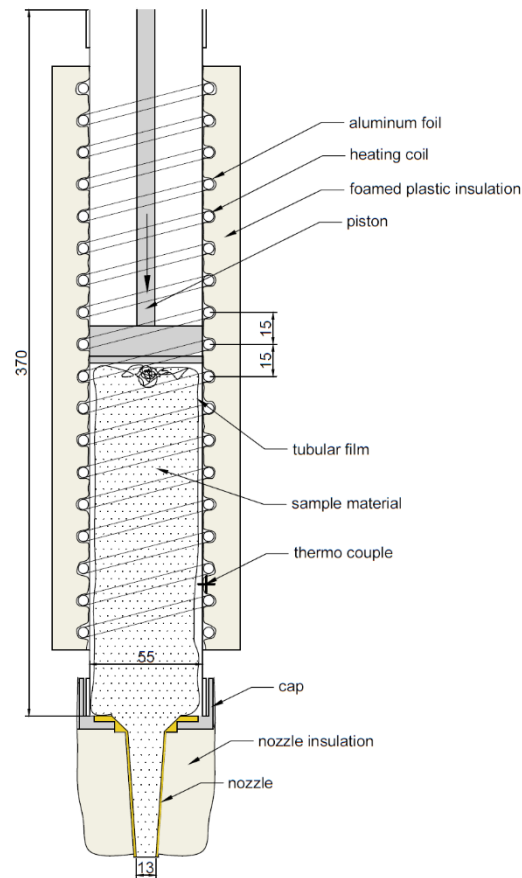
Figure 6-4 Ram extruder design. An automated caulking gun DEWALT DCE581E was altered to be able to heat its cartridge with a heating coil and connected insulation. Measurements are given in [mm]. Adapted from (Christ et al., 2023).

6.3.3. Fan

A fan was used at a distance of about 50cm to accelerate the cooling of the freshly printed layers.

A 35cm box fan from the producer MALMBERGS with the model number FB3501 was utilized.

The fan flowrate was adjusted to create a constant airflow with a speed of 2-3 m/s around the

sample. The air velocity was measured with a hand-held digital vane anemometer. The setup can

be seen in Figure 6-4.

6.3.4. Preheating of material

A UF160 oven from MEMMERT was used to preheat the material. At the temperature of 50°C,

the material was placed in the oven on a metal tray.

6.4. Methods

6.4.1. Material preparation

The binder was produced similar to earlier studies (Christ et al., 2019b)(Christ et al., 2023), using

a Kenwood KCC9060S cooking chef machine. The machine is in general quite similar to mixers as widely used for manufacturing test specimens for cement and mortar testing (Dansk Standard, 2016) but allows additionally the control of heat input.

The mammal gelatin granulate was soaked in water for 30 min under low stirring and without heating in normal ambient room conditions. Subsequently, the material was heated under low stirring to 65°C for 10min. At this stage, the material proved to be nearly homogeneous and the granulate was fully dissolved. To produce the composite material, the binder was mixed with sand, pre-heated to 50°C. Thereafter, the temperature and mechanical blending speed was kept unchanged for 20 minutes. The composite was then filled in tubular bags from low-density polyethylene with a wall thickness of 50μm and a width of 80mm. Closing both ends of the tubular bag with a simple knot prevented the material from drying during the preparation period. The material was stored in the tubular bags and under cooled conditions until printing preparation (see Figure 6-3).

The material preparation was designed to avoid denaturing the polymer structure, creating a porous material, and preventing drying. Therefore, the material was not exposed to long heating periods, fast stirring, and storing the material outside closed containers for extended amount of time.

6.4.2. Printing preparation

The extruder was pre-heated to 60°C and kept at this temperature for another 30min before filling the composite material bag. Simultaneously, the cool material bags were warmed in the oven to 50°C. The materials were placed in the oven not longer than 2 hours and at a minimum of one hour. This time frame aimed to ensure that the materials exhibited the same rheological properties and an even temperature profile between the batches. It could be observed that the material's porosity would decrease for more extended heating periods. The bags were kneaded for one min before usage and after preheating to ensure a homogenous material at extrusion. The robot arm

with the extruder was manually turned upwards for the refill (see Figure 6-3). The warm bag was slid into the extruder, and the tip of the bag was cut off before reattaching the nozzle on the cartridge. The piston of the extruder was manually engaged, and the robot was brought in start position.

6.4.3. Printing

The extrusion speed from the 13mm wide nozzle was kept constant at 10mm/s ($1.33cm^3$/s) and could be turned on/off manually with an external switch. The engagement of extrusion was timed with the manual onset of the robot arm movement. However, due to the material's elasticity and yield stress characteristic, the material extrusion showed some inertia in stopping and starting extrusion, especially when the cartridge was filled. Therefore, the extrusion was started slightly before the robot arm movement to enable a simultaneous onset of extrusion and movement.

Proper operation was controlled after each completed layer. The average printing time for a layer of a circular tube was about 40 seconds with an averaged extrusion or print head speed of 16mm/s along the printing path. Time and speed varied for layers within the tube curvature to enable the creation of a varying layer thickness. The time between each layer, i.e., the rest time after completing the previous layer and starting the subsequent layer, was varied depending on the layer inclination and based on the rigidity assessment of the previous layer. The production time for each layer was estimated from 20s time lapsed photographs.

The filling procedure of the cartridge gave an additional waiting time of 6-7min after each 9th layer.

6.4.4. Multi-directional slicing and tool path calculation

A planar multi-directional slicing approach, similar to (Wang et al., 2019) was used to create a tool path. The slicing methodology was further edited and adjusted to the needs of the experimental setup:

1. For small scale polymer slicers, the print bed is usually rotated instead of the print head (Dai et al., 2018)(Wang et al., 2020) to enable multi-directional printing – this is not feasible for extrusion-based 3D concrete printing since an on-site fabrication is envisaged.

2. The KUKA robot uses the manufacturer's own KUKA robotic language contrary to the conventionally used G-code language, i.e. the commands needed to be translated to this syntax.

3. The robot uses different location definitions for base and tool as well as for its coordinates, speed and acceleration.

4. Compared to desktop polymer printers, the extrusion rate of the used extruder could not be adjusted due to high inertial effects in the ram extrusion system. To be enable the printing of layers with variable thicknesses, the extruded volume per unit length was controlled by its traversing speed.

A flow chart of the slicing methodology is seen in Figure 6-5. The program incorporates the main steps of loading the model geometry, calculating a skeleton spline curve that serves as a normal vector to the slicing planes, generating a tool path. The tool path was created as G-code, and later translated to the Kuka-robot-language.
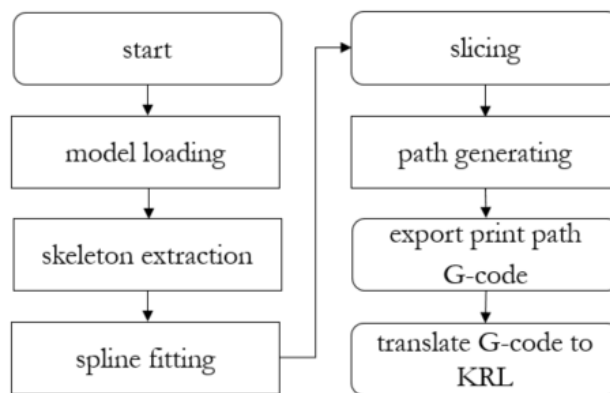
Figure 6-5 Flow-chart of slicing algorithm.

Model loading

The models were prepared as Standard Triangle Language file (STL). The file contains a triangulated mesh, approximating the object (see Figure 6-6 and Figure 6-7), consisting of three vertices, defining a plane between them and, if required, the corresponding plane normal vector.
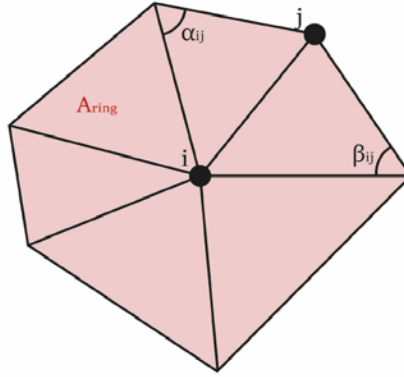
Figure 6-6 Mesh cut-out with the vertices i and j and the opposite angles α_{ij} and β_{ij} of line $\overline{IJ}$. (Leusink, 2020)
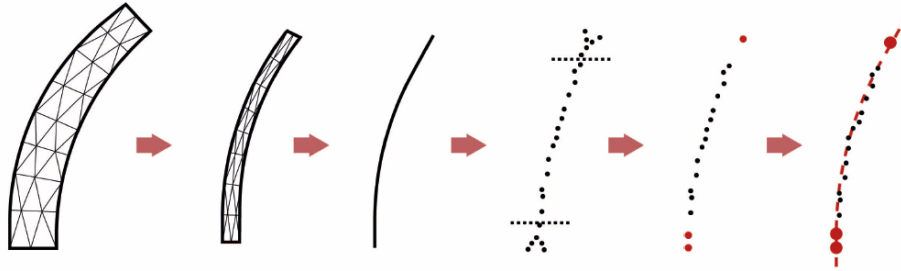
Figure 6-7 Skeleton line calculation. The mesh of the STL file is being contracted to a point cloud, trimmed and approximated by a spline curve. (Leusink, 2020)

Skeleton extraction

The STL mesh was further abstracted to a skeleton line to identify a slicing curve representing the longitudinal direction of the object. Some approaches to calculate the skeleton line, such as the shape diameter function (Shapira et al., 2008), mesh contraction method (Au et al., 2008), and mean curvature flow method (Tagliasacchi et al., 2012), were considered. Here, the method of (Au et al., 2008) was used, providing itself as least computational demanding. The approach abstracts the mesh by contracting the object based on local curvature (see Figure 6-7). The vertices of the

model surface S are thereby moved in the direction of the local surface normal n by a distance Δp proportionate to the local curvature H. As in (Tagliasacchi et al., 2012):

$$\Delta p = Hn \tag{6.1}$$

This was done by using the discrete Laplacian equation of $LV' = 0$, with V' being the vertex position and L being the $n \times n$ Laplace operator as described by equation (6.2) (Au et al., 2008):

$$L_{ij} = \begin{cases} \omega_{ij} = \cot\alpha_{ij} + \cot\beta_{ij} & if\ (i,j) \in E \\ \sum_{(i,k)\in E}^{k} -\omega_{ik} & if\ i = j \\ 0 & other \end{cases} \tag{6.2}$$

In which α_{ij} and β_{ij} are the opposite angles from the vertices i and j (see Figure 6-6). To prevent the mesh contracting to a single point, the diagonal weighting matrices W_L and W_H are introduced according to (Au et al., 2008), balancing the contraction and attraction, respectively:

$$\begin{bmatrix} W_L L \\ W_H \end{bmatrix} V' = \begin{bmatrix} 0 \\ W_H V \end{bmatrix} \tag{6.3}$$

The contraction process is iterative and is performed after (Au et al., 2008) by:

1. Solving the Laplacian equation $\begin{bmatrix} W_L^t L^t \\ W_H^t \end{bmatrix} V^{t+1} = \begin{bmatrix} 0 \\ W_H^t V^t \end{bmatrix}$ for the vertex position V^{t+1}.

2. Update the matrices $W_L^{t+1} = s_L W_L^t$ and $W_{H,i}^{t+1} = W_{H,i}^0 \sqrt{A_i^0/A_i^t}$ where A_i^0 and A_i^t are the areas of the mesh ring around point i.

3. Calculate the Laplace operator L^{t+1} for step $t + 1$ with equation (6.1)

Similar parameters, as in (Au et al., 2008), but slightly altered by trial and error were chosen to control the amount of detail in the contracted mesh: $W_L^0 = 1.0$; $W_H^0 = 10^{-2}\sqrt{A}$; $s_L = 2.0$; $\varepsilon = 5 \cdot 10^{-4}$. The contracted mesh was further processed from a contracted mesh to a point cloud of vertices (see Figure 6-7). Terminating closures of 3D objects lead to deviations in the point cloud. Therefore, a margin of 5% was removed at top and bottom of the curves.

Spline fitting

A 3rd order Bezier spline as in (Wang et al., 2019) was fit through the created point cloud to produce the final skeleton line. The spline was extrapolated beyond the end of the object to offset for the removed 5% margin.

Slicing

The object was sliced into layers by dividing the skeleton spline into sections with the length of the layer thickness t_{layer}. The number of layers n_{layer} could be calculated by dividing the length of the spline $S(u)$ at a parametric distance u by t_{layer} (Wang et al., 2019):

$$n_{layers} = \frac{S(u)}{t_{layer}} = \frac{1}{t_{layer}} \int_0^1 \sqrt{x'(u)^2 + y'(u)^2 + z'(u)^2} du \qquad (6.4)$$

The slicing planes were defined at points along this curve, where S(u) is an integer multiple of the layer thickness.

$$S(u) = i \cdot t_{layer} \qquad (6.5)$$

The corresponding normal vector of the slicing plane is S'(u). The printed thickness of the lines on the layers was calculated with the dynamic line thickness method as in (Wang et al., 2019).

The intersection of the slicing planes with the 3D surface is used to calculate the planar tool path, using conventional slicing methods (Choi and Kwok, 2002). Since the extrusion speed was fixed to a constant value, the extruded volume per millimeter printing track, i.e. the layer thickness, was controlled by adjusting the print speed (see appended video in Appendix 6.I) with:

$$v = \frac{Q}{t_L \cdot w_L} \qquad (6.6)$$

Where Q is the flow rate of the nozzle, t_L is the local layer thickness and w_L is the layer width. Since Q and w_L are constant, Q/w_L can be seen as a factor.

Export

The printing path was exported to G-code to allow an ubiquitous export format for computer numerical controlled machining. The printing path was noted as a `G1` movement for constant speed, while all other relocation motions were denoted as `G0` for faster movements.

The G-code could then be translated to the KRL syntax by using the correlations stated in Table 6-1. Most parameters can directly be correlated. However, some values, such as speed and acceleration, require additional lines in KUKA-robot-language and therefore need special translation. Also, units differed from G-code to KRL and needed to be adjusted. The tool and base definition was done manually with the KUKA robot's built-in software.

The implemented *slicing-* and *G-code to KRL translation algorithm* that was used in this paper can be found in (Leusink, 2020).

Table 6-1 Conversion from G-code to KUKA. The Section 'common commands' show directly convertible values between the G-code and KRL syntax. Underneath, the Kuka specific variable are specified which do not have a value in G-code.

		G-code	KRL
common commands	Coordinate (cdnt)	`X.. Y.. Z.. A.. B.. C..`	`{X .., Y .., Z .., A .., B .., C ..}`
	Tool Selection	`T..`	`$TOOL = TOOL_DATA[..]`
	Base Selection	`G92 X.. Y.. Z..`	`$BASE = BASE_DATA[..]`
	Rapid motion	`G0 [cdnt]`	`PTP[cdnt]`
	Controlled linear mot.	`G1 [cdnt]`	`LIN[cdnt]`
	Controlled circular mot.	`G2 [cdnt] I.. J..`	`CIRC[cdnt], [cdnt]`
		`G3 [cdnt] I.. J..`	`CIRC[cdnt], [cdnt]`
	Home all axis'	`G28`	`PTP HOME`
	Velocity	`F..`	`$VEL.CP = ..`

	Acceleration	`M204 S..`	`$ACC.CP = ..`
	Initialize	`G21; G90; G92 E0;`	`INI`
	Pause	`M1`	`HALT`
	Comments	`;`	`:`
Add. KRL commands	Approximate linear mot.		`[lin motion] C_DIS`
	Approximate distance		`$APO.CDIS = ..`
	Orientation control		`$ORI_TYPE #..`

6.4.5. Printed geometries

To test the maximum overhangs that can be produced with the bio-based composite material in vertical and the multi-directional slicing, eight shapes were defined (see Figure 6-8). To simplify the test of the concept, a circular cross-section was chosen with a diameter of 20cm. Inclinations of 10°, 20°, 30°, 40°, 50°, 60°, 70° and 80° were defined to identify the limit for material and printing method. The average layer height was defined as 5mm (see Figure 6-9). The layer width resulted, as discussed before, from the defined extrusion-, printing speed, nozzle size, and layer height in 13-15mm (see Figure 6-9).
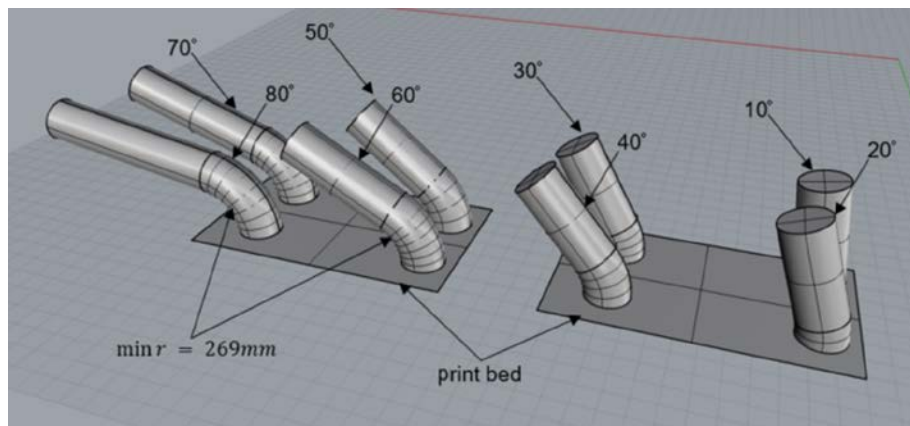
Figure 6-8 Modelled printing objects in Rhinoceros 6. Cylinders with an inclination of 10°-80° and a cylindrical cross section with a diameter of 20cm. The minimum radius of the rotation was calculated after equation 6.7. Four objects were fitted on the dimension of the printing bed.

Figure 6-9 Vertical cross-section of 80° inclination as seen in Figure 6-8. The layer width of 13-15mm and a layer height of approx. 5mm is identifiable. Picture: Julian Christ

Naturally, if a layer thickness shall be larger than zero at any point, the change of inclination between two successive layers, or the curvature of skeleton is limited. Figure 6-10 shows the geometry for a multi-axial 3D printing approach. The inner layers, closest to the center of rotation should not lay beneath a certain thresh-hold to enable a good print quality. In the case of this study, the thresh hold was chosen to be ±2mm respective to the average layer thickness. A general formulation for the minimum rotation radius for this boundary condition could be derived of the geometrical circumstances in Figure 6-10.
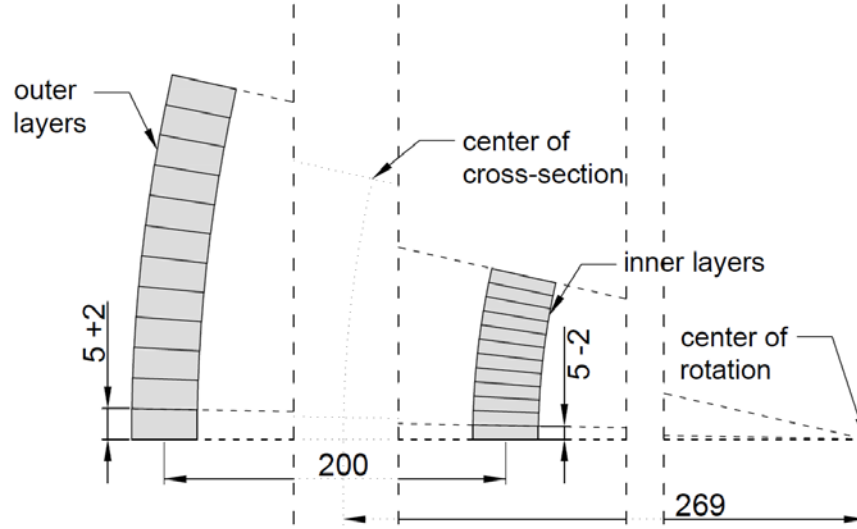
Figure 6-10 Geometrical limits for rotation radius with a layer height variance of ±2mm. All measurements are given in [mm].

The layers, laying on the inside of the rotation can be 2mm decreased, the layers on the outside can be 2mm increased, related to

the chosen layer height of 5mm. Equation 6.7 shows the calculation of the minimum radius of 269mm to satisfy those limits.

This can be seen in equation 6.7:

$$\min r = \frac{R + 0.5w}{x}$$

(6.7)

With: r - radius of pipe's curvature from rotational center to center of cross-section

R - radius of circular pipe's cross-section center

w - layer width

x - possible variance of layer (printability boundary); layer height $H \pm xH$;

$0 \le x \le 1$

For the layer thickness, a variation factor of $x = 2/5$ was defined, i.e. the standard layer height of

$H = 5mm$ was varied by: $\pm xH = \pm\frac{2}{5} \cdot 5mm = \pm 2mm$. The minimum radius of the cylinders

was calculated as $\min r = 269mm$.

It was expected to be able to print larger overhang geometries with the multi axes slicing direction, rather than the standard vertical build directions as known from other projects (Brun et al., 2020)(Vantyghem et al., 2020a). Therefore, the prints were started out with a vertical build direction, horizontal slicing, and a low overhang. The overhang was increased for each print, up to the point of observable failure in the manufacturing. To push beyond this point, the slicing methodology was switched to the multi axial slicing approach and continued to the maximum overhang/inclination of 80° (see Figure 6-8).

6.5. Results and discussion

6.5.1. Printing cylinders

The printed elements are shown in Figure 6-11. The top row shows the cylinders that were sliced with a vertical build direction – a maximum of 40-50° could be reached. The second row shows the multi-directionally sliced cylinders, for which a significantly higher layer inclination of 80° could be achieved.

The 50° overhang of the vertically sliced element was not printable. The areas of the layers that present the largest overhang (see bottom left of Figure 6-11) showed deformation during the print and later failure. In the regions of outmost lateral offset, the layer geometries lacked support and could therefore not be pressed onto the preceeded layer by the tip of the nozzle, thus keeping its cylindrical shape. The connection of the printed layer was insufficient to keep the material in place; it deformed and fell down. The identified printability limit in overhang originated from the material's loss of equilibrium and thus the lack of connection. To avoid this issue, small-scale polymer printers incorporate a temporary support structure that needs to be removed after completion of the print (Ligon et al., 2017). This is due to practical reasons not feasible for concrete printing, leaving to reach larger overhangs to increase the tack (adhesion strength of printed

174

layers), normal strength, and yield stress of the material, or creating increased support by layer inclination as explored in this study and shown in Figure 6-11.
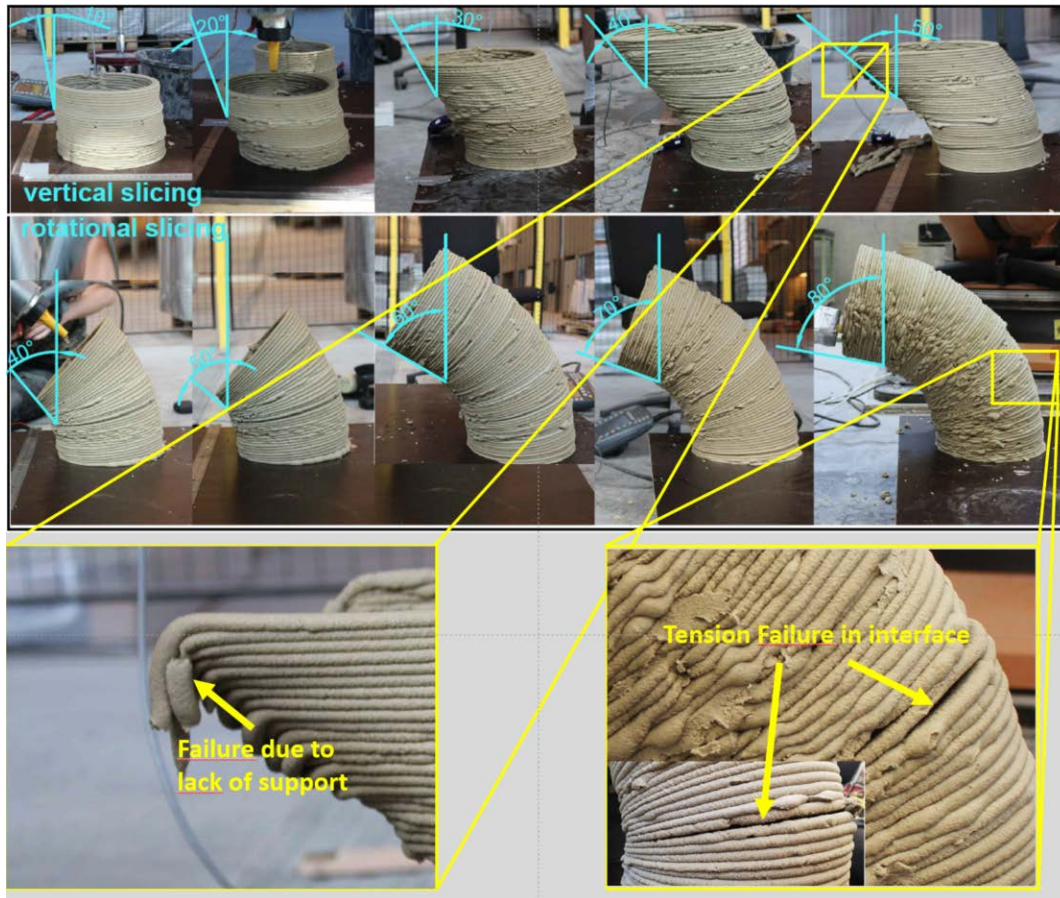
Figure 6-11 Prints of varying overhang geometry. Cross-section of pipe kept constantly circular with diameter of 20cm. Increasing overhang from 10° (top left) to 80° bottom right. Built with varying slicing strategies: vertical slicing (top) and rotational slicing (middle). 40° inclination was the largest inclination possible for vertical slicing methods, for rotational slicing, 80° inclination was achieved. Mechanisms of the respective failures can be seen in the bottom of this figure. Pictures: Julian Christ

An overhang of 50° could be reached without any further complications with the multi axial printed objects, suggesting that the increased layer inclination gives better buildability for overhang constructions. The overhang inclination was increased to 80°. The material showed at the reached inclination still good buildability without significant deformation. A failure occurred in the

location of high tensile stresses normal to the layer interface plane due to a large moment induced by self-weight of the cantilevering arch of the curved tube (see bottom right of Figure 6-11). Even though a failure was observed, the local deposition of the layer under an 80° inclination was still sufficient to meet the occurring tensile and shear stresses. The structural failure at 80° could be avoided by choosing a greater layer time to give the material a longer hardening time before being loaded.

The layer times were chosen, as seen in Figure 6-12. For close to vertical build-up without overhang, a continuous print was conducted without any resting time between the layers, i.e., the layer time matched the time for the nozzle to print one layer – 40s, as described in Section 6.4.3. As the built inclination increased, a more significant yield strength increase was needed to keep the material in place. As described in (Christ et al., 2023), the yield stress and stiffness of the material increase when given time to settle (thixotropy) and by cooling the material. Therefore, the increase of the layer time could add to the obtainable layer stability. A continuation of a 40s layer time would have led to an earlier collapse of the overhang structures. The layer times were increased in regards to the layer inclination. The average layer time did not exceed 5min for reasons of manufacturing practicability.
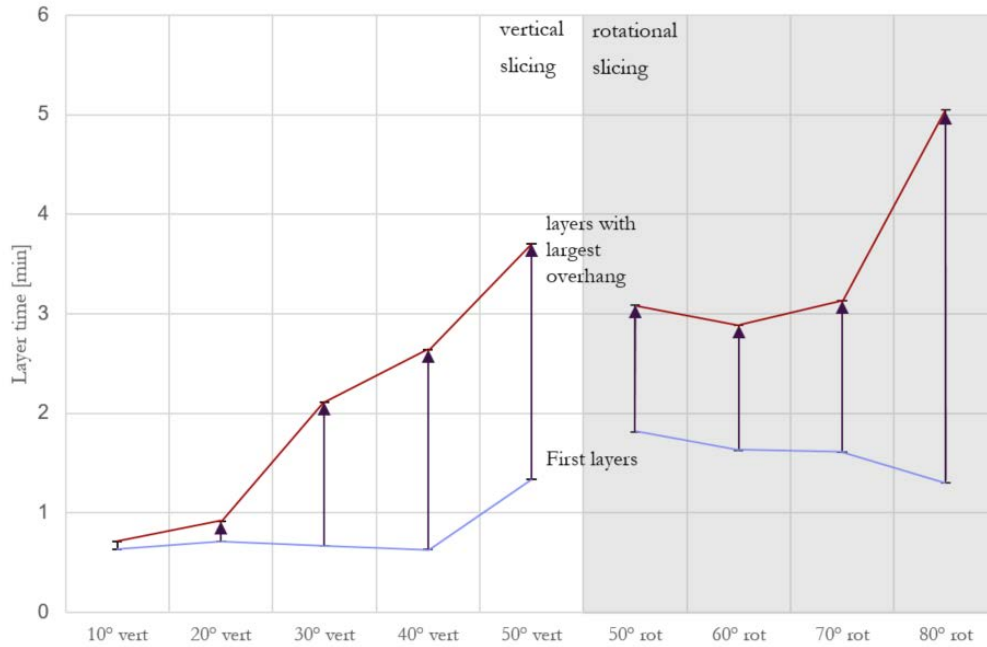
Figure 6-12 Mean layer time for (left) vertically sliced objects, (right) for multi-directionally sliced objects. The mean is taken over approx. 9 layers or each cartridge of the caulking gun.

Similar studies were attempted to reach a high inclination of overhang with vertical build direction methodologies for polymer printers (Mass and Amir, 2017) and cementitious concrete printers (Brun et al., 2020)(Vantyghem et al., 2020a). In (Brun et al., 2020), a maximum overhang in the vertical direction of 17.5° could be reached by optimizing the composition of cementitious material with the addition of fly ash. Similar results to this study give limits of polymer printers which are communicated with approx. 45° (Wulle et al., 2017). Depending on the layer thickness, a limit of 45° is often noted as a theoretical limit for a vertically sliced object (Mass and Amir, 2017). Since the layer width matches the layer's height, 50% of the deposited material lacks support, giving equilibrium issues of the supported layer, without relying on the materials tack.

Also in concrete printing, significant overhangs can be reached by either increasing the layer width or inclining the layers (Dressler et al., 2020)(Twente, 2020). For inclined layers, larger overhangs than 17.5° can be achieved (Twente, 2020). However, the material's buildability is still limited,

i.e., the rather slow setting characteristics are the limiting factor. For the presented concrete composite, a fast setting time through thermoplastic hardening can be reached and, therefore, high layer inclinations compared to conventional concrete composites. The high density and mass of the material also limits the overhang constructions due to the induced moment, not being able to reach as high overhangs as for other, less dense materials, such as plastics.

6.5.2. 6-axis printing

The robot arm allowed a 6-axes control, i.e., movement along 3 axis and adjustment of yaw and pitch angles of the print head. Therefore, the extrusion system could be placed normal to the layer plane for all slicing direction hence optimizing the material deposition. A limiting factor is the size of the print head, which could for complex geometries and small operation space collide with the already existing part of the structure. If not solved otherwise through advanced print head design, the print inclination would need to be limited for larger overhangs or limited printing spaces to give the print head enough room without damaging already printed parts. Similar processes can be seen in (XTree, 2019)(Twente, 2020).

The sliced planes were printable both for the vertical and multi-directional printing approach. The layers of the conventional slicer showed, as expected, a uniform layer height, while the layer height of the multi-directional sliced pipes varied. The allowed variation of the layer thickness of $\pm 2mm$ as determined in Section 6.4.5, was for some layers exceeded or undercut but without damaging the proceeding layer (see Figure 6-11). The intended maximum variation was exceeded. It can therefore be concluded that the calculated skeleton line and the centerline of the circular cross-section are similarly placed but not alike.

6.5.3. Extrusion and material

The extrusion through a caulking gun with preheated material as seen in Figure 6-4, was a simple but effective design successfully applied for building the geometries intended. The material

showed good homogeneity at extrusion. The material's consistency could vary slightly from batch to batch depending on pre-heating duration. This consistency change originates from mixing variations and the vapor permeability of the low density polyethylene film tube bags. During the heating period, the water content in the material is being decreased. In addition, the material is given time to settle while being heated and air enclosures in the material from the mixing process are being driven to the surface. The volume of solid material in the tube bag could therefore decrease through segregation in the solid- and gas phase, leaving the solid phase with varying consistencies.

The printability of the material is proved to show sufficient robustness for large layer inclinations. No tearing was observed from the deformation, and no plastic deformation due to self-weight was observed. The filament could be deformed from a cylinder shape of 13mm diameter to a layer with a height of 5mm through nozzle placement and movement.

6.6.   Conclusion

The process and the related material to print structures with large overhangs were presented. It was shown that with a multi-directional planar slicing methodology larger overhang structures could be reached than with the conventionally used vertical build direction methods. The multi-directional slicing approach, for which a skeleton line presents the slicing normal, offered better support for the freshly printed layers and could therefore enable higher degrees of freedom. The biopolymer-based thermoplastic concrete composite material developed early-age properties that showed sufficient rigidity to hold a freshly printed layer in place - also under 80° layer inclination. The heated ram extruder could keep the preheated composite material at temperature and allow for homogeneous extrusion with a rapid early-age yield stress development.

The improvement of rheological properties are decreasing the overhang limitations for 3D printed construction materials. With larger overhangs, higher degrees of structural optimization in building components and therefore a lower material consumption are possible. This paper could show that freedom of shape and large overhangs can be enabled by thermoplastic substitutes for conventional binders in concretes like the presented mammal gelatin.

Acknowledgements

7.   Discussion and conclusion

Photo: Julian Christ. A structure printed with a natural polymer based composite.

7.1. Printing optimized designs with gelatin-based concrete composite (Proof-of-concept)

This PhD study could prove (i) the applicability of natural polymer based concrete composites to construction and (ii) that the rheological properties of this material are suitable to realize freely shaped constructions with 3D printing. As introduced, the aim of this research was to pave the way for the realization of structurally optimized designs for a minimum resource consumption. While the journal papers embedded in this thesis, show 'in-vitro' studies for the mechanical strength, rheological properties and the limitation of realized free geometries, this chapter aims on demonstrating 'ex-vitro' application possibilities of building topology optimized construction designs with the material and printing process proposed in Chapter 6. Additional experiments were therefore performed in this chapter.

7.1.1. Topology-optimized structural design

To demonstrate that the material can realize topology optimized designs, a biomorph structure was designed with Rhinoceros 6 and the Grasshopper plug-in 'TOPOS' from 'archiseb'. One support was defined, that would branch out into four arms, loaded with a downwards facing surface load (see Figure 7-1 – bottom-right). The topology optimization algorithm minimized the material use to sustain the forces under the given support conditions and optimize its stiffness (see also (Christ, 2016) or (Bendsøe and Sigmund, 2003)). The optimized design aimed on representing a building column.

7.1.2. Material and method

The same material and methods of a gelatin based composite, printed with a robotic arm, as presented in Chapter 6 were used. However, a planar slicing tool was applied because, in this case, no inclinations of the design were larger than 45°.

7.1.3. *Printing of topology optimized design*

As seen in Figure 7-1, the structurally optimized design could be printed. The layers could be deposited without larger deformations and presented a good form stability for the connected overhangs. This goes in line with the findings of Chapter 6. Interesting to note is that at the beginning of the branching, a gap of several centimeters occurred that needed to be bridged with a material layer (see Figure 7-1 – bottom – middle). This was possible without support due to the cohesive strength of the freshly printed mortar and temperature controlled setting behavior (see Chapter 6).

7.1.4. *Overview of proof-of-concept*
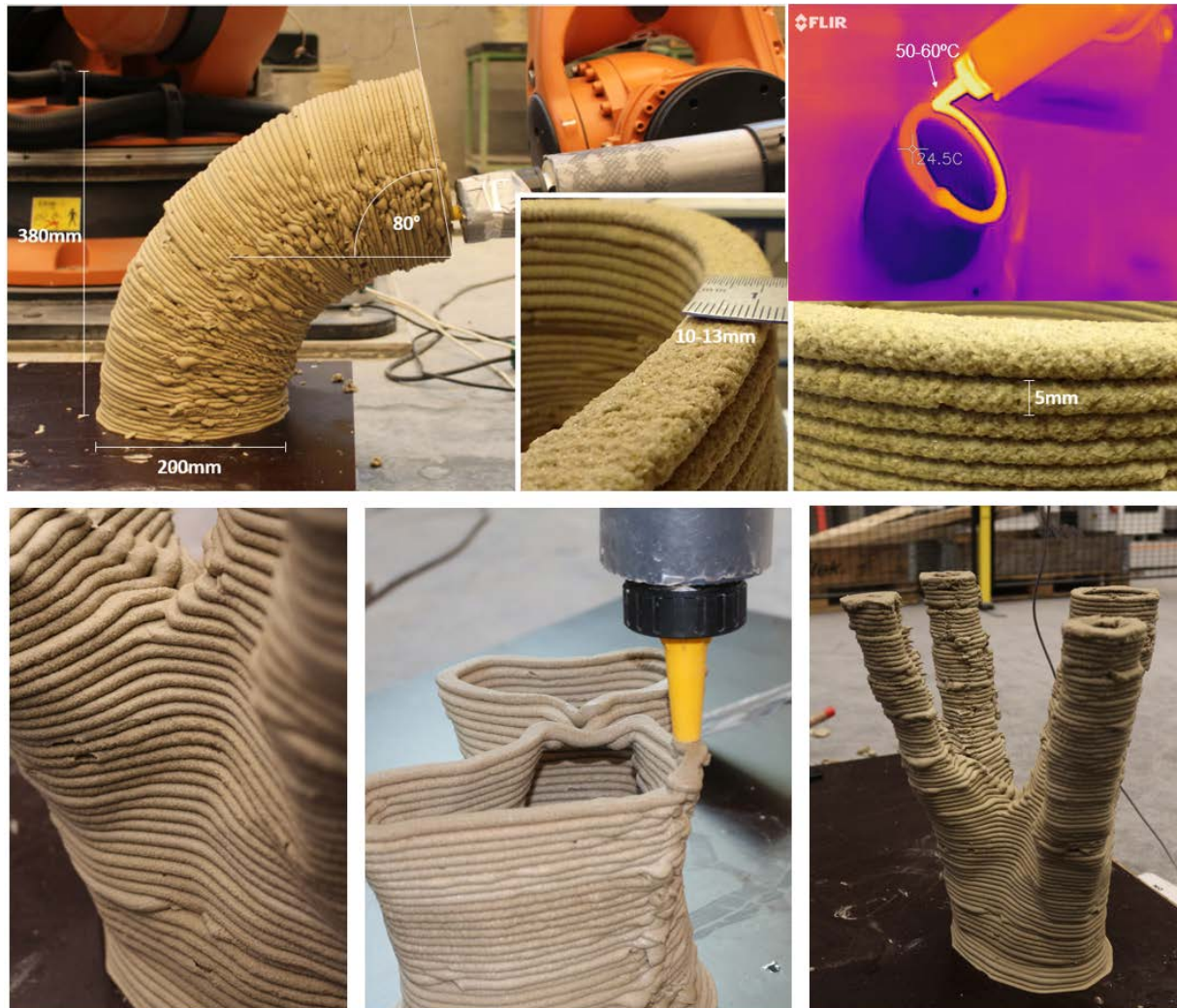
Figure 7-1 The composite of gelatin and mineral aggregates proved to realize optimized and geometrically free designs with a

temperature controlled print-head. (Top) A cylindrical overhang structure with layer inclination of 80° could be printed – The printing process and sample dimensions are shown, as well as a recording with an infrared camera to visualize the temperature differences during extrusion. (Bottom) A topology optimized structure could be printed with 4 branches that could be used as a building column. Picture from: (Christ et al., 2022).

The realization of the two building components, shown in Figure 7-1 with a mechanically strong gelatin and sand based composite with 3D printing proved the intended concept of this study.

This shall inspire designers and architects to create larger and more intricate optimized designs that can fully utilize the load-bearing capacity, as well as the free form potential of the material and process, thereby igniting their passion for innovative and daring building designs. In fact, the work of this thesis is already gaining attention as inspiration for future construction and design practices: the two building components are currently exhibited at the Designmuseum Denmark within the exhibition 'The Future is Present' (see Appendix 0.I).

7.2.   Discussion and future work

In this thesis, concrete composites produced from natural polymer binders and mineral aggregates which are suitable for load carrying applications in terms of their mechanical strength, have successfully been presented. Especially gelatin-based composites developed high strengths in the same order of magnitude as cementitious concrete composites (see Chapter 4). Furthermore, it could be proven that the thermoplastic natural polymer composites can be extruded with a temperature controlled ram extruder and that the thermoplastic setting of the material allows for fast stiffening, right after extrusion (see Chapter 5). The production and extrusion of these concretes allowed for the realization of free-formed and load carrying structures (see Chapter 6). The fast setting of the material allowed for 80⁰ layer inclination and overhang. These advanced rheological properties for the 3D printing application increase the building freedom, so that

realizing computationally optimized and organically shaped structural components as introduced in Chapter 1 is possible.

In the following, the intermediate conclusions of Chapter 4-6 are summarized and tied to the three research questions presented in Section 2.1. The findings are discussed in relation to each question. An outlook on future work and a description of impact of the work is given.

7.2.1. Discussions and future work on mechanical strength investigations

Chapter 4 concludes that all of the six natural polymer based composites present mechanical strength in the dried state. These composites were prepared so the fresh material mix is workable and sustains its shape under gravitational loading, ensuring that the tested mixtures are printable. In this assessment, especially gelatin-bound sand presented high compression strengths at the lower end but in the same order of magnitude as conventional cementitious concretes. The presented research could therefore answer positively to the first research question, presented in Section 2.1: 'Is it possible to build something from a concrete composite from natural polymers and mineral aggregates?'

Since all natural polymers presented an appropriate mechanical strength and the fresh concrete material was workable, it can be stated that it is possible to build load-carrying structures using a composite from natural polymers and mineral aggregates. However, the hardening required an extensive drying process for the material to reach its final strength, which sets a certain limitation for constructing with these materials. If bulky parts are intended to be casted from the concrete, the drying process could be very lengthy, and the large amounts of free water could lead to molding and deterioration of the organic binders. Therefore, a thin walled construction method without the use of formwork like the presented 3D printing technique is preferred.

The study showed that the materials can function as building components, but generally, durability issues could be identified. The materials swell easily with exposure to moisture and lose some of their mechanical strength. The exposure to moisture reintroduces free water to the natural polymers, which in turn can lead to molding. In future studies these issues need to be addressed, and can potentially be solved by inducing cross-linking agents which cross-link the natural polymer strands with stronger bonds, making the material set and more resistant to moisture. The natural polymers rely on hydrogen bonding for their cohesive strength development. The strength of these bonds is decreased by introducing a polar solvent, e.g. water. Cross-linking agents could create covalent bonding between the polymer strands, which cannot be dissolved by water. In addition, coatings can potentially prevent moisture from reaching the material.

Fire resistance is an additional concern. The presented binders are organic and do decompose at lower temperatures than mineral or metal based construction materials. However, the presented thermoplastic principles would let the reader expect that the material could lose its strength when reheated to printing temperatures. This however is not the case because the material is dried before being used as load carrying material. The removed water leads to an increase in solution concentration of the natural polymer composite and, as found in Chapter 5, to a melting point that is higher in temperature. Still, the heat and fire resistance of the material needs to be further investigated and developed. Also here, covalent cross-linking of the polymers can potentially improve the material. Protecting the material from heat through insulation or adding fire retarding materials is another possibility.

Despite the issues of fire and moisture resistance, a material, which could withstand mechanical force, was successfully produced. Since the production of these natural polymer based construction materials do not use Portland cement, the application could lower the CO_2 emissions of the

construction industry. This, however, needs further developments on the specific processing and construction techniques to conduct a subsequent life-cycle assessment comparison between full-scale conventionally cast concrete buildings and buildings built with the natural polymer based composite materials.

7.2.2. *Discussions and future work on the material's rheological behavior*

In Chapter 5, it was shown that a composite from mineral aggregates with carrageenan or gelatin as a binder has beneficial properties for 3D concrete printing. In addition to the conventionally used thixotropic principle in 3D concrete printing, the proposed material also undergoes a thermoplastic hardening in the fresh state. This can be utilized by extruding the heated material and therefore increase the stiffening after extrusion through cooling. Printing trials confirmed these beneficial rheological properties. Especially gelatin showed good consistency for extrusion and subsequent stiffening under cooling. The second research question of Section 2.1, i.e. 'Is it possible to use these composites to 3D print structures?' could therefore be answered with: yes, it is possible to 3D print structures with natural polymer based composites. The thin-walled character of the constructed components enabled the drying of the material after the construction phase. This creates a dependency of the material to the 3D printing construction process. Even when enabling the material application, the 3D printed and thin walled structure needs to be designed for this drying process. When working with closed or dense prints, again, molding issues could arise.

Generally, the change in rheological properties during extrusion is essential for an efficient extrusion-based 3D printing process. Even though the composite of natural polymers and sand was proven suitable for 3D printing by this work, the rheological properties can be further improved by (i) improving the grain size distribution and incorporating a higher share of fines and (ii) editing the binder's setting characteristics. In (i), a finer grain content could be introduced to increase the

thixotropic behavior of the composite and ease printability. The here investigated composite levers primarily on the thermoplastic stiffening principles for extrusion. The thixotropic principles could be elevated to a level of conventional cementitious printing materials and be supported by the thermoplastic thickening. Organic thixotropic additives like nano-crystalline cellulose can also be used to improve these phase changing properties. For (ii), mixtures of natural polymers can be used as binders. Carrageenan presented a very sudden viscosity change, while gelatin is more continuous in its stiffening. A combination of those two binders can potentially design the rheological properties for a specific application. Also additives that change the viscosity of the material could be applied and are left for future work.

The main objective of the embedded journal paper in Chapter 5 was the investigation of the two natural polymers carrageenan and gelatin due to the gelatin's workability and load carrying properties and the carrageenan's rapid setting characteristics. The other four natural polymer composites, which were identified with load carrying capability in Chapter 4 can be investigated further on their rheological properties and possible 3D printing applications. Some of these show thermosetting properties by adding an thermosetting additive or with heat. This principle could be utilized in a two-component extrusion system that mixes or heats the material in the nozzle for fast setting. E.g.: A combination of a sodium alginate based composite with an ion-solution that is injected at the extruder could enable sudden stiffening and good printability. In addition, a combination of a heated extruder and such an injection system for a second component that modifies the composite's rheology could be researched

The presented material in Chapter 5 showed a significant change in rheological properties during extrusion. With this setting behavior and promising printing properties, the research and material has the potential to greatly influence the development of the 3D printing community. Not only are

the setting characteristics of the presented material highly suited for 3D printing processes but the primary binder of natural polymers also present an alternative to the Portland cement used in cementitious concretes. Alternative binders like the presented natural polymers could alleviate the large requirement of Portland cement for the thixotropic properties necessary for 3D printing of concrete.

7.2.3. *Robotic printing with gelatin-based composite*

In Chapter 6, the range of possible geometrical complexity using the gelatin-based composite was studied, considering the presented printing technology. With a gelatin-based concrete composite, planar printing methods came to the limits of 40° overhangs, while multi-axial prints could show realizable layer inclinations and overhangs of up to 80º. These large degrees of freedom were enabled by the rheological properties of the material. The setting of the material through temperature change made the printed layer keep its shape and position right after extrusion, even with a layer inclination of 80º. Therefore, the answer to the third research question of Section 2.1, i.e., 'Do the advanced setting characteristics enable the realization of freely formed constructions?' is: yes, printing large overhangs could demonstrate the advanced rheological properties of the material.

For future work and further insights to the material's behavior, building components and printed structures should be tested. The incorporation of numerical models can link the material properties and limitation of geometrical freedom with structural optimization algorithms. This link can minimize the material use for the given process boundaries. For these numerical models, printing trials need to be assessed for their mechanical properties, which might differ from the tested samples in Chapter 4 due to the different sample preparation methods.

In this present study, the focus laid on the material. Further studies testing the use of several structural optimization methods and elaborating their potential for the application are recommended. These optimized and possibly geometrically free designs can subsequently be investigated for their architectural utilization and load carrying ability.

The developed printing process shows promising results for sample sized building components. To realize actual building sized components, building a larger print-head setup is recommended (see suggestion in Section 2.3.2). In addition, implementing a continuous material feeding process is recommended for future print head designs.

7.2.4. *Impact of this research*

The development of advanced material properties of concrete composites with a potentially more sustainable binder compared to conventional Portland cement, has the potential of introducing a radically new building philosophy to civil engineering. The high degrees of freedom which can be reached with the presented material and building process enables organic structural designs and the incorporation of new structures into architectural spaces. High degrees of optimization can be applied to building components and realized with natural polymer based 3D printing without the use of extensive formwork. This can reduce the consumed amount of material of the construction sector to a minimum.

The presented research represents a significant step forward for the field of civil engineering, as it responds to the growing demand for sustainable binders in concrete composites. Moreover, this research takes advantage of this need to strengthen innovative building technologies, like 3D printing. Thus, it contributes to the sustainable transition of the construction sector, and simultaneously, supports the automation of processes for higher productivity.

The author hopes that this interdisciplinary study inspires other researchers to seek out new research terrains and supplement the known grounds of their own research area. In times of imminent threats, such as the climate and environmental crisis, there is a pressing need to broaden knowledge through collaborations across all disciplines to create novel and ground breaking technologies for a more sustainable society.

7.3.   Conclusion

In this thesis, the possibility of using natural polymers as replacement for conventional binding material in 3D printing mortar was researched. A general proof-of-concept study was conducted.

κ-carrageenan, sodium alginate, agar, chitin, mammal gelatin and cold water fish gelatin showed potential for the use as binder in a natural polymer based concrete composite. Especially gelatin composites showed mechanical properties suitable for construction purposes.

In rheological testing, the mammal gelatin composite also proved suitable for a temperature controlled printing process. The material could change its consistency from extrudable at 50-60°C to buildable at around 20°C.

A printing process specifically designed for these materials, showed that freely formed constructions and optimized structures could be built.

Appendix 7.I shows the milestones of this study and concludes these in form of a Conference poster and extended abstract.

This study could show that the composite of mammal gelatin and sand is the most suitable of the 14 natural polymer binders investigated for the application in concrete. The composite has the ability of creating load carrying structures, which can be 3D printed in advanced free form

geometries, due to its thermoplastic setting characteristics. This concept was proven. Further research and development efforts on improving the materials durability, as well as research on specific application possibilities, should be undertaken.

The developments of potentially sustainable and biologically-based concrete composites with advanced rheological properties for 3D printing applications has the potential to largely impact civil engineering by enabling organic structural designs, reducing material consumption and a high degree of optimization in building components.

References

Aday, A., Osio-Norgaard, J., Foster, K., Srubar, W., 2017. Carrageenan-based superabsorbent biopolymers mitigate autogeneous shrinkage in ordinary portland cement. Mater. Struct.

Akbarzadegan, R., Ahari, H., Sharifan, A., Ali Anvar, A., 2020. Overview of the studies on authentication of gelatin using Fourier Transform Infrared spectroscopy coupled with chemometrics. J. Human, Heal. Halal Metrics 1, 86–93.

Ali, M.H., Issayev, G., Shehab, E., Sarfraz, S., 2022. A critical review of 3D printing and digital manufacturing in construction engineering. Rapid Prototyp. J.

ASTM International, 2014. D638 - 14 Standard test method for tensile properties of plastics. West Conshohocken.

Au, O.K.C., Tai, C.L., Chu, H.K., Cohen-Or, D., Lee, T.Y., 2008. Skeleton extraction by mesh contraction. ACM Trans. Graph. 27, 1–10.

Aykin-Dinçer, E., Koç, A., Erbas, M., 2017. Extraction and physicochemical characterization of broiler (Gallus gallus domesticus) skin gelatin compared to commercial bovine gelatin. Poult. Sci. 96, 4124–4131.

Baxter, A., Dillon, M., Taylor, A., 1992. Improved method for i.r. determination of the degree of N-acetylation of chitosan. Int. J. Biol. Macromol. 14, 166–169.

Behrens, S.H., Grier, D.G., 2001. The Charge of Glass and Silica Surfaces. Chem. Phys. 6716–6721.

Bendsøe, M.P., Sigmund, O., 2003. Topology Optimization. Theory, Methods, and Application, 2nd editio. ed. Springer Science & Business Media, 2003.

Biazar, E., Najafi S, M., Heidari K, S., Yazdankhah, M., Rafiei, A., Biazar, D., 2018. 3D bio-printing technology for body tissues and organs regeneration. J. Med. Eng. Technol. 42, 187–202.

Biggerstaff, A., Fuller, G., Lepech, M., Loftus, D., 2021. Determining the yield stress of a Biopolymer-bound Soil Composite for extrusion-based 3D printing applications. Constr. Build. Mater. 305, 124730.

Błaszak, B., Gozdecka, G., Shyichuk, A., 2018. Carrageenan as a functional additive in the production of cheese and cheese-like products. Acta Sci. Pol. Technol. Aliment. 17, 107–116.

Block Research Group, 2023. Block research group - 3D printed floor system [WWW Document]. Res. Gr. web site. URL https://www.block.arch.ethz.ch/brg/research/3d-printed-floor-system (accessed 3.2.23).

References

Bloom, O., 1925. Machine for testing jelly strength of glues, gelatins, and the like. US1540979.

Bos, F., Wolfs, R., Ahmed, Z., Salet, T., 2016. Additive manufacturing of concrete in construction: potentials and challenges of 3D concrete printing. Virtual Phys. Prototyp. 11, 209–225.

Bove, M., Uricek, M., 2022. 3D printed homes from waste materials [WWW Document]. WOHN - home as a Serv. URL https://www.wohnhomes.com/ (accessed 7.17.22).

Brun, F., Gaspar, F., Mateus, A., Vitorino, J., Diz, F., 2020. Experimental Study on 3D Printing of Concrete with Overhangs. RILEM Bookseries 28, 778–789.

Buchanan, C., Gardner, L., 2019. Metal 3D printing in construction: A review of methods, research, applications, opportunities and challenges. Eng. Struct. 180, 332–348.

Burgos, M., 2023. World's first 100% bio-based 3D-printed home in maine is built with sawdust and corn [WWW Document]. designboom. URL https://www.designboom.com/architecture/biohome3d-3d-printed-bio-based-university-of-maine-01-06-2023/ (accessed 3.2.23).

Buswell, R.A., Leal de Silva, W.R., Jones, S.Z., Dirrenberger, J., 2018. 3D printing using concrete extrusion: A roadmap for research. Cem. Concr. Res. 112, 37–49.

Campo, V.L., Kawano, D.F., Silva, D.B. da, Carvalho, I., 2009. Carrageenans: Biological properties, chemical modifications and structural analysis - A review. Carbohydr. Polym. 77, 167–180.

Cao, X., Yu, S., Cui, H., Li, Z., 2022. 3D Printing Devices and Reinforcing Techniques for Extruded Cement-Based Materials: A Review. Buildings 12, 1–19.

Cao, Y., Wang, Y., Zhang, Z., Ma, Y., Wang, H., 2021. Recent progress of utilization of activated kaolinitic clay in cementitious construction materials. Compos. Part B Eng. 211, 108636–108636.

Carro-López, D., González-Fonteboa, B., De Brito, J., Martínez-Abella, F., González-Taboada, I., Silva, P., 2015. Study of the rheology of self-compacting concrete with fine recycled concrete aggregates. Constr. Build. Mater. 96, 491–501.

Castagnino, S., Rothballer, C., Gerbert, P., 2016. What's the future of the construction industry? | World Economic Forum [WWW Document]. URL https://www.weforum.org/agenda/2016/04/building-in-the-fourth-industrial-revolution/ (accessed 7.15.22).

Choi, S.H., Kwok, K.T., 2002. A tolerant slicing algorithm for layered manufacturing. Rapid Prototyp. J. 8, 161–179.

Christ, J., 2016. Topology Optimization under Stochastic Wind Loading. Master Thesis, Technical University of Denmark.

References

Christ, J., Bak, J., Fiebig, J., Koss, H., 2019a. On the Ecology of climate and structures. In: IASS Symposium 2019 - 60th Anniversary Symposium of the International Association for Shell and Spatial Structures; Structural Membranes 2019. Barcelona, Spain, pp. 385–396.

Christ, J., Engelsen, T.K., Ottosen, L.M., Koss, H., 2020. Potential of natural polymers as alternative binder for 3D printing concretes. In: Digital Concrete 2020. Eindhoven, Netherlands.

Christ, J., Koss, H., Ottosen, L.M., 2019b. A concrete composite from biologically based binders and mineral aggregates for constructional 3D-printing. In: 2nd International Conference of Sustainable Building Materials. Eindhoven, The Netherlands.

Christ, J., Ottosen, L.M., Koss, H., 2022. Gelatin as biologically-based binder in temperature-sensitive printing mortar for advanced free form constructions. In: 3rd RILEM International Conference on Concrete and Digital Fabrication – Digital Concrete, 26-29 June 202. Loughborough, UK.

Christ, J., Perrot, A., Ottosen, L.M., Koss, H., 2023. Rheological characterization of temperature-sensitive biopolymer-bound 3D printing concrete. Constr. Build. Mater. (submitted - Curr. under Rev.).

Christiaen, D., Bodard, M., 1983. Spectroscopie Infrarouge de Films d'agar de Gracilaria Verrucosa (Huds.) Papenfuss. Bot. Mar. 26, 425–428.

COBOD, 2023. COBOD - World leader in 3D construction printing solutions [WWW Document]. Web site. URL https://cobod.com/ (accessed 3.2.23).

Dai, C., Wang, C.C.L., Wu, C., Lefebvre, S., Fang, G., Liu, Y.J., 2018. Support-free volume printing by multi-axis motion. ACM Trans. Graph. 37.

Dansk Standard, 2012. Dansk standard DS / EN 933-1 Prøvningsmetoder for geometriske egenskaber ved tilslag – Del 1 : Bestemmelse af kornstørrelses- fordeling – Sigteanalyse Tests for geometrical properties of aggregates – Part 1 : Determination of particle size distribution –.

Dansk Standard, 2013. DS/EN 12390-1 Dansk standard Prøvning af hærdnet beton – Del 1 : Form , dimensioner og andre krav til prøvelegemer og forme Part 1 : Shape , dimensions and other requirements.

Dansk Standard, 2016. DS/EN 196-1:2016 - Dansk standard Metoder til prøvning af cement – Del 1 : Styrkebestemmelse Methods of testing cement – Part 1 : Determination of strength.

Dansk Standard, 2019. DS/EN 932-3 - Prøvningsmetode for generelle egenskaber ved tilslag – Del 3 : Procedure og terminologi for forenklet petrografisk beskrivelse Tests for general properties of aggregates.

De Larrard, F., Ferraris, C.F., Sedran, T., 1996. Fresh concrete: A Herschel-Bulkley material. Mater. Struct. Constr. 31, 494–498.

References

Deshmukh, K., Ahamed, M.B., Deshmukh, R.R., Pasha, S.K.K., Bhagat, P.R., Chidambaram, K., 2017. 3 - Biopolymer Composites With High Dielectric Performance: Interface Engineering. In: Biopolymer Composites in Electronics. Elsevier Inc., pp. 27–128.

DesignNews, 2014. 3D Printing Water-Based, Biodegradable Composites - with Robots! [WWW Document]. URL https://www.designnews.com/3d-printing-water-based-biodegradable-composites-robots (accessed 3.2.23).

DeWALT, 2018. 18V XR Fugepistol med holder til patron, løs enhed [WWW Document]. URL https://www.dewalt.dk/powertools/productdetails/catno/DCE581N/ (accessed 7.18.22).

DICTUM, 2019. More than Tools - Dictum [WWW Document]. URL https://www.dictum.com/en/ (accessed 4.23.19).

Dillenburger, B., Hansmeyer, M., 2016. Digital Grotesque II at centre pompidous "impreimer le monde" [WWW Document]. Chair Digit. Build. Technol. ETH Zurich. URL https://dbt.arch.ethz.ch/project/digital-grotesque-at-centre-pompidou/

Donayre, A., Sanchez, L.F., Kim, S., Aguilar, R., Nakamatsu, J., 2018. Eco-friendly Improvement of Water Erosion Resistance of Unstable Soils with Biodegradable Polymers. IOP Conf. Ser. Mater. Sci. Eng. 416.

Dressler, I., Freund, N., Lowke, D., 2020. The effect of accelerator dosage on fresh concrete properties and on interlayer strength in shotcrete 3D printing. Materials (Basel). 13.

DS-EN-196-3, 2016. Dansk standard Metoder til prøvning af cement – Del 3 : Bestemmelse af afbindingstid og volumenbestandighed Methods of testing cement – Part 3 : Determination of setting times and soundness. Nordhavn.

DUS, 2023. 3D print canal house [WWW Document]. URL https://houseofdus.com/project/3d-print-canal-house/ (accessed 3.2.23).

Engbert, A., Gruber, S., Plank, J., 2020. The effect of alginates on the hydration of calcium aluminate cement. Carbohydr. Polym. 236, 116038.

Ferretti, E., Moretti, M., Chiusoli, A., Naldoni, L., de Fabritiis, F., Visonà, M., 2022. Rice-Husk Shredding as a Means of Increasing the Long-Term Mechanical Properties of Earthen Mixtures for 3D Printing. Materials (Basel). 15.

Foox, M., Zilberman, M., 2015. Drug delivery from gelatin-based systems. Expert Opin. Drug Deliv. 12, 1547–1563.

Frihart, C.R., Lorenz, L.F., 2018. Protein adhesives. In: Handbook of Adhesive Technology, Third Edition. CRC Press Taylor & Francis Group, pp. 145–176.

Galán-Marín, C., Rivera-Gómez, C., Petric, J., 2010. Clay-based composite stabilized with natural polymer and fibre. Constr. Build. Mater. 24, 1462–1468.

References

Garside, M., 2022. • Cement production global 2021 | Statista [WWW Document]. URL https://www.statista.com/statistics/1087115/global-cement-production-volume/ (accessed 7.15.22).

Global Alliance for Buildings and Construction, International Energy Agency, United Nations Environment Programme, 2019. Towards a zero-emissions, efficient and resilient buildings and construction sector. 2019 Global Status report.

Godoi, F.C., Prakash, S., Bhandari, B.R., 2016. 3d printing technologies applied for food design: Status and prospects. J. Food Eng. 179, 44–54.

Gomaa, M., Jabi, W., Soebarto, V., Xie, Y.M., 2022. Digital manufacturing for earth construction: A critical review. J. Clean. Prod. 338, 130630.

Gomez-Guillen, M.C., Gimenez, B., Lopez-Caballero, M.E., Montero, M.P., 2011. Functional and bioactive properties of collagen and gelatin from alternative sources: A review. Food Hydrocoll. 25, 1813–1827.

Gosselin, C., Duballet, R., Roux, P., Gaudillière, N., Dirrenberger, J., Morel, P., 2016. Large-scale 3D printing of ultra-high performance concrete - a new processing route for architects and builders. Mater. Des. 100, 102–109.

Guihéneuf, S., Rangeard, D., Perrot, A., Cusin, T., Collet, F., Prétot, S., 2020. Effect of bio-stabilizers on capillary absorption and water vapour transfer into raw earth. Mater. Struct. Constr. 53.

Guo, L., Colby, R.H., Lusignan, C.P., Howe, A.M., 2003. Physical gelation of gelatin studied with rheo-optics. Macromolecules 36, 10009–10020.

Guo, X., Wang, Y., Qin, Y., Shen, P., Peng, Q., 2020. Structures, properties and application of alginic acid: A review. Int. J. Biol. Macromol. 162, 618–628.

Hack, N., Lauer, W.V., 2014. Mesh-mould: Robotically fabricated spatial meshes as reinforced concrete formwork. Archit. Des. 84, 224–231.

Haghdan, S., Renneckar, S., Smith, G.D., 2016. Sources of Lignin. In: Lignin in Polymer Composites. Elsevier Inc., pp. 1–11.

Hamard, E., Cazacliu, B., Razakamanantsoa, A., Morel, J.-C., 2016. Cob, a vernacular earth construction process in the context of modern sustainable building. Build. Environ. 106, 103–119.

Homayouni, A., Ehsani, M.R., Azizi, A., Yarmand, M.S., Razavi, S.H., 2007. Effect of lecithin and calcium chloride solution on the microencapsulation process yield of calcium alginate beads. Iran. Polym. J. (English Ed. 16, 597–606.

Inozemtcev, A., Korolev, E., Qui, D.T., 2018. Study of mineral additives for cement materials for 3D-printing in construction. IOP Conf. Ser. Mater. Sci. Eng. 365.

References

IPCC, Pörtner, H.-O., Roberts, D.C., Poloczanska, E.S., Mintenbeck, K., Tignor, M., Alegría, A., Craig, M., Langsdorf, S., Löschke, S., Möller, V., Okem, A., 2022. Climate Change 2022 - Impacts, Adaptation and Vulnerability - Summary for Policymakers, Cambridge University Press. Switzerland.

Jacquet, Y., Picandet, V., Rangeard, D., Perrot, A., 2020. Gravity induced flow to characterize rheological properties of printable cement-based materials. RILEM Tech. Lett. 5, 150–156.

Jain, S., Fang, C., Achal, V., 2021. A critical review on microbial carbonate precipitation via denitrification process in building materials. Bioengineered 12, 7529–7551.

Jayathilakage, R., Rajeev, P., Sanjayan, J., 2020. Yield stress criteria to assess the buildability of 3D concrete printing. Constr. Build. Mater. 240, 117989.

Kaszyńska, M., Skibicki, S., Hoffmann, M., 2020. 3D Concrete Printing for Sustainable Construction. Energies 13.

Khatami, H.R., O'Kelly, B.C., 2013. Improving Mechanical Properties of Sand Using Biopolymers. J. Geotech. Geoenvironmental Eng. 139, 1402–1406.

Khunawattanakul, W., Puttipipatkhachorn, S., Rades, T., Pongjanyakul, T., 2010. Chitosan-magnesium aluminum silicate nanocomposite films: Physicochemical characterization and drug permeability. Int. J. Pharm. 393, 220–230.

Kolawole, J.T., Boshoff, W.P., Babafemi, A.J., Combrinck, R., 2021. Shear and viscoelastic properties of early-age concrete using small-amplitude and low-rate rheometry - From fresh state to initial set. Cem. Concr. Compos.

Kontovourkis, O., Tryfonos, G., 2020. Robotic 3D clay printing of prefabricated non-conventional wall components based on a parametric-integrated design. Autom. Constr. 110, 103005.

Krcma, M., Skaroupka, D., Zikmund, T., Kaiser, J., Palousek, D., 2021. Use of polymer concrete for large-scale 3D printing. Rapid Prototyp. J. 27, 465–474.

Kromoser, B., Reichenbach, S., Hellmayr, R., Myna, R., Wimmer, R., 2022. Circular economy in wood construction – Additive manufacturing of fully recyclable walls made from renewables: Proof of concept and preliminary data. Constr. Build. Mater. 344, 128219.

Laborel-Préneron, A., Aubert, J.E., Magniont, C., Tribout, C., Bertron, A., 2016. Plant aggregates and fibers in earth construction materials: A review. Constr. Build. Mater. 111, 719–734.

Laureano-López, B., Pérez-López, A., Espinosa-Solares, T., del Carmen Núñez-Santiago, M., 2022. Application of the tan δ method in the determination of the melting temperature of κ-carrageenan gels in the presence of calcium ions. Rheol. Acta 61, 183–189.

Le, T.T., Austin, S.A., Lim, S., Buswell, R.A., Gibb, A.G.F., Thorpe, T., 2012. Mix design and

fresh properties for high-performance printing concrete. Mater. Struct. Constr. 45, 1221–1232.

Leusink, S., 2020. Development of a slicing and control application for construction - scale 3D printing with polymeric concrete composites. Master Thesis. Technical University of Denmark - Supervised by J. Christ, H. Koss.

Ligon, S.C., Liska, R., Stampfl, J., Gurr, M., Mülhaupt, R., 2017. Polymers for 3D Printing and Customized Additive Manufacturing. Chem. Rev. 117, 10212–10290.

Lim, J.H., Panda, B., Pham, Q.C., 2018. Improving flexural characteristics of 3D printed geopolymer composites with in-process steel cable reinforcement. Constr. Build. Mater. 178, 32–41.

Liu, J., Nguyen-Van, V., Panda, B., Fox, K., Du Plessis, A., Tran, P., 2022. Additive Manufacturing of Sustainable Construction Materials and Form-finding Structures: A Review on Recent Progresses. 3D Print. Addit. Manuf. 9, 12–34.

Liu, Y., An, D., Xiao, Q., Chen, F., Zhang, Y., Weng, H., Xiao, A., 2022. A novel κ-carrageenan extracting process with calcium hydroxide and carbon dioxide. Food Hydrocoll. 127, 107507.

Lothenbach, B., Scrivener, K., Hooton, R.D., 2011. Supplementary cementitious materials. Cem. Concr. Res. 41, 1244–1256.

Lowke, D., Dini, E., Perrot, A., Weger, D., Gehlen, C., Dillenburger, B., 2018. Particle-bed 3D printing in concrete construction – Possibilities and challenges. Cem. Concr. Res. 112, 50–65.

Luhar, S., Suntharalingam, T., Navaratnam, S., Luhar, I., Thamboo, J., Poologanathan, K., Gatheeshgar, P., 2020. Sustainable and renewable bio-based natural fibres and its application for 3d printed concrete: A review. Sustain. 12, 1–25.

Lv, S., Cao, Q., Zhou, Q., Lai, S., Gao, F., 2013. Structure and characterization of sulfated chitosan superplasticizer. J. Am. Ceram. Soc. 96, 1923–1929.

Lyu, F., Zhao, D., Hou, X., Sun, L., Zhang, Q., 2021. Overview of the Development of 3D-Printing Concrete: A Review. Appl. Sci. 11, 9822.

Ma, S., Qian, Y., Kawashima, S., 2018. Experimental and modeling study on the non-linear structural build-up of fresh cement pastes incorporating viscosity modifying admixtures. Cem. Concr. Res. 108, 1–9.

Martens, P., Mathot, M., Bos, F.P., Coenders, J., 2017. Optimising 3D printed concrete structures using topology optimisation. In: Proceedings of the 2017 Fib Symposium, Held in Maastricht, The Netherlands, June 12-14. pp. 301–309.

Mass, Y., Amir, O., 2017. Topology optimization for additive manufacturing: Accounting for

overhang limitations using a virtual skeleton. Addit. Manuf. 18, 58–73.

Matsunaga, T., Shibayama, M., 2007. Gel point determination of gelatin hydrogels by dynamic light scattering and rheological measurements. Phys. Rev. E - Stat. Nonlinear, Soft Matter Phys. 76.

Mechtcherine, V., Bos, F.P., Perrot, A., da Silva, W.R.L., Nerella, V.N., Fataei, S., Wolfs, R.J.M., Sonebi, M., Roussel, N., 2020. Extrusion-based additive manufacturing with cement-based materials – Production steps, processes, and their underlying physics: A review. Cem. Concr. Res. 132, 106037.

Meibodi, M., Bernhard, M., Jipa, A., Dillenburger, B., 2017. the Smart Takes From the Strong: 3D printing stay-in-place formwork for concrete slab construction. In: Fabricate 2017. pp. 210–217.

Menasria, F., Perrot, A., Rangeard, D., 2017. Using Alginate Biopolymer To Enhance the Mechanical Properties of Earth-Based Materials. 2nd Int. Conf. Bio-based Build. Mater. 1st Conf. Ecol. Valoris. Granul. fibrous Mater. 35, 143–147.

Mignon, A., Vermeulen, J., Snoeck, D., Dubruel, P., Van Vlierberghe, S., Belie, N. De, 2016. Use of methacrylated alginate for self-healing concrete. HealCON 28–29.

Minghou, J., Lahaye, M., Yaphe, W., 1988. Structural studies on agar fractions extracted sequentially from chinese red sea weeds:Gracilaria sjeostedtii, G. textorii and G. salicornia using13C-NMR and IR spectroscopy. Chinese J. Oceanol. Limnol. 6, 87–103.

Mokhtar, A., Djelad, A., Bengueddach, A., Sassi, M., 2018. Biopolymer-layered polysilicate micro/nanocomposite based on chitosan intercalated in magadiite. Res. Chem. Intermed. 44, 6469–6478.

Mokhtari, H., Tavakoli, S., Safarpour, F., Kharaziha, M., Bakhsheshi-Rad, H.R., Ramakrishna, S., Berto, F., 2021. Recent advances in chemically-modified and hybrid carrageenan-based platforms for drug delivery, wound healing, and tissue engineering. Polymers (Basel). 13.

Monteiro, P.J.M., Miller, S.A., Horvath, A., 2017. Towards sustainable concrete. Nat. Mater. 16, 698–699.

Muguda, S., Hughes, P.N., Augarde, C.E., Perlot, C., Walter Bruno, A., Gallipoli, D., 2021. Cross-linking of biopolymers for stabilizing earthen construction materials. Build. Res. Inf. 0, 1–13.

Muguda, S., Lucas, G., Hughes, P.N., Augarde, C.E., Perlot, C., Bruno, A.W., Gallipoli, D., 2020. Durability and hygroscopic behaviour of biopolymer stabilised earthen construction materials. Constr. Build. Mater. 259, 119725.

Muhammad, R., Mohammad, S.S., Ashok, K., Peter, B., Carl, T., Pulickel, A., 2020. Cement-based direct ink for 3D printing of complex architected structures. US2020181014A1.

References

Nakamatsu, J., Kim, S., Ayarza, J., Ramírez, E., Elgegren, M., Aguilar, R., 2017. Eco-friendly modification of earthen construction with carrageenan: Water durability and mechanical assessment. Constr. Build. Mater. 139, 193–202.

Ngo, T.D., Kashani, A., Imbalzano, G., Nguyen, K.T.Q., Hui, D., 2018. Additive manufacturing (3D printing): A review of materials, methods, applications and challenges. Compos. Part B Eng. 143, 172–196.

Nhari, R.M.H.R., Ismail, A., Che Man, Y.B., 2012. Analytical methods for gelatin differentiation from bovine and porcine origins and food products. J. Food Sci. 77.

Nitsuwat, S., Zhang, P., Ng, K., Fang, Z., 2021. Fish gelatin as an alternative to mammalian gelatin for food industry: A meta-analysis. Lwt 141, 110899.

Ohama, Y., 2008. Polymer concrete. In: Developments in the Formulation and Reinforcement of Concrete. Woodhead Publishing Limited, pp. 256–269.

Pacheco-Torgal, F., Jalali, S., 2012. Earth construction: Lessons from the past for future eco-efficient construction. Constr. Build. Mater. 29, 512–519.

Panda, B., Unluer, C., Tan, M.J., 2018. Investigation of the rheology and strength of geopolymer mixtures for extrusion-based 3D printing. Cem. Concr. Compos. 94, 307–314.

Paris, J.M., Roessler, J.G., Ferraro, C.C., Deford, H.D., Townsend, T.G., 2016. A review of waste products utilized as supplements to Portland cement in concrete. J. Clean. Prod. 121, 1–18.

Paul, S.C., van Zijl, G.P.A.G., Gibson, I., 2018. A review of 3D concrete printing systems and materials properties: current status and future research prospects. Rapid Prototyp. J. 24, 784–798.

Perrot, A., 2019. 3D Printing of Concrete - State of the Art and Challenges of the Digital Construction Revolution. ISTE Ltd and John Wiley & Sons, Inc.

Perrot, A., Rangeard, D., Courteille, E., 2018a. 3D printing of earth-based materials: Processing aspects. Constr. Build. Mater. 172, 670–676.

Perrot, A., Rangeard, D., Mélinge, Y., 2014. Prediction of the ram extrusion force of cement-based materials. Appl. Rheol. 24.

Perrot, A., Rangeard, D., Menasria, F., Guihéneuf, S., 2018b. Strategies for optimizing the mechanical strengths of raw earth-based mortars. Constr. Build. Mater. 167, 496–504.

Perrot, A., Rangeard, D., Pierre, A., 2016. Structural built-up of cement-based materials used for 3D-printing extrusion techniques. Mater. Struct. Constr. 49, 1213–1220.

Piculell, L., 2020. Gelling Carrageenans. In: Food Polysaccharides and Their Applications. pp. 239–276.

References

Rahul, A. V., Santhanam, M., 2020. Evaluating the printability of concretes containing lightweight coarse aggregates. Cem. Concr. Compos. 109, 103570.

Ranjbar, N., Mehrali, M., Kuenzel, C., Gundlach, C., Pedersen, D.B., Dolatshahi-Pirouz, A., Spangenberg, J., 2021. Rheological characterization of 3D printable geopolymers. Cem. Concr. Res. 147, 106498.

Refilda, E., Munaf, R., Zein, A., Dharma, I., Indrawati, I., Lim, L.W., Takeuchi, T., 2009. Optimation study of carrageenan extraction from red algae (Eucheuma cottonii). J. Ris. Kim. 2, 120–121.

Rhein-Knudsen, N., Ale, M.T., Meyer, A.S., 2015. Seaweed hydrocolloid production: An update on enzyme assisted extraction and modification technologies. Mar. Drugs 13, 3340–3359.

Rhim, J.W., Ng, P.K.W., 2007. Natural biopolymer-based nanocomposite films for packaging applications. Crit. Rev. Food Sci. Nutr. 47, 411–433.

Rinaudo, M., 2006. Chitin and chitosan: Properties and applications. Prog. Polym. Sci. 31, 603–632.

Ritchie, H., Roser, M., Rosado, P., 2020. Energy - Our World in Data [WWW Document]. URL https://ourworldindata.org/energy (accessed 7.15.22).

Rizvi, H., Mehta, Y., Weis, D., Purdy, C., Ali, A., 2019. Fuel Resistance Asphalt Binder: Mixing Procedure and Fuel Damage Resistance, Sustainable Civil Infrastructures. Springer International Publishing.

Rosa, I., Roedel, H., Allende, M.I., Lepech, M.D., Loftus, D.J., 2020. On designing biopolymer-bound soil composites (BSC) for peak compressive strength. J. Renew. Mater. 8, 845–861.

Roser, M., Ortiz-Ospina, E., Ritchie, H., 2019. Life Expectancy - Our World in Data [WWW Document]. Publ. online OurWorldInData.org. URL https://ourworldindata.org/life-expectancy (accessed 7.15.22).

Roser, M., Ritchie, H., Ortiz-Ospina, E., 2020. World Population Growth - Our World in Data [WWW Document]. URL https://ourworldindata.org/world-population-growth (accessed 7.15.22).

Roussel, N., 2018. "Rheological requirements for printable concretes." Cem. Concr. Res. 112, 76–85.

Saji, S., Hebden, A., Goswami, P., Du, C., 2022. A Brief Review on the Development of Alginate Extraction Process and Its Sustainability. Sustain. 14, 1–20.

Samimi Gharaie, S., Habibi, S., Nazockdast, H., 2018. Fabrication and characterization of chitosan/gelatin/thermoplastic polyurethane blend nanofibers. J. Text. Fibrous Mater. 1, 251522111876932.

References

Schrieber, R., Gareis, H., 2007. From Collagen to Gelatine, Gelatine Handbook.

Schutter, G. De, Lesage, K., Mechtcherine, V., Nerella, V.N., Habert, G., Augusti-Juan, I., 2018. Vision of 3D printing with concrete - Technical, economic and environmental potentials. Cem. Concr. Res. 112, 25–36.

Sen, M., Erboz, E., 2010. Determination of critical gelation conditions of k-carrageenan by viscometric and FT-IR analyses. Food Res. Int. 43, 1361–1364.

Seok, H.W., 2005. Manufacturing method for building panel of yellow earth. KR20050049136A.

Shakor, P., Nejadi, S., Paul, G., 2019. A study into the effect of different nozzles shapes and fibre-reinforcement in 3D printed mortar. Materials (Basel). 12.

Shapira, L., Shamir, A., Cohen-Or, D., 2008. Consistent mesh partitioning and skeletonisation using the shape diameter function. Vis. Comput. 24, 249–259.

Siddika, A., Mamun, M.A. Al, Ferdous, W., Saha, A.K., Alyousef, R., 2020. 3D-printed concrete: applications, performance, and challenges. J. Sustain. Cem. Mater. 9, 127–164.

Singh, B., Ishwarya, G., Gupta, M., Bhattacharyya, S.K., 2015. Geopolymer concrete: A review of some recent developments. Constr. Build. Mater. 85, 78–90.

Singh, P., Dutta, D., 2001. Multi-direction slicing for layered manufacturing. J. Comput. Inf. Sci. Eng. 1, 129–142.

Sinka, M., Zorica, J., Bajare, D., Sahmenko, G., Korjakins, A., 2020. Fast setting binders for application in 3d printing of bio-based building materials. Sustain. 12, 1–12.

Soldevila, L.M., Royo, J.D., Oxman, N., 2014. Water - Based Robotic Fabrication : Large - Scale Additive Manufacturing of Functionally Graded Hydrogel Composites via Multichamber Extrusion.

Soltan, D.G., Li, V.C., 2018. A self-reinforced cementitious composite for building-scale 3D printing. Cem. Concr. Compos. 90, 1–13.

Sonebi, M., Amziane, S., Page, J., 2019. Proceedings of the 3 rd International Conference on Bio-Based Building Materials ICBBM 2019 Third International RILEM Conference on Bio-based Building Materials. Belfast.

Sri Bhanupratap Rathod, R., Venkatarama Reddy, B. V., 2021. Strength and stress–strain characteristics of fibre reinforced cement stabilised rammed earth. Mater. Struct. Constr. 54, 1–13.

Surahyo, A., 2019. Sustainable concrete. In: Concrete Construction. Springer Nature Switzerland AG 2019, pp. 105–121.

Tagliasacchi, A., Alhashim, I., Olson, M., Zhang, H., 2012. Mean curvature skeletons.

Eurographics Symp. Geom. Process. 31, 1735–1744.

Tay, Y.W.D., Lim, J.H., Li, M., Tan, M.J., 2022. Creating functionally graded concrete materials with varying 3D printing parameters. Virtual Phys. Prototyp. 17, 662–681.

Teizer, J., Blickle, A., King, T., Leitzbach, O., Guenther, D., 2016. Large scale 3D printing of complex geometric shapes in construction. ISARC 2016 - 33rd Int. Symp. Autom. Robot. Constr. i, 948–956.

Teter, J., Feuvre, P. Le, Bains, P., Re, L.R., 2020. Tracking Aviation 2020 – Analysis - IEA [WWW Document]. URL https://www.iea.org/reports/tracking-aviation-2020 (accessed 7.15.22).

Thành, T.T.T., Yuguchi, Y., Mimura, M., Yasunaga, H., Takano, R., Urakawa, H., Kajiwara, K., 2002. Molecular characteristics and gelling properties of the carrageenan family, 1: Preparation of novel carrageenans and their dilute solution properties. Macromol. Chem. Phys. 203, 15–23.

The World Bank, 2019. Fertility rate, total (births per woman) | Data [WWW Document]. URL https://data.worldbank.org/indicator/SP.DYN.TFRT.IN (accessed 7.15.22).

Thomas, S., Durand, D., Chassenieux, C., Jyotishkumar, P., 2013. Handbook of Biopolymer-Based Materials - Volume 2 - From Blends and Composites to Gels and Complex Networks. Wiley-VCH Verlag GmbH & Co. KGaA.

Tice, L.F., Moore, A.W., 1952. Heat Denatured Gelatin. J. Am. Pharm. Assoc. 631–633.

Tsavdaridis, K.D., Nicolaou, A., Efthymiou, A., 2018. Application of structural topology optimization to slender telecommunication lattice towers. In: Proceedings of CST 2018. 13th International Conference, Computational Structures Technology, 04-06 Sep. Barcelona, Spain.

Twente, 2020. 3D Printing Concrete Live - World's Records (Time Lapse) [WWW Document]. Youtube video. URL https://www.youtube.com/watch?v=uCE0ojKWqSM (accessed 7.19.22).

United Nations, 2015. The paris agreement. Paris.

Vantyghem, G., De Corte, W., Shakour, E., Amir, O., 2020a. 3D printing of a post-tensioned concrete girder designed by topology optimization. Autom. Constr. 112, 103084.

Vantyghem, G., Ooms, T., Shakour, E., Amir, O., 2020b. 3D-Printed Concrete Bridge Designed by Topology Optimization. In: Conference: 2nd RILEM International Conference on Concrete and Digital Fabrication.

Vollmert, B., 1973. Polymer Chemistry, Paper Knowledge . Toward a Media History of Documents. Springer-Verlag Berlin Heidelberg New York, Brooklyn.

References

Wagner, D., 2017. Holzbeton-Wandbauplatten in der DDR [WWW Document]. URL https://www.gutachter-wagner.de/holzbeton-wandbauplatten-in-der-ddr/ (accessed 3.9.23).

Walker, P., Stace, T., 1997. Properties of some cement stabilised compressed earth blocks and mortars. Mater. Struct. Constr. 30, 545–551.

Wang, M., Zhang, H., Hu, Q., Liu, D., Lammer, H., 2019. Research and implementation of a non-supporting 3D printing method based on 5-axis dynamic slice algorithm. Robot. Comput. Integr. Manuf. 57, 496–505.

Wang, S., Guo, S., Gao, X., Zhang, P., Li, G., 2022. Effects of cement content and soil texture on strength, hydraulic, and microstructural characteristics of cement-stabilized composite soils. Bull. Eng. Geol. Environ. 81.

Wang, X., Chen, L., Lau, T.Y., Tang, K., 2020. A skeleton-based process planning framework for support-free 3+2-axis printing of multi-branch freeform parts. Int. J. Adv. Manuf. Technol. 110, 327–350.

Wangler, T., Pileggi, R., Gürel, S., Flatt, R.J., 2022. A chemical process engineering look at digital concrete processes: critical step design, inline mixing, and scaleup. Cem. Concr. Res. 155, 106782.

Wangler, T., Roussel, N., Bos, F.P., Salet, T.A.M., Flatt, R.J., 2019. Digital Concrete: A Review. Cem. Concr. Res. 123.

WEF, W.E.F., 2016. Shaping the Future of Construction A Breakthrough in Mindset and Technology, Industry Agenda.

Whittington, T., 2021. Construction's productivity problem requires technology-based solutions [WWW Document]. Oxford Econ. URL https://blog.oxfordeconomics.com/world-post-covid/constructions-productivity-problem-requires-technology-based-solutions (accessed 7.15.22).

Wolfs, R.J.M., Bos, F.P., Salet, T.A.M., 2018. Early age mechanical behaviour of 3D printed concrete: Numerical modelling and experimental testing. Cem. Concr. Res. 106, 103–116.

Wolfs, R.J.M., Bos, F.P., Salet, T.A.M., 2019. Hardened properties of 3D printed concrete: The influence of process parameters on interlayer adhesion. Cem. Concr. Res. 119, 132–140.

Wulansari, R., Mitchell, J.R., Blanshard, J.M.V., Paterson, J.L., 1998. Why are gelatin solutions Newtonian? Food Hydrocoll. 12, 245–249.

Wulle, F., Coupek, D., Schäffner, F., Verl, A., Oberhofer, F., Maier, T., 2017. Workpiece and Machine Design in Additive Manufacturing for Multi-Axis Fused Deposition Modeling. Procedia CIRP 60, 229–234.

Xiao, Q., Gu, X., Tan, S., 2014. Drying process of sodium alginate studied by two-dimensional correlation ATR-FTIR spectroscopy. Food Chem. 164, 179–184.

References

XTree, 2019. 3D Printed Wall with integrated window frame [WWW Document]. Youtube video. URL https://www.youtube.com/watch?v=0byQtXW5Gm8 (accessed 7.18.22).

XTree, 2023. XTreeE - The large-scale 3D [WWW Document]. Web site. URL https://xtreee.com/en/ (accessed 3.2.23).

Yammine, J., Chaouche, M., Guerinet, M., Moranville, M., Roussel, N., 2008. From ordinary rhelogy concrete to self compacting concrete: A transition between frictional and hydrodynamic interactions. Cem. Concr. Res. 38, 890–896.

Yong, H., Liu, Jing, Kan, J., Liu, Jun, 2022. Active/intelligent packaging films developed by immobilizing anthocyanins from purple sweetpotato and purple cabbage in locust bean gum, chitosan and κ-carrageenan-based matrices. Int. J. Biol. Macromol. 211, 238–248.

Yuelin, L., 2018. Preparation method of 3D printing mortar with high thermal insulation performance. CN108083759A.

Zegard, T., Hartz, C., Mazurek, A., Baker, W.F., 2020. Advancing building engineering through structural and topology optimization. Struct. Multidiscip. Optim. 62, 915–935.

Zhang, Yu, Zhang, Yunsheng, She, W., Yang, L., Liu, G., Yang, Y., 2019. Rheological and harden properties of the high-thixotropy 3D printing concrete. Constr. Build. Mater. 201, 278–285.

Zou, S., Xiao, J., Zhenhua, D., Ding, T., Hou, S., 2021. On rheology of mortar with recycled fine aggregate for 3D printing. Constr. Build. Mater. 311.

Appendix 0.I - Dissemination and communications

Throughout the course of this project, the findings were (or are intended to be) disseminated in peer-reviewed journal publications, conference papers, - poster publications and -presentations. In addition to scientific dissemination, communication channels to the general public were chosen to extend the outreach. A list of dissemination and communication actions can be seen here:

Dissemination in peer-reviewed journals

J. Christ, T. K. Engelsen, E. Thybring, L. Ottosen and H. Koss. 'Screening of natural polymers as binder in concrete composites'. *Submitted to and currently under review in*: Construction and Building Material, 2023, manuscript reference no.: CONBUILDMAT-D-23-02616.

J. Christ, A. Perrot, L.M. Ottosen, H. Koss. 'Rheological characterization of temperature-sensitive biopolymer-bound 3D printing concrete'. *Submitted and currently under review in*: Building and Construction Materials, 2023, manuscript reference no.: CONBUILDMAT-D-23-01335.

J. Christ, S. Leusink, H. Koss. 'Multi-axial 3D printing of biopolymer-based concrete composites in construction'. *Submitted and currently under review in*: Materials and Design, 2023, manuscript reference no.: JMADE-D-23-00609.

Dissemination in conference proceedings and -posters

Christ, J., Ottosen, L.M., Koss, H. 'Gelatin as biologically-based binder in temperature-sensitive printing mortar for advanced free form constructions', 3rd RILEM International Conference on Concrete and Digital Fabrication – Digital Concrete, 26-29 June 2022, Loughborough [UK] – Loughborough University

Christ, J., T. K. Engelsen, L. M. Ottosen, H. Koss, 'Potential of natural polymers as alternative binder for 3D printing concretes', Proceedings of the 2nd RILEM International Conference on Concrete and Digital Fabrication – Digital Concrete, 6-9 July 2020, Eindhoven [NE] – Eindhoven University of Technology.

Christ, J., H. Koss, L. M. Ottosen, 'A concrete composite from biologically based binders and mineral aggregates for constructional 3D-printing', Proceedings of the 2nd International Conference of Sustainable Building Materials – ICSBM 2019, 12-15 August 2019, Eindhoven [NE] – Eindhoven University of Technology.

Christ, J., J. Fernandoy-Bak, J. Fiebig, H. Koss, ' On the Ecology of Climate & Structures', Proceedings of the IASS Annual Symposium 2019 – Structural Membrane 2019 – Form and Force, 7-10 October 2019, Barcelona [ES]

Additional conferences with presentation

Christ, J*, 'Kan man lave beton af madaffald?', Danish bio-economy conference 2021, Engestofte Gods, Maribo (DK), [Invited Speaker]

Communication activities

'The Future is Present'. June 22, 2022 – May 28, 2023, **Designmuseum Denmark** (DMD), Copenhagen. Exhibition of the two main proof-of-concept pieces in this study for 11 months. (see picture below)

'**TV2** Nyheder', Danish National TV News (2021) by Søren Juhler - 19:00, 9 September, Danmark Lyngby/Odense. Interview with Holger Koss and Julian Christ and filming of the 3D concrete printing equipment. (see picture below)

Christ, J., H. Koss, 'Her skal de printe organiske strukturer – med cementfri beton'. Magazine **DYNAMO**: 3D-beton-print, (65) June 2021, Article by Lotte Krull - Technical University of Denmark, accessible at: https://issuu.com/dtudk/docs/dynamo65?fr=sOGQyMTQ4NjgwMg

Eight **LinkedIn** posts, average-reach per post: 4800 impressions. Through personal profile https://www.linkedin.com/in/julian-christ-84343511b/; **LinkedIn** communications through DTU Civil Engineering's (https://www.linkedin.com/company/dtu-byg/mycompany/) and DTU central's profile (https://www.linkedin.com/school/technical-university-of-denmark/)

Appendix 0.II - Supervised master and special course projects

As part of this PhD project, the following student projects were supervised:

Jonas Holmer Bigom & Oliver Kragelund Vittrup, *Juxtaposition of two biopolymer based composites and cementitious mortar for extrusion based 3D printing,* Master Thesis, 2022

Olivia Balenciaga Sanchez, *Study on the bonding strength of a biopolymer-based 3D printed concrete*, Special Course, 2021

Maria Husarcikova, *Rheological study of biopolymer-based concrete composites for extrusion-based 3D printing*, Master Thesis, 2021

Sander Leusink, *Development of a slicing and control application for construction-scale 3D printing with polymeric concrete composites*, Master Thesis, 2020

Madeleine Durieux Rostrup-Nielsen, *Bio-based building materials*, Special Course, 2019

Marvin Glissner, *Organic secondary resources in Greenland*, Student Assistant, 2019

Appendix 0.III - Attended Courses

As part of this PhD study, the following courses were attended:

Rheology of complex fluids (7.5 ECTS), DTU Department of Chemical Engineering , course nr. 28908, Denmark

Biochemistry (5 ECTS), DTU Department of Biotechnology and Biomedicine, course nr. 27022, Denmark

Basics of robot programming (2.5 ECTS), KUKA College Augsburg, Germany

How to write a scientific paper (5 ECTS), DTU Department of Civil Engineering, course nr. 11621, Denmark

Patent Course (3 ECTS), DTU Department of Management Engineering, course nr. 42799, Denmark

Methods for experimental materials characterization (5 ECTS), DTU Department of Mechanical Engineering, course nr. 41658, Denmark

Appendix 0.IV - Teaching Activities

In addition to the carried out research work, this PhD study included the following departmental work:

Teaching in the course 'Building Design 2', DTU Department of Civil Engineering, course nr. 11825, Greenland

Teaching in course 'Interdisciplinary Bioengineering', interdepartmental course at DTU, course nr. 27020, Denmark

Appendix 1.I - Conference Paper – 'On the Ecology of Climate & Structures'

Christ, J., J. Fernandoy-Bak, J. Fiebig, H. Koss, ' On the Ecology of Climate & Structures',

Proceedings of the IASS Annual Symposium 2019 – Structural Membrane 2019 – Form and Force,

7-10 October 2019, Barcelona [ES]

On the Ecology of Climate & Structures

J. CHRIST, J. FERNANDOY-BAK[a], J. FIEBIG[a], H. KOSS[a]

*DTU Civil Engineering, Brovej 118, 2800 Kgs. Lyngby
julch@byg.dtu.dk

[a] DTU Civil Engineering, Brovej 118, 2800 Kgs. Lyngby

Abstract

The paper discusses various aspects of the interrelation between climate and structures as part of the biosphere's ecosystem. Structural design is hereby understood as a subsystem of humanity, seen as a biological organism, and the climate, as part of the organism's abiotic environment. Possibilities within recent advancements in digitalization and automation to adopt structural design to climatic loading conditions and to mitigate the effect of the manufacturing of structures on the climate are presented as core disciplines of the research group 'Climate&Structures' and are placed within the ecosystem's interrelations. These disciplines are: observation and simulation of climatic loading phenomena (icing, snow- and wind loading), adaption of structures to these with parametric multi-objective and topology optimization, and realization of these structures with additive manufacturing with circular and recycled construction materials.

Keywords: ecological structures, climate, climatic loading, wind load, snow load, icing, parametric multi-objective optimization, topology optimization, constructional 3D-printing, biologically based concrete composites

1. Introduction

Ecology, a science evolving from biology, describes the interrelation of organisms with their biotic and abiotic environment [1]. The investigated body within an ecological unit is thereby the ecosystem and includes the interaction of its biological, physical and chemical components [2]. This relation exists and is subjected to investigation at different scales: from Petri-dish bacteria cultures to our planetary biosphere [3]. On the example of the largest anthropogenic affected ecosystem, humans affect their environment by changing available resources in their physical, chemical and biological state [2]. In the same way, humans in turn are affected by other living components of the ecosystem and by the availability of non-living resources and physical states in nature. An ecosystem is often misunderstood as a community, limited to a field in ecology describing the interrelation of living biotic components (plants animals, microbes, etc.). By the definitions introduced above, a full view of an ecosystem includes as well numerous abiotic factors like climate, soil, and general energy and material consumption [1][4].

In fields, such as ecological economics [5], ecological agriculture, or ecological building [1], the objective is to adopt the respective human systems (economics, industry, etc.) to be co-existent in symbiosis [6] (or mutualism [7]) with their environment. Consequently, these disciplines are a subsystem of the human organism within the ecosystem [5] of our own biosphere. The term 'ecological building' describes this role for the field of Civil Engineering and is explained in Daniels [1]. Focusing on a specific part of this field, the paper describes the interrelation of the load carrying structure (design and construction) as a subsystem of the human organism, with the climate as its abiotic environment. Conceptual relations are laid out by mapping interdependencies between climate and structures. Furthermore, strategies and methodologies are presented to understand, quantify and influence the

ecological processes and are presented as part of the core disciplines of the research group 'Climate&Structures' at DTU Civil Engineering.

1.2. Climate and structures – A concept of interrelation

Throughout the history of humankind, structures were erected to create shelter from weather and environmental impacts, starting by using locally available materials. Structural geometry and concepts of the load carrying system were adapted and optimized through trial-and-error and systematic experimentation. Available resources were refined, material properties enhanced, and design methods improved, leading gradually to optimized structures within the associated ecosystem.

With the advent of globalization and industrialization, the supply chain for raw materials changed significantly and with that the advancement in architecture, design and structural performance. Construction materials, like concrete and steel, were produced from large-scale centralized industrial branches, affecting the environment by heavy resourcing of raw materials and changing its chemical state [8]. Such, not only standing in the direct interrelation with its local ecosystem, but rather affecting the biosphere and global climate, marking hence the era of the Anthropocene.
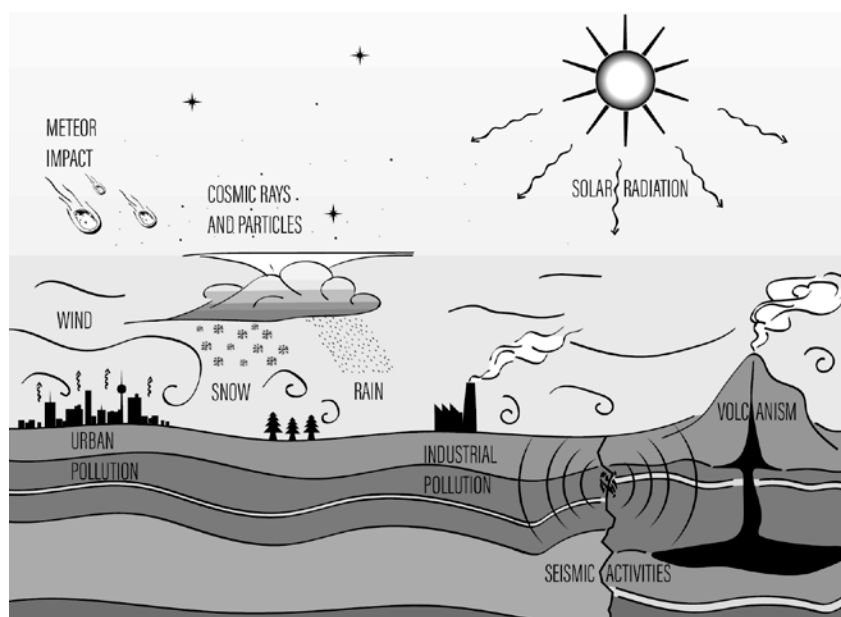
Figure 1: Aspects of climate-structures interrelation, including direct load impacts and long-term exposures of structures and humans within the built environment.

Figure 1 illustrates some of the main natural and anthropogenic elements in the ecology of natural environment, climate, structures and humans in the built environment. Structures are designed to withstand the impact from natural forces such as wind, snow, ice and earthquakes and are subjected to deterioration by climate impact like temperature, humidity and solar radiation. The climate in turn is affected by the manufacturing process of structures, e.g. through the herewith connected particle- and greenhouse gas emission, and through the expansion of urban land (e.g. surface albedo change). As described by the International Panel on Climate Change (IPCC), CO_2-emissions are one of the key drivers in climate change [10], for which the construction sector plays a major role [8], [11], [12] - Cement production alone is responsible for around 4% of the world's fossil fuel emissions [13]. The material use in structural building components has therefore a direct influence on the climate and the change of its physical state. The drivers of climate change derive from anthropogenic sources of aerosols and greenhouse gases like other fossil fuel consuming industries and of natural origin like volcanism, solar radiation flux, impacts from cosmic rays and particles [9] or even extraterrestrial objects, etc. [10]

some of which are still under discussion (Figure 1). Other natural- but not climate related boundary conditions include soil and seismic activities. These conditions influence the choice for material, manufacturing technology, design of structural components and transportation and consequently the extent of associated emissions. Figure 2 illustrates the circular dependency of climatic boundary conditions, choice of resources and building technology, associated impact on environment and climate.

1.2. Ecological structures

Centralization of material resourcing and the establishment of ubiquitous architectural and engineering standards are increasing the construction industry's economical efficiency and safety. Construction materials are produced by large-scale industry branches and transported to construction sites, making it simple to apply proven and time-efficient structural designs. However, the same set of designs is used for all types of geographical highly diverse regions, giving less priority to the exploitation of local raw materials and customized designs. In this respect, current building practice has a significant impact on climate and environment caused by unnecessary greenhouse gas emission, resource consumption [11], and waste production.

As part of the UN-Sustainable Development goals [14], expressed by the EU-Commission [15] and the IPCC [10], sustainable solutions for mitigating climate change are needed. Therefore, awareness of an overuse of resources is also increasing in the construction sector, causing a call for more efficient technologies [16]. Recent advancements towards digitalization and automation could enable a high degree of structural customization for local climatic loading and resource availability. Technologies, such as advanced load simulation techniques, structural optimization methods, free form construction techniques, and novel material alternatives could increase the effectiveness of the industry [11] in terms of its ecological mutualism by rendering safe structures with minimal use of local materials.
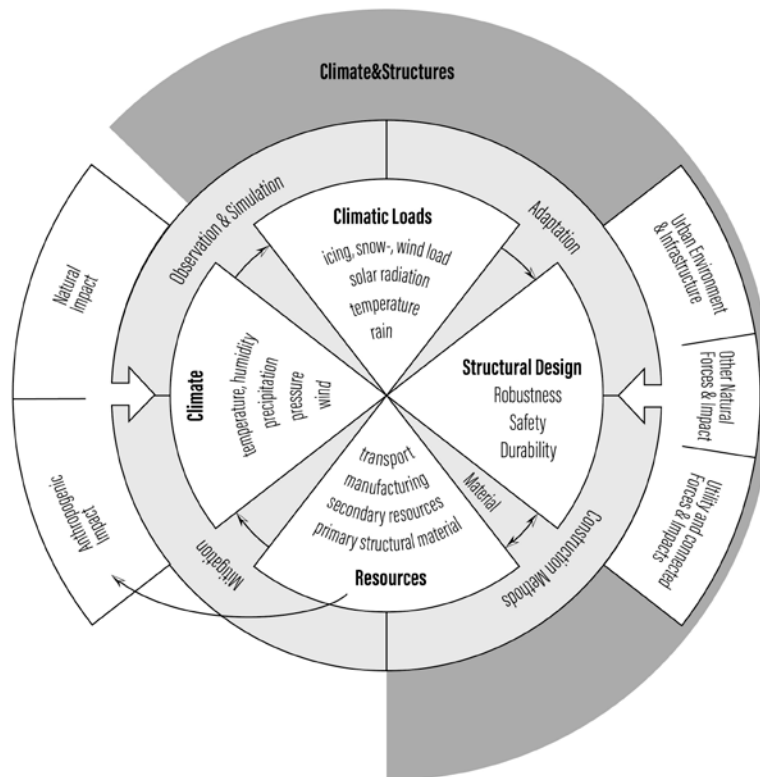

Figure 2: Illustration of circular dependency of climatic boundary conditions, resulting climatic loading, choice of resources and building technology, and the associated impact on environment and climate.

The central strategy of the research group 'Climate&Structures' is to contribute to sustainable advancements in the technological aspects of the circular interdependency between climate and structures. To this end, the research work focuses on three main areas: 1) observation and simulation of loading processes (physical states of the climate action), 2) response, deterioration and adaptation of structural designs to climate and environmental loads, and 3) advancement of material science and construction methods to render ecological structures with optimized performance.

2. Climatic loads

In structural engineering, climatic loads are extreme impacts resulting from the fluctuating state of the Earth's climate system in general or of processes in the Earth's atmospheric in particular. They are considered as single events such as extreme storms (e.g. hurricanes, extratropical cyclones) to ensure structural safety or as long-term processes to ensure durability. When planning development projects in urban areas not only the safe and durable design of the building or structure in question is of importance. With a trend to a high level of global urbanization, the effect of the local microclimate on human well-being has increasingly gained attention. A resourceful and climate conscious design of both, the built (structures and buildings) and urban (space between buildings) environment is indispensable to ensure sustainable urban planning [17].

2.1. Wind

Few other forces have so universally shaped the diverse terrains and waters of the earth. Few other phenomena have exerted such profound influence on the history of humankind, on the way we live and how we build and where [18]. Being one of the principal forces in structural engineering, wind loads are determined by two main factors: the local climate and the shape of the object exposed to the wind. With the latter, the architectural form language plays a significant role for the loading the structure or building has to sustain throughout its lifetime. Hence, the load-carrying system on the inside and the outside shape of the building skin are key elements of any structural optimization process.

Wind loading is a fluctuating process governed by the aerodynamic behavior of the building, structure or structural element. To identify the extreme characteristic used for structural design, a large quantity of data is usually required and obtained through simulations with experimental or numerical models. Main challenge in these simulations is the accurate reflection of the turbulent atmospheric boundary-layer (ABL) in the lower part of the Earth's atmosphere. A mismatch in the turbulent structure and velocity distribution has a significant influence on the safety [19] or lifetime prediction of the structure designed with the data obtained through simulation. Wind tunnel testing (Figure 3a) is a proven and reliable method to investigate the complex wind loading process and allows amassing a large amount of data for reliable statistical analysis and probabilistic modelling of the structural response. On the other hand, a disadvantage of wind tunnel model is limit of shape variability. Depending on the type of model, a shape-load optimization has to done manually, i.e. through stepwise variation of the model shape (force balance models). Here, the numerical simulation provides the possibility of an automated process, linking aerodynamic optimization of the outer shape with a topology optimization of the load carrying structure. The present state-of-the-art of numerical simulation software and computational power puts some limits to a reliable and reasonably fast application. Current research effort within the group 'Climate&Structures' aims on numerical modelling strategies of sufficient accuracy and acceptable computation time [20], [21].

2.2. Icing

Icing of structures is part of phenomena occurring under cold climate conditions starting just under 0°C. The type of icing and magnitude of its effect on structural and aerodynamic loading is a function of temperature, wind speed and precipitation. All types have in common that the precipitating water is still liquid at the instant of impact on the object's surface and solidifies gradually in the subsequent thermodynamic process. Air temperature, wind speed, droplet size (median volume diameter), liquid

water content (LWC) in air, object's surface and core temperature, thermal conductivity, geometric shape and surface roughness determine the ice accretion process and with that the quantity of additional mass on the object and the alteration of the object's geometry, i.e. its aerodynamic performance. The phenomenon of atmospheric icing on structural elements is the observable manifestation of a complex thermodynamic process which is best studied by recreating the governing climatic and structural boundary conditions as true-to-life as possible. For this reason, the 'Climate&Structures' group uses a climatic wind tunnel (CWT) jointly developed and operated with the Department of Hydro- and Aerodynamics of FORCE Technology [22]. Amongst other, in-cloud icing on structural bridge cables [23] and wind turbine wings are investigated. The wind tunnel allows using prototype samples of cables and wing section are studies at reduced scale compared as validation data to numerical icing simulations [24] (Figure 3b,c). Apart from additional mass and increase of aerodynamic resistance amplifying static loads or reducing energy production, ice accretion also bears a risk of aerodynamic instabilities such as galloping or flutter. Both can lead to large-amplitude vibrations reducing significantly structural lifespan and/or lead to structural failure. With respect to structural ecology, controlling and reducing the driving mechanisms behind aerodynamic instabilities for extreme and changing climate conditions allows minimizing maintenance and material consumption. The CWT is part of a wind tunnel network at DTU including test facilities at the Departments of Civil and Mechanical Engineering and of Wind Energy.

a) Wind tunnel study of surface pressure on a high-rise building in urban terrain for comparison with numerical simulation.

b) Study in climatic wind tunnel of ice accretion on structural bridge cable and its effect on overall aerodynamic performance and instability [25]

c) Icing study on an airfoil to specify the geometric characteristic of the ice layer at leading edge and the change of aerodynamic force coefficients during icing process.

Figure 3: Examples for investigations of wind actions on civil engineering structures under different climatic conditions.

2.3. Snow

With respect to structural loading snow is a considerable factor in cold climates, which in extreme cases exceeds the carrying capacity of roofs and, as in Arctic regions, can remain for months on the structure leading to densification and water penetration. Long-term penetration leads to mold growth deteriorating the integrity of the mostly wooden load carrying system and contaminating the indoor climate. The research group on 'Climate&Structures' looks at the relation of architectural design of Arctic residential buildings and snow accumulation on and around the buildings. The former address snow loading events whereas the latter focuses on the usability of buildings and their accessibility to formulate guidelines and recommendation for Arctic architecture and urban planning. Especially for Arctic regions, an increase of the annual mean temperature may lead to an increase of snow and wind event frequency and intensity. To investigate the mechanics of wind-driven snow accumulation the small closed-circuit boundary-layer wind tunnel at DTU Civil Engineering is fitted with a seeding mechanism of substitutional material. For validation of model-scale tests, a reference cube was installed in Nuuk (Greenland) with simultaneous monitoring of climatic conditions and snow accumulation throughout, up to now, two winter seasons.

3. Climatic structural design

Structures today are conceived from experience, mathematical description of mechanical behavior, experimental and numerical modelling, and are a result of a complex interaction of economical-, building performance- and infrastructural optimization. Automation and digitalization will possibly lower the dependency on large industrial manufacturing infrastructure and create structural customization for specific local climatic and loading condition (Section 2). It will thereby decrease resource consumption and increase the sustainability account of the construction sector. The interface between local loading conditions (climatic, natural forces, function, dead weight) and the construction material (primary material consumption, transport, manufacturing, waste) is the structural design (Figure 2). 'Climate&Structures' aims on the creation of climate-oriented structural designs, i.e. resource conscious structures that use a minimum of material to withstand extreme local climatic loading conditions using parametric and topology optimization tools.

3.1. Topology optimization

Structural optimization in terms of topology optimization can minimize the material use for a maximized structural performance within a given domain. A computational algorithm places material within a space of finite volumes at the location of high strain energy according to the given loading boundary conditions. To design structural components with this tool, a set of detailed loading conditions is required to prevent over- and under-dimensioning of the structure. 'Climate&Structures' uses topology optimization to create high performance structures for fluctuating loading impacts, obtained from wind tunnel simulations (Section 2.1). In Fernandoy-Bak, et al. [26], a vault-shaped structure was optimized (Figure 4-a) to withstand the stochastic loading process of wind-induced surface pressures. The turbulent structure of the simulated ABL-flow is visualized in Figure 4-b. First results indicate a common solution of the topology optimization for all loading instants [26]. This in turn could lead to a full stochastic topology optimization of the load carrying system for extreme climate impacts. Placing even inferior material strategically where it serves best structural safety and durability, will lead to a significant reduction of material consumption (Figure 2).
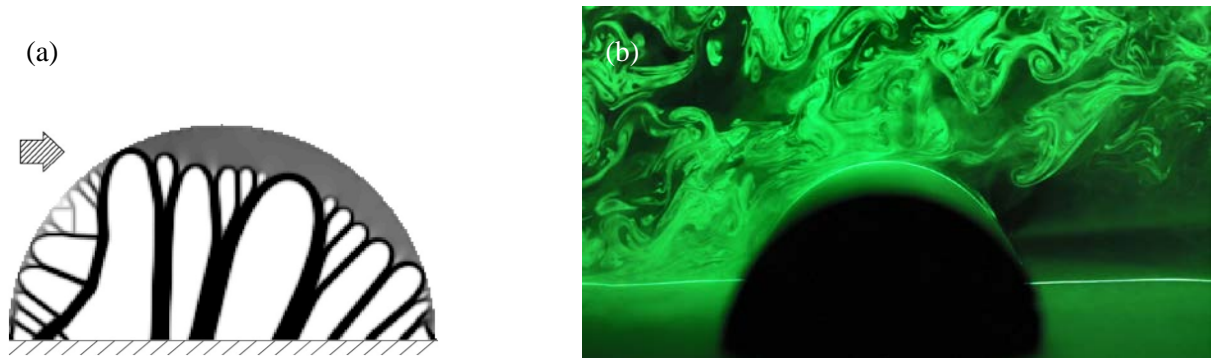
Figure 4: (a) Result from structural optimization (topology optimization) for wind loading scenarios [26], (b) visualization of turbulent flow over model in wind tunnel (flow from left to right).

3.2. Parametric multi-objective-optimization

'Climate&Structures' uses parametric design tools to optimize the performance of structural components. Through the inclusion of various performance objectives, the optimization process can consider not only material minimization of the structure as in Section 3.1, but include also e.g. manufacturing- and architectural boundary conditions. In Fernandoy-Bak, et al. [26], a frame-supported membrane structure has been parametrically designed for the use as an Antarctic research station. The structure was dimensioned to withstand extreme climatic loading conditions, to be transported to remote sites and assembled without mechanical help. The optimization scheme has therefore been adopted to

the objectives of reaching a minimal number of structural components with limited dimensions and to create structures, being light in weight. Some of the outcomes are shown in Figure 5.
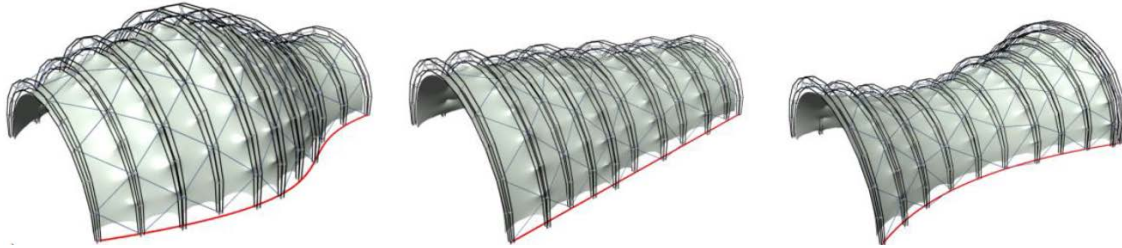
Figure 5: Frame-supported membrane structure, designed with multi-objective-optimization to withstand climatic loading impact and to fit several architectural boundary conditions. *Image:* [26].

Multi-objective optimizations with parametric tools give therefore the possibility, to design structural representations of climatic loading impacts, and at the same time respecting boundaries of manufacturing technologies, material resourcing, and architecture. Hence, representing the interface of all technological aspects (dark grey) in Figure 2.

4. Construction methods and resources

Computational optimized biomimetic structural design is a highly advanced field [27], pathing the way to create more sustainable and resource conscious constructions. However, the mostly biomorphic and freely shaped structural designs (Figure 4 - a) have a large draw-back in conventional manufacturing due to intensive use of non-standard molding and manufacturing shapes. Recent advancements in additive manufacturing (AM) [28] show possibilities in computer numerical controlled production without formwork and little waste material. The most advanced technology in constructional AM is 3D-printing of concrete using cementitious composites as a filament for construction. Judging the State-of-Art, designs manufactured by using this technology show a high potential for reaching construction-site-readiness in near future. Using cementitious filament allows relying on proven properties regarding performance as building material, but implies as well disadvantages such as lack of tensional strength, long setting times and environmental impact.

Novel construction methods and the associated material choices are the link between optimized structural designs, resource consumption feeding into the impact on the global climate (Figure 1). The aim of 'Climate&Structures' is to advance construction methods using materials, that enable the realization of the complex and optimized geometries presented in Section 3.

4.1. Additive manufacturing

The group explores possibilities of applying and advancing layered, extrusion-based constructional 3D-printing. The up to date, rather limited free form construction techniques, show difficulties in printing overhanging geometries needed for the realization of structures as shown in Figure 4. Climate&Structures focuses on the advancement of the filament's performance in terms of hardening characteristics, early age material strength, printed induced dead load and increasing tensional strengths by attempting and introducing novel choices of extruded materials [29].

4.2. Use of secondary resources

Filaments for constructional 3D-printing can be taken from secondary resources of local industry branches as attempted before (e.g. in Guan [30]). These could deliver solutions to waste problems and increase reuse possibilities of secondary resources in constructions through modern construction technologies.
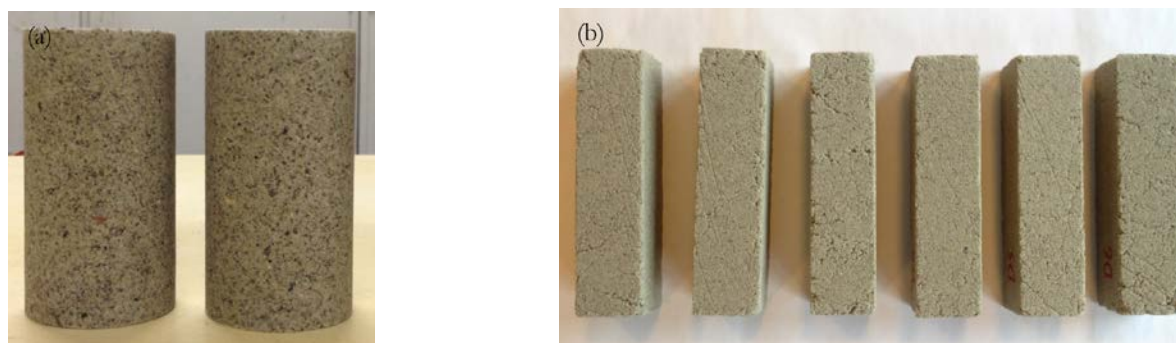
Figure 6: (a), (b) Concrete composite samples with biologically based binding materials, envisaged as filament for constructional 3D-printing. *Image:* [29].

Local resourcing from waste products reducing or even avoiding long transportation ways and production infrastructures is thereby one of the group's core ideas. The approach aims on the use of basic biological secondary materials connected with the food industry. The reuse of these materials could decrease emission and waste products due to lower production temperatures and recycle/reuse possibilities [29], falling in line with the EU's bioeconomic strategy [31]. Current research shows that use of secondary materials from food industry (biologically gels) as bio-based binding material for concrete (Figure 6) has a high potential for advanced applicability as filament in constructional 3D-printing [29].

5. Discussion

The discussed methodologies and technological fields of the research group 'Climate&Structures' have been presented and placed within the interrelation of climate and structural design (Figure 2). Being part of the biosphere's ecosystem, the interrelation between climate and structures is described by defining the structural design as a subsystem of humanity, seen as a natural organism, and the climate as its abiotic environment. The research group's activities are placed within the technological aspects of this interdependence. In this context, the observation and simulation of climatic conditions (snow-, ice-, wind loading) allow for detailed understanding and description of the associated loading processes. With the application of this information in structural design (topology optimization, parametric multi-objective optimization), structures can be adopted to different climates, dependent on geographical regions and to changing boundary conditions. Key approach is herein the close link between manufacturing methods (additive manufacturing), the "free form" (topology) optimization of structures and the use of novel circular materials (secondary resources) in these manufacturing technologies to mitigate climate change (Figure 2).

Overall, the work conducted by the 'Climate&Structures' research group seeks to improve existing and develop new technologies for ecological designs of buildings, structures and built environment by exploring advanced digitalization and automation methods. To succeed with this endeavor, the work depends on collaboration with other research groups and sections within the department, institutes at DTU and other universities and with partners from industry. Thoughtful consideration of human made structures within the boundaries of rapidly advancing technology and a changing climate is, considering the scale of the construction sector's pollutants and emissions, one of the most important of our time.

Acknowledgements

References

[1]   K. Daniels, J. Stoll, and L. Ilg, *Technology of Ecological Building*. Birkhäuser Verlag, 1997.

[2]   P. Calow, "E," in *The Encyclopedia of Ecology & Environmental Management*, Blackwell Science Ltd., 1998, pp. 209–264.

[3]   A. J. Willis, "The Ecosystem: An Evolving Concept Viewed Historically," *Source Funct. Ecol.*, vol. 11, no. 2, pp. 268–271, 1997.

[4]   P. Calow, "C," in *The Encyclopedia of Ecology & Environmental Management*, Blackwell Science Ltd., 1998, pp. 107–169.

[5]   R. Goodland, "Inegration of Economy and Ecology," *Ecol. Econ.*, vol. 2, pp. 343–359, 1990.

[6]   P. Calow, "S," in *The Encyclopedia of Ecology & Environmental Management*, Blackwell Science Ltd., 1998, pp. 652–738.

[7]   P. Calow, "M," in *The Encyclopedia of Ecology & Environmental Management*, Blackwell Science Ltd., 1998, pp. 420–467.

[8]   L. Huang, G. Krigsvoll, F. Johansen, Y. Liu, and X. Zhang, "Carbon emission of global construction sector," *Renew. Sustain. Energy Rev.*, vol. 81, no. June 2016, pp. 1906–1916, 2018.

[9]   Svensmark, H., Friis-Christenssen, E., "Variation of cosmic ray flux and global cloud coverage - A missing link in solar-climate relationships", J. of Atmospheric and Solar-Terrestrial Physics, Vol.59 No.11, 1997, pp. 1225-1232

[10]   T. F. Stocker *et al.*, "IPCC - Summary for Policymakers," Cambridge, United Kingdom and New York, NY, USA, 2013.

[11]   S. C. C. R. and A. R. Philipp Gerbert, "Shaping the Future of Construction A Breakthrough in Mindset and Technology," *World Econ. Forum*, no. May, pp. 1–64, 2016.

[12]   D. G. Dhavale and J. Sarkis, "Greenhouse gas emissions in the construction industry : An analysis and evaluation of a concrete supply chain," vol. 167, 2017.

[13]   R. M. Andrew, "Global CO 2 emissions from cement production , 1928 – 2017," pp. 2213–2239, 2018.

[14]   UNDP, *UN -Sustainable Development Goals 2030.* .

[15]   G. Amanatidis, "European policies on climate and energy towards 2020, 2030 and 2050," 2019.

[16]   S. Castagnino, C. Rothballer, and P. Gebert, "What's the future of the construction industry?," *World Economic Forum (WEF)*, 2016. [Online]. Available: https://www.weforum.org/agenda/2016/04/building-in-the-fourth-industrial-revolution/. [Accessed: 14-Jun-2019].

[17]   Koss, H.H. "Understanding urban environments and developing methods for sustainable urban design". In preparation for publication in *Journal Building and Environment*, 2019

[18]   J. DeBlieu, "Wind - How the Flow of Air Has Shaped Life, Myth, and the Land ", *Open Road Distribution*, 2nd Ed. 2015

[19]   H.H. Koss, "Influence of the natural wind simulation on the prognosis of overload risk of industrial low-rise structures" *Doctoral thesis, Ruhr-University of Bochum, Faculty for Civil Engineering*, Germany, 2001 (German language)

[20]   M.S. Thordal, J.C. Bennetsen, H.H. Koss, "Review for practical application of CFD for the determination of wind load on high-rise buildings" *Journal of Wind Engineering and Industrial Aerodynamics*, 2019, Vol. 186, pp. 155-168

[21]   H.H. Koss, L. Jørgensen, P. Jørgensen, N.G. Jørgensen, M.K. Rasmussen, "Benchmark for self-accreditation", in Proc. *European-African Conference on Wind Engineeing (EACWE)*, Liege, 2017

[22]   C.T. Georgakis, H.H. Koss and F. Ricciardelli, 2009, "Design Specifications for a Novel Climatic Wind Tunnel for the Testing of Structural Cable*s"*. Proceedings *8th International Symposium on Cable Dynamics*, Paris, France

[23]   H.H. Koss, J.F. Henningsen, I. Olsen, 2013, "Influence of Icing on Bridge Cable Aerodynamics", In: *15th International Workshop on Atmospheric Icing of Structure*s, St. John's, Newfoundland and Labrador, Canada

[24]   C. Son, H.H. Koss, T. Kim. "Development of 3D icing simulation code for wind turbines". Proc. of *International Workshop on Atmospheric Icing of Structures (IWAIS)*, Reykjavik, Iceland, June 23-28 2019

[25]   H.H. Koss, "Investigating the influence of cold climate conditions on structural dynamics". Proc. of *International RILEM Conference on Materials, Systems and Structures in Civil Engineering*, 22-24 August 2016

[26]   J. Fernandoy-bak, J. Christ, P. Shepherd, and H. Koss, "Cases of Lightweight Structures for Polar Areas," 2017.

[27]   J. F. Dynowski *et al.*, *Evolution of Lightweight Structures*. Springer Dordrecht Heidelberg New York London, 2015.

[28]   P. Shakor, S. Nejadi, G. Paul, and S. Malek, "Review of Emerging Additive Manufacturing Technologies in 3D Printing of Cementitious Materials in the Construction Industry," vol. 4, no. January, 2019.

[29]   J. Christ, H. Koss, and L. M. Ottosen, "A concrete composite from biologically based binders and mineral aggregates for constructional 3D-printing," in *2nd International Conference of Sustainable Building Materials*, 2019.

[30]   G. Heng, A. Ting, Y. Wei, D. Tay, Y. Qian, and M. Jen, "Utilization of recycled glass for 3D concrete printing : rheological and mechanical properties," *J. Mater. Cycles Waste Manag.*, vol. 0, no. 0, p. 0, 2019.

[31]   European Commission, *A sustainable Bioeconomy for Europe: strengthening the connection between economy, society and the environment*. 2018.

Appendix 1.II – Conference Paper – 'A concrete composite from biologically based binders and mineral aggregates for constructional 3D printing'

Christ, J., H. Koss, L. M. Ottosen, 'A concrete composite from biologically based binders and mineral aggregates for constructional 3D-printing', Proceedings of the 2nd International Conference of Sustainable Building Materials – ICSBM 2019, 12-15 August 2019, Eindhoven [NE] – Eindhoven University of Technology.

A concrete composite from biologically based binders and mineral aggregates for constructional 3D-printing

J. Christ[1], H. Koss[1], L.M. Ottosen[1]

[1]Department of Civil Engineering, Technical University of Denmark, Brovej 118, 2400 Kgs. Lyngby

Abstract - The paper presents an alternative binder for structural 3D-printing with composite materials. The binder eases the control of setting times after extrusion through thermoplastic hardening properties. The material could therefore enable the production of thin-walled geometries in large-scale 3D-printing with higher degrees of freedom in respect to overhanging geometries without supporting structures. The proposed composite material is made from mineral aggregates and biological gels, resourced from animal tissue and bone. The used mineral aggregates are not deviating significantly from conventional concrete or mortar.

So far, the research determined a maximum flexural- and compressive strength of 8 MPa and 21 MPa. Furthermore, first material compositions are introduced and respective material properties tested. As a conclusion, the paper presents limitations and potentials of the concrete for the use as structural building material and the use within large-scale 3D-printing.

Keywords: Bio-based concrete, constructional 3D-printing, biopolymers, concrete composite, mineral aggregates

1   Introduction

Additive manufacturing and 3D-printing in the construction sector is a rapidly growing field of interest in research and industry [1], [2]. Possible material savings and a higher degree of freedom in shape forming increase both, sustainability in construction and architectural expression [3]. Some of the materials used for constructional three dimensional extrusion processes are steel ([4], [5]) , carbon fibre[6], or polymers ([7], [8], [9]). The main focus however lays on the printing with concrete ([1], [3], [10]), due to proven beneficial properties of cementitious materials, such as durability, inexpensiveness, fire resistance, structural strength and its plasticity during extrusion.

The current focus on cementitious concrete has its drawback regarding its sustainability account. This is due to the high amount of energy used under production, the CO_2-emissions of the chemical process during calcination of limestone and the high transport efforts due to dependency on centralised large-scale production sites. In many cases, the extruded material comprises substantially higher cementitious shares than conventionally casted concretes [11]–[13]. Additionally, extensive admixtures are being used to adapt the composite's performance as intended, enabling rapid viscosity change from liquid to solid during the printing process by thixotropic or chemical procedures. The combination of large limitations in reinforcement integration [3] and low early-age strength of concrete causes buckling and moment failures during printing, and restrain degree-of-freedom to an almost vertical build up.

The here presented research proposes an alternative concrete composite, based on biologically (bio-) based binding materials, for constructional 3D-printing. This concrete is in the following referred to as Biopolymer Concrete (BPC). The novelty of the material is the compound of biopolymers, resourced from animal tissue, bones, fish, shellfish, or algae as binding material in concrete, purposed for additive manufacturing processes. The intention is to completely replace any cementitious share in the composite with the biopolymer- and water- based binders. Sought after properties of the BPC with regards to constructional 3D-pinting are rapid viscosity change due to its thermoplastic hardening. Possibly, higher material savings in comparison to cementitious concrete could be reached by enabling higher resolution prints, i.e. thin-walled and overhanging geometries, through the rapid solidification.

Different sources for the binding material are considered. As a first prove of construction-worthiness of the novel material, the research presented here is conducted with BPC samples made of bone glue, a biologically resourced gel from animal tissue and bones (meat industrial waste products). The samples were tested for compressive- and flexural strength with different binder contents in the composite material. Other properties relating to the construction process, i.e. printability of the concrete, such as hardening and drying time as well as shrinkage, density and thermoplasticity have been tested explicitly or will be discussed based on available information.

2

2 Methodology

2.1 Materials

The tested BPC composite material was manufactured using bone glue as bio-based binding material, and mineral aggregates. In the following, the individual components, are described and characterized.
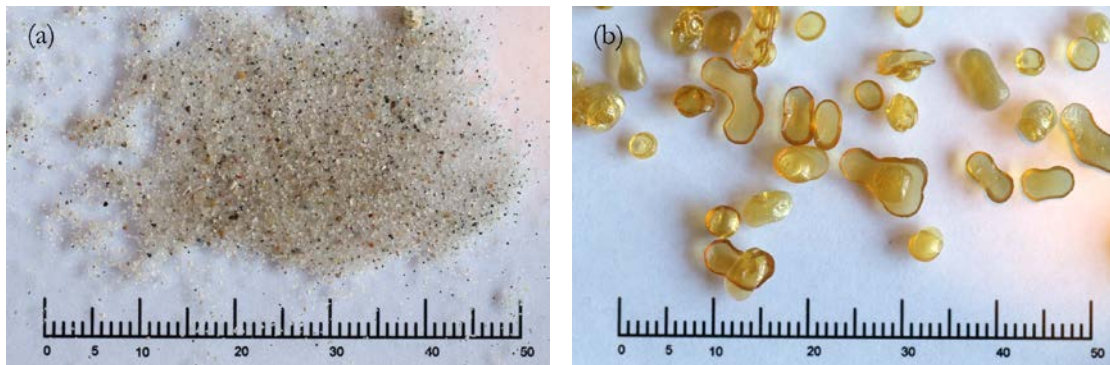
Figure 1: Raw materials used for BPC – (a) Mineral aggregates: Sand with a grain size distribution between 0-2mm, (b) biologically based binder granulate: bone glue – in [mm]

2.1.1 Mineral Aggregates

The used mineral aggregates are limited to sand with a grain size composition of 0-2mm (Figure 1 - a). The used sand is taken from the Great Belt strait in Denmark, part of the Baltic Sea. Due to the maritime origin, round grained characteristics can be assumed. The sands density is $2.6\frac{g}{cm^3}$ [1].

 The small grain size was chosen to:

- reach a sufficient homogeneity of the composite material for small sample sizes
- assure applicability for constructional 3D printing, for which rather small grained aggregates are used (as in [12], [13]) to enable thin extrusion processes and high resolution.
- the rounded shape adds to good workability of the fresh concrete mix

2.1.2 Bio-based binding material

Bone glue is used as a biologically based binder to produce test specimen in this paper. The material is commercially available and extracted from industrial waste in food production (animal tissue and bones). It is traditionally used as adhesive for carpentry, woodwork, as well as for restauration and instrument making. Under soaking of water and the influence of heat, covalent bonds of long chained bio-polymers dissolve and a biological gel is separated from the raw biological material by Gelatinization. The adhesive is dried and sold in form of granulate (see Figure 1 – b).

---

[1] Characterised by weight and volumetric analysis with water bath. A weight scale with an accuracy of 0.01g was used, as well as a single graduated 100ml cylinder to measure the volumetric increase of 50ml of water by adding 50g of binder granulate.

The bone glue was purchased from DICTUM [14], a supplier for woodworking tools and materials. The delivered glue granulate has a grain size of 2-7mm (Figure 1 – b). Covered with water, the granulate dissolves and the gel liquefies. This process is intensified when adding heat to the solution. Both, water content and temperature in particular affect the viscosity of the gel significantly (thermoplasticity) and are hence pivotal to the workability of the composite material. The viscosity decreases significantly when increasing the binder's temperature to 70°C. The raw granulates density is $1.3\frac{g}{cm^3}$ [2].

2.1.3   Nomenclature

To specify the composition of the tested BPC materials, a coding indicating the different constituents by letters and numbers of mass percent is used. In this study, specific constituents are water **(W)**, bone glue **(BG)** and Great Belt sea sand 0-2mm **(Z1)**. Symbols for less specified groups or more general terms would be glue granulate **(GG)** or binder **(b)**. This system allows to write unspecific (1) and specified (2) balanced equations describing BPC materials:

$$b1 = 44GG + 56W \tag{1}$$

$$BPC1 = 10(44BG56W)90Z1 \tag{2}$$

Equation (2) omits arithmetic operators (+) as used in equation (1). The unspecified glue granulate in equation (1) is in equation (2) replaced with the specific reference to bone glue. In this way, the notation allows defining parent types and sub groups of binders and composites. Finally, a specific sample of any BPC material is identified by a unique number at the end of the material code separated by a dot. The fifth sample made of BPC1 would bear the code:

$$BPC1.5 = 10(44BG56W)90Z1.5 \tag{3}$$

All numeric values and ratios refer to the material's weight and to compositions under mixing. The specified material proportions do not account for hardened samples, since water content decreases during drying.

2.1.4   Mixture

The tested compositions consist of bone glue, water and mineral aggregates. The specifications of the different BPC materials are listed in Table 1. In all cases, a W/GG-ratio of 1.25 has been chosen due to benefits in the workability of the heated mass. This was found during preliminary experiments. Material coding is according to Section 2.1.3.

---

[2] Characterised by weight and volumetric analysis with water bath. A weight scale with an accuracy of 0.01g was used, as well as a single graduated 100ml cylinder to measure the volumetric increase of 50ml of water by adding 20g of binder granulate.

Table 1: Overview of the used material compositions.

#	Sample	Binder-content	Glue granulate-content	Water-content	Aggregate-content
[-]	[-]	[wt.%]	[wt.%]	[wt.%]	[wt.%]
BPC1	10(44BG56W)90Z	10	4.44	5.56	90
BPC2	15(44BG56W)85Z	15	6.67	8.33	85
BPC3	20(44BG56W)80Z	20	8.89	11.11	80
BPC4	25(44BG56W)75Z	25	11.11	13.89	75

2.2   Methods

The used methods for mixing, moulding and testing are largely inspired by the standardised procedures for cementitious mortar and concrete as described in EN 196-1 [15]. However, due to thermoplastic properties of the binding material, some adaptions were made. The steps in sample production, testing and property characterisation are in the following described in more detail.

2.2.1   Composite production

The production of the concrete composite, including the process for moulding and drying is compiled in Table 2, with approximate durations of the individual steps.

Table 2: In-sum process specifications for the production of bio-based concrete composite samples.

Process #	Process specification	Duration	Notes
1	Soaking of GG in W	>1h	Soaking of glue granulate in water
2	Heating	~1h	Heating of Z and b in oven to 70°C
3	Mixing	2min	Mixing in mortar blender, standardised in EN196-1 [15]
4	Moulding	3min	Moulded on vibration table until solidity is reached
5	Thermoplastic hardening	1 day	1 day left in mould - actual thermoplastic hardening time substantially lower - dependant on geometry, ambient temperature, etc.
6	Demoulding	-	Demoulding 1day after casting
7	Dry-hardening A	1 day	Dry hardening under room temperature
8	Dry-hardening B	4-48 days	Dry hardening in well ventilated oven at 50°C

1) Soaking of GG in W: Soaking the glue granulate in water for >1 hour, until a homogenous concentration of gel in the GG-W mix could be reached. The granulate increases its volume in reaction with water. The viscosity in this step depends on both, amount of added water and soaking time, and can range from solid to liquid. Frequently, the mix has been stirred with a glass spatula.

2) Heating of constituents: The viscosity of the GG-W mix can be decreased by heating (thermoplasticity). The water addition can be thereby decreased due to temperature control. To avoid sudden cooling and undesired hardening during the mixing process of the binder, aggregates

ICSBM 2019

2nd International Conference of Sustainable Building Materials

12-15 August, Eindhoven The Netherlands

----

are heated as well. Both materials are heated to 70°C to ensure the plasticity of the mix. Higher temperatures were avoided to prevent damage of the molecular structure.

3) Mixing of constituents: The heated constituents are mixed with a mortar blender for conventional cementitious material (Mixer specification: Seger – Tonindurtie), standardised in EN196-1 [15]. The mixing vessel is prior tempered to 70°C to prevent premature cooling of the mass. A homogenous material mix could be assumed after 2 minutes of mixing. The mixing and moulding was conducted at room temperature, giving a time limitation for the mixing. Due to cooling, the mass becomes unworkable after a short time (about 5-10min).

4) Moulding: The composite material is poured into moulds. This is done in a rather rapid fashion to prevent the material from premature stiffening. The moulds were filled on a vibration table to prevent large captivities and larger inhomogeneity inside the sample. The vibration was conducted with 60-80Hz until the material increased in viscosity (approx. 3min). Prism moulds with dimensions of 40x40x160mm (width/height/length) after EN 196-1 [15], as well as cylinders with a measurement of 50x100mm (diameter/height) were used. Metal surfaces of the moulds needed to be covered with a thin PE-foil to prevent the corrosion caused by the acidic nature of the bio-binder.

5) Thermoplastic hardening: Thermoplastic hardening occurs directly after the binding material is removed from a heat source and placed in a cooler ambient temperature. The material's viscosity increases noticeably throughout mixing and moulding process.

6) Demoulding of the samples was conducted one day after moulding, to support the integrity of the sample by reaching additional strength through the outset of the dry hardening process.

7) Dry hardening: Even if the material shows stiffness after the thermoplastic hardening process, the material still contains water which prevents the biopolymers to form stronger bonds. After all water is evaporated, the material is considered as hardened. The duration of this process is dependent on water content, dimension of the sample, aggregate content and porosity. To accelerate the process for testing, samples were, after one day drying under room temperature, placed in a well ventilated oven (Oven specification: Memmert UF 160) at 50°C. For most samples, an oven drying time of 21 days was chosen.

2.2.2 *Structural testing of cylindrical samples*

A total of 12 cylindrical samples, 50mm diameter and 100mm height, were casted to determine compressive strengths. For loading tests, an 'Instron-6025' with a capacity of 100kN was used to load the samples, as well as for recording of force and displacement. Circular platens with a diameter of 50mm were used to slender the apparatus' loading surface down to the geometry of the material cylinders. Force was applied with a loading rate of 2400 N/s.

The moulding and drying of the samples left the top and bottom surfaces of the cylinders uneven. The samples were cut with a circular saw to a length of ~90mm before testing and after drying. The sawing was conducted slowly and without any water-cooling of the blade to prevent the material from weakening by water soaking.

2.2.3   Structural testing of prism samples

Prism samples with the size of 40x40x160mm were tested for flexural- and compressive strength according to EN196-1 [15].

For flexural strength, the prism samples were tested in a three-point bending test as standardized with a distance of the supporting rollers of 100mm and a loading rate of 50N/s on an 'Instron-6022' with a loading capacity of 10kN. The specimen was mounted with the from the moulding created even surfaces in contact with the flexure device.

The compressive strength was measured for each of the two fragments obtained from the segmentation when measuring the flexural strength. Above and below, the specimen was loaded on a surface of 40x40mm. The orientation of the samples for compressive strength was in accordance to the flexural tests, described above. Loading was applied at a rate of 2400N/s with an 'Instron-6025' testing machine with a loading capacity of 100kN.

2.2.4   Density-measurements of the composite

Calculated as ratio of individually measured mass (accuracy 0.01g) and volume (accuracy 0.01mm).

2.2.5   Shrinkage

Shrinkages of prism samples were determined by evaluating the differences in length before and after dry hardening, i.e. immediately after demoulding and before testing. Therefore, shrinkage information relates only to the dry-hardening process during this time and not to thermoplastic-hardening.

2.2.6   Dry-hardening times

The binding material develops strength over the thermoplastic- and the dry-hardening period. The duration of the thermoplastic hardening was short and easy controllable by temperature. The duration of the dry-hardening depends on geometry, porosity, ambient temperature and binder or water contents. A total of 12 cylindrical samples of BPC3 have been tested in compression (see Section 2.2.1 and 2.2.2) to evaluate the rapidity of the drying process. The sample production was conducted as indicated in Table 2. The duration of step 8 was varied. Three samples have been tested, respectively after 4, 12, 22 and 48 days of oven drying at 50°C. To keep samples comparable, the W/GG and b-content has not been varied and kept on 1.25 and 20%.

3   Results and discussion

3.1   Results
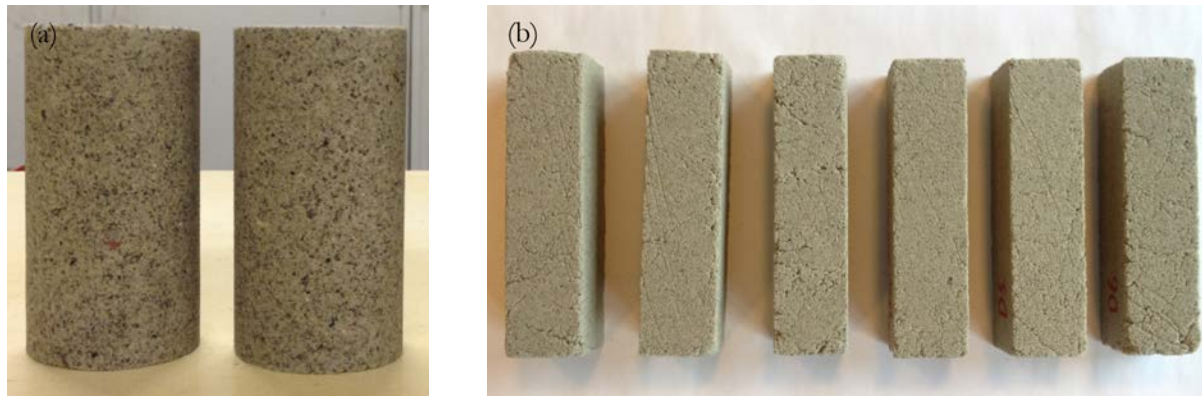
Examples of BPC are seen in Figure 2.

Figure 2: Biopolymer Concrete (BPC) Samples: (a) circular cylinders 100mm high and 50mm in diameter, (b) square prism samples with a length of 160mm and a cross-section of 40x40mm.

3.1.1   *Property variations under hardening*

The two hardening characteristics, thermoplastic- and dry-hardening, are key-influencer on the materials strength and viscosity. The thermoplastic hardening time already occurs after several minutes after discontinuity of heat exposure, the material's viscosity increases and the composite gains integrity. Due to the obvious relation of the material's temperature to its fluidity, the rapidity of the process is thought to be connected with the composite's geometry, heat capacity, water content, initial- and ambient temperature. The observations of this process proposes therefore, its simple controllability. The subsequent dry hardening can be described as the water loss through evaporation and extends, dependant on the water content, over a longer period of time.

Figure 3 shows the dependency of the compressive strengths on this dry-hardening duration. Illustrated results display that the material strength is increasing for an increase of dry-hardening time, suggesting that the strength of the material is strongly dependant on its water content. Hence, a high water content implies low strength and an advanced drying process a higher strength. The four data points were tested with a respective sample quantity of three, namely samples BPC3.1-12 (Figure 2 – a). The mean of each tested point in time has been connected by a smoothened line. A substantial increase of compressive strength was observed (until 22 days), where after the graph flattens. The flattening starts between 12 days and 22 days, an exact point in time, however, could not be determined. For the values around the flattening, the graph shows larger variabilities. Contrary, minor variations were observed for short and extensive dry-hardening durations. A bend in the smoothened curve of Figure 3 denotes a characteristic change of drying rapidity.
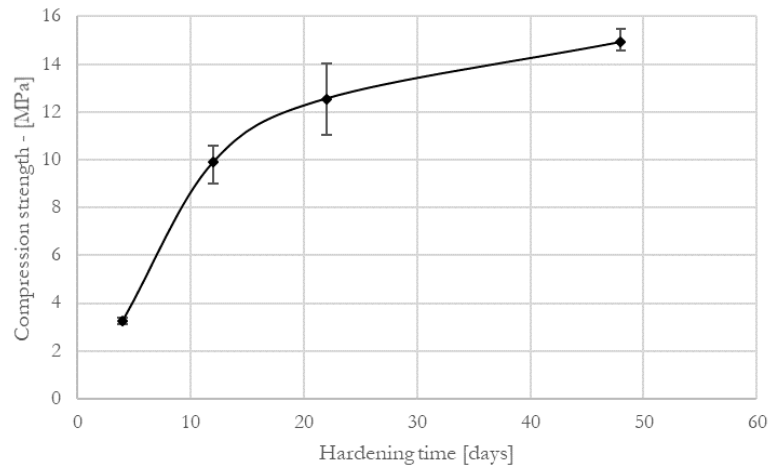
Figure 3: Compressive strength of cylindrical samples BPC3.1-12. over dry hardening times at 50°C (corresponding to step 8 in Table 2). The error bars show maximum and minimum values. The connecting line has been smoothened.

The drying characteristics are expected to be geometry dependent, as well as reliant on initial water content, ambient temperature and humidity. Other than the thermoplastic hardening, dry hardening is expected to not conclude, but rather to approximate asymptotically to an upper bound, which is dependent on the ambient humidity. Therefore, varying water contents through differing binder to aggregate compositions, possibly show divergent hardening times. This, however is up to date not experimentally verified.

3.1.2   Density

Characterizing density and shrinkage is useful to evaluate the material on its suitability for constructional 3D printing by limiting self-weight and shrinkage cracking. For sample batches BPC1, BPC2, BPC3, and BPC4 (cf. Table 1); volume, weight and length have been measured before testing and after drying. Respectively calculated density values can be seen in Figure 4. The mean values range from 1.6g/cm^3 to 1.4g/cm^3 for varying binder contents. Densities generally decrease with a decrease in aggregate shares in the mix.

Figure 4: Density of sample batches with varying binder contents. Whiskers show maximum and minimum value of the data set; boxes define upper, middle and lower quartile; the marker shows mean values. Each boxplot is substantiated with a data point quantity of six measurements.

The material's density is scattered around a value of about 1.5 g/cm³. The composite is therefore lighter than cementitious mortar, which is here assumed with the typical value of 2.2 g/cm³. The mixing ratios influences the material's density only marginally for a binder content of 10%-20% (BPC1, BPC2, BPC3). A content of 25%, however, causes a large density loss of 10%. Due to the comparably high density of the used sand (2.6 g/cm³), low density binder (1.3 g/cm³), and the continuous change of mixing ratios (10%, 15%, 20%, 25% binder content) throughout the tests, a linear decrease of density could have been expected. Contrary, the non-linear appearing measurements of Figure 4 let suppose, that the pore content for samples with a binder content of over 20% increases substantially, i.e. its density decreases.

3.1.3   Shrinkage

The densities tendency is reversely reflected by shrinkage ratios in Figure 5. The continuous increase of the data set ranges from 0.3% to 2% and increases for higher binder contents. Therefore, shrinkage appears to be directly interlinked to the materials composition, or rather to the binder's water content. The results suggest that the evaporation of water causes the material to shrink.

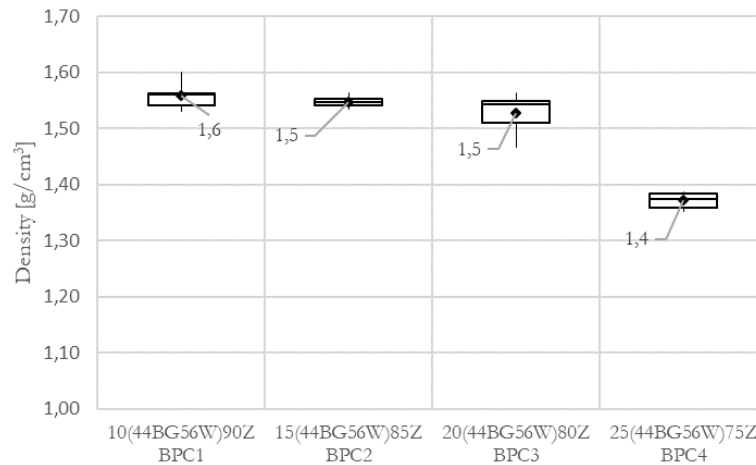

Figure 5: Shrinkage of sample batches with varying binder contents. Whiskers show maximum and minimum value of the data set; boxes define upper, middle and lower quartile; the markers show mean values. Each boxplot is substantiated with a data point quantity of six measurements.

3.1.4   Strength of BPC

The composite's properties are expected to be strongly dependant on the material's composition. Therefore, the dependencies on varying binder-contents were measured to determine performance peaks of flexural and compressive strength. Six prisms (Figure 2-b) for each composition were casted with a binder content of 10%, 15%, 20% and 25% (BPC1-4) and a W/GG-ratio by weight of 1.25. Corresponding mixtures can be found in Table 1, a dry-hardening duration of 21 days was chosen for all samples. Figure 6 and 7 show the obtained results for flexural and compressive strengths.

Flexural strength: As shown in Figure 6, batch BPC2 had the highest flexural strength, i.e. the batch with a binder content of 15%. When lowering the binder content to 10% (Batch BPC1), the flexural strength was more than halved. Increasing the binder content to 20% and 25%, i.e. BPC3 and BPC4, resulted in a decreased flexural strength, though not as significant as for the prisms with 10% binder.

Compressive Strength: The compressive strength for the prisms are shown in Figure 7. A tendency to a maximum mean compressive strength of batch BPC3 can be identified as a peak performance value. However, the upper error bar for batch BPC3 has a relatively large magnitude and is decisive for an increased mean value, being higher than middle and upper quartile. Therefore, a difference between batch BPC2 and BPC3 can not be concluded. A major drop in strength is located between BPC3 and BPC4.
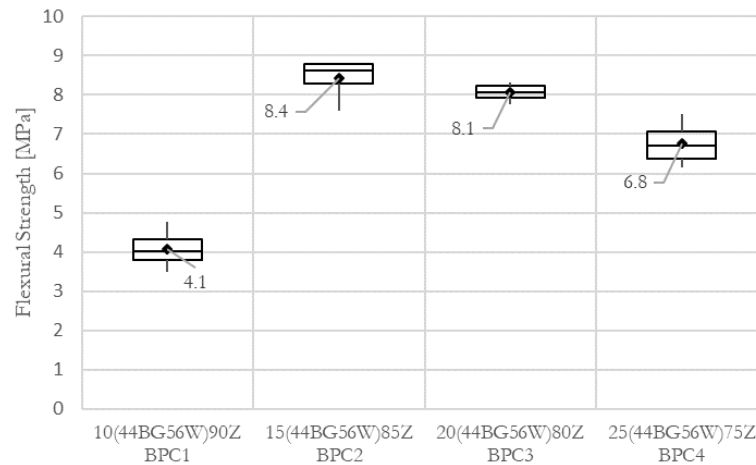
Figure 6: Flexural strength of prism samples with varying binder contents. Whiskers show maximum and minimum value of the data set; boxes define upper, middle and lower quartile; the marker shows mean values.
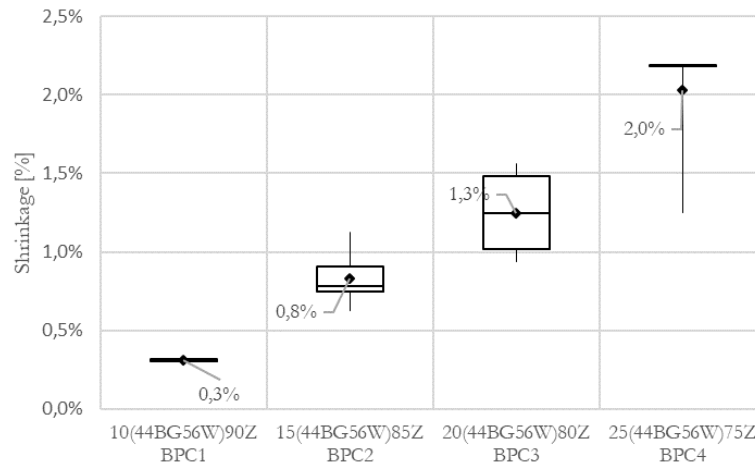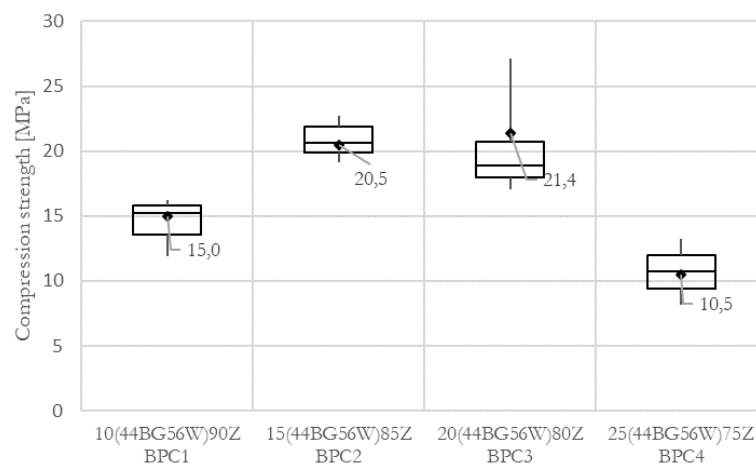

Figure 7: Compressive strength testing of prism samples with varying binder contents. Whiskers show maximum and minimum value of the data set; boxes define upper, middle and lower quartile; markers show mean values.

Both, flexural and compressive strength suggest a performance peak between 15% and 20% binder content. The peaking of strength in this range, and the subsequent decrease for higher binder contents can potentially be explained with: 1) an increase of porosity due to the higher binder content and therefore decrease in density and strength (see Figure 4), or 2) an incomplete or not comparable dry-hardening process between varying binder contents as described in Section 3.1.1.

Even though in similar range, flexural- and compressive strength propose diverging mean performance peaks in the margin of 15%-20%. The boxplots however do show similar order for both stresses in Figure 6 and 7. The correlation of mean flexural- and compressive strength was therefore evaluated to determine the consequences of an increase of binder content in the mixture. The results are shown in Figure 8. It

ICSBM 2019
 2nd International Conference of Sustainable Building Materials
12-15 August, Eindhoven The Netherlands

----

appears that the two properties react differently on the composition change. A consistent ratio in strength could therefore be excluded. A general observed trend is that higher binder contents cause an increase in relative flexural strength. Contrary, low binder contents lay the performance's focus on the compressive strength. The maximum ratio in Figure 8 has a magnitude of 65% for a binder content of 25% (BPC4). The indicated performance peaks for BPC2 and BPC3 show a strength ratio of around 40%. In all cases, the ratio of flexural- to compressive strength surpasses the performance of conventional cementitious concrete, which is around 10%, as a rule of thumb.
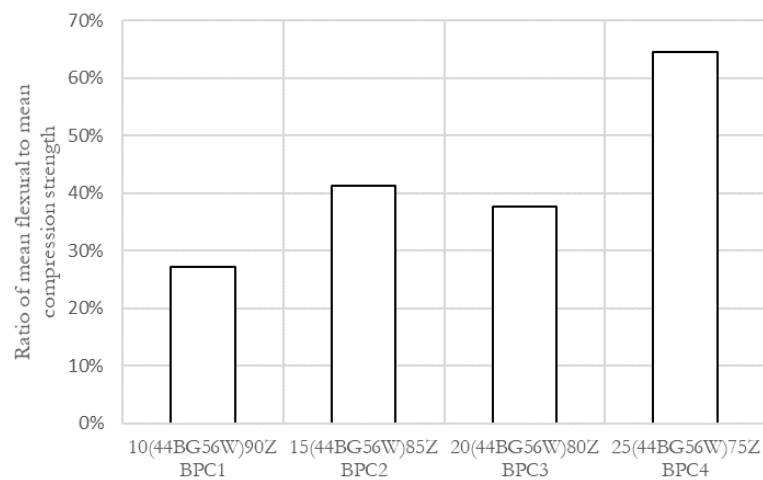
Figure 8: Ratio of flexural strength to compressive strength for varying binder contents. Mean values of measured strengths as in Figure 6 and 7 were used.

3.2   Discussion

The BPC's properties were tested to assess the materials suitability for constructional 3D-printing. In the following, the results are brought into context, i.e. 'suitable'- and 'to be further advanced' properties are listed and compared.

Suitable properties of BPC for constructional 3D-printing:

- *Printability of BPC:* Primary advantage of BPC for constructional 3D-printing is the easy controllable thermoplastic hardening and thickening of the material. The in Section 2.2 and 3.1.1 discussed thermoplasticity shows, that the material increases rapidly in viscosity only by the exposure to room temperature. During an envisaged printing process, the material itself would therefore not only rely on the thixotropic build-up of the composite material, as for 3D-printing with cementitious concrete [16]. By the ability of controlling the thermoplasticity to a high degree, and increasing the early age strength of the matrix, the thinness of layers could be increased and potential early age moment failure of the built up prevented. More slender constructions and higher degree of freedom in terms of overhanging prints, could possibly be realised. This is also supported by the material's

ICSBM 2019
 2nd International Conference of Sustainable Building Materials
12-15 August, Eindhoven The Netherlands

----

low density and high relative flexural strength, as described in Section 3.1.4, which can increase the early age moment resistance and lower the dead load added to the system under construction.

- *Composite strength:* As proposed in Section 3.1.4, BPC shows generally a strength in the order of magnitude of cementitious concrete, though not comparable with high performance printing concretes [12]. One of the biggest challenges of constructional 3D-printing is the integration of reinforcement [3]. The printing process prevents the placing of extensive steel reinforcement and limits the freedom of shape for cementitious concrete substantially due to the lack of flexural strength in cementitious materials. With a high ratio of flexural- to compressive strength of BPC, as described in Section 3.1.4, the BPC material could deliver a filament that could render building components loaded in flexure and thereby diminish the need for reinforcement.

- *Structural integrity of prints:* Assuming a layer-by-layer 3D-printing process for the constructional use of the material, the integrity of the meso-scale structure is at risk by possibly exceeded shrinkage limits or detachment of layers through lacking interface adhesion [17]. Shrinkage, as evaluated in Section 3.1.3, can be controlled by editing the binder content. Possibly, fibre reinforcement could be added to limit shrinkage cracking. The found shrinkage ratios of 0.3% to 2% is therefore evaluated as suitable for constructional 3D-printing. The bone glue has furthermore been traditionally used for carpentry constructions and instrument making and adheres well to itself. It is therefore expected, that the contact surface of a printed layer bonds well to precedent layers. This, however needs to be experimentally verified in further work.

- *Sustainability:* The substitution of high cement contents and extensive admixtures in constructional 3D-printing filaments with biologically based binders such as bone glue could have a positive impact on the sustainability account of the method. This is due to lower production temperatures of bone glue in comparison to cement, and avoidance of CO_2-emissions under the calcination of limestone.

BPC properties, crucial to be further advanced:

- *Durability:* BPC has, due to its organic compounds and hygroscopic behaviour, a high risk of fast deterioration. During the testing, some of the samples, especially for binder contents over 20%, showed moulding attack.

- *Fire resistance:* The thermoplastic properties of the material are expected to be beneficial for the 3D-printing process but disadvantageous for its fire-resistance. The fireproofing of the material is crucial for further development.

- *Hygroscopic properties:* As described in Section 3.1.1, the water content is decisive for the structural strength of the material. Removing the water contents, hardens the material. The process can also be reversed, i.e. exposure of the hardened material to water softens its strength, which is critical for the use as structural material.

An overview of the above described can be found in Table 4.

Table 4: In sum – advantageous properties in comparison to ongoing advancements

Properties of BPC, suitable for constructional 3D-printing	Properties of BPC, crucial to be advanced
- Thermoplasticity	- Durability
- Flexural- /compressive strength	- Fire resistance
- Low density	- Water resistance
- Self-adhesion	
- Shrinkage	

4   Conclusions

A composite of a biopolymer binding material (bone glue – a bio-gel produced from the meat industry's waste) in conjunction with mineral aggregates was evaluated on its suitability as a filament for constructional 3D-printing of concrete. The findings show structural strengths in the order of magnitude of conventional concrete, i.e. flexural strength of 8 MPa and compressive strength of 21 MPa, and suggest therefore the composite's usability as a structural building material. A density of around 1.5 g/cm³, easy controllable thermoplastic hardening characteristics, and a high moment resistance through high flexural- to compressive strength ratios of up to 65%, propose furthermore the benefit for additive manufacturing processes. Low induced dead loads, early-age material strength and high moment resistance, could diminish the need for reinforcement integration of 3D-printed structures, and enable higher degrees of freedom in terms of overhanging and thin geometries. The results suggest the suitability of bone glue as a binding material for concrete and the use in constructional 3D printing, linked with further research and development work for the composite's durability, fire- and water resistance.

5   Acknowledgment

6   References

[1]   Y. W. D. Tay, B. Panda, S. C. Paul, N. A. Noor Mohamed, M. J. Tan, and K. F. Leong, "3D printing trends in building and construction industry: a review," *Virtual Phys. Prototyp.*, vol. 12, no. 3, pp. 261–276, 2017.

[2]   N. Labonnote, A. Rønnquist, B. Manum, and P. Rüther, "Additive construction: State-of-the-art, challenges and opportunities," *Autom. Constr.*, vol. 72, pp. 347–366, 2016.

[3]   F. Bos, R. Wolfs, Z. Ahmed, and T. Salet, "Additive manufacturing of concrete in construction: potentials and challenges of 3D concrete printing," *Virtual Phys. Prototyp.*, vol. 11, no. 3, pp. 209–225, 2016.

----

[4]   S. Ren and S. Galjaard, "Topology Optimisation for Steel Structural Design with Additive Manufacturing Shibo," in *Modelling Behavior*, 2015, pp. 35–36.

[5]   "MX3D Bridge." [Online]. Available: https://mx3d.com/projects/bridge-2/. [Accessed: 26-Apr-2019].

[6]   A. Menges, "BUGA Fibre Pavilion 2019 | Institute for Computational Design and Construction," 2018. [Online]. Available: https://icd.uni-stuttgart.de/?p=22271. [Accessed: 26-Apr-2019].

[7]   S. J. Keating, J. C. Leland, L. Cai, and N. Oxman, "Toward site-specific and self-sufficient robotic fabrication on architectural scales," *Sci. Robot.*, vol. 2, no. 5, 2017.

[8]   G. Pasquarelli, W. Sharples, C. Sharples, and R. Caillouet, "Additive Manufacturing Revolutionizes Lightweight Gridshells," 2017.

[9]   L. Mogas-Soldevila and N. Oxman, "Water-based engineering & fabrication: Large-scale additive manufacturing of biomaterials," *Mater. Res. Soc. Symp. Proc.*, vol. 1800, pp. 46–53, 2015.

[10]   I. Perkins and M. Skitmore, "Three-dimensional printing in the construction industry: A review," *Int. J. Constr. Manag.*, vol. 15, no. 1, pp. 1–9, 2015.

[11]   D. Marchon, S. Kawashima, H. Bessaies-Bey, S. Mantellato, and S. Ng, "Hydration and rheology control of concrete for digital fabrication: Potential admixtures and cement chemistry," *Cem. Concr. Res.*, vol. 112, no. December 2017, pp. 96–110, 2018.

[12]   T. T. Le, S. A. Austin, S. Lim, R. A. Buswell, A. G. F. Gibb, and T. Thorpe, "Mix design and fresh properties for high-performance printing concrete," *Mater. Struct. Constr.*, vol. 45, no. 8, pp. 1221–1232, 2012.

[13]   Y. Zhang, Y. Zhang, W. She, L. Yang, G. Liu, and Y. Yang, "Rheological and harden properties of the high-thixotropy 3D printing concrete," *Constr. Build. Mater.*, vol. 201, pp. 278–285, 2019.

[14]   "More than Tools | Dictum." [Online]. Available: https://www.dictum.com/en/. [Accessed: 23-Apr-2019].

[15]   DS/En 196-1, "Metoder til prøvning af cement – Del 1: Styrkebestemmelse Methods of testing cement – Part 1: Determination of strength," 2016.

[16]   R. J. M. Wolfs, F. P. Bos, and T. A. M. Salet, "Early age mechanical behaviour of 3D printed concrete: Numerical modelling and experimental testing," *Cem. Concr. Res.*, vol. 106, no. May 2017, pp. 103–116, 2018.

[17]   Y. W. D. Tay, G. H. A. Ting, Y. Qian, B. Panda, L. He, and M. J. Tan, "Time gap effect on bond strength of 3D-printed concrete," *Virtual Phys. Prototyp.*, vol. 14, no. 1, pp. 104–113, 2019.

Appendix 3.I – Conference Poster I – 'Potential of natural polymers as alternative binder for 3D printing concrete'

Christ, J., T. K. Engelsen, L. M. Ottosen, H. Koss, 'Potential of natural polymers as alternative binder for 3D printing concretes', 2nd RILEM International Conference on Concrete and Digital Fabrication – Digital Concrete, 6-9 July 2020, Eindhoven [NE] – Eindhoven University of Technology.

2020 Digital Concrete

RILEM · TU/e EINDHOVEN UNIVERSITY OF TECHNOLOGY

Potential of natural polymers as alternative binder for 3D printing concretes

Julian Christ, Thor Kell Engelsen, Lisbeth M. Ottosen, Holger Koss
DTU Civil Engineering
julch@byg.dtu.dk

DTU

Introduction

Cementitious concrete/mortar in 3DCP:

Problem
- does not satisfy the need for fast change in viscosity without extensive admixtures
- has a negative impact on the method's sustainability through the use of high cementitious shares and the connected high energy demanding processes
- is reliant on large scale industries

Natural hydrogels as binding material in concrete composites:

Motivation
- could *enhance the freedom of shape* in 3D printing through thermosetting or thermoplastic properties (easy controllable setting characteristics)
- could *decrease the energy demand* through low extraction temperatures and the utilisation other industry's byproducts (reuse of secondary products)
- can *decrease, the dependency on large industrial facilities* through simple production processes – especially important for remote living societies

Idea To assess 14 natural polymers on its suitability as binding material in concrete/mortar, i.e. as cement substitute.

Bio-binder + Sand
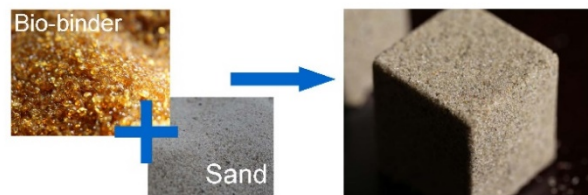
Materials and methodology

Methodolgy
The natural polymers have been assessed on the basis of mixing and observing the hydrogel's behavior (Category A-B), by evaluating literature (Category C-D), and assessing on the aspects of origin, scarcity and extraction method (Category E).

Bone glue: thermoplastic hydrogel in water, denaturated collagen extracted from butchery waste products.

Casein: milk protein, acid induced, thermosetting under elevated temperature (forms weak curd)

Soy protein: thermosetting under elevated temperature (forms weak curd), extracted from soybean

Isinglass: thermoplastic hydrogel in water, denaturated collagen extracted from swim bladder of fish

Cold water fish gelantine: thermoplastic hydrogel in water, denaturated collagen extracted from fish

Ovalbumin: egg white protein, thermosetting under elevated temperature

Materials
Alginate: forms gel under high concentration and/or with addition of catalysts (eg. Ca++ ion-solution), extracted from brown algae

κ-carrageenan: forms gel under addition of catalysts (eg. K+ ion-solution), extracted from red algae

Agar: thermoplastic hydrogel in water, extracted from red algae

Pectin: forms acid induced gel with addition of sugar, or with ion solution. Extracted from fruits (e.g. lemon fruit or apples)

Chitosan: acid induced gel, extracted from exosceletons of crustaceans

Cellulose: no gelling properties with water, extracted from wood

Starch: thermoplastic properties in water, extracted from vegetables

Lignin: no gelling properties with water, extracted from wood

	Natural polymer	Category A: Binding properties	Category B: Setting characteristics	Category C: Abundance	Category D: Raw material extraction	Category E: Ethical concerns	Overall Rating
Protein	Bone glue	++	+	+ [1]	+	o	5
	Casein	o	++A	o	o	-	1
	Soy protein	o	++A	o	+	-	2
	Isinglass	++	+	--	+	--	0
	Cold water fish gelantine	++	+	o	+	o	4
	Ovalbumin	+	++A	o	++	--	3
Polysaccharide and others	Alginate	+	++C	+ [2]	- [7]	+	4
	κ-carrageenan	+	++C	+ [3]	+ [8]	+	6
	Agar	+	+	o [3]	+ [9]	+	4
	Pectin	+	++C	o	o	o	2
	Chitosan	+	++C	+ [4]	o	o	4
	Cellulose	--	-	+ [5]	-	+	-2
	Starch	+	+	+	+	+	3
	Lignin	--	-- (++B)	+ [6]	+	+	-3

Category A
- ++ forms hydrogel with both strong adhesive and cohesive properties
- + forms hydrogel with either strong adhesive or cohesive properties
- o forms hydrogel without cohesive or adhesive strength
- - forms a thick suspension but no hydrogel
- -- does not form a hydrogel - with low viscosity

Category B
- ++A sudden thermosetting with temperature change
- ++B sudden thermosetting with UV radiation
- ++C sudden thermosetting with catalyst
- + thermoplastic / thermoreversible
- o does not show sudden viscosity change
- - low setting of suspension by temperature change
- -- no setting
- 0 unconfirmed

Category C
- ++ abundancy equal or higher than mineral binding materials
- + high abundancy
- o mediocre abundancy
- - smaller amounts easy accessible
- -- rare

Category D
- ++ raw material can be used
- + easy process by decocting raw material
- o extraction by addition of simple additives (eg. acids)
- - complex extraction method
- -- large industrial and complex process necessary for extraction

Category E
- ++ no ethical concerns - non reusable secondary material
- + low ethical concerns - primary material, no food application
- o secondary material, reusable as food application
- - primary material, usable for food production
- -- use of large quantities of life stock

Conclusion

- **Bone glue, Cold water fish gelantine, Alginate, κ-carrageenan, Agar and Chitosan show the highest potential and overall rating of natural polymers as binding materials in concrete composites**

References

[1] Lodish, H et al. (2004). ISBN 0716743663: Sect. 22.3
[2] Pegg, A (2012). ISBN 9781845698119: 175-196
[3] Therkelsen, G H (1993). ISBN 9780080926544: 145-180
[4] Daraghmeh, N H et al. (2011). Prof. Dr. Sub. Exc. 36: 35-102
[5] Aspinall, G O, (1970). ISBN 9780080134093: 1-12
[6] Gathergood, N et al. (2018). ISBN 9781786345219: 1-214
[7] Verma, A et al. (2019). DOI 10.1201/9780429023439-15
[8] Husin, A (2014). Extraction of kappa carrageenan from local seaweed. Universiti Malasia Pahang
[9] http://www.fao.org/3/y4765e/y4765e06.htm, [Accessed: 15-06-2020]

Appendix 3.I

	Natural polymer	Category A: Binding properties	Category B: Setting characteristics	Category C: Abundance	Category D: Raw material extraction	Category E: Ethical concerns	Overall Rating
Protein	Bone glue	++	+	+ [1]	+	o	5
	Casein	o	++A	o	o	-	1
	Soy protein	o	++A	o	+	-	2
	Isinglass	++	+	--	+	--	0
	Cold water fish gelantine	++	+	o	+	o	4
	Ovalbumin	+	++A	o	++	--	3
Polysaccharide and others	Alginate	+	+	+ [2]	- [7]	+	4
	К-carrageenan	+	+	+ [3]	+ [8]	+	6
	Agar	+	+	o [3]	+ [9]	+	4
	Pectin	+	++C	-	o	o	2
	Chitosan	+	++C	+ [4]	o	o	4
	Cellulose	--	-	+ [5]	-	+	-2
	Starch	+	+	+	+	-	3
	Lignin	--	-- (++B)	+ [6]	-	+	-3

Category A
++ forms hydrogel with both strong adhesive and cohesive propertie
+ forms hydrogel with either strong adhesive or cohesive propertie
o forms hydrogel without cohesive or adhesive strength
+ forms a thick suspension but no hydrogel
- - does not form a hydrogel - with low viscosity

Category B
++A sudden thermosetting with temperature change
++B sudden thermosetting with UV radiation
++C sudden thermosetting with catalyst
+ thermoplastic / thermoreversible
o does not show sudden viscosity change
- low setting of suspension by temperature change
-- no setting
0 unconfirmed

Category C
++ abundancy equal or higher than mineral binding materials
+ high abundancy
o mediocre abundancy
- smaller amounts easy accessible
-- rare

Category D
++ raw material can be used
+ easy process by decocting raw material
o extraction by addition of simple additives (eg. acids)
- complex extraction method
-- large industrial and complex process necessary for extraction

Category E
++ no ethical concerns - non reusable secondary material
+ low ethical concerns - primary material, no food application
o secondary material, reusable as food application
- primary material, usable for food production
-- use of large quantitities of life stock

Appendix 4.I – FT-IR spectra of natural polymers

The FT-IR spectra of biopolymers are raw product (red) and gelled dried film (blue). Each spectrum shows one representative result of triplicates. The denoted peaks are the mean value of these triplicates. All materials could be identified with their spectrum and compared to the following: (Sen and Erboz, 2010) for k-Carrageenan, (Xiao et al., 2014) for sodium alginate, (Christiaen and Bodard, 1983) for agar, (Baxter et al., 1992) for chitosan, and (Akbarzadegan et al., 2020) for gelatin.
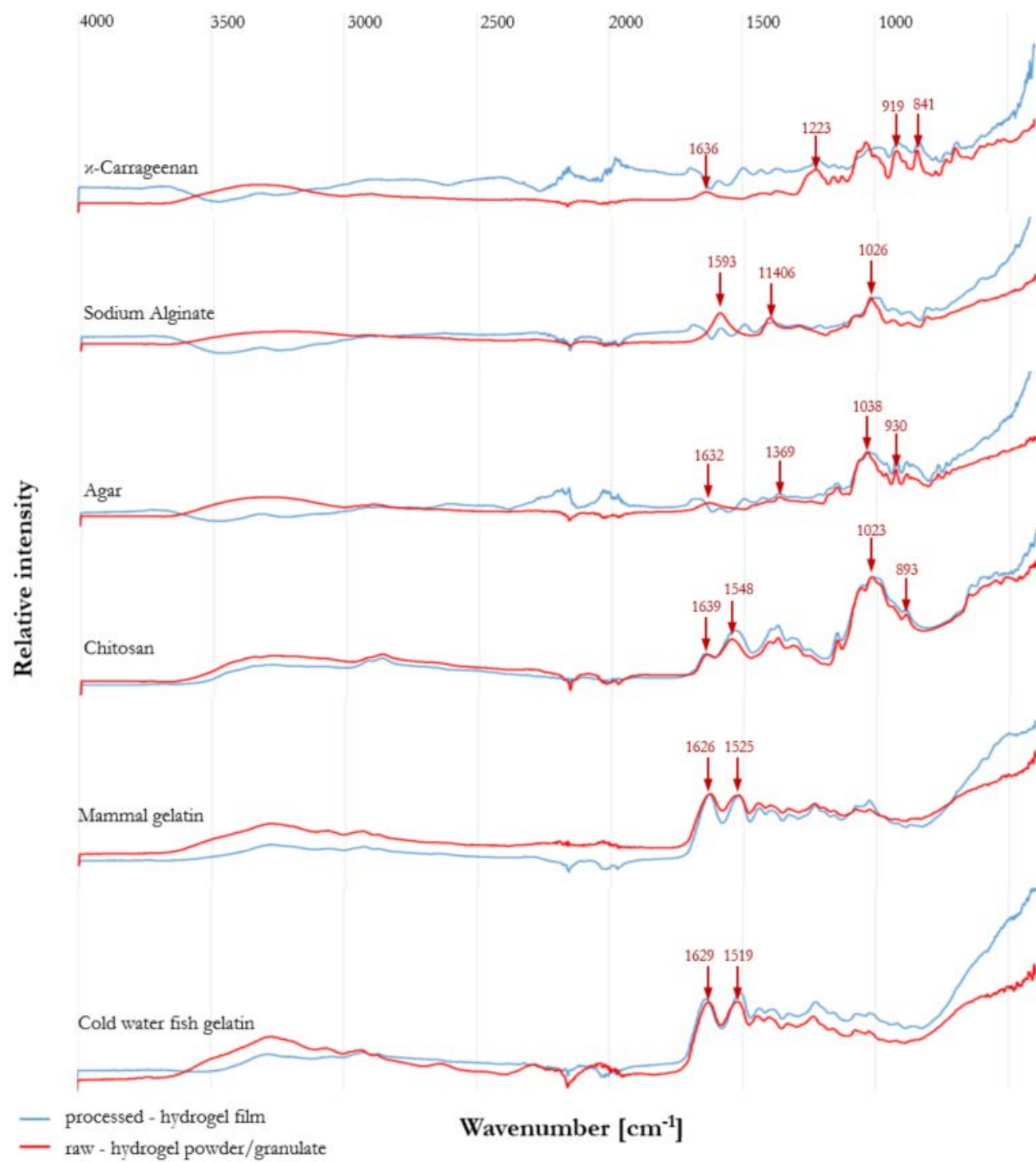
Appendix 4.II – FT-IR spectra of natural polymers under drying

FT-IR spectra of hydrogel's drying process are shown. The green line shows the pure hydrogel drying, while the blue lines show the composite drying. An increase in color intensity shows an increase in drying time. Sampling was conducted under constant drying every 5min. Concentrations according to the hydrogel solubility limit were chosen as described in Figure 4-4.
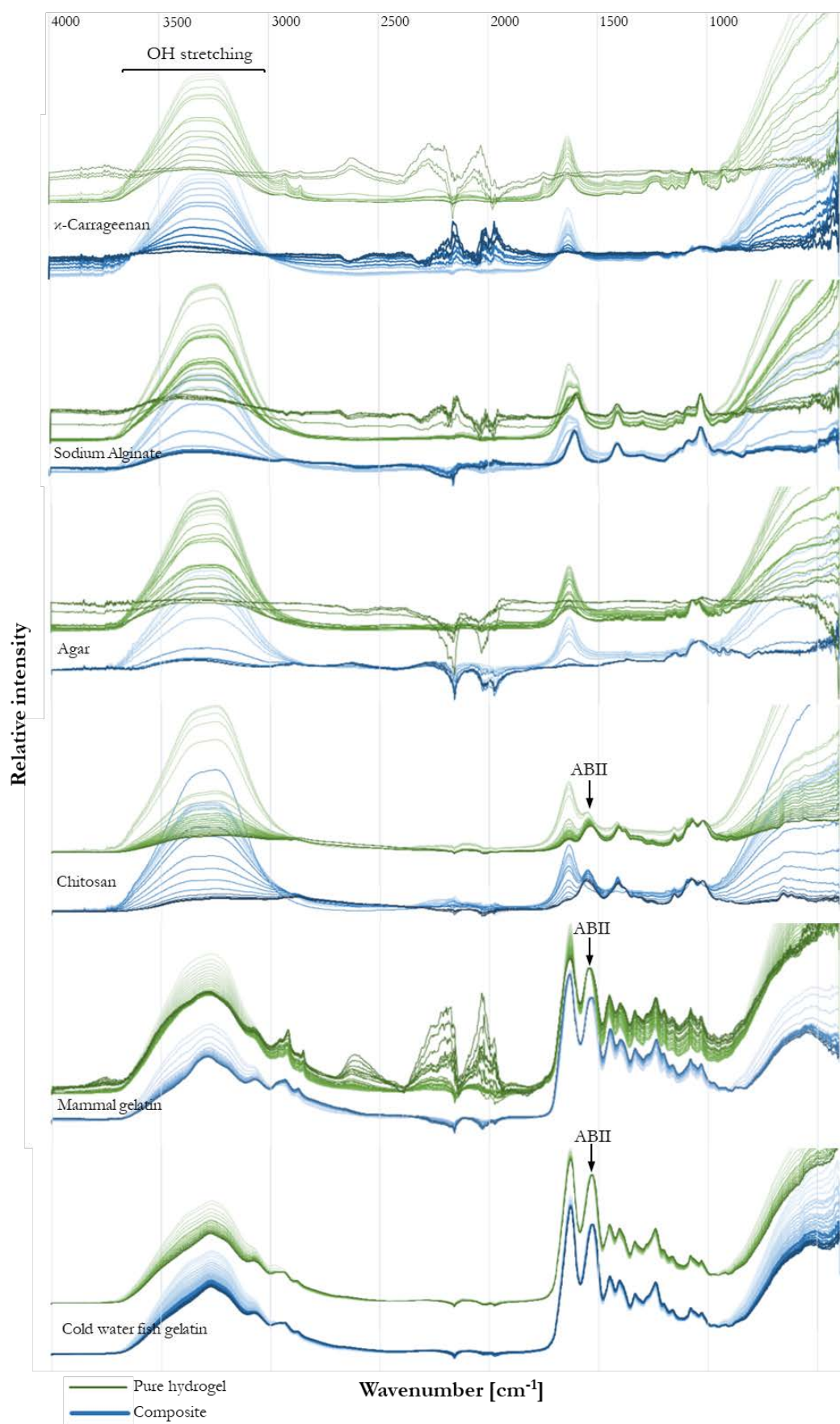
Appendix 6.I – Video of printing process

Video describing the variety of speed during a printed layer with constant extrusion speed and varying layer thickness.

Appendix 7.I – Conference Poster II – 'Gelatin as biologically based binder in temperature-sensitive printing mortar for advanced free-form constructions'

Christ, J., Ottosen, L.M., Koss, H. 'Gelatin as biologically-based binder in temperature-sensitive printing mortar for advanced free form constructions', 3rd RILEM International Conference on Concrete and Digital Fabrication – Digital Concrete, 26-29 June 2022, Loughborough [UK] – Loughborough University

The extended abstract can be seen, following the poster.

Gelatin as biologically-based binder in temperature-sensitive printing mortar for advanced free form constructions

Julian Christ, Lisbeth M. Ottosen, Holger Koss*
DTU Construct
julch@byg.dtu.dk

Introduction

To increase the efficient placement of 3D-printed building materials and increase architectural freedom, it is pursued to print in an inclined fashion. In 3D printing of cementitious mortars, high amounts of cements and advanced admixtures are consumed, in order to satisfy sophisticated rheological requirements. This adds up to a high share of CO_2 emissions per material unit. Therefore, other material compositions from earth, bio-based composites or geopolymers are investigated for their feasability, presenting a possible sustainable alternative.

Gelatin shows beneficial properties as binding material. The mix's thermoplastic behavior improves the stiffening of the composite after extrusion. It includes an additional rheological changing parameter besides the commonly used principle of thixotropy. The higher degree of freedom reached with the material can enable architecturally advanced and highly optimized designs.
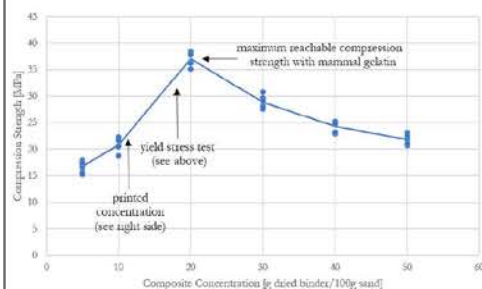
Yield strength development

- Rotational shear-vane-in-cup test
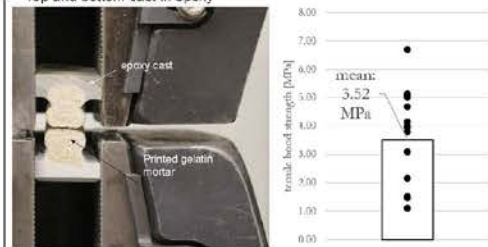- 0.1/s - shear-rate controlled by Rheometer
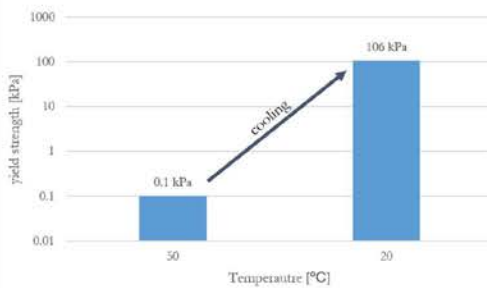
Compression strength (dried)

- 20x20x20mm samples casted
- dried under ambient conditions
- tested in compression

Interface adhesion

- Samples printed with layer time of 3min
- 4 layers, cut after printing to 50mm length
- Top and bottom cast in epoxy

mean: 3.52 MPa

Materials

Mammal gelatin (MG) was utilized as a binder. A granulate was purchased at DICTUM (pr#450141). The granulate was soaked in conventional tap water and heated to 60° C to produce a solution. For the printed samples, a binder solution of 80%-w/v of MG was used in a wet binder to sand weight-ratio of 0.35. The sand had a maximum grain size of 0.25mm. For the yield strength development, a higher concentration of 150%-w/v with a wet binder to sand ration of 0.4 was chosen. The composite shows a thermoplastic setting in the early hardening stage and develops its maximum strength under drying.

Printing Method

A printing setup was constructed by mounting an automated caulking gun, modified by a heating apparatus to warm the material, to a 6-axis KUKA robotic arm. The nozzle used had an inner diameter of 13mm. The layer time of 20s - 5min was chosen. The caulking gun was refilled every ~8 layers, which took between 5-6min. The material was extruded at 50-60°C. A 10-13mm layer width was defined by the chosen printing speed of 3mm/s and a layer height of 5mm. A tubular pipe with a diameter of 20cm and a maximum layer inclination of 80° was attempted as a printing object, as well as a topology optimized, organic shape.

Temperature controlled printing of free-form structures
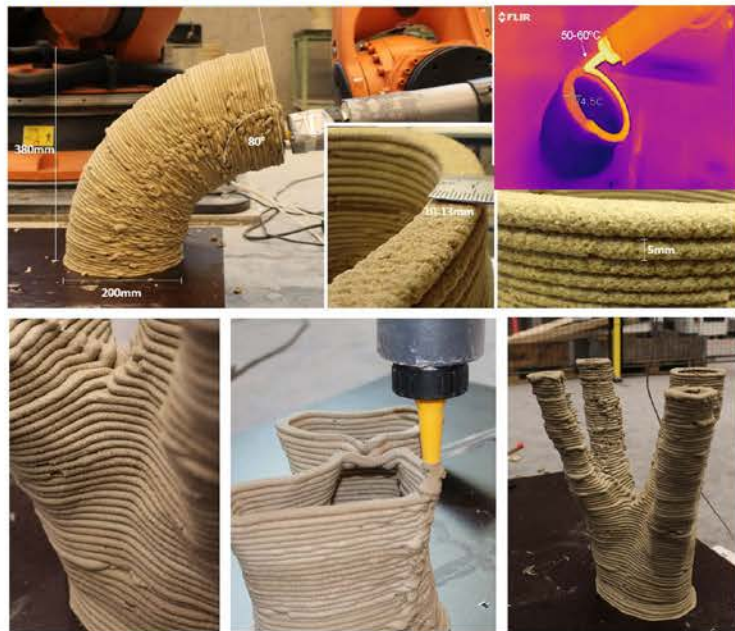
Conclusion

Gelatin-bound concrete composites show good properties for the realization of overhang constructions and large layer inclination. The material proofed the concept for completion of architecturally advanced designs. For structural applications, the material shows compression strengths in the same order of magnitude as cementitious concrete composites.

Julian Christ – julch@byg.dtu.dk
Holger Koss – hko@byg.dtu.dk

Gelatin as biologically-based binder in temperature-sensitive printing mortar for advanced free form constructions

Julian Christ[1][0000-0002-1945-4438], Lisbeth M. Ottosen[1][0000-0001-7756-382X] and Holger Koss[1][0000-0002-0274-4340]

[1] Department for Civil Engineering, Technical University of Denmark, Brovej 118, 2800 Lyngby, Denmark
julch@byg.dtu.dk

Abstract. Presented is the hydrogel gelatin as cement replacement in printing mortar to enable higher degrees of freedom for constructions built with extrusion-based 3D printing. Gelatin composites have a temperature-sensitive rheological behavior in the fresh state, improving the setting characteristics of the composite and thereby its buildability. It is shown that with a binder to sand ratio of 0.35 and a print temperature of 50°C, an 80° layer inclination and overhang could be realized. The binder consisted of an 80%-w/v granulate-water mixture. Protein binders could be more environmentally friendly than portland cement due to their low extraction temperature of <100°C and side streams as a resource. The high degree of freedom in the building process reached with the material enables architecturally advanced and highly optimized designs.

Keywords: Gelatin, 3D printing, concrete composite, overhang constructions, biopolymer.

1 Introduction

In recent years, 3D concrete printing technology gained in popularity. Automated construction of concrete elements on-site without formwork promises lower costs and enables the construction of optimized building components with less material use.
To increase the efficient placement of the material, it is pursued to print in an inclined fashion [1]. In order to satisfy the sophisticated rheological requirements, printing-concretes usually consume large amounts of cement, adding up to a high share of CO_2 emissions per material unit. Therefore, other material compositions from earth, bio-based composites or geopolymers are investigated for their feasability, presenting a possible sustainable alternative. Gelatin shows similar potential to be used as a cement replacement in printing mortar [2]. The mix's thermoplastic behavior improves the stiffening of the composite. It includes an additional rheological changing parameter besides the commonly used principle of thixotropy. The higher degree of freedom reached with the material can enable architecturally advanced and highly optimized designs. In this study, a material mixture of Gelatin, sand and water is presented. It was attempted to print a 80° layer inclination to proof its concept.

2 Materials and Methodology

Mammal gelatin (MG), resourced from bones, was utilized as a binder. A granulate was purchased at DICTUM (pr#450141). The granulate was soaked in conventional tap water and heated to 60°C. A binder mixture of 80%-w/v of MG was used in a binder to sand weight-ratio of 0.35. The sand had a maximum grain size of 0.25mm.

A printing setup was constructed by mounting an automated caulking gun, modified by a heating apparatus to warm the material, to a 6-axis KUKA robotic arm. The nozzle used had an inner diameter of 13mm. The layer time of 3 min was chosen. The caulking gun was refilled every ~8 layers, which took between 5-6min. The material was extruded at 50°C. A 10-13mm layer width was defined by the chosen printing speed of 3mm/s and a layer height of 5mm. A tubular pipe with a diameter of 20cm and a maximum layer inclination of 80° was attempted as a printing object.

3 Results

Fig. 1. 3D object printed from gelatin composite with a heated extruder

As shown in Figure 1, the composite material from Gelatin and mineral aggregates could realize the tubular 3D object with a layer inclination of 80°. The freshly applied layers did not show significant deformation under self-weight. After reaching the overhang shown, the interface between layers 25 and 26 failed under tension caused by the self-weight induced moment. Larger overhangs are possible by increasing the drying time to strengthen the layer interfaces.

4 Conclusion

Gelatin-bound concrete composites show good buildability for the realization of overhang constructions and large layer inclination. The material proofed the concept for completion of architecturally advanced designs.

1. Vantyghem, G., Corte, W., Shakour, E., Amir, O.: 3D printing of a post-tensioned concrete girder designed by topology optimization. Aut. in Constr. 112 (2020).
2. Christ, J., Ottosen, L.M., Koss, H.: A concrete composite from biologically based binders and mineral aggregates for constructional 3D-printing. In: ICSBM 2019: 2nd International Conference on Sustainable Building Materials, Vol.5, p.93-105.